Metabolomics and Proteomics Investigations of Alzheimer's Disease and Related Conditions

Jingshu Xu

A thesis submitted in partial fulfilment of the requirements for the degree of Doctor of Philosophy in Biological Sciences, The University of Auckland, 2016.

Abstract

Alzheimer's disease (AD) causes the commonest form of dementia, and remains the largest unmet medical need in neurology. The cause of AD is largely unknown and to date, there are no treatments with proven disease-modifying actions.

Substantial evidence has accumulated to support an important association between type-2-diabetes (T2D) and AD. Specifically, the vasculopathy aspects of T2D and AD have gained significant scientific attention, with a potential link being atherosclerosis.

This study aimed to improve understanding of the molecular basis of AD pathogenesis, with focus on vascular mechanisms. Case-control studies were performed in *ex-vivo* rabbit aortic tissue, and *post-mortem* brain tissue from patients. Specifically, we aimed to generate a detailed molecular profile representative of pathogenetic processes in aortic tissue from a rabbit model of atherosclerosis, and brain from AD patients. Furthermore, we aimed to measure and compare molecular changes in seven structurally and functionally distinct brain regions, to improve understanding of disease distribution in the human brain.

I performed parallel proteomic analyses and metabolic profiling studies: target tissues were analysed by iTRAQ-proteomics and tissue metabolites profiled by gas-chromatography-mass-spectrometry and liquid-chromatography-mass-spectrometry.

We derived a detailed description of molecular changes in human AD brain at both protein and metabolite levels, and generated quantitative protein and metabolite profiles from seven distinct brain regions. AD brain exhibited clear evidence of global perturbations in phospholipid content and defects in energy-producing mechanisms, the latter characterised by impaired glycolytic pathway and TCA cycle enzymes and metabolites, with concomitant activation of the pentose-phosphate and polyol pathways.

Compared to severely affected brain regions (hippocampus and entorhinal cortex), the least affected brain region (cerebellum) exhibited molecular signatures indicative of earlier disease processes and activation of molecular defence mechanisms: these included better-preserved systems for protein folding, protein degradation, and Aβ-clearance, and lesser activation of the immune response and oxidative phosphorylation.

I concluded that: accumulation of free glucose, sorbitol and fructose in AD brain is a probable cause of decreased cerebral glucose uptake as observed in patients; glycosylated proteins/lipids, interacting with relevant receptors may promote vasculopathy in atherosclerosis, T2D and AD; and, in the latter, different brain regions undergo molecular damage at different rates.

Acknowledgements

I would like to express my deepest gratitude to my supervisor Professor Garth Cooper for his patience, guidance and immense knowledge. He has been a tremendous mentor for me who supported my research with enthusiasm and encouraged me to strive for excellence in science.

I would also like to thank my co-supervisor, Dr Mia Jüllig, for her brilliant comments and suggestions, and her constant presence during the ups and downs of my research.

I would especially like to thank my lab manager, Cynthia Tse, for her impeccable administrative skill and her caring support throughout my doctoral years.

I would like to extend my thanks to my advisor Professor Richard Faull for his generosity in providing precious human brain tissue and supporting my study.

I would like to thank my parents for their unconditional love, allowing me to embrace my life without fear and regret. I also thank my son Sywon, a bright gentle soul bringing me happiness and courage in my life. I dedicate this thesis to them.

Lastly, I would also like to thank my friend Saem, who encouraged me to strive towards my goal throughout the study.

THE UNIVERSITY OF AUCKLAND
SCHOOL OF GRADUATE STUDIES

Co-Authorship Form

Graduate Centre
ClockTower – East Wing
22 Princes Street, Auckland
Phone: +64 9 373 7599 ext 81321
Fax: +64 9 373 7610
Email: postgraduate@auckland.ac.nz
www.postgrad.auckland.ac.nz

This form is to accompany the submission of any PhD that contains research reported in published or unpublished co-authored work. **Please include one copy of this form for each co-authored work.** Completed forms should be included in all copies of your thesis submitted for examination and library deposit (including digital deposit), following your thesis Acknowledgements.

Please indicate the chapter/section/pages of this thesis that are extracted from a co-authored work and give the title and publication details or details of submission of the co-authored work.	Molecular changes in the ascending aorta of cholesterol-fed rabbits (unpublished co-authored work)
Nature of contribution by PhD candidate	Designed experiments and obtained ethics approval for the study. Carried out animal monitoring, end-point tissue dissection, protein sample extraction, analysis/interpretation of the iTRAQ data, histological and immunohistochemical examination, and western blots.
Extent of contribution by PhD candidate (%)	70%

CO-AUTHORS

Name	Nature of Contribution
Mia Jüllig	Assisted with end-point tissue dissection, protein extraction, iTRAQ data processing and interpretation.
Martin Middleditch	Performed mass spectrometry analysis (on Q-star)
Garth Cooper	Supervised the entire study

Certification by Co-Authors

The undersigned hereby certify that:

- the above statement correctly reflects the nature and extent of the PhD candidate's contribution to this work, and the nature of the contribution of each of the co-authors; and
- in cases where the PhD candidate was the lead author of the work that the candidate wrote the text.

Name	Signature	Date
Mia Jüllig	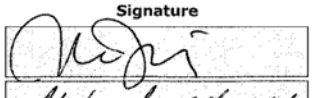	Click here 17/11/2014
MARTIN MIDDLEDITCH	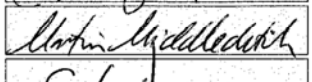	Click here 17/11/2014
GARTH COOPER	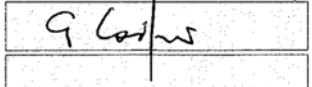	Click here 17/11/2014
		Click here
		Click here
		Click here

Last updated: 25 March 2013

THE UNIVERSITY OF AUCKLAND
SCHOOL OF GRADUATE STUDIES

Co-Authorship Form

Graduate Centre
ClockTower – East Wing
22 Princes Street, Auckland
Phone: +64 9 373 7599 ext 81321
Fax: +64 9 373 7610
Email: postgraduate@auckland.ac.nz
www.postgrad.auckland.ac.nz

This form is to accompany the submission of any PhD that contains research reported in published or unpublished co-authored work. **Please include one copy of this form for each co-authored work.** Completed forms should be included in all copies of your thesis submitted for examination and library deposit (including digital deposit), following your thesis Acknowledgements.

Please indicate the chapter/section/pages of this thesis that are extracted from a co-authored work and give the title and publication details or details of submission of the co-authored work.	Molecular profiling of the Alzheimer's disease brain: Metabolomics study comparing seven brain regions from human subjects with Alzheimer's disease (unpublished co-authored work)
Nature of contribution by PhD candidate	Designed the experiment and collected a total of 126 brain samples from seven brain regions of nine Alzheimer's disease patients and nine control patients. Performed tissue dissection, sample extraction, data analysis and data interpretation.
Extent of contribution by PhD candidate (%)	70%

CO-AUTHORS

Name	Nature of Contribution
Paul Begley	Performed GC/MS analysis and assisted data processing
Stephanie Church	Performed LC/MS analysis and assisted data processing
Katherine Hollywood	Adviced on data processing
Stefano Patassini	Assisted with human brain tissue dissection
Henry Waldvogel	Assisted with human brain tissue dissection

Certification by Co-Authors

The undersigned hereby certify that:

- the above statement correctly reflects the nature and extent of the PhD candidate's contribution to this work, and the nature of the contribution of each of the co-authors; and
- in cases where the PhD candidate was the lead author of the work that the candidate wrote the text.

Name	Signature	Date
PAUL BEGLEY	P. Begley	Click here 17/11/14
STEPHANIE CHURCH		Click here 17/11/14
		Click here
STEFANO PATASSINI	Stefano Patassini	Click here 17/11/2014
Henry Waldvogel	Waldvogel	Click here 17/11/2014
		Click here

Last updated: 25 March 2013

THE UNIVERSITY OF AUCKLAND
SCHOOL OF GRADUATE STUDIES

Co-Authorship Form

Graduate Centre
ClockTower – East Wing
22 Princes Street, Auckland
Phone: +64 9 373 7599 ext 81321
Fax: +64 9 373 7610
Email: postgraduate@auckland.ac.nz
www.postgrad.auckland.ac.nz

This form is to accompany the submission of any PhD that contains research reported in published or unpublished co-authored work. **Please include one copy of this form for each co-authored work.** Completed forms should be included in all copies of your thesis submitted for examination and library deposit (including digital deposit), following your thesis Acknowledgements.

Please indicate the chapter/section/pages of this thesis that are extracted from a co-authored work and give the title and publication details or details of submission of the co-authored work.

Molecular profiling of the Alzheimer's disease brain: Metabolomics study comparing seven brain regions from human subjects with Alzheimer's disease (unpublished co-authored work)

Nature of contribution by PhD candidate	Designed the experiment and collected a total of 126 brain samples from seven brain regions of nine Alzheimer's disease patients and nine control patients. Performed tissue dissection, sample extraction, data analysis and data interpretation.
Extent of contribution by PhD candidate (%)	70%

CO-AUTHORS

Name	Nature of Contribution
Paul Begley	Performed GC/MS analysis and assisted data processing
Stephanie Church	Performed LC/MS analysis and assisted data processing
Katherine Hollywood	Adviced on data processing
Stefano Patassini	Assisted with human brain tissue dissection
Henry Waldvogel	Assisted with human brain tissue dissection

Certification by Co-Authors

The undersigned hereby certify that:

- the above statement correctly reflects the nature and extent of the PhD candidate's contribution to this work, and the nature of the contribution of each of the co-authors; and
- in cases where the PhD candidate was the lead author of the work that the candidate wrote the text.

Name	Signature	Date
		Click here
		Click here
KATHERINE HOLLYWOOD	K Hollywood	Click here 17/11/2014
STEFANO PATASSINI	Stefano Patassini	Click here 17/11/2014
Henry Waldvogel	Waldvogel	Click here 17/11/2014
		Click here

THE UNIVERSITY OF AUCKLAND
SCHOOL OF GRADUATE STUDIES

Co-Authorship Form

Graduate Centre
ClockTower – East Wing
22 Princes Street, Auckland
Phone: +64 9 373 7599 ext 81321
Fax: +64 9 373 7610
Email: postgraduate@auckland.ac.nz
www.postgrad.auckland.ac.nz

This form is to accompany the submission of any PhD that contains research reported in published or unpublished co-authored work. **Please include one copy of this form for each co-authored work.** Completed forms should be included in all copies of your thesis submitted for examination and library deposit (including digital deposit), following your thesis Acknowledgements.

Please indicate the chapter/section/pages of this thesis that are extracted from a co-authored work and give the title and publication details or details of submission of the co-authored work.	Molecular profiling of the Alzheimer's disease brain: Metabolomics study comparing seven brain regions from human subjects with Alzheimer's disease (unpublished co-authored work)
Nature of contribution by PhD candidate	Designed the experiment and collected a total of 126 brain samples from seven brain regions of nine Alzheimer's disease patients and nine control patients. Performed tissue dissection, sample extraction, data analysis and data interpretation.
Extent of contribution by PhD candidate (%)	70%

CO-AUTHORS

Name	Nature of Contribution
Wanchang Lin	Assisted with data processing
Richard L. M. Faull	Provided the human brain samples and useful consultation
Andrew W. Dowsey	Assisted with data processing and analysed the data for three major metabolites: Glucose, Sorbitol, and Fructose
Garth Cooper	Supervised the entire study

Certification by Co-Authors

The undersigned hereby certify that:

- the above statement correctly reflects the nature and extent of the PhD candidate's contribution to this work, and the nature of the contribution of each of the co-authors; and
- In cases where the PhD candidate was the lead author of the work that the candidate wrote the text.

Name	Signature	Date
WANCHANG LIN	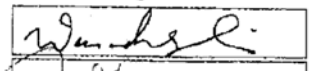	Click here 18/11/14
Richard L M Faull	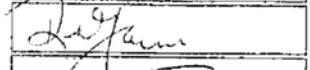	Click here 17/11/14
ANDREW DOWSEY	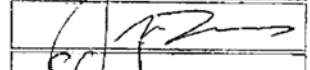	Click here 28/7/15
G COOPER	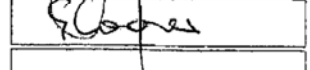	Click here 17/11/2014
		Click here
		Click here

Last updated: 25 March 2013

THE UNIVERSITY OF AUCKLAND
SCHOOL OF GRADUATE STUDIES

Co-Authorship Form

Graduate Centre
ClockTower – East Wing
22 Princes Street, Auckland
Phone: +64 9 373 7599 ext 81321
Fax: +64 9 373 7610
Email: postgraduate@auckland.ac.nz
www.postgrad.auckland.ac.nz

This form is to accompany the submission of any PhD that contains research reported in published or unpublished co-authored work. **Please include one copy of this form for each co-authored work.** Completed forms should be included in all copies of your thesis submitted for examination and library deposit (including digital deposit), following your thesis Acknowledgements.

Please indicate the chapter/section/pages of this thesis that are extracted from a co-authored work and give the title and publication details or details of submission of the co-authored work.	Molecular profiling of the Alzheimer's disease brain: Proteomics study comparing seven brain regions from human subjects with Alzheimer's disease (unpublished co-authored work)
Nature of contribution by PhD candidate	Designed the experiment and collected a total of 126 brain samples from seven brain regions of nine Alzheimer's disease patients and nine control patients. Performed tissue dissection, sample extraction, data analysis and data interpretation for the iTRAQ experiment.
Extent of contribution by PhD candidate (%)	70%

CO-AUTHORS

Name	Nature of Contribution
Mia Jüllig	Adviced the iTRAQ experimental design and assisted with data processing and interpretation
Stefano Patassini	Assisted with human brain tissue dissection
Henry Waldvogel	Assisted with human brain tissue dissection
Nitin Rustogi	Performed mass spectrometry analysis (on Q-star)
Richard L. M. Faull	Provided the human brain samples and useful consultation

Certification by Co-Authors

The undersigned hereby certify that:

- the above statement correctly reflects the nature and extent of the PhD candidate's contribution to this work, and the nature of the contribution of each of the co-authors; and
- in cases where the PhD candidate was the lead author of the work that the candidate wrote the text.

Name	Signature	Date
Mia Jüllig		Click here 17/11/2014
STEFANO PATASSINI		Click here 17/11/2014
Henry Waldvogel		Click here 17/11/2014
NITIN RUSTOGI		Click here 18/11/2014
RICHARD L.M. FAULL		Click here 17/11/2014
		Click here

Last updated: 25 March 2013

THE UNIVERSITY OF AUCKLAND
SCHOOL OF GRADUATE STUDIES

Co-Authorship Form

Graduate Centre
ClockTower – East Wing
22 Princes Street, Auckland
Phone: +64 9 373 7599 ext 81321
Fax: +64 9 373 7610
Email: postgraduate@auckland.ac.nz
www.postgrad.auckland.ac.nz

This form is to accompany the submission of any PhD that contains research reported in published or unpublished co-authored work. **Please include one copy of this form for each co-authored work.** Completed forms should be included in all copies of your thesis submitted for examination and library deposit (including digital deposit), following your thesis Acknowledgements.

Please indicate the chapter/section/pages of this thesis that are extracted from a co-authored work and give the title and publication details or details of submission of the co-authored work.	Molecular profiling of the Alzheimer's disease brain: Proteomics study comparing seven brain regions from human subjects with Alzheimer's disease (unpublished co-authored work)
Nature of contribution by PhD candidate	Designed the experiment and collected a total of 126 brain samples from seven brain regions of nine Alzheimer's disease patients and nine control patients. Performed tissue dissection, sample extraction, data analysis and data interpretation for the iTRAQ experiment.
Extent of contribution by PhD candidate (%)	70%

CO-AUTHORS

Name	Nature of Contribution
Andrew W.Dowsey	Software development and statistical analysis for dataset generated from this study
Richard Unwin	Adviced the experimental design and supervised this study
Garth Cooper	Supervised the entire study

Certification by Co-Authors

The undersigned hereby certify that:

- the above statement correctly reflects the nature and extent of the PhD candidate's contribution to this work, and the nature of the contribution of each of the co-authors; and
- in cases where the PhD candidate was the lead author of the work that the candidate wrote the text.

Name	Signature	Date
ANDREW. DOWSEY		Click here 28/7/15
RICHARD UNWIN		Click here 18/11/2014
GARTH. COOPER		Click here 17/11/14
		Click here
		Click here
		Click here

Last updated: 25 March 2013

Table of Contents

List of Figures

List of Tables

Abbreviations

ACN	Acetonitrile
AD	Alzheimer's disease
APP	Amyloid precursor protein
Aβ	Amyloid beta, product of APP cleavage
BACE1	APP cleaving enzyme 1
BAG	Bcl-2-associated athanogene
BH4	Tetrahydrobiopterin
BSA	Bovine serum albumin
BW	Body-weight
CCT	Chaperonin containing Tcp1
CE	Cholesterol ester
CERAD	Consortium to Establish a Registry for AD
CI	Confidence interval
CNS	Central nervous system
CSF	Cerebral-spinal fluid
CSN	COP9 signalsome complex
DBHS	Drosophila behaviour/human splicing
DG	Diradylglycerol
DTT	Dithiothreitol
ECM	Extracellular matrix
EDTA	Ethylenediaminetetraacetic acid
ER	Endoplasmic reticulum
ETC	Electron transport chain
FAO	Fatty acid oxidation
FDR	False-discovery rates
GABA	γ-hydroxybutyric acid
GAPDH	Glyceraldehyde 3-phosphate dehydrogenase
GC-MS	Gas-chromatography/mass-spectrometry
GlcCer	Glucosylceramide
Gpnmb	Glycoprotein (transmembrane) nmb-like
H&E	Haematoxylin and Eosin
HCD	High cholesterol diet
HESI	Heated electrospray ionisation source
hnRNP	Heterogeneous nuclear ribonucleoprotein
HpHRP	High pH reverse phase
HPLC	High-performance liquid chromatography
Hsc	Heat shock cognate
Hsp	Heat shock protein
IDA	Information dependent acquisition
IDL	Intermediate-density lipoprotein
IHC	Immunohistochemistry
IPA	Ingenuity Pathway Analysis
IPI	International Protein Index
iTRAQ	Isobaric tags for relative and absolute quantitation

KGDHC	Alpha-ketoglutarate dehydrogenase complex
LC-MS	Liquid-chromatography mass-spectrometry
LDL	Low-density lipoprotein
MCI	Mild cognitive impairment
MG	Monoradylglycerol
MSTFA	N-methyltrimethylsilyltrifluoroacetamide
OCT	Optimal cutting temperature compound
OGDC	Oxoglutarate dehydrogenase complex
OxPhos	Oxidative phosphorylation
PA	Glycerophosphate
PBS	Phosphate buffered saline
PC	Glycerophosphocholine
PCA	Principal component analysis
PDHC	Pyruvate dehydrogenase complex
PE	Glycerophosphoethanolamine
PEG	Polyethylene glycol
PG	Glycerophosphoglycerol
PI	Glycerophosphoinositol
PS	Glycerophosphoserine
PSEN1	Gene encoding presenilin 1
PSEN2	Gene encoding presenilin 2
QC	Quality control
RGD	Rat Genome Database
ROS	Reactive oxygen species
RT	Retention time
Serpin	Serine protease inhibitor
snRNP	Small nuclear ribonucleoprotein
SOD	Superoxide dismutase
SPAN	Snake presynaptic phospholipase A2 neurotoxins
SPE	Solid phase extraction
TEAB	Triethyl ammonium bicarbonate buffer
TFA	Trifluoroacetic acid
TG	Triradylglycerol
TTBS	Tris-buffered saline containing Tween20
UPS	Ubiquitin-proteasome system
VLDL	Very-low-density lipoprotein

Amino acid nomenclature

Full Name	3-letter code	1-letter code
Alanine	Ala	A
Arginine	Arg	R
Asparagine	Asn	N
Aspartic Acid	Asp	D
Cysteine	Cys	C
Glutamic Acid	Glu	E
Glutamine	Gln	Q
Glycine	Gly	G
Histidine	His	H
Isoleucine	Ile	I
Leucine	Leu	L
Lysine	Lys	K
Methionine	Met	M
Phenylalanine	Phe	F
Proline	Pro	P
Serine	Ser	S
Threonine	Thr	T
Tryptophan	Trp	W
Tyrosine	Tyr	Y
Valine	Val	V

Brain region abbreviations

HP	Hippocampus
ENT	Entorhinal cortex
MTG	Middle-temporal gyrus
SCx	Sensory cortex
MCx	Motor cortex
CG	Cingulate gyrus
CB	Cerebellum

Chapter 1. Introduction

1.1. Introductory summary

This summary provides an overarching framework through which the linkages between the different sections of the thesis document can be understood. It is intended to act as a guide for the reader.

This thesis comprises five chapters: an introduction (Chapter One); three results chapters (Chapters Two to Four) which also have specific introductory and methods sections; and a concluding chapter (Chapter Five), which provides an overarching summary and suggestions for further work.

In this work, I have placed particular emphasis on the linkages between defective regulation of lipid metabolism and the causation of Alzheimer's disease (AD). This is because there is emerging evidence that the mechanisms of atherosclerosis are linked to those of dementia, particularly AD [1,2]. Moreover, there is also substantive evidence linking defective lipid metabolism to aspects of the pathogenesis of vasculopathy in AD [3]. In designing my overall approach, I was also cognisant of the emergent link between type-2 diabetes (T2D) and AD [4,5]: this was particularly significant in the interpretation of the metabolomic and proteomic studies of human brain tissue described in Chapters Three and Four.

In this thesis programme, I undertook a series of linked proteomic and metabolomic studies of AD (Chapters Three and Four), and a related metabolic state hypercholesterolaemic vasculopathy as it manifests in the aorta (Chapter Two). The focus of the studies in the experimental chapters was chosen because each was considered to illustrate key aspects of the underlying pathogenetic mechanisms of AD.

Methods, results and conclusions related to each major area of investigation are presented in the respective chapters in the thesis document.

The principal aim of the work was to generate improved understanding of the pathogenetic mechanisms that lead to or cause AD, and its linkages to atherosclerosis and to T2D. The main methodologies employed were proteomics and metabolomics, accompanied where necessary by other methodologies, for example the classical pathological approaches of clinical biochemistry and histopathology.

A further aim was to study aspects of the effects of vasculopathy in the aetiopathogenesis of AD. In particular, there is now substantive evidence that amyloid angiopathy plays a major role in the pathogenesis of AD [6-8]: this process has also been linked to concomitant atherosclerosis [9]. Here, this aspect of the work was begun by proteomic analysis in the hypercholesterolaemic rabbit. The intended aim was subsequently to compare and contrast the aortic proteome with equivalent proteomic data derived from analysis of the cerebral arteries from patients with AD and vasculopathy. In the event, the second aspect of the planned studies, the proteomic analysis of the middle cerebral artery in AD cases and matched controls without neurodegeneration, was not completed before the end of the thesis period

due to unavailability of sufficient number of samples, and therefore has not been included here: the planned study is currently underway and will employ the results from Chapter Two as comparators, as originally planned.

Here, proteomics and metabolomics have been applied to elucidate the molecular basis of disease mechanisms in two models, the aortas of cholesterol-fed rabbits and matched controls, and brain tissue from cases with AD and matched controls.

Proteomic studies were initially performed in a widely-accepted animal model of hypercholesterolaemic vasculopathy, cholesterol-fed rabbit [10,11]: these are described in Chapter Two. It is noteworthy that the cholesterol-fed rabbit is also employed as a model for AD [12], wherein the AD-like phenotype is accentuated when the drinking water is supplemented with low levels of added Cu^{2+} [13-15]. These studies were performed using tissue from the wall of the ascending aorta. Atherosclerosis is considered by some to contribute to the pathogenesis of the vasculopathy in AD [9] and other related forms of chronic, age-related dementia such as Huntington's dementia [16,17] and age-related Parkinson's dementia [18].

I chose to perform these studies in the animal model rather than in *post-mortem* human tissue because this rabbit model is considered to provide a more specific model of atherosclerosis than would, for example, be provided by ageing human aorta, which is usually subject to other disease processes in addition to atherosclerosis, and therefore is expected to yield a mixed picture which would be more difficult to interpret.

The aim of this section of the work was to define a series of changes in the aorta that were specific for atherosclerosis, so that they could be compared with changes in human cerebral arteries from patients with AD. The idea was to use the animal model of atherosclerosis to identify those aspects of the pathogenesis that might be attributable to the atherosclerotic process. To our knowledge, these studies are original and there was no equivalent data in the literature known to us.

Secondly, I undertook detailed metabolomic and proteomic studies of *post-mortem* human brain from patients diagnosed with severe AD and resulting dementia, and from matched control patients who had no evidence of neurodegeneration or mental impairment at the time of death: these are presented in Chapter Three and Chapter Four, respectively. Molecular composition of brain tissues was compared and contrasted between seven brain regions. Brains were pre-dissected by a qualified neuroanatomist: they were sourced from the New Zealand Neurological Foundation Human Brain Bank, in the Centre for Brain Research, Faculty of Medical and Health Sciences, University of Auckland, Auckland, New Zealand. These studies are described in detail in the relevant sections of the thesis.

A substantive paper describing the work in Chapter Two had been accepted for publication in the journal ***Atherosclerosis*** at the time this thesis was submitted to the University: a reference to this submission is provided at the end of the thesis document.

A major paper describing the work in Chapter Three was in submission at the time this thesis was submitted to the University: a reference to this submission is provided at the end of the thesis document.

1.2. Social impact of dementia

Dementia, a disease characterised by progressive decline in cognitive function, has currently reached epidemic scale as the world's population ages. In 2013, ~44 million of the world-wide population was estimated to be affected by dementia. This number was predicted to reach ~76 million by 2030 and 136 million by 2050 [19]. The majority of cases of dementia (~70%) are accounted for by AD [20] and the prevalence of AD has been predicted to exceed one hundred million by 2050 [21]. To date, there are no treatments with proven disease-modifying effects and AD remains the largest unmet medical need in neurology [22]. In 2010 alone, AD has cost the world an estimated $604 billion [23] and with the estimated rise in AD population in the foreseeable future, health systems will struggle to cope with the staggering cost associated with AD. As a result, there is an urgent need to understand the underlying aetiology of AD for development of genuinely effective treatment.

1.3. Characteristics of Alzheimer's disease

AD is clinically characterised by a progression from episodic memory problems to a slow global decline of cognitive function [22]. Its pathobiology is characterized by accumulation of extracellular beta amyloid (Aβ) plaques and intracellular formation of neurofibrillary tangles (NFT) in the brain [24].

To date, the precise underlying aetiology of AD is unknown. Generally accepted molecular mechanisms associated with the disease include the accumulation of misfolded proteins in the brain and resulting oxidative and inflammatory damage, which leads to impaired energetics and synaptic function, ultimately leading the neurodegeneration [20].

More than two decades ago, the amyloid hypothesis was formulated: in brief, it put forward the idea that pathological accumulation of Aβ is the root cause of AD pathogenesis [25]. Aβ is generated from proteolysis of the amyloid precursor protein (APP) through sequential enzymatic cleavages. The amyloid hypothesis is strongly supported by autosomal dominant familial AD (fAD) syndromes, which are caused by mutations in three genes encoding proteins that are integrally involved in Aβ production, namely *APP* and the processing enzymes *PSEN1* and *PSEN2* [26].

Similarities between fAD and sporadic AD pathology are integral to the amyloid hypothesis. Excessive accumulation of toxic forms of Aβ that are present in both fAD and sporadic AD (or Late-Onset Alzheimer's Disease) is the main basis for extension of the amyloid hypothesis in sporadic AD. However, not only are both forms of AD are highly heterogeneous and show mixed pathological presentations, the genetic components of sporadic AD, which comprises the vast majority (~95%) of AD cases, are much more complex than the familial form. In general, the risk genes identified for sporadic AD are subtle, with no direct genetic association to the *APP* gene or its processing enzymes. Nevertheless, most of the genetic link to sporatic AD (eg. *Apolipoprotein* genotype E4 (*APOE4*) and

triggering receptor expressed on myeloid cells 2 gene (*TREM2*)) have been interpreted through the lens of the dominating amyloid hypothesis although other interpretations are equally valid [27].

Accumulating evidence is urging the researchers to practice caution when interpreting results from AD studies in the context of the amyloid hypothesis, due to the remaining uncertainties on the causality of Aβ deposits in AD. One of the first questions regarding the validity of the amyloid hypothesis arises from poor correlation between the Aβ deposition and neuropathology in AD, both temporally and anatomically [28,29]. More recently, there has been a shift in the amyoloid hypothesis towards soluble Aβ oligomers, rather than plaques, being responsible for neurodegeneration in AD [30]. However, the current over-reliance on low-resolution techniques (eg. Sodium dodecyl sulphate (SDS) polyacrylamide gel electrophoresis (PAGE)) as a detection method for Aβ oligomers [31] introduces the possibility of Aβ oligomerization as a result of experimental manipulations and hence, uncertainties surrounding the presence of Aβ oligomers in the human brain *in vivo* [27]. Furthermore, studies investigating Aβ oligomer toxicity in vivo are still largely constrained by methodological limitations and therefore, its physiological relevance to the pathogenic mechnisms in brain should be interpreted with caution [27]. Secondly, the fact that around 25% to 30% of individuals carrying substantial amyloid burdens in their brains are without overt clinical symptoms of dementia also indicates that amyloid is not a sufficient cause of the disease [32], and it has been suggested that amyloid deposition is predominantly associated with normal ageing and not a disease *per* se [27]. Perhaps the strongest evidence arguing against the amyloid hypothesis comes from continuous failure in clinical trials based on the premises of the amyloid hypothesis [33]. Drugs targeting Aβ and BACE1 failed to show disease-modifying effects, suggesting inconsistency between the available human pharmacology of this system and its exerting major effects in sporadic AD.

Despite the aforementioned discrepancies, amyloid continues to be considered strongly associated with AD. Actually, none of the previous data necessarily argue against a pathogenic role for Aβ in AD. The critical shift in how researchers see the amyloid hypothesis is related to causality: Is Aβ the primary cause of sAD? And based on accumulated evidence, the aggregation of Aβ and the development of neuritic plaques are neither necessary nor sufficient to produce the neuronal losses and clinical changes of AD [32,34]. It is perhaps preferable to consider that Aβ is not the primary direct neurotoxin that itself alone causes AD, but rather that it acts as the initiator of a complex network of pathologic changes in the brain [34] or even a consequence of other upstream events.

With this paradigm shift, alternative causative mechanisms underlying AD have been put forward. In particular, cerebrovascular pathology as the primary trigger in the development of sporadic AD has gained a significant amount of recognition[35]. Some have also suggested that both amyloid plaques and neurofibrillary tangles formed by tau protein are the results of upstream pathogenic processes, such as defects in brain carbohydrate metabolism [36].

In summary, there is currently an urgent need for a systematic and holistic approach in AD research where the role of Aβ can be accommodated within a broadened view of AD, accounting for the extensive

data with unprejudiced interpretation. This would accommodate the search for other possible targets as treatment strategies for AD in the future.

1.4. Role of vasculopathy in Alzheimer's disease: link to vascular dementia and diabetes

The coexistence of AD and vascular dementia (VaD) pathologies in the same patient is one of the biggest challenges for diagnosis [37]. About 30% of AD cases present with intracerebral vascular disease [20]. In reverse, around 40% of VaD cases have AD pathological features including senile plaque and NFT deposits [38]. The significant overlap in pathological features may not be surprising, considering the fact that the diagnosis of two diseases were previously defined to be mutually exclusive. According to the diagnostic and *Statistical Manual of Mental Disorders, Fourth Edition (DSM-IV)*, the presence of cerebrovascular disease in a demented individual would be diagnosed as VaD and excluded from the diagnosis of AD [39]. The observation of mixed brain pathologies characteristic of both AD and VaD, not only made it difficult to distinguish between these two diseases but also indicates an as yet uncharacterized connection between AD and VaD, which, together account for ~90% of all dementia cases [40].

Ever-growing evidence now suggest that sporadic AD is initiated by vascular factors that precede the neurodegenerative process [38]. Both epidemiological and neuropathological studies suggest that vascular risk factors are associated with AD [41-44]. Furthermore, the diseases that are known as risk factors for AD, including diabetes [4] and atherosclerosis [2], also have a vascular involvement [45].

The severity of both AD and VaD was found to be significantly correlated with the severity of atherosclerosis according to the Rotterdam study [2] and it was suggested that atherosclerotic carotid artery flow that leads to brain hypoperfusion can lead to gradual cognitive loss over several decades [38]. Atherosclerosis is intimately related to high blood cholesterol, and cholesterol is known to increase the production and affect the clearance of Aβ [46], which may underlie the link between atherosclerosis and AD.

Epidemiological studies have previously revealed that diabetic patients have higher risk of developing dementia [4,47]. More recently, increased blood glucose levels have been suggested to increase the risk of dementia even among patients without diabetes [48] and impaired glycaemia has been positively associated with cognitive decline in cases of mild cognitive impairment and progression to AD [49]. These data not only suggest that glucose homeostasis is critically involved in the development of dementia but also indicate the existence of a potential link between AD and T2D.

1.5. Case-control study of the molecular composition of the hypercholesterolaemic aorta in cholesterol-fed rabbits

In light of previous findings, we aimed to investigate the possible vascular link between AD and diabetes via direct comparison of molecular signatures of AD- and diabetes-like pathology in nonclinical animal models. The main research hypothesis investigated is that the common dementias, AD and VaD, are caused by vascular pathologies associated with hypercholesterolaemia and hyperglycaemia.

A pilot study was performed to establish thee experimental groups: non-diseased control, hypercholesterolaemic, and diabetic, in New Zealand White (NZW) rabbits. An animal larger than rats/mice was required in order to enable sufficiently sensitive analyses of tissue responses. Hypercholesterolaemic NZW rabbits have been shown to develop dementia when treated with a high cholesterol diet, which resembles AD in humans [12,50]. However, the STZ-induced diabetic model is not well established in NZW rabbit. Therefore, we undertook a dose-escalation study in order to characterise STZ-induced diabetes in the NZW rabbit. We concluded that the STZ dose required to induce diabetes is much higher in the rabbit compared to rats and mice (it was found to be either ~at or higher than the lethal dose) and that the conversion rate is very low. Therefore, the use of STZ as a diabetogenic agent in the rabbit is neither feasible nor ethical, and that the model is not valid as an animal model of diabetes. This section of the thesis work has not been written up in the thesis document: however, a paper describing these results was in submission at the time this thesis document was submitted to the University.

As a consequence of these findings, the planned full-scale study using the STZ-treated rabbit was not performed. From this study, a total of 12 rabbits (six controls, six cholesterol-fed) were studied to elucidate the effects of hypercholesterolaemia in the aorta. We applied proteomics to profile the molecular changes that occur in the ascending aorta of hypercholesterolaemic animals in comparison to control animals and these data are reported in Chapter Two.

1.6. Case-control studies of the molecular composition of the human brain in Alzheimer's disease

In continued pursuit of better understanding of AD, we have obtained *post-mortem* human brains from AD patients and matched controls from the New Zealand Neurological Foundation Human Brain Bank. With this rare set of human brain tissue samples, we aimed to perform systematic analysis using metabolomics and proteomics to ascertain disease mechanism at the molecular level. With the highly systematic and *a posteriori* hypotheses-generating approach, we aimed to better define pathogenetic mechanism to aid the identification of new potential diagnostic and therapeutic strategies for AD. Furthermore, we aimed to examine and compare seven functionally-distinct brain regions that are

known to be differentially affected by AD, which would substantially increase our knowledge about the disease processes that take place in different regions of the brain in AD.

Here we have applied metabolomics to profile the metabolic changes that occur in AD human brain in a brain-region-specific manner in Chapter Three. The same brain regions were examined again by applying proteomics with the aim of profiling changes in various molecular pathways that occur in AD: these studies in Chapter Four.

1.7. Overarching objectives

With the ongoing failure of development of drugs for preventing the progression of AD, there is a widely-agreed unmet clinical need for new approaches for the diagnosis, monitoring and therapeutics of AD. Due to the nature of the complexity of the disease, which may involve defects in numerous molecular pathways, therapies targeting several neurodegenerative mechanisms may be necessary, along with well-chosen timing of the introduction of these therapies and an appropriate sequence of treatments [34]. To achieve this, a better global understanding of the molecular pathologies and how they interact, is of critical importance.

In this study, we sought to achieve better understanding of the molecular basis of AD pathogenesis by using systematic approaches that combined both metabolomics and proteomics, to provide accurate descriptions of the molecular profiles of the changes that may underlie the pathogenesis of AD. Furthermore, this study was also designed to identify potential biomarkers for diagnosis, ascertainment of prognosis, or therapeutic monitoring in AD patients. We hypothesized that the outcome would provide potential targets for future drug development, and also act as a valuable platform for the rigorous testing of drug efficacy.

Chapter 2. Modelling atherosclerosis: Molecular changes in the ascending aorta of cholesterol-fed rabbits

2.1. Introduction

Atherosclerosis is a chronic inflammatory disease of the large and medium-sized arteries [51] characterised by the accumulation of lipids and fibrous elements in the arterial wall, and the activation of both the innate and adaptive immune systems [51-53]. Atherosclerosis is the primary cause of heart disease and stroke, which accounts for about 50% of all deaths in the westernised societies [53].

The progression of atherosclerosis is characterised by early lesions displaying accumulation of cholesterol-engorged macrophages in the sub-endothelial matrix, followed by accumulation of lipid-rich necrotic debris and smooth muscle cells. At the late stage, complex plaques with calcification, ulceration and haemorrhage are present. Thrombosis associated with rupture or erosion of these lesions is the most important clinical complication of atherosclerosis, causing myocardial infarction or stroke [53].

The pathogenic process of atherosclerosis is still incompletely understood at the molecular level. It is clear that elevated blood cholesterol contributes to the development of atherosclerosis, although different species respond in different ways to increased dietary cholesterol. In humans, hypercholesterolaemia appears to be more closely correlated to dietary saturated fat than the amount of cholesterol obtained from food [54]. Some animals, including rabbits, display a more direct relationship and will develop hypercholesterolaemia in response to increased dietary intake of cholesterol. High cholesterol diets have been widely used to establish atherosclerosis in experimental animals. Rabbits exhibit hypercholesterolaemia within a few days of administration of a high cholesterol diet and their sensitivity to the induction of atheromatous lesions has made them the most popular animal model for atherosclerosis. Furthermore, compared to rabbits, most rodents are highly resistant to the effects of high cholesterol diets due to a phenomenon that can be attributed to low cholesterol ester transfer protein activity, and primate models are costly and come with various technical difficulties [10].

In rabbits, the percentage of cholesterol added to the diet and the duration of the diet are known to result in different lesion morphology, representing various degrees and stages (early fatty streaks to fibrous plaques) of atherosclerotic lesions [11,55,56]. Supplementation of the diet with ≥0.5% cholesterol for short period (weeks) causes predominantly monocyte/macrophage-enriched fibrofoamy changes in the arterial intima comparable to early human lesions, whereas <0.5% cholesterol for longer period (months) causes fibromuscular lesions similar to advanced human atherosclerotic plaques [55,56].

The development of novel proteomic techniques has enabled the identification and quantitation of a multitude of proteins in complex proteinaceous samples. Proteomic profiling of diseased tissues is used to gain detailed knowledge of the molecular processes causing and/or resulting from a pathobiological process. Atherosclerotic lesions have previously been subjected to proteomic study; however only a

relatively small number of proteins were identified in these studies from patients [57] and rabbit models [58], 27 and 100 proteins were identified respectively.

Here we aimed to use a combination of isobaric (iTRAQ) labels and LC-MS/MS to examine the molecular changes evident in the ascending aorta of NZW rabbit maintained on a 2% cholesterol diet for 10 weeks, a model which corresponds to early atherosclerosis in humans.

2.2. Methods

2.2.1. Animal preparation and sample preparation

All animal experiments were conducted in accordance with ethics approval from the University of Auckland Animal Ethics Committee (in accordance with the Animal Welfare Act 1999). Twelve male NZW rabbits were purchased through the Vernon Jansen Unit (University of Auckland, New Zealand). All rabbits were acclimated to the laboratory environment for at least 2 weeks and confirmed to be specific-pathogen-free before entering the study. Body-weights (BW) were 2.8 ± 0.3 kg at the time of enrolment. Rabbits were individually housed, kept in a temperature- and humidity-controlled room with a 12/12 h light/dark cycle and given *ad libitum* access to food and distilled water. The animals were randomly divided into two diet groups; the control group was fed high-fibre low-starch rabbit pellets, whereas the high cholesterol diet (HCD) group was fed the equivalent high-fibre low-starch with 2% cholesterol (w/w) added (diet formulation by Specialty Feeds, WA, Australia). BW was measured weekly for the entire 10 weeks of the experimental period.

At the end of the 10-week diet-treatment, a surgical level of anaesthesia was induced using ketamine/xylazine (35 mg/kg and 5 mg/kg mixture) via intraperitoneal injection, following which cardiac puncture and heparin (35,000 IU/35 mL, DBL Heparin Sodium Injection BP, Hospira) injection at 1 µL/g BW were performed. After allowing 2-3 min for distribution of heparin via the circulation, the animals were exsanguinated and death was confirmed. Rabbits were then dissected through a ventro-medial incision for tissue collection.

All analyses in the current study were performed on 5 HCD-fed rabbits and 6 control diet-fed rabbits (one rabbit from the HCD group died unexpectedly before the final phase of the experiment).

Plasma samples were prepared under standard clinical centrifugation conditions (2,500 × g for 15 min) and stored at -80 °C until analysed. Ascending aortic tissues were collected and cleaned from blood using ice-cold PBS; equal portions of each sample were then immediately frozen in liquid nitrogen (for proteomics), or immersed in 4% paraformaldehyde (for histological and immunohistochemical (IHC) examination). For histological and IHC examination, samples were submerged in 4% paraformaldehyde for 4-8 h, washed with PBS, blocked into OCT (Optimal Cutting Temperature compound) and then kept

at -80 °C. Plasma samples chemically analysed for total cholesterol content (Gribbles Veterinary Pathology Limited, Auckland, NZ).

2.2.2. iTRAQ

2.2.2.1. Protein extraction and digestion

Tissue samples, weighing ~150 mg each, were ground individually into fine powder in liquid nitrogen using an agate mortar and pestle, and then supplemented with 400 µL extraction buffer (7 mol/L urea, 2 mol/L thiourea, 0.8% Surfact-Ampss X-100 (Life Technologies, Grand Island, NY, USA), 10 mmol/L DTT, 5 mmol/L EDTA, 10% v/v glycerol, 8 mmol/L pepstatin A and 16 mmol/L bestatin hydrochloride in 15 mM phosphate buffer, pH 8.3). For grinding, I alternated between the HCD and control groups and within each group, the processing order was randomised. Samples were subjected to 3 freeze/thaw cycles on a dry ice/ice mixture and 3-5 rounds of sonication (Vibra-Cell; Newton, CT, USA) at 15 Amps for 15 s. Following centrifugation at 16,000 × g for 20 min at 4 ^{o}C, supernatants were transferred to fresh microtubes. Each supernatant sample was further subdivided into 3 tubes: one contained 100 µL for further processing, and two containing aliquots of ~95 µL that were stored -80 °C for follow-up validation studies.

Protein samples were alkylated with 500 mM iodoacetamide (Bio-Rad, Hercules, CA, USA) at 75 mM concentration for 1 h in the dark. Protein concentration was determined using a portion of the alkylated samples. Standards used for protein assay were prepared with fatty acid-free BSA (ABFF-100G, MP Biomedicals, NZ) in 15 mM phosphate buffer, at concentrations of 2, 1, 0.5, 0.25, and 0.125 mg/mL. Alkylated samples were diluted 10-fold in 15 mM phosphate buffer (pH 8.3) for protein assay. Protein assay reagent (500-0006, Bio-Rad) was diluted 1:4 in 18 MΩ (MilliQ, Millipore) water and used according to the manufacturer's instructions: 200 µL of reagent was mixed with 2.5 µL of proteins standards (in triplicate) and diluted alkylated samples (in triplicate) in a 96-well plate. The plate was then incubated at room temperature for 5 min and read at A595 using a micro-plate reader (SoftMaxPro 4.1.7, Spectra Max 340, Molecular Devices, USA). Protein concentrations were calculated using the standard curve and corrected for the dilution factor. Alkylation was followed by reduction with DTT at a final concentration of 25 mM. Protein extracts were diluted 10-fold with 15 mM phosphate buffer (pH 8.3) and the volume corresponding to 50 µg of protein transferred into new tubes. Sample volumes were equalised across all samples using extraction buffer diluted 10-fold with 15 mM phosphate buffer to achieve uniform concentration of both the proteins and the buffer chemicals.

A reference sample representing a pool of equal amounts of proteins from each individual sample was created after the alkylation/dilution steps to be used for normalisation between two iTRAQ runs. To cover two iTRAQ runs, the reference sample constituted to contain 100 µg of protein and the volume adjusted with the diluted extraction buffer as per the above method, to double that of the other individual samples. The pH value of each sample was determined and adjusted as necessary to ~8.0, prior to the digestion. Protein was digested with trypsin (Promega, Madison, WI, USA) at a 25:1 ratio at 37 ^{o}C for 5

h. Digestion was stopped by the addition of 10% (v/v) formic acid (10 µL for every 25 µg of protein) and the samples left at 4 °C overnight before proceeding to solid phase extraction (SPE).

2.2.2.2. SPE and iTRAQ label

Following acidification of the digests by addition of 10% (v/v) formic acid, sample pH values were measured and adjusted if needed to ~pH 3-4 for efficient column binding during SPE. Sample volumes were doubled by addition of 0.1% (v/v) formic acid and centrifuged at 16,000 × g for 3 min before proceeding to SPE. Ten mg Oasis HLB solid-phase-extraction cartridges (Waters, Milford, MA, USA) were used for SPE. Cartridges were washed with 0.5 mL of methanol followed by 0.5 mL 0.1% formic acid before the samples were loaded. Following sample injection, cartridges were washed again with 0.5 mL 0.1% formic acid and finally 0.5 mL 18 MΩ water (MilliQ; Millipore, Billerica, MA, USA). After the completion of the washing steps, samples were eluted with 250 µL 70% (v/v) acetonitrile into fresh Axygen microtubes. The pooled reference sample was eluted with 500 µL 70% (v/v) acetonitrile and divided into two tubes to be used in two iTRAQ runs. The resulting tryptic-digest samples were then desalted and dried using a vacuum concentrator (Savant SPD121P SpeedVac concentrator, Thermo Scientific) and stored at -30 °C until labelled.

Labelling was carried out in two batches according to the labelling schedule (**Table 2-1**). For each batch, eight samples were supplemented with 30 µL of the dissolution buffer provided in the iTRAQ labelling kit and each sample labelled with an 8-plex iTRAQ label (Applied Biosystems, Foster City, CA, USA) according to the manufacturer's instructions: samples were briefly vortexed and spun after the addition of dissolution buffer. To each of the 8-plex iTRAQ labels, 50 µL isopropanol was added followed by brief vortex and centrifugation steps. Labels were them mixed with appropriate samples according to the labelling schedule (**Table 2-1**).

Table 2-1: iTRAQ labelling scheme

Label	113	114	115	116	117	118	119	121
Run I	Ref	Ctrl-1	Ctrl-2	HCD-4	Ctrl-3	HCD-1	HCD-2	HCD-3
Run II	Ctrl-4	HCD-5	Other	Un-used	Other	Ctrl-5	Ctrl-6	Ref

Labelled samples were vortexed gently and spun briefly before incubation at room temperature for 2 h. Each sample was then acidified with 5 µL 50% (v/v) formic acid to quench the reaction prior to pooling all eight samples; the combined sample was then reduced to 200 µL using a vacuum concentrator, then diluted to 2 mL with 0.1% (v/v) formic acid and centrifuged at 16,000 × g for 3 min before undergoing SPE as described above. Cartridges were then washed with 0.5 mL methanol followed by 0.5 mL 0.1% (v/v) formic acid before loading. Following assembly of the combined sample, cartridges were washed twice with 0.5 mL 0.1% (v/v) formic acid and finally eluted with 250 µL 70% (v/v) acetonitrile. The eluted sample was then concentrated to ~40 µL, acidified with 10% (v/v) formic acid and diluted to 250 mL with water (18 MΩ/cm resistivity, MilliQ) prior to LC-MS/MS analysis.

2.2.2.3. iTRAQ – LC-MS/MS analysis

Labelled digests were fractionated on a 0.3 x 35 mm Zorbax Bio-SCX II column (Agilent, Santa Clara, CA, USA) in an on-line fashion using 10-µL aliquots of KCl in 0.1% (v/v) formic acid (15, 25, 40, 60, 80, 100, 120, 150, 200, 600 mM final). Peptides were captured on a 0.3 × 5 mm PepMap cartridge (LC Packings, Dionex Corporation, Sunnyvale, CA, USA) before separation on a 0.3 × 100 mm Zorbax 300SB- C18 column (Agilent). The HPLC gradient between Buffer A (0.1% (v/v) formic acid in water) and Buffer B (0.1% (v/v) formic acid in acetonitrile) was formed at 6 µL/min as follows: 10% B for the first 3 min, increasing to 35% B by 85 min, increasing to 98% B by 90 min, held at 98% until 93 min, back to 10% B at 95 min and held at 10% until 100 min. The LC effluent was directed into the Ionspray source of QSTAR XL hybrid Quadrupole-Time-of-Flight mass spectrometer (Applied Biosystems) scanning from 320-1600 m/z. The top three most abundant multiply-charged peptides were selected for MS/MS analysis (75-1600 m/z) with the Enhance All feature enabled. The mass spectrometer and HPLC system were under the control of the Analyst QS 2.0 software package (Applied Biosystems).

The two LC-MS/MS datasets obtained were searched both individually and in combination against the rabbit subset of NCBI's protein database (51,902 sequences, March 2013) using ProteinPilot v 4.0 with the following settings: Sample Type: iTRAQ 8plex (Peptide Labeled); Cys - Alkylation, Iodoacetamide; Digestion, Trypsin; Instrument, QSTAR or QSTAR XL ESI; Search Effort, Thorough; FDR Analysis, Yes. False-discovery rates (FDR) for protein identifications were estimated by performing identical searches using the same database with all sequences reversed. Discordant peptides allowed were: carbamidomethyl (C), deamidated (N), deamidated (Q), formyl@N-term, Gln->pyro-Glu@N-term, iTRAQ8plex (Y), oxidation (M), oxidation (P) and Pro->pyro-Glu (P).

In cases where the protein names assigned by IPI were deemed too general, we adopted the protein names used in linked pages in either the Rat Genome Database (RGD) or UniProt databases, when available. Alternatively, the amino-acid sequence of the matched protein was used to perform a BLAST search (http://blast.ncbi.nlm.nih.gov), which typically resulted in identification of an identical protein with an established name.

2.2.2.4. iTRAQ – data processing

Initial data processing revealed that ProteinPilot v 4.0 performs an overly strict designation of "discordant peptides" in the raw dataset, excluding by default any peptides matched to peptide sequences with any modifications, including hydroxylations. Exclusion of these matches would remove a large portion of the relevant findings whereas allowing all discordant peptides into the calculations would introduce an excessive number of errors of identification into the results. After careful examination of all the types of discordant peptides present in the dataset, all of the following types of discordant peptides were allowed in a revised programme: carbamidomethyl (C), deamidated (N), deamidated (Q), formyl@N-term, Gln->pyro-Glu@N-term, iTRAQ8plex (Y), oxidation (M), oxidation (P) and Pro->pyro-Glu (P). Allowing the above discordant types resulted in the inclusion of a further >2500 spectra per run for subsequent calculation. All compromised spectra were excluded from quantification; thereby, all

spectra with low iTRAQ signal (i.e. with a used score of 0) and spectra matched to peptides carrying proline in the C-terminus and /or including a proline-glutamine couple were eliminated.

Normalisation was performed in log space to equalise the average log-value of all non-compromised spectra between the channels, and separate normalisation factors for correctly cleaved and mis-cleaved peptides were used to exclude any bias from differential tryptic cleavage. Normalised data were then back-transformed to the raw format and the entire dataset was sorted by "N" to combine correctly cleaved and mis-cleaved peptides for each unique protein. This process allowed for the relative abundance of each individual protein to be calculated by summing up all peak areas for each protein from each label.

After both LC-MS/MS runs had been filtered and processed as described above, the final numbers for each protein within each sample were brought forward into a Master file, where average abundances and confidence intervals were calculated for each protein. A typical complication of performing more than one LC-MS/MS run is that a protein is often assigned to different database entries in different runs, complicating the assembly of the Master file. In order to avoid this problem, a third database search was routinely performed wherein the LC-MS/MS outputs from both runs were combined. Proteins identified within the third search were then used as a guide to determine which proteins were truly present in the samples, and the peptide summary from the third search was used as a template to align all proteins across the prior two individual runs. Therefore, the FDR cut-off scores from two individual runs were disregarded and all proteins that were identified with at least 99% certainty in the combined search were included into the final master file. This approach is considered to be more stringent than that of using the individual FDR cut-off value from each individual run.

Sample C3 (run 1) showed markedly-lower iTRAQ levels prior to normalisation, suggesting a markedly-lower protein load. Normalisation works best with minor variations between samples and in this case, considering the observation that exclusion of C3 substantially improved *p*-values, normalisation was not sufficient to overcome the differences in loading between samples. For this reason, the final analysis was based on the comparison between five control samples and five HCD samples only.

Among 453 unique proteins that were thus identified in the two runs with >99% confidence and with sufficient iTRAQ signal to enable calculations of their relative abundance, statistical testing was performed on 347 proteins containing at least 3 samples in each of the groups compared.

2.2.3. Histology: Congo red and H&E

Three sets of 7 µm sections separated by at least 200 µm were obtained from each fixed and paraffin-embedded specimen. Congo-red and haematoxylin and eosin (H&E) staining was performed on consecutive sections prepared from prefixed tissue by following routine histological protocols. Bright-field microscopy (for H&E stained sections) and polarised-light microscopy (for Congo-red-stained sections) were performed using a Leica DMRE microscope (Leica Microsystems, Wetzlar, Germany), fitted with a CCD camera (Leica DC500) to capture images.

2.2.4. Western blots

For each target protein, relative protein levels were measured by western blot in each individual protein sample prepared during protein extraction for iTRAQ analysis (2.2.2.1). Protein samples for western blot loading were prepared to achieve equal volume between samples (<15 µL). Each sample contained 1 × NuPAGE LDS sample buffer (Invitrogen), MilliQ water, and DTT to a final concentration of 50 mM. The amount of protein loaded varied between 10 µg and 20 µg among experiments.

For SDS-PAGE runs, NuPAGE 4-12% or 12% Bis-Tris Gels and a Novex Mini-Cell gel box (all Invitrogen) were used. The upper (inner) buffer chamber was filled with 200 mL of 1 × NuPAGE SDS running buffer containing 500 µL NuPAGE antioxidant. The lower (outer) buffer chamber was filled with 600 mL of 1 × NuPAGE SDS running buffer. A 10 µL-ladder (dual colour Precision Plus Protein Standards; Bio-Rad) was loaded into the gel along with the protein samples. Gels were run at 100 V (constant) for 1 h and transferred using the iBlot Gel Transfer Device (Invitrogen). Membranes were then removed and stained with Ponceau S (0.1% (w/v) in 5% (v/v) acetic acid) and images captured using a scanner (Epson Perfection 4990 Photo).

The membrane was then washed in TTBS and incubated with blocking buffer (5% (w/v) BSA in TTBS) either overnight in a shaker at 4 ^{o}C, or for 2 h at room temperature. Thereafter, membranes were incubated with primary antibody (diluted in TTBS containing 1% BSA) at room temperature for 3 h with shaking. Unbound primary antibodies were washed off with TTBS for 3 × 10 min. Secondary antibody diluted in TTBS containing 1% BSA was then added and incubated at room temperature for 2 h with shaking. Unbound secondary antibodies were removed by washing with TTBS for 3 × 10 min.

Specific antibody-reactive protein bands were detected using an ECL Plus detection kit (Amersham, GE Healthcare) according to manufacturer's instructions. A FUJIFILM Luminescent Image Analyzer LAS-4000 was used to image and digitise the membranes. Relative protein levels were analysed by Multigauge software using Ponceau S-stained samples as normalisers for protein loading. Student's *t*-test was performed to test the statistical significance of differences in values of variables between the two diet groups.

Primary antibodies used for the validation of iTRAQ results included two custom-made polyclonal antibodies (**Table 2-2**) and four monoclonal antibodies that were commercially available (**Table 2-3**). For all primary antibodies, a range of concentrations was used to cover the full range of recommended dilutions (1:100, 1:500, 1:1000). For the custom-made primary antibodies only, peptide blocking was also performed using the peptide provided by the antibody manufacturer. The secondary antibody used in this study was goat anti-mouse IgG-HRP (sc-2031; Santa Cruz).

Table 2-2: Anti-Gpnmb primary antibodies

Gpnmb_N1	**Order ID: 295193-1**
Antigen	NENPHGSTREHPQ-C (top BLAST hit: glycoprotein (transmembrane) nmb-like [*Oryctolagus cuniculus*] 100% identical, next hit in rabbit is phosphorylated CTD interacting factor 1 [*Oryctolagus cuniculus*] which is only 80% identical)
Concentration	0.792 mg/mL 9.19 mg in 11.60 ml PBS (pH 7.4) with 0.02% sodium azide
Gpnmb_N2	**Order ID: 295193-3**
Antigen	LDGWSPEENNWNEK-C (top BLAST hit: glycoprotein (transmembrane) nmb-like [*Oryctolagus cuniculus*] 100% identical, next hit in rabbit is hCG40831-like [*Oryctolagus cuniculus*] which is only 64% identical)
Concentration	1.212 mg/mL 12.12 mg in 10.00 ml PBS (pH 7.4) with 0.02% azide
Common for Gpnmb_N1 & N2	
Immunogen	Peptide-KLH conjugate
Host	BALB/c Mouse
Order	GenScript, USA

Table 2-3: Monoclonal primary antibodies

Antibody	Type	Clone	Order
CD31	Monoclonal Mouse Anti-Human	JC70A	M0823 Dako (Denmark)
CD68	Monoclonal Mouse Anti-Human	KP1	M0814 Dako (Denmark)
ADAM10	Mouse monoclonal Anti-Human	11G2	ab59482 (Abcam)
VEGFA	Monoclonal Mouse Anti-Human	JH121	LS-C88111

2.2.5. Immunohistochemistry

Immunohistochemistry was performed on ascending-aorta tissue sections prepared as described in Section: 2.2.3. Immunohistochemistry was performed both with and without antigen retrieval.

Sections were fixed with cold acetone for 5-10 min at room temperature, washed with PBS and blocked with 10% (v/v) goat serum in PBS for 10 min at room temperature. Following 3 × 5 min washes with PBS, sections were incubated with primary antibodies at 1:20, 1:50, 1:100, 1:200, and 1:500 dilution for 1-2 h at room temperature. Then 3 × 5 min washes with PBS were carried out followed by incubation with goat anti-mouse IgG (Alexa Fluor® 488) secondary Ab at 1:200 dilution, for 30-60 min, and finally

washed with PBS 3 × 5 min, then mounted with ProLong Gold Antifade Reagent with DAPI (Life Technologies).

Sections were submerged in PickCell Buffer A (Electron Microscopy Sciences, Hatfield, PA, USA) in a within-slide chamber for antigen retrieval using an antigen retrieval programmed for 20-min heating, and 2 h subsequent cooling. Sections were rinsed with dH_2O × 5 and washed in PBS for 2 × 10 min. Steps for primary and secondary antibody incubations and mounting were performed as above. Slides were then examined with a light microscope (Leica DMRE) fitted with a CCD camera (Leica DC500).

2.2.6. Multiple Reaction Monitoring (MRM)

2.2.6.1. LC-MS/MS analysis

Individual aorta samples were solubilised, digested and SPE-processed as before, but were analysed individually without iTRAQ labelling, using LC-MS/MS to monitor seven proteins of interest. A multiple Product Ion Scan method was created based on the observed fragment-ion patterns (gathered from an Information Dependent Acquisition LC-MS/MS run of a pooled digest, or from the iTRAQ datasets themselves, allowing for the mass shift due to labelling) for at least two peptides per protein. Due to the number of peptides being monitored and the cycle times required to give measurable peak areas, the method was split into three separate time periods to generate a reasonable number of data points across the chromatographic peaks. Peptides were captured on a 0.3 × 5 mm PepMap C18 cartridge (LC Packings) followed by separation on a Zorbax 300SB-C18 0.3 × 100 mm column (Agilent) using the following gradient at 6 µL/min: 0-3 min 10% B, 85 min 35%B, 90 min 97%B, 94 min 97%B, 96 min 10%B, 100 min 10%B, where buffer A was 0.1% (v/v) formic acid in water and buffer B 0.1% (v/v) formic acid in acetonitrile. The column effluent was directed into the Ionspray source of a QSTAR XL hybrid mass spectrometer (Applied Biosystems) using the above method. The resulting data were processed using the Quantitate function in Analyst QS 2.0 (Applied Biosystems) whereby selected fragment-ion chromatograms were extracted, summed and integrated to give raw peak areas for each peptide. As some peptides gave no significant peak above the background noise level in the control subjects, the peak height and local background noise heights were reported in order to provide a metric for comparison with the control subjects.

2.2.6.2. MRM – data processing

Our iTRAQ results indicated that versican expression at the protein level was not affected by HCD. Therefore, we have chosen versican to monitor and correct for loading during the MRM studies.

Two versican peptides (VER-VSV and VER-YEV) were used for normalisation of the datasets. The analyte peak areas for both peptides in each sample were divided by the average area for all samples for the appropriate peptide. Then the relative values for both peak areas were averaged to obtain a value for relative abundance of versican (i.e. the relative abundance of overall protein) to be used as a normaliser for peak areas corresponding to all non-versican peptides. For fibronectin 1 and transgelin,

the analyte peak areas (for each peptide individually) were normalised by dividing them by the corresponding versican value obtained for the sample in question. In order to obtain a value for HCD samples in relative terms to the control samples, for each of the two peptides (for each protein), an average value of all the control samples was calculated and used to scale the normalized values. The relative abundance for fibronectin 1 and transgelin in HCD relative to control groups was calculated by averaging the two scale-values for each protein in each sample and then averaging these values for the HCD and control groups. To test the statistical significance by assessing values for two peptides for each protein, two-way ANOVA was performed.

Most of the proteins of interest were elevated several-fold in the cholesterol group but present in such low amounts in the control group that no signal was detected that could be deemed to be higher than the background “noise”. Therefore, the signal-to-noise ratio was used for interpretation. The signal-to-noise ratio was calculated by dividing each analyte peak-height by the associated noise- peak height for all peptides whose peak areas were >90. For those peak areas <90 (in control samples), the corresponding signal-to-noise ratio was considered to be 1. Signal-to-noise values for the two (or, in the case of Plastin-3, four) peptides monitored for each protein were then averaged for each sample, and the groups were compared using unpaired *t*-tests (Prism). The same approach was also applied to fibronectin and transgelin, solely for the purpose of comparing the two approaches. Note that C1 was excluded from the control group due to the aberrant versican levels, which meant that it could not be properly normalised.

2.3. Results

2.3.1. Blood cholesterol

Significant changes in circulating levels of cholesterol were observed in NZW rabbits after the 10-week treatment. Total cholesterol measured in plasma was significantly elevated in the HCD group (0.9±0.1 mmol/L for controls, 50.6±4.2 mmol/L for the HCD group, $p<0.0001$).

2.3.2. iTRAQ results

2.3.2.1. iTRAQ summary

Among the total of 347 proteins that were identified and quantified in the current study, 61% were up-regulated and 21% down-regulated in tissue from cholesterol-fed rabbits compared with control values (**Figure 2-1**). Proteins with fold-changes of between 0.95 and 1.05 contributed to 18% of the total and were considered to be stable. Eleven proteins whose fold-change values were > 2.3 have not been included in the figure (**Figure 2-1**): this was because their inclusion would severely skew the balance of the data, obscuring the underlying pattern present in the rest of the data.

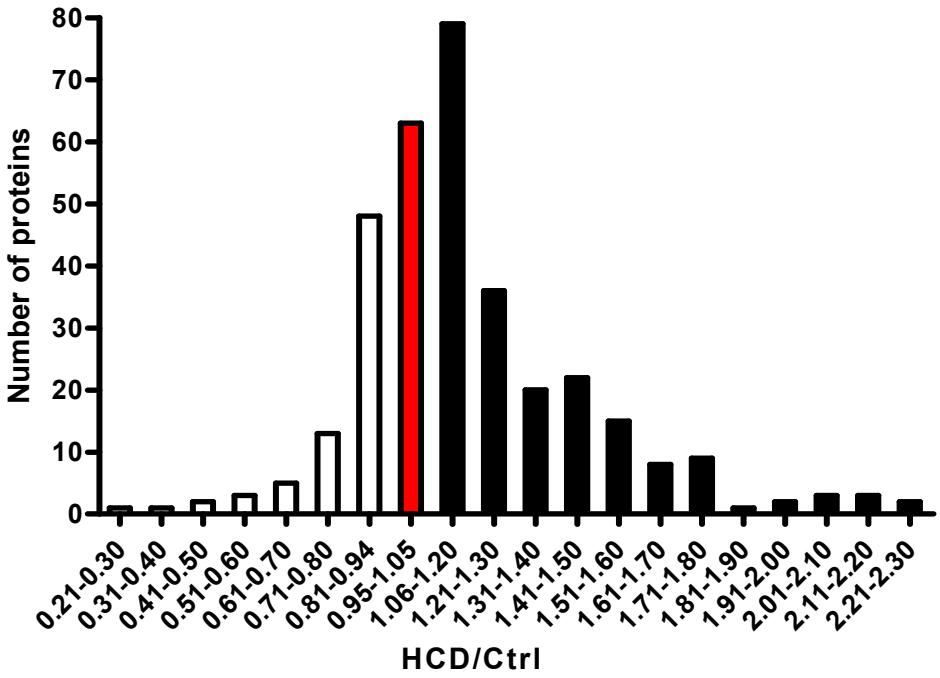

Figure 2-1 Distribution of 347 proteins according to the level of fold-change comparing the HCD treated vs controls.

Of 347 proteins detected in this study, ~18% had fold-change 0.95≤fc≥1.05 (Red bar), ~61% had fold-change >1.05 (black bars) and ~21% had fold-change <0.95 (white bars).

The observed trend of more proteins being increased than decreased became more evident when only proteins with significance were considered. According to the statistical analysis, 76 proteins differed significantly ($p<0.05$) and a further 50 showed a trend (defined as $0.05 \geq p < 0.1$) in the HCD group compared to the Control group (HCD/Ctrl).

Within the 76 proteins that were differentially expressed ($p<0.05$) between the HCD and Control groups, 71 were elevated and 5 were decreased (**Figure 2-2**). The highest number of proteins was found in the group with 1.41~1.60-fold elevation and in general, the number of proteins decreased as the level of fold-change increased. Six proteins with fold-changes above 3.40 have not been shown in **Figure 2-2**.

The distribution of 50 proteins with corresponding p-values above 0.05 but below 0.1 is shown in **Figure 2-2 b**. Again, following the same trend, more than 5 times as many proteins were elevated as opposed to lowered (42 vs 8). There was no protein with more than 2.20-fold elevation in this group. In both groups (**Figure 2-2 a & b**), there are no proteins in the stable range (0.95~1.05). The following sections refer only the proteins with p-value less than 0.1.

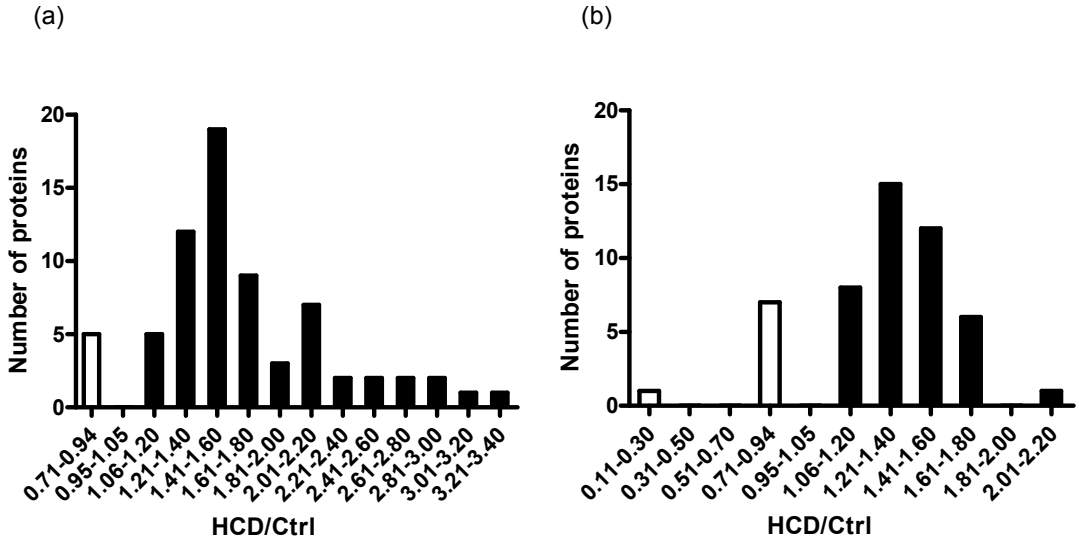

Figure 2-2 Distribution of proteins with significant fold-change comparing the HCD treated vs controls.

(a) Of 76 proteins with significant fold-changes (p-value < 0.05), 71 were increased while 5 were decreased in abundance. (b) Of 50 proteins with near-significant fold-changes (0.05 ≥ p-value <0.1), 42 were increased while 8 were decreased in abundance.

2.3.2.2. Proteins changes between diet groups – iTRAQ analysis

Apolipoproteins were among the most dramatically affected proteins as a result of HCD treatment in the current study. We noted the marked elevation of apolipoproteins in HCD-treated tissues: apolipoprotein E and apolipoprotein B were elevated 8.6 -fold (p=0.0005) and 4.5-fold (p=0.0071) respectively (Table 2-4).

Numerous blood-related proteins were significantly altered in response to HCD treatment (Table 2-4): all were elevated except for haemoglobin, which was trending downwards (0.3-fold, p=0.077). Proteins that are involved in the immune response were generally up-regulated (typically by 1.8~3.3-fold), including the histidine-rich glycoprotein (HRGP), fetuin-A, complement pathway proteins, and vitamin D-binding protein. Various other plasma proteins were elevated in the HCD-treatment group, including serotransferrin, transthyretin, and immunoglobulin gamma1 constant region.

All the identified nucleus-related proteins were elevated in the HCD group compared to the control group, either significantly or trending (Table 2-5). There are five major families of histones: H1/H5, H2A, H2B, H3, and H4. Histones H2A, H2B, H3 and H4 are known as the core histones, while histones H1 and H5 are known as the linker histones. Here, two of the four core histone were elevated: H4 was increased by 1.6 fold (p=0.030), and both predicted H2A variants were elevated by ~1.4-fold (p<0.05).

Nucleosome assembly protein-1-like 4 (NAP1L4) was also elevated (2.2-fold, p=0.033). Heterogeneous nuclear ribonucleoproteins (hnRNPs), including hnRNP-E1 (1.7-fold, p=0.015) and hnRNP-K (1.4-fold, p=0.054) were both elevated, whereas the synaptotagmin-binding, cytoplasmic RNA-interacting

protein/hnRNP-Q (1.6-fold, p=0.10) also trended upwards. A protein of the nuclear envelope, transmembrane protein 43 (TMEM43) was increased by 1.5-fold (p=0.021).

Ribosomes, also known as 80S ribosomes, consist of two subunits, a small 40S subunit and a large 60S subunit. Here we report an increase in the ribosomal proteins, as seen in 5 small subunit proteins and 3 large subunit proteins; the small and large subunit proteins were elevated within the range of 1.5~2.1-fold and 1.7~1.8-fold respectively. The 60S acidic ribosomal protein P2 is an acidic ribosomal P protein and here trended towards elevation (1.5-fold, p=0.065). Elongation factor-1 alpha, was also elevated (1.2-fold, p=0.014): it is an isoform of the alpha subunit of the elongation factor-1 complex, which is responsible for the enzymatic delivery of aminoacyl-tRNAs to the ribosome. The eukaryotic initiation factor-4A (eIF4A) family consists of 3 closely-related isoforms and these factors are required for the binding of mRNA to 40S ribosomal subunits. We observed a 1.3-fold increase (p=0.034) in translation initiation factor 4A (EIF4A2). Although all measured proteasomal proteins were unchanged, the ubiquitin-specific peptidase 5 (USP5) trended upwards (1.5-fold, p=0.069). Two proteases active both in lysosomes and in the extracellular matrix, cathepsin B (cath-B) (2.6-fold, p=0.018) and cathepsin D (cath-D) (2.8-fold, p=0.0073), were strongly upregulated. Apart from these proteases, few protease inhibitors in the Serine Protease Inhibitor (Serpin) family were also affected by HCD: the levels of serpin peptidase inhibitor, clade C, member 1 (SERPINC1)/Antithrombin III (2.0-fold, p=0.0030), serpinA9 (1.8, p=0.030), and serpinA3N (1.5, p=0.058) were all increased in HCD compared to controls (**Table 2-6**).

Table 2-4: Summary statistics of the effect of HCD on apolipoproteins and blood-related proteins

		Ctrl		HCD		N		
Protein name	NCBI accession	average	95% CI	HCD	95% CI	Ctrl	HCD	p-value
Apolipoprotein								
Apolipoprotein E	gi|225946	1	0.62-1.61	7.80	3.63-16.78	5	5	0.0005
PREDICTED: Apolipoprotein B	gi|291387156	1	0.74-1.35	4.50	1.84-10.91	5	5	0.0071
Blood related proteins								
PREDICTED: Histidine-rich glycoprotein (HRGP)	gi|291400273	1	0.83-1.2	3.33	1.88-5.87	5	5	0.0030
Fetuin-A	gi|12644357	1	0.76-1.31	1.79	1.13-2.83	5	5	0.0210
PREDICTED: Complement component C4a	gi|291395827	1	0.89-1.13	2.93	1.62-5.31	5	5	0.0064
Complement component C9 precursor	gi|126723572	1	0.68-1.48	2.59	1-6.75	5	5	0.0478
Vitamin D-binding protein	gi|126723668	1	0.8-1.25	2.20	1.75-2.77	5	5	0.0001
Albumin	gi|407943895	1	0.74-1.35	1.73	0.86-3.46	5	5	0.0969
Serotransferrin (TF)	gi|156119356	1	0.84-1.19	2.18	1.01-4.71	5	5	0.0457
PREDICTED: Transthyretin (TTR)	gi|136466	1	0.82-1.22	1.95	1.32-2.92	5	5	0.0059
Immunoglobulin gamma1 constant region	gi|291415360	1	0.86-1.17	3.15	1.96-5.05	5	5	0.0016
PREDICTED: Haemoglobin	gi|218456301	1	0.24-4.1	0.3	0.21-0.42	5	5	0.0766

Table 2-5: Summary statistics of the effect of HCD on histones and heterogeneous nuclear ribonucleoproteins

		Ctrl		HCD		N		
Protein name	NCBI accession	average	95% CI	HCD	95% CI	Ctrl	HCD	p-value
PREDICTED: GK13546-like/H4	gi|291400879	1	0.68-1.47	1.56	1.24-1.96	5	5	0.0302
PREDICTED: Histone cluster 1, H2ag-like	gi|291410763	1	0.74-1.35	1.44	1.18-1.77	5	5	0.0260
PREDICTED: Histone cluster 1, H2ac-like	gi|291395657	1	0.71-1.4	1.41	1.18-1.67	5	5	0.0471
PREDICTED: Nucleosome assembly protein 1-like 4	gi|291415556	1	0.7-1.42	2.24	1.09-4.62	5	5	0.0327
hnRNP-E1	gi|12230408	1	0.67-1.49	1.74	1.31-2.32	5	5	0.0154
hnRNP-K	gi|2644968	1	0.8-1.25	1.42	1-2.02	5	5	0.0541
PREDICTED: Synaptotagmin binding, cytoplasmic RNA interacting protein (hnRNP-Q)	gi|291396562	1	0.78-1.28	1.59	0.88-2.86	5	5	0.0959
PREDICTED: Transmembrane protein 43 (TMEM43)	gi|291393466	1	0.74-1.36	1.47	1.33-1.64	5	5	0.0210

Table 2-6: Summary statistics of the effect of HCD on protein synthesis and degradation

		Ctrl		HCD		N		
Protein name	NCBI accession	average	95% CI	HCD	95% CI	Ctrl	HCD	p-value
Ribosomal proteins and protein biosynthesis								
PREDICTED: Ribosomal protein S23-like	gi|291388092	1	0.58-1.73	2.1	1.64-2.69	5	5	0.0160
PREDICTED: Ribosomal protein S16-like	gi|291399079	1	0.74-1.35	1.79	1.11-2.92	5	5	0.0253
PREDICTED: Ribosomal protein S10-like (60S L10)	gi|291408682	1	0.69-1.46	1.76	1.02-3.06	5	5	0.0492
PREDICTED: Ribosomal protein S3-like	gi|291389681	1	0.81-1.24	1.67	1.32-2.1	5	5	0.0019
PREDICTED: Ribosomal protein S7-like	gi|291409903	1	0.69-1.46	1.45	0.97-2.15	5	5	0.0983
PREDICTED: Ribosomal protein 10-like (Rps10)	gi|291396063	1	0.76-1.31	1.48	1.19-1.83	5	5	0.0146
PREDICTED: Ribosomal protein L15-like	gi|291399716	1	0.68-1.47	1.7	1.62-1.78	5	5	0.0185
Ribosomal protein L4-like	gi|307775447	1	0.53-1.88	1.8	1.27-2.56	5	5	0.0617
RecName: 60S acidic ribosomal protein P2	gi|133062	1	0.71-1.41	1.49	1.01-2.19	5	5	0.0646
Elongation factor 1 alpha	gi|126723647	1	0.88-1.14	1.2	1.12-1.28	5	5	0.0135
PREDICTED: Initiation factor 4AII (eIF4A)	gi|227239	1	0.85-1.17	1.26	1.04-1.52	5	5	0.0336
PREDICTED: Ubiquitin specific peptidase 5	gi|291392775	1	0.67-1.49	1.51	1.04-2.19	5	5	0.0686
Proteases								
Cathepsin D	gi|291416142	1	0.68-1.47	2.84	1.48-5.42	5	5	0.0073
PREDICTED: Cathepsin B	gi|291385792	1	0.63-1.6	2.58	1.27-5.26	5	5	0.0178
Protease inhibitors								
PREDICTED: SERPINC1/antithrombin III	gi|291397262	1	0.81-1.23	2.04	1.41-2.94	5	5	0.0030
SerpinA9	gi|1008928	1	0.92-1.09	1.82	1.1-3.03	5	5	0.0296
PREDICTED: Serpin A3N	gi|291413837	1	0.66-1.52	1.52	1.11-2.09	5	5	0.0577

Numerous HSPs and chaperones were found to be elevated in the HCD group, the one exception being cyclophilin 18. All endoplasmic reticulum (ER) proteins in this category associated with protein production were strongly elevated (by 1.3~1.7-fold). These included: calreticulin (1.7-fold, p=0.011); heat shock 70kDa protein 5 (HspA5) (1.6-fold, p=0.064); heat shock protein 47 (Hsp47) (1.5-fold, p=0.029); heat shock protein 90kDa beta, member 1 (Hsp90B1) (1.3-fold, p=0.087); and protein disulfide-isomerase (1.4-fold, p=0.0038). All of these act as ER chaperones. Apart from the ER Hsp90B1, cytoplasmic Hsp90 proteins were also elevated. Hsp90AB1 was strongly elevated (1.5, p=0.0037) and Hsp90A slightly elevated (1.2, p=0.0098). The Hsp70 family contains both heat-inducible and constitutively expressed members, the latter being known as heat-shock cognate (Hsc) proteins. The heat shock 70kDa protein 8, also known as Hsc70, belongs to the Hsc subgroup. Our result showed that the increase in Hsc70 (1.1-fold, p=0.023) is not as marked as that of HspA5, albeit at a higher significance level. Chaperonin, also known as the Hsp60 protein, trended towards increase (1.4-fold, p=0.084), and cytoplasmic chaperonin-containing Tcp1 (CCT) was also elevated (1.3-fold, p=0.030). Cyclophilin A was the only protein in this category that trended towards down-regulation (0.7-fold, p=0.09) (**Table 2-7**).

Several proteins involved in the pathway from ER to Golgi transport system and beyond were strongly elevated, including Rab1a (2.0-fold, p=0.0062); Rab11a (1.7, p=0.046); B-cell receptor-associated protein 31 (BCAP31; 1.6-fold, p=0.020); clathrin heavy-chain 1 (CLTC; 1.4-fold, p=0.024); and transmembrane emp24 domain-containing protein 10 precursor (1.7-fold, p=0.023). As a group, the elevation of this cluster of proteins was highly significant. Other proteins involved primarily in ER-Golgi transport were also moderately elevated: atlastin-3 (1.3-fold, p=0.055); ADP-ribosylation factor (1.3-fold, p=0.0098); and valosin-containing protein (1.2-fold, p=0.063). Proteins known to be involved in ER stress, namely niban (1.2-fold, p=0.087) and calnexin (1.4-fold, p=0.011) were also elevated (**Table 2-8**).

Table 2-7: Summary statistics of the effect of HCD on chaperones

		Ctrl		HCD		N		
Protein name	NCBI accession	average	95% CI	HCD	95% CI	Ctrl	HCD	p-value
Located in ER								
Calreticulin precursor	gi|117504	1	0.86-1.17	1.71	1.19-2.46	5	5	0.0112
PREDICTED: Heat shock 70kDa protein 5	gi|291408341	1	0.62-1.61	1.63	1.07-2.49	5	5	0.0643
PREDICTED: Heat shock protein 47	gi|291384245	1	0.79-1.27	1.51	1.07-2.14	5	5	0.0289
Protein disulfide-isomerase	gi|283549170	1	0.86-1.17	1.42	1.18-1.7	5	5	0.0038
Located in Cytoplasm/nucleus								
PREDICTED: Heat shock 90kDa protein 1, beta (Hsp90AB1)	gi|291396282	1	0.82-1.22	1.54	1.24-1.93	5	5	0.0037
PREDICTED: Heat shock 90kDa protein 1, beta (Hsp90A)	gi|291410975	1	0.91-1.1	1.16	1.07-1.26	5	5	0.0098
PREDICTED: Heat shock 70kDa protein 8	gi|291383777	1	0.95-1.05	1.08	1.02-1.15	5	5	0.0231
PREDICTED: Chaperonin	gi|291391974	1	0.72-1.38	1.39	0.99-1.95	5	5	0.0844
Chaperonin-containing T-complex polypeptide beta subunit	gi|209981451	1	0.87-1.15	1.3	1.05-1.63	5	5	0.0269
Cyclophilin A	gi|6651171	1	0.82-1.22	0.71	0.49-1.04	5	5	0.0675

Table 2-8: Summary statistics of the effect of HCD on ER proteins

		Ctrl		HCD		N		
Protein name	NCBI accession	average	95% CI	HCD	95% CI	Ctrl	HCD	p-value
ER_Golgi transport								
PREDICTED: Rab1A	gi|291386694	1	0.69-1.46	1.97	1.4-2.75	5	5	0.0062
PREDICTED: Rab11A	gi|291411545	1	0.6-1.66	1.7	1.21-2.38	5	5	0.0457
PREDICTED: B-cell receptor-associated protein 31	gi|291412844	1	0.76-1.32	1.55	1.13-2.11	5	5	0.0195
PREDICTED: Clathrin heavy chain 1	gi|291405680	1	0.79-1.27	1.43	1.1-1.85	5	5	0.0238
Transmembrane emp24 domain-containing protein 10 precursor	gi|127140999	1	0.8-1.25	1.69	1.1-2.58	5	5	0.0229
PREDICTED: Atlastin 3	gi|291409484	1	0.79-1.26	1.28	1.04-1.58	5	5	0.0552
PREDICTED: ADP-ribosylation factor	gi|291389073	1	0.9-1.11	1.26	1.08-1.46	5	5	0.0098
PREDICTED: Valosin-containing protein	gi|291383033	1	0.9-1.12	1.15	1-1.33	5	5	0.0629
ER stress								
PREDICTED: Niban protein	gi|291412446	1	0.83-1.2	1.17	1.03-1.34	5	5	0.0870
PREDICTED: Calnexin	gi|291410136	1	0.84-1.19	1.41	1.12-1.77	5	5	0.0113

Many glycolytic enzymes were elevated in the HCD group compared to the control group (**Table 2-9**). Lactate dehydrogenase-A chain (LDH-A) was strongly elevated (1.5-fold, p=0.0061) and LDH (B chain) also trending towards elevation (1.2-fold, p=0.062). Other glycolytic enzymes showing significant or near-significant between-group differences included pyruvate kinase (1.3-fold, p=0.059), enolase (1.2-fold, p=0.052), phosphoglycerate mutase (1.4-fold, p=0.031), phosphoglycerate kinase (1.2-fold, p=0.036), and triose-phosphate isomerase (1.1-fold, p=0.088).

Among the TCA cycle enzymes, oxoglutarate dehydrogenase (1.4-fold, p=0.014) and mitochondrial malate dehydrogenase (1.4-fold, p=0.074) were both up-regulated. These two enzymes are involved in the malate-aspartate shuttle, which also involves cytosolic malate dehydrogenase (1.1-fold, p=0.076). Mitochondrial ATP synthase is composed of multiple F1 and F0 subunits. The mitochondrial ATP synthase beta subunit belongs to the F1 family and is the only one which demonstrated a trend towards change (1.1-fold, p=0.076). Two nucleoside/nucleotide kinases were also present at higher levels: adenylate kinase 3 (AK3), from the mitochondrial matrix (1.2-fold, p=0.094), and nucleoside diphosphate kinase B (NDK B) (1.5-fold, p=0.0071).

Some proteins involved in maintaining actin filaments were decreased, including: destrin (to 0.7-fold p=0.025); transgelin (0.7, p=0.0035); and filamin-A (0.9, p=0.082). On the other hand, actin-bundling protein plastin-3 isoforms were increased: plastin 3 L-isoform (4.7-fold, p=0.0011), and X2-isoform (1.5-fold, p=0.040). Two members of the Arp 2/3 complex were also up-regulated: Arp3 (1.3-fold, p=0.025), and Arp 2/3 complex subunit 2 (Arpc2) (1.3-fold, p=0.049) in HCD-treated compared with control tissue (**Table 2-10**).

Intermediate filament protein desmin (1.6-fold, p=0.064) and actin-binding protein moesin (1.2-fold, p=0.058) both trended towards increase in the HCD group. Proteins playing important functions in cytoskeletal structure, including rhea-like protein (0.9-fold, p=0.021), smoothelin (0.8-fold, p=0.0049), and smooth muscle caldesmon (0.8-fold, p=0.049) were all significantly down-regulated. Smooth-muscle myosin components, myosin heavy chain (MHC11) and myosin light chain 6 (MYL6) both trended downwards, respectively by (0.9-fold, p=0.063) and (0.9-fold, p=0.078). Another important contractile protein, tropomyosin alpha-1 (TPM1), also trended towards down-regulation (0.9-fold), although only its B-chain was detected (**Table 2-10**).

Two of the four S100 calcium-binding proteins, S100-A4 (1.4-fold, p=0.048) and S100-A6 (1.3-fold, p=0.014), were elevated. CREC proteins, constituting a family of EF-hand calcium binding proteins localised to the secretory pathway, calumenin (1.2-fold, p=0.012) and the ER protein, reticulocalbin 3 (1.7-fold, p=0.053), were also elevated (**Table 2-11**).

A number of intra- and extracellular enzymes related to reactive species metabolism were not identified in this study. We did however detect a trend towards elevated levels of monoamine oxidase B (MAOB) (1.4-fold, p=0.051) and extracellular superoxide dismutase (SOD3) (1.6-fold, p=0.082). Obg-like ATPase 1 (OLA1; 1.6-fold, p=0.060) trended towards up-regulation and is also involved in oxidative stress regulation (**Table 2-11**). Cytochrome b5 was also increased in the HCD group.

Proteins involved in cell matrix adhesion were also elevated (**Table 2-12**), including fibronectin 1 (2.1-fold, p=0.018) and dystroglycan (2.0-fold, p=0.081). The ECM protein, transforming growth factor-beta-induced protein 1 (TGFB1) (1.6-fold, p=0.0065) was also increased, whereas another vascular ECM protein, osteoglycin (0.8-fold, p=0.072) was decreased.

Perhaps the most strikingly-elevated protein in this study was the glycoprotein (transmembrane) nmb-like (Gpnmb), which was increased by 15.4-fold (p=0.0003). Galecin-3 was increased by > 2-fold (p=0.0024), and both annexin 5 and annexin A3 were elevated over 1.3-fold (**Table 2-12**).

Other miscellaneous proteins that displayed significant or near-significant trends included the following: ras-related protein Rap-1A (1.2-fold, p=0.047); 14-3-3 protein eta (tyrosine 3-monooxygenase/tryptophan 5-monooxygenase activation protein; 1.1-fold, p=0.072); SH3P2-like (1.3-fold, p=0.061); cytoplasmic dynein 1 heavy chain 1 (1.3-fold, p=0.077); dihydropyrimidinase-like 2-like (1.4-fold, p=0.065); EF-hand domain family, member D1 (1.3-fold, p=0.056); and ras suppressor protein 1 (RSU1; 0.9-fold, p=0.077) (**Table 2-12**).

Table 2-9: Summary statistics of the effect of HCD on metabolic enzymes

		Ctrl		HCD		N		
Protein name	NCBI accession	average	95% CI	HCD	95% CI	Ctrl	HCD	p-value
Glycolytic enzymes								
Lactate dehydrogenase (A chain)	gi|126050	1	0.92-1.08	1.51	1.19-1.91	5	5	0.0061
Lactate dehydrogenase (B chain)	gi|307611949	1	0.85-1.17	1.21	1.01-1.46	5	5	0.0617
Pyruvate kinase	gi|307548868	1	0.92-1.09	1.3	0.98-1.71	5	5	0.0585
PREDICTED: Enolase 1-like	gi|291399590	1	0.88-1.14	1.17	1.01-1.36	5	5	0.0523
PREDICTED: Phosphoglycerate mutase 1-like	gi|291404565	1	0.74-1.35	1.44	1.13-1.83	5	5	0.0310
PREDICTED: Phosphoglycerate kinase 1	gi|291384724	1	0.86-1.16	1.21	1.04-1.41	5	5	0.0364
PREDICTED: Triosephosphate isomerase	gi|136066	1	0.89-1.12	1.13	0.99-1.29	5	5	0.0876
TCA cycle enzymes								
PREDICTED: Oxoglutarate dehydrogenase	gi|291394911	1	0.84-1.19	1.39	1.11-1.74	5	5	0.0136
PREDICTED: Cytosolic malate dehydrogenase	gi|291386712	1	0.94-1.06	1.11	0.98-1.26	5	5	0.0757
PREDICTED: Mitochondrial malate dehydrogenase	gi|291390903	1	0.83-1.2	1.4	0.95-2.05	5	5	0.0743
PREDICTED: Mitochondrial ATP synthase beta subunit	gi|291389459	1	0.88-1.14	1.13	1.02-1.26	5	5	0.0757
Adenylate kinase 3	gi|15778674	1	0.79-1.26	1.23	1.02-1.48	5	5	0.0943
PREDICTED: ATP synthase, H+ transporting, mitochondrial F1 complex, gamma subunit [*Oryctolagus cuniculus*]	gi|291401980	1	0.74-1.34	1.48	1.33-1.65	5	5	0.0182
Nucleoside diphosphate kinase B	gi|291405780	1	0.88-1.14	1.48	1.16-1.88	5	5	0.0071

Table 2-10: Summary statistics of the effect of HCD on contractile and cytoskeleton proteins

		Ctrl		HCD		N		
Protein name	NCBI accession	average	95% CI	HCD	95% CI	Ctrl	HCD	p-value
Cytoskeleton								
PREDICTED: Destrin	gi|291388996	1	0.86-1.17	0.73	0.56-0.95	5	5	0.0247
PREDICTED: Transgelin	gi|291383827	1	0.88-1.14	0.74	0.64-0.86	5	5	0.0035
Filamin-A (FLNa)	gi|217418270	1	0.96-1.04	0.93	0.85-1.01	5	5	0.0818
PREDICTED: Plastin 3 (L-isoform)	gi|291392980	1	0.57-1.77	4.68	2.47-8.85	5	5	0.0011
PREDICTED: Plastin 3 isoform X2 (T-plastin)	gi|291407827	1	0.73-1.37	1.45	1.09-1.93	5	5	0.0396
PREDICTED: Actin related protein 3 (ARP3)	gi|291391454	1	0.85-1.18	1.32	1.06-1.64	5	5	0.0254
PREDICTED: Actin related protein 2/3 complex subunit 2 (Arpc2)	gi|291392221	1	0.84-1.19	1.29	1.01-1.64	5	5	0.0491
Desmin	gi|284005349	1	0.72-1.39	1.56	0.99-2.47	5	5	0.0639
PREDICTED: Moesin	gi|291407599	1	0.92-1.09	1.17	0.99-1.38	5	5	0.0583
PREDICTED: Rhea-like (highly similar to talin)	gi|291383009	1	0.93-1.08	0.9	0.89-0.92	5	5	0.0209
PREDICTED: Smoothelin	gi|291406858	1	0.94-1.06	0.84	0.76-0.93	5	5	0.0049
Contractile proteins								
Smooth muscle caldesmon protein (h-CaD)	gi|16226131	1	0.9-1.11	0.82	0.68-1	5	5	0.0485
Myosin heavy chain 11 (MHC11)	gi|165490	1	0.93-1.08	0.9	0.81-1	5	5	0.0628
PREDICTED: Myosin, light chain 6 (MYL6)	gi|291389425	1	0.92-1.09	0.9	0.81-1.01	5	5	0.0778
PREDICTED: Tropomyosin alpha-1, Chain B	gi|230768	1	0.96-1.05	0.94	0.87-1.02	5	5	0.0979

Table 2-11: Summary statistics of the effect of HCD on calcium-binding proteins and proteins participating in oxidative stress

		Ctrl		HCD		N		
Protein name	NCBI accession	average	95% CI	HCD	95% CI	Ctrl	HCD	p-value
Calcium-related								
PREDICTED: S100-A4	gi|291397940	1	0.92-1.09	1.44	1-2.09	5	5	0.0484
Protein S100-A6	gi|1173337	1	0.87-1.15	1.29	1.09-1.53	5	5	0.0136
Cardiac calumenin	gi|130492398	1	0.92-1.08	1.22	1.06-1.4	5	5	0.0121
PREDICTED: Reticulocalbin 3	gi|291415444	1	0.86-1.16	1.69	0.98-2.92	5	5	0.0527
Oxidative stress								
PREDICTED: Monoamine oxidase B-like (MAOB)	gi|291407377	1	0.78-1.28	1.44	1.01-2.05	5	5	0.0506
Extracellular superoxide dismutase (SOD3)	gi|3250881	1	0.59-1.69	1.59	1.11-2.29	5	5	0.0818
PREDICTED: Obg-like ATPase 1	gi|291391759	1	0.63-1.6	1.56	1.18-2.08	5	5	0.0602
Cytochrome b5	gi|117811	1	0.91-1.09	1.19	1.05-1.35	5	5	0.0166

Table 2-12: Summary statistics of the effect of HCD on proteins with various functions

		Ctrl		HCD		N		
Protein name	NCBI accession	average	95% CI	HCD	95% CI	Ctrl	HCD	p-value
Adhesion/ECM/cell proliferation								
PREDICTED: Fibronectin 1	gi|291392188	1	0.7-1.42	2.14	1.2-3.82	5	5	0.0181
Dystroglycan	gi|1546	1	0.44-2.29	2.02	1.26-3.25	5	4	0.0808
ECM and related								
PREDICTED: Transforming growth factor, beta-induced, 68kDa (TGFB1)	gi|291387372	1	0.89-1.13	1.56	1.2-2.04	5	5	0.0065
Osteoglycin	gi|75073382	1	0.85-1.18	0.81	0.64-1.02	5	5	0.0722
PREDICTED: Ras suppressor protein 1 (RSU1)	gi|291402256	1	0.87-1.15	0.87	0.75-1	5	5	0.0767
Miscellaneous								
PREDICTED: Glycoprotein (transmembrane) nmb-like	gi|291394533	1	0.39-2.56	15.43	6.62-35.87	5	5	0.0003
Galectin-3	gi|606795	1	0.87-1.16	2.24	1.54-3.25	5	5	0.0024
PREDICTED: Annexin 5	gi|291401824	1	0.85-1.17	1.39	1.29-1.49	5	5	0.0023
PREDICTED: Annexin A3	gi|291401561	1	0.75-1.34	1.33	1-1.78	5	5	0.0899
PREDICTED: Ras-related protein Rap-1A	gi|291398271	1	0.88-1.14	1.19	1.01-1.41	5	5	0.0466
PREDICTED: 14-3-3 protein eta (tyrosine 3-monooxygenase/tryptophan 5-monooxygenase activation protein)	gi|284004958	1	0.9-1.11	1.12	1-1.26	5	5	0.0717
PREDICTED: SH3P2-like	gi|291383396	1	0.77-1.3	1.33	1.04-1.71	5	5	0.0612
PREDICTED: Cytoplasmic dynein 1 heavy chain 1	gi|291410977	1	0.9-1.12	1.31	0.95-1.8	5	5	0.0765
PREDICTED: Dihydropyrimidinase-like 2-like	gi|291385863	1	0.74-1.36	1.39	1.02-1.9	5	5	0.0654
PREDICTED: EF-hand domain family, member D1	gi|291410402	1	0.88-1.14	1.27	0.99-1.64	5	5	0.0555

2.3.3. Histology

Three sections from each staining run were examined per individual, with very similar results. The most prominent histological feature evident in H&E-stained - tissues was that intimal thickening was present in the ascending aorta from all five HCD specimens examined, but in none of the five control specimens (Figure 2-3). The HCD aortic samples were also more fragile than samples obtained from the control group, and tended to break during handling. Congo red staining did not show any notable difference between the treatment groups and did not produce any evidence for amyloid deposition in the artery in this model of atherosclerosis.

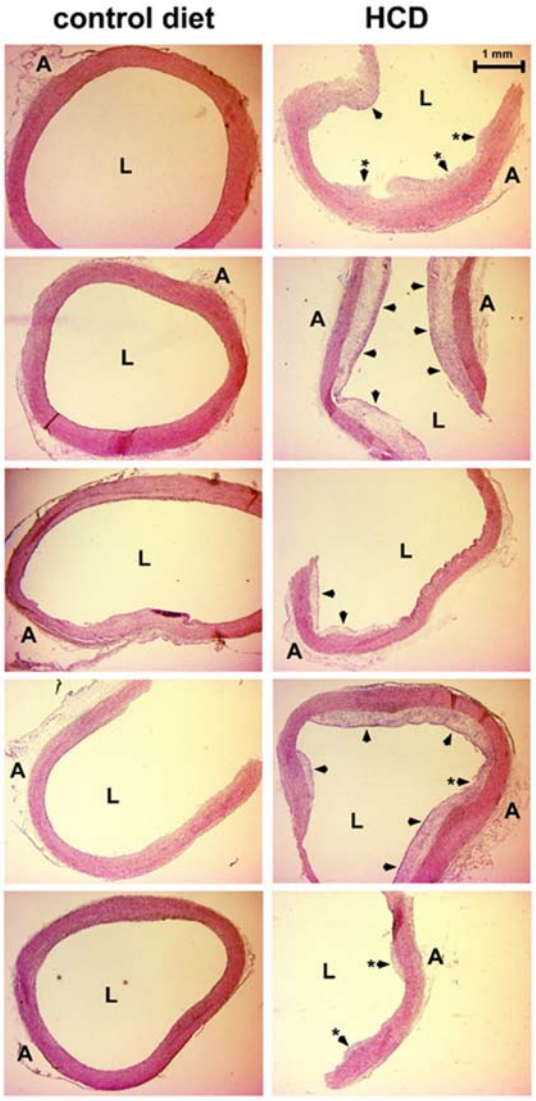

Figure 2-3 H&E staining of ascending aorta from NZW rabbits which received a control diet or HCD.

Ascending aortas from five individuals per group at 2.5 x magnification. The images shown are representative of three separate slides examined for each individual. Abbreviations: A, Adventitia; L, vessel lumen. Arrows indicate regions with distinct intimal thickening and asterisks highlight areas with damaged thickened intima, which may have broken during processing of the samples.

2.3.4. Western blots and Immunohistochemistry

Western blots and immunohistochemistry showed nonspecific antibody reactivity towards tested samples and therefore, validation of iTRAQ results was not achieved with these methods.

2.3.5. MRM results

MRM was performed to validate the finding of the iTRAQ study by measuring selected proteins, including the representative up-regulated proteins apolipoprotein E, cathepsin D, Gpnmb, palstin 3 and fibronectin 1, and the down-regulated protein transgelin.

Table 2-13: MRM analysis by peak areas

Proteins	iTRAQ result (HCD Vs Ctrl)	HCD areas Vs Ctrl areas	p-value
Fibronectin 1	2.14 (p=0.0181)	2.60	0.0002
Transgelin	0.74 (p=0.0035)	0.78	< 0.0001

Fibronectin 1 was elevated 2.6-fold and the significance of the increase (p-value) derived from the MRM analysis was comparable to the 2.1-fold increase detected by iTRAQ. Transgelin was decreased to 0.7-fold (p< 0.0001) in the HCD group compared to the control group (**Table 2-13**), which is also consistent with the observation from the preceding iTRAQ study, where transgelin was also down-regulated (0.7-fold, p=0.0035).

Table 2-14: MRM analysis by peak height vs noise ratio

Proteins	iTRAQ result (HCD Vs Ctrl)	HCD peak height Vs noise	Ctrl peak height Vs noise	HCD Vs Ctrl	p-value
Apo-E	7.80 (p=0.0005)	20.56±12.80	1:1 (at noise level)	n/a	0.019
Cathepsin D	2.84 (p=0.0073)	37.63±22.98	1:1 (at noise level)	n/a	0.071
Gpnmb	15.43 (p=0.0003)	35.69±19.88	1:1 (at noise level)	n/a	0.018
Plastin 3	4.68 (p=0.0011)	14.57±12.08	1:1 (at noise level)	n/a	0.066
Fibronectin 1	2.14 (p=0.0181)	62.6±30.19	30.64±13.00	2.04	0.077
Transgelin	0.74 (p=0.0035)	130.07±33.07	193.65±42.72	0.67	0.048

For apolipoprotein E, cathepsin D, Gpnmb, and palstin 3, the analyte peak in the control samples were at the noise level and therefore, peak height vs noise ratio was used for interpretation of the results. The HCD group showed significantly higher protein levels of apolipoprotein E and Gpnmb compared to the controls; in the HCD group, peak-to-noise ratio was 20.6 (p=0.019) and 35.7 (p=0.018) for apolipoprotein E and Gpnmb respectively, while in the control group, peak-to-noise ratio was 1 for both proteins. Consistent with the iTRAQ result showing elevations in cathepsin D and plastin 3, MRM results showed peak-to-noise ratios of 37.6 (p=0.071) and 14.6 (p= 0.066) for cathepsin D and plastin 3 respectively in the HCD group compared to 1 for both proteins in the control group (**Table 2-14**).

Changes in the level of fibronectin 1 and transgelin in response to HCD were calculated using the more robust method employing analyte peak areas for analysis. Nevertheless, changes were recalculated

with the peak-to-noise ratio to compare results from the two methods. The peak height-to-noise approach produced similar results as did the peak area approach, albeit with decreased statistical power.

2.4. Discussion

The prominent thickening in the intimal region of the arterial wall observed for all five HCD-treated subjects is consistent with intimal thickening/hyperplasia, the precursor lesion of atherosclerosis [59]. This finding provides substantive evidence that the HCD-treated animals in this study were progressing towards overt atherosclerosis in response to the dramatically elevated blood cholesterol levels seen for this group.

Many of the specific changes in proteins identified in the iTRAQ study were consistent with current understanding of the atherosclerotic process. The dramatic increase in apolipoproteins B and E in the HCD group was expected, given the accepted role of these proteins in cholesterol clearance [60,61]. Furthermore, HCD appeared to specifically affect lipoproteins that promote atherosclerosis [62], including low-density lipoprotein (LDL), very-low-density lipoprotein (VLDL), and intermediate-density lipoprotein (IDL), whereas, lipoproteins that regulate chylomicrons and HDL were not altered/detected.

HCD in the rabbit not only leads to atherosclerosis but has also been used to model AD [12]. The 2-fold elevation of the plasma protein transthyretin in aortic tissue may be relevant to both atherosclerosis and AD. The dissociation of transthyretin homotetramer into monomers with internal tertiary structural changes [63], reportedly acts as a rate-limiting step in amyloid fibril formation [64]. Transthyretin also cleaves apolipoprotein A-I, leading to reduced ability to promote cholesterol efflux and increased amyloidogenic potential [65]; and it has previously been associated with senile systemic amyloidosis [66], familial amyloid polyneuropathy [67], and familial amyloid cardiomyopathy [68].

2.4.1. Immune response

Atherosclerotic lesions are characterised by activation of both the innate and the adaptive immune response [53]. The complement system is part of the innate immune system and assists in the ability of antibodies and phagocytic cells to clear pathogens from an organism. On the other hand, complement activation is also necessary for removal of immune complexes, debris and apoptotic cells and has therefore been suggested to exert dual proatherogenic and atheroprotective effects within the vessel wall [69]. The complement system consists of nine major complement proteins (C1 through C9) which normally circulate in the bloodstream as inactive precursors. In the current study, we observed 2.9- and 2.6-fold increases in the complement components C4a and C9 precursor in HCD-treated aortic tissue, respectively. Complement component C4a is an anaphylatoxin, which can mediate chemotaxis, inflammation, and generation of cytotoxic oxygen radicals [70]. Complement component C9 is a component of the membrane attack complex and forms pores in the plasma membrane of target cells

[71]. Activation of the complement system is a major aspect of many chronic inflammatory diseases and has been suggested to be involved in the pathogenesis of atherosclerosis, which is a classical inflammatory disease [69].

Other proteins that are involved in the immune response were also up-regulated in the HCD treated group. HRGP, increased 3.3-fold, is an alpha-glycoprotein present in human plasma which is also present in monocytes and macrophages, and which has been reported to modulate the immune, vascular and coagulation systems [72]. HRGP has been shown to neutralise the anticoagulant activity of heparin. Furthermore, it has also been reported to specifically inhibit the anti-proliferative effect of heparin on arterial smooth muscle cells. The multicellular inflammatory response to endothelial injury is partially characterised by the influx of platelets and macrophages, and it has been suggested to under the influence of HRGP release into the arterial microenvironment which may allow smooth muscle cell proliferation and atherogenesis by inhibiting the action of endothelial cell-derived heparinoid substances [73].

Fetuin-A, elevated 1.8-fold, is a glycoprotein present in the serum which acts as a potent inhibitor of pathological calcification by forming soluble complexes with calcium and phosphate, which prevents their precipitation [74,75]. In both patients and animal models, it was reported that fetuin-A has an anti-inflammatory property although more recently, evidence showed that fetuin-A promotes inflammatory cytokines and that a major mediator of inflammatory cytokine action, NF-kB, upregulates hepatic fetuin-A synthesis [76].

Vitamin D-binding protein (VDBP), elevated 2.2-fold, is also involved in modulation of immune and inflammatory responses [77,78]. At the site of endothelial injury, release of VDBP confers chemotactic function as well as inducing proliferation of vascular smooth muscle cells [79]. Elevated VDBP level has been detected in the serum and fresh thrombotic plaques of patients with myocardial infarction [80], and in the plasma of patients with acute coronary syndromes [81].

Albumin also trended upwards (1.7 fold) in the HCD group. Lower levels of serum albumin have been associated with increased risk of coronary disease [82] and cardiovascular mortality [83]. Serum albumin has been suggest to limit atherogenesis through its anti-oxidative properties, and low albumin levels may reflect activation of pro-inflammatory cytokines and ongoing subclinical inflammation [84]. Haemoglobin was the only blood-related protein that showed a trend towards decrease (0.3-fold, $p=0.077$) in the HCD group. This is consistent with previously reported phenomena of hypercholesterolaemia-associated decrease in haemoglobin levels in rabbits on a high fat diet, possibly due to increased osmotic fragility of the red blood cells [85].

Overall, this study clearly demonstrated findings consistent with activation of the immune response in line with current understanding of atherosclerosis.

2.4.2. Oxidative stress

There is general consensus that the initiation and progression of atherosclerosis is heavily influenced by oxidative processes affecting primarily lipids, such as those contained in LDL particles. This in turn induces oxidative stress generated by cells such as macrophages, which are thought to bring about necrosis of the foam cells in the arterial wall. Proteins implicated in oxidative defence responses were also significantly elevated in this study.

Here, transferrin was increased by 2.2 fold. Transferrin functions as an iron-binding blood-plasma glycoprotein whose primary role is transporting iron through the body and delivering it to the cells that utilise it. Increased transferrin expression has been associated with a rise in antioxidant activity which may act as a defence reaction towards hypercholesterolaemia in the rabbit [86]. Furthermore, antioxidative system ceruloplasmin-transferrin activity and the severity of pathological lesions were found to correlate in both experimental (rabbit) and clinical atherosclerosis; antioxidative system activity was higher in the mild disease state while in the severe disease course, antioxidative system activity was threefold lower [87]. It has been proposed that transferrin, by binding of iron, exerts a protective role by preventing oxidative stress and associated lipid peroxidation which has a direct role in atherosclerosis [88].

MAO-B (1.4-fold trend) is an intracellular H_2O_2-generating enzyme present on the outside of mitochondria. SOD3 (1.6-fold trend) converts extracellular superoxide anion ($O_2^{-\cdot}$) to H_2O_2. An increase in these proteins is suggestive of increased generation of H_2O_2. Interestingly, while it is known that $O_2^{-\cdot}$ is generated by the entire vessel wall, including cells in both the ECM and smooth-muscle in atherosclerosis [89], H_2O_2 has been suggested to play a bigger part in atherogenesis than $O_2^{-\cdot}$[90]. OLA1 (1.6-fold trend) not only regulates the oxidative stress response [91], but also stabilises HSP70 and increases cell survival during heat shock stress [92]. Cytb5 is a membrane-bound protein which functions as an electron carrier for several membrane-bound oxygenases [93] and is also known to modulate the catalytic activity of its redox partner, cytochrome P450 (cytP450) [94]. Therefore, dysregulation of this protein could affect cytP450-associated oxidative stress.

2.4.3. Protein production and turnover

Histones are proteins found in cell nuclei that package and order the DNA into structural units called nucleosomes. In this study, core histones as well as the nucleosome assembly protein NAP1L4 were increased in the HCD group. NAP1L4 can shuttle between the cytoplasm and nucleus, and has been suggested to act as a histone chaperone [95]. Increased levels of TMEM43, a protein that maintains nuclear-envelope structure, and mRNA processing hnRNPs were also seen the HCD group. Previously, it was shown that mRNA-processing activity of endothelial cell was increased in arterial regions susceptible to atherosclerosis [96]. The hnRNP-E1 has been shown to stabilise the mRNA of endothelial nitric oxide synthase, which plays a pivotal role in the maintenance of homeostasis in the blood vessel

wall [97]. Our findings are also consistent with the previously reported up-regulation of the hnRNP-K in the smooth muscle cells of HCD-fed rabbits [98]. A significant increase in the expression of hnRNP-E1 and -K was found in patients with cardiovascular disease relative to controls and furthermore, they have been shown to act as positive effectors of collagen synthesis at the post-transcriptional level [99]. Ribosomal proteins were significantly increased in the HCD group; 5 small subunit proteins and 3 large subunit proteins were elevated within the range of 1.5~2.1 fold and 1.7~1.8 fold respectively. P2, a constituent of the 60S ribosomal subunit involved in interactions with elongation factors during the course of protein synthesis [100], Elongation factor 1 alpha, and translation initiation factor EIF4A2 were all increased in the DCH group, collectively suggesting increased protein production or turnover.

In line with the evidence for increased protein production, enzymes involved in protein degradation were also increased in abundance, including ubiquitin-specific peptidase 5, cathepsin B and cathepsin D. Cathepsin B has been mentioned in the context of angiogenesis, acting upstream of vascular endothelial growth factor (VEGF) [101] and cathepsin D is known to be expressed in the aortic extracellular space (as well as in lysosomes) with a role in atherosclerosis [102]. Furthermore, cathepsin D has also been suggested to be a crucial paracrine factor for endothelial and fibroblastic cells as they were found to be in macrophage-rich regions of atherosclerotic lesions [103]. We found that protease inhibitors of the serpin family were also increased by HCD. SerpinA9 is involved in maturation and maintenance of naïve B lymphocytes, which play a role in atherogenesis. Variants in the *SERPINA9* gene presenting as single-nucleotide polymorphism have been shown to be associated with characteristics of carotid atherosclerotic plaques [104]. SerpinC1, which is synthesised by endothelial cells, modulates intravascular coagulation and could play a central role in the initiation and progression of atherosclerosis [105]. SerpinA3 is another secreted serpin that has previously been associated with atherosclerosis; it is expressed in endothelial cells and medial smooth muscle cells in human atherosclerotic lesions, and a 14-fold increased expression of serpinA3n mRNA was found in lesions from ApoE-/- mice compared to lesion-free vessels [106]. Increases in proteases and protease inhibitors are likely to be related to the increased protein production and may also play a significant role through their role in immune-related functions.

2.4.4. Chaperones

In accordance with changes discussed above, increased levels of HSPs and chaperones were also observed in this study. Molecular chaperones prevent inappropriate protein aggregation and mediate transport of immature proteins to the target organelles for final packaging, degradation, or repair [107]. In this study, both calrecticulin and calnexin were up-regulated in the HCD group. The calreticulin/calnexin cycle plays an important role in the ER quality control system; calreticulin promotes folding and oligomeric assembly and was suggested to act as a vascular regulator in reducing intimal hyperplasia after arterial injury [108]. Calnexin has a dual role of promoting the accurate folding of glycoproteins and targeting the misfolded proteins to ER-associated degradation [109]. Other ER chaperones increased in abundance include HspA5, Hsp47, protein disulfide-isomerase and Hsp90B1. HspA5 is the most abundant HSP70 in the ER which promotes correct folding and assembly of proteins and is believed to play a key role in monitoring protein transport through the cell [110]. Hsp47 is a collagen-binding stress

protein and its expression under normal conditions correlates with that of collagen molecules in various cell-types and tissues [111]. Hsp90B1 is crucial for the maturation and exportation of toll-like receptors (TLRs) and contributes to innate immunity [112]. Furthermore, it interacts with the MHC class I molecules of DCs and other APCs and also has a significant role in the adaptive immune system [113]. Protein disulfide-isomerase is an oxidoreductase that catalyses formation and isomerisation of disulfide bonds, thereby participating in protein folding. It has been suggested that lipid peroxidation products in atherosclerotic lesions may modify and lead to a loss of function in Protein disulfide-isomerase, which in turn, contributes to local ER stress, apoptosis, and plaque progression [114].

Cytosolic chaperones were also increased in abundance in the HCD group, inducing Hsp90, Hsp70, chaperonin, and CCT. HSP90 is highly expressed in human atherosclerotic plaques with increased vascular smooth muscle cells and collagens, suggesting that HSP90 contributes to the instability of advanced human atherosclerotic plaques by regulating their collagen contents [115,116] as well as vascular smooth muscle cell migration and proliferation [117]. Hsc70 is only mildly induced during stress situations while Hsp70 is highly inducible during stress [118]. It has been proposed that Hsc70, together with Hsp70, interacts with lipids and plays a role in the folding of membrane proteins and the translocation of polypeptides across membranes [119]. Chaperonin is expressed in the mitochondria that can be translocated to the cytosol and later, transported to the cell surface and shed into the environment. It has been shown to trigger innate and adaptive immune responses that initiate the earliest still reversible inflammatory stage of atherosclerosis [120]. CCT is known to play an important role in the folding and biogenesis of tubulin and actin, as well as other proteins such as α- and β-globin and cofactor A [121,122]. Therefore, increased levels of HSPs not only regulate protein folding but also play a significant role in immune response.

Cyclophilin A has peptidyl prolyl *cis-trans* isomerase (PPIase) and chaperone activity, and is the only chaperone showing decreased abundance in this study. Cyclophilin A is a crucial mediator of vascular remodelling and atherosclerosis; as atherosclerosis progresses, inflammatory stimuli induce the secretion of cyclophilin A from vascular smooth muscle cells, endothelial cells and macrophages [123]. The decreased levels of cyclophilin A in our study are consistent with induced secretion of this protein in the ascending aorta of the HCD-treated group.

2.4.5. ER-Golgi transport

Consistent with the elevated production/turnover of proteins, ER transport/membrane trafficking-related proteins were also strongly increased in this study. Both Rab1A and Rab11A belong to the Rab small GTPase family; these are major regulatory proteins involved in membrane transport [124]. Rab1a controls vesicle traffic/protein transit from the ER to the Golgi apparatus and regulates early endosome sorting for multiple cargo species [125]. Rab11a is associated with both constitutive and regulated secretory pathways [126]. Rab11 family proteins are shown to participate in recycling processes at perinuclear recycling endosomes and they are transported along microtubules to the cell periphery through association with recycling carriers [127]. In line with this, we also observed elevation in atlastin-3, an

integral membrane GTPases that interact with the tubule-shaping proteins. Atlastin-3 is involved in the formation of the tubular ER network that plays an important role in ER and Golgi morphology [128,129].

Bap31 is an integral protein of the ER membrane implicated in regulating the export of selected membrane proteins, especially those prone to ER-associated degradation, from the ER to downstream compartments of the secretory pathway [130,131]. Clathrin also is a key protein in endocytosis and intracellular vesicles. Transmembrane emp24 domain-containing protein recycles amongst the membrane-bound organelles; transmembrane protein cargo destined for internalisation is known to be mediated by clathrin during the endocytosis [132]. ADP-ribosylation factor controls the formation of transport vesicles during intracellular transport and membrane trafficking, while the Rab family controls the specific delivery of vesicles to target membranes [133]. Valosin-containing protein, crucial for ER-associated degradation, removes the ubiquitinated proteins from the ER to the cytosol for proteasomal degradation [134]. Increases in the above proteins indicate elevated endocytosis, and combined with increases in ER stress protein Niban and Calnexin, further supports increased protein production in the HCD group.

2.4.6. Metabolism

The trend of increase in the glycolytic enzymes suggests an increased reliance on anaerobic energy production. Increased LDH may be a mechanism to ensure replenishing of NAD^+ to enable glycolysis to continue. As shown in (**Figure 2-4**), all glycolytic enzymes showing significant/trending difference are found in the second half of the glycolytic pathway; these include pyruvate kinase, enolase, phosphoglycerate mutase, phosphoglycerate kinase and triose phosphate isomerase. It is possible that this pattern is related to elevated catabolism of a carbohydrate other than glucose (e.g. fructose, which enters glycolysis at the level of glyceraldehyde-3-P). Increases in TCA-cycle enzymes and proteins involved in mitochondrial energy production are consistent with altered energy metabolism.

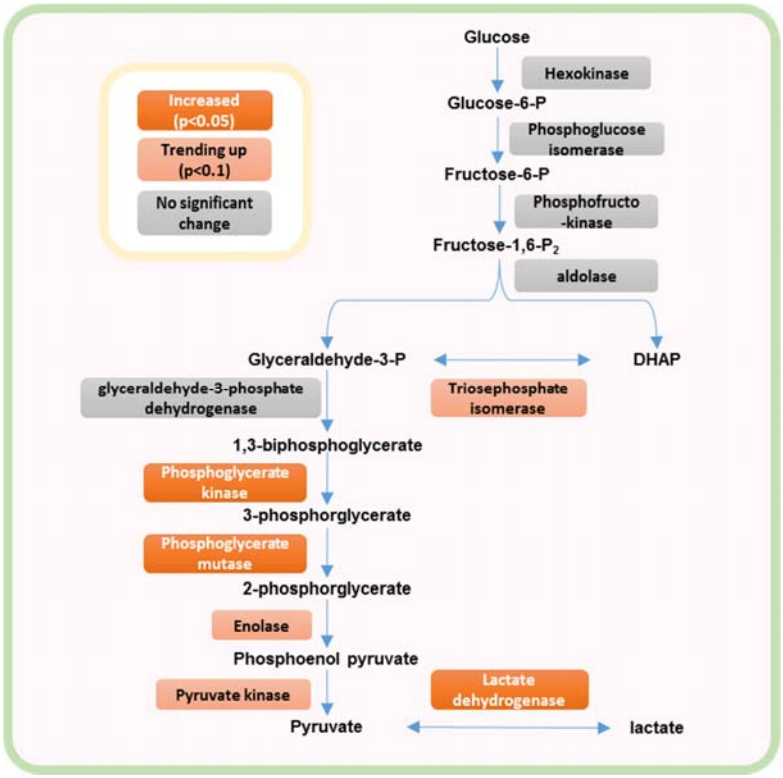

Figure 2-4 Changes in glycolytic enzymes in ascending aorta from HCD-fed NZW rabbits.

Changes in relative abundance of glycolytic enzymes were based on measurements from five HCD-fed NZW rabbits and five control diet-fed NZW rabbits. Altered glycolytic enzymes were all increased in abundance, including and subsequent to triosephosphate isomerase in the pathway. Consistent with an elevation of anaerobic glucose handling, lactate dehydrogenase was also increased.

2.4.7. Muscle contractile and cytoskeleton proteins

As stated earlier, only five proteins were found at significantly lower levels in the HCD group, and all of these are known to be involved in muscle contraction. Furthermore, several of them are specific for smooth muscle cells, the only muscle cell type found in the arterial wall.

Significant decrease in proteins involved in actin filament organisation has been reported in the HCD group, including destrin, an actin-depolymerizing protein [135], and transgelin and filamin-A, both of which are known to crosslink actin filaments and regulate actin cytoskeleton organization [136,137]. Reduction in the expression of the smooth muscle cell marker transgelin has been reported in atherosclerotic arteries previously [138], and filamin-A was suggested to have a regulatory role in vascular remodelling and smooth muscle cell migration at the site of vascular injury [139]. Rhea-like protein, which is highly similar to talin, is essential for integrin function and acts by stably linking clusters of ECM-linked integrins to the cytoskeleton [140]. Talin is also an essential mediator of integrin activation for its various downstream effects on the vascular system [141,142]. Therefore, reduction in the rhea-like protein may further impair cytoskeleton structure.

Smooth muscle caldesmon protein binds to myosin and actin simultaneously whereby it modulates the actomyosin interaction and hence, muscle contraction [143]. Furthermore, contractile proteins including myosin heavy chain, myosin light chain, and tropomyosin were also reduced in abundance in the HCD group, further consistent with compromised contractile function in the ascending aorta as a result of HCD diet. Previously, a decrease in MHC11 was observed in the smooth muscle cells of coronary atherosclerosis, along with the loss of desmin [144].

Desmin is a constitutive subunit of the intermediate filament (in skeletal, cardiac, and smooth muscles) with a role in maintaining structural integrity and myogenesis [145]. Desmin expression decreases during the functional and morphological damage of the endothelium in the late stages of atherosclerosis [144]. However, desmin up-regulation has been associated with proliferation of smooth muscle cells during neointima formation [146]. Smoothelin is a recently-identified cytoskeletal protein exhibiting a filamentous organisation. It is found only in contractile smooth muscle cells and does not belong to any of the classes of structural proteins [147]. It has been shown that in the carotid artery of rats following vascular injury, the smoothelin level was decreased in the media and neointima during early formation/proliferation phase but increased in both media and neointima at later phase, correlating with a decrease in proliferation [148]. The presence of smoothelin-positive cells in various advanced lesion sites of atherosclerotic arteries, was considered to be indicative of ceased expansion [149]. Therefore, increased desmin and decreased smoothelin as seen in our study, provides two lines of evidence that our model represents early stages of atherosclerosis-like lesions during neointimal thickening.

Actin related proteins that were increased in abundance are known to be involved in cell motility and invasion. Plastin 3 is an actin-bundling protein that significantly influences cell invasion and metastasis in cancer [150,151], is known to be up-regulated by VEGF, and may be associated with angiogenesis [152]. Actin-related protein (Arp) 2/3 complex is capable of inducing actin polymerisation and controls the assembly of a branching network of actin filaments at the leading edge of motile cells [153]. Moesin is involved in rearrangement of the actin cytoskeleton and an established marker for smooth muscle cell migration that may also contribute to changes in phenotype of smooth muscle cell following stress [154]. Increases in these proteins suggest induction of cell migration and may also be associated with neointima formation and expansion in cell numbers. Consistent with this interpretation, the few calcium-binding proteins measured here that are involved in mediating cell proliferation, were also increased in abundance. S100A4 is known as a mediator of cancer metastasis, and down-regulation of S100A4 by small interfering RNAs has been shown to decrease cell invasion, metastasis, and angiogenesis [155]. Increased S100A4 has also been observed in diseases where both fibrosis and inflammation are involved - processes greatly dependent on tissue remodeling and cell motility, such as fibrosis (of kidney, heart and liver) and arterial disease [156]. S100A6 is up-regulated in proliferating and differentiating cells [157] and is known to be present at elevated levels in different tumours. Through interaction with different protein partners such as annexins, p53 and HSPs, S100A6 is able to modulate endothelial cell-cycle progression [158]. Calumenin was suggested to elicit an autocrine or paracrine effect on cells in its vicinity and to exert a role during processes in which the cytoskeleton is rearranged, or in cell proliferation [159]. It was found in atherosclerotic lesions but not in normal vasculature [160]. Overall,

these changes are consistent with our observation of expanding cell numbers during neointima formation.

Considering the inflammatory nature of the disease we are modelling herein, it is interesting to note the immune-related aspects of the above changes in actin-regulating proteins. The recognition of MHC molecules loaded with antigen at the surface of antigen-presenting cells by the T-cell receptor results in the formation of an immunological synapse, which is accompanied by a major accumulation of actin at the contact site. At the immunological synapse, clathrin is responsible for actin polymerisation by acting as a molecular platform for the recruitment of actin-polymerising proteins such as the Arp2/3 complex [161]. The increased abundance of clathrin and Arp2/3 complex protein may have a significant role in mediating immune response in the ascending aorta of the HCD-treated rabbit.

2.4.8. Other significant findings

A critical step in the initiation of an atherosclerotic plaque is the subendothelial retention of apolipoprotein B and associated expansion of intimal space with the deposition of extracellular matrix (ECM) [162]. Fibronectin is one of the earliest ECM proteins deposited at atherosclerosis-prone sites and was suggested to promote the formation of the atherosclerotic lesion. In this study, increases in fibronectin 1, which is known to increase the atherogenic plaque area by promoting VMSCs migration [163], may be closely associated with the cell proliferation during neointima formation.

Dystroglycan, an adhesion molecule that act as a a signalling scaffold in a variety of cell types and tissues [164], was suggested to play a protective role in the artery wall against injury-induced intimal thickening [165]. Dystroglycan precursor is cleaved into dystroglycan-A (residues 30 – 653) and dystroglycan-B (residues 654 – 895) that link to laminins and actin respectively. While dystroglycan-A levels were very similar between groups, dystroglycan-B was clearly elevated in the HCD group (>2.6-fold). It is possible that the two chains also have independent roles in regulating adhesion processes in our model.

Another basic component of the vascular ECM, osteoglycin, was significantly lowered in the HCD group. In the vascular smooth muscle cells that had undergone proliferation, osteoglycin expression was shown to decrease through the action of TGF-beta [166]. Our observation of increased TGFB1 with concomitantly decreased osteoglycin is consistent with this description. Ras suppressor protein 1 (RUS1), significantly decreased in this study, is an endogenous inhibitor of the Ras signalling pathway. Ras has a critical role in smooth muscle cell proliferation and inhibition of the Ras signalling pathway has been shown to attenuate neointimal formation following vascular injury [167]. Our result is consistent with previously-reported RUS1 down-regulation during lesion progression in the mouse model of atherosclerosis [168]. The decrease in both osteoglycin and RUS1 is consistent with smooth muscle cell proliferation and progression of the atherosclerotic lesion in the ascending aorta of our rabbit model.

2.4.9. Glycoprotein (transmembrane) nmb-like

The most dramatically-altered protein was Gpnmb, a transmembrane glycoprotein also known as osteoactivin. The *GPNMB* gene was first reported in cancer cells but later found in many non-cancerous cell types, including melanocytes, osteoclasts, osteoblasts, and dendritic cells. The Gpnmb protein is related to a number of processes, including bone mineralisation, cell adhesion, and angiogenesis. However, this protein has not been reported in the context of atherosclerosis before.

Gpnmb expression appears to promote migration, invasion and metastasis of breast cancer cells, and *GPNMB*-expressing tumours exhibited increased recruitment of endothelium [169]. The 15-fold elevation here detected in response to HCD could thus be part of a similar, albeit non-cancerous, process. Endothelial migration was linked to shedding of the Gpnmb extracellular domain through a proteolytic process governed by A disintegrin and metalloproteinase (ADAM) domain-containing proteins [169]. Shedding of extracellular domain-Gpnmb was linked to elevated levels of VEGF [169] and matrix metalloprotease-3 (MMP-3) previously [170].

If the extracellular domain is shed from Gpnmb in the ascending aorta with similar effects, elevated VEGF likely promotes angiogenesis within the neointima, while elevated MMP-3 probably contributes to vascular remodelling by degradation of protein components of the ECM. Altered proteins that are known to regulate actin cytoskeleton, cell proliferation and migration as described earlier in Section 2.4.7 was supportive of the vascular remodelling process being present in the ascending aorta studied here.

Interestingly, high levels of MMP-3 have been reported in smooth muscle cells in atherosclerotic coronary arteries, and were suggested to be part of the local connective tissue remodelling process in association with plaque formation and growth [171]. Furthermore, focal overexpression of MMP-3 was suggested to promote destabilisation and complication of atherosclerotic plaques [171,172]. In light of this, our finding of Gpnmb at 15-fold higher levels in aortic tissue exhibiting pronounced intimal thickening suggests a causative role for Gpnmb in atherosclerosis and highlights Gpnmb as a possible therapeutic target.

In this study, over 2-fold elevation was observed for galectin-3 in the ascending aorta of the HCD group, consistent with previously identified galectin-3 up-regulation within atherosclerotic lesions [173]. This protein is known to be: 1) enriched in activated macrophages in chronic inflammatory conditions; 2) involved in cell proliferation, adhesion and migration [174], and 3) part of VEGF- and basic fibroblast growth factor (bFGF)-mediated angiogenesis [175]. Also, increased fibronectin expression (described earlier) may be linked to the up-regulation of galectin-3, which has been associated with an “epithelial-to-mesenchymal-transition”-like phenomenon that is partially characterised by fibronectin fibrillogenesis [174]. Early fibronectin fibrillogenesis is an integrin-dependent process [176], in which the integrin-mediated fibronectin assembly by a subpopulation of smooth muscle cells acts as a key response step in arterial injury [177]. Therefore, increased galectin-3 is likely to be involved in both the inflammatory response and vascular remodelling in response to arterial injury, through its role in cell proliferation/migration and

angiogenesis. Another line of evidence for induced angiogenesis in our study comes from increased annexin-A3, which not only induces VEGF production through the hypoxia-inducible factor-1 (HIF-1) pathway but also induces migration and tube formation of human umbilical vein endothelial cells [178].

Increased annexin-5, along with fibronectin1, may exert their protective effect toward atherosclerotic lesions by preventing plaque rupture atherothrombosis [163,179].

Finally, several other proteins that were significantly elevated in the ascending aorta of HCD-treated rabbit have no previously-defined role in atherosclerosis. Ras-related protein Rap-1A (RAP1A) is one of the two Rap1 isoforms that forms a complex with other proteins (talin and Rap1-GTP-interacting adaptor molecule (RIAM)) and activates integrin signalling [180]. Tyrosine 3-monooxygenase/tryptophan 5-monooxygenase activation protein, epsilon (14-3-3ε), belongs to the 14-3-3 family of proteins which mediate signal transduction. Elevation in 14-3-3ε expression was shown to promote epithelial-to-mesenchymal-transition and cell migration in tumours [181]. Cytoplasmic dynein 1 heavy chain 1 (DYNC1H1) is the core protein of the cytoplasmic dynein 1 complex and acts as a motor for the intracellular retrograde motility of vesicles and organelles along microtubules. The dynein complex has housekeeping functions in all cells, including orientation of the mitotic spindle, nuclear positioning, Golgi maintenance, and endosomal dynamics [182]. Dihydropyrimidinase-like 2-like (DPYSL2), a member of the collapsin response-mediator protein family whose members facilitate neuronal differentiation and axonal guidance, plays a role in synaptic signalling through interactions with calcium channels [183]. EFHD1 is an EF-hand domain-containing protein that displays increased expression during neuronal differentiation [184]. These changes appear to be associated with altered neuronal function and differentiation based on what is known to date. However, their role in atherosclerosis requires further investigation.

2.5. Conclusion

In the ascending aorta of HCD-treated rabbits, the most prominent histopathological feature was intimal thickening. Intimal hyperplasia is generally thought to precede overt atherosclerosis. Deposition of proteoglycans in the intima has been proposed to contribute to thickening and, specifically, as a mechanism for incorporation of lipoproteins. Proteoglycans in the ECM can bind and retain lipoproteins such as apolipoprotein B (here up-regulated by 4.5-fold), which attracts macrophages and hence leads to induction of an inflammatory cascade. Despite the significant elevation in apolipoproteins in response to the HCD, we observed no significant change in proteoglycans in our study. Therefore, the increased apolipoprotein levels as seen here is unlikely to be associated with changes in proteoglycan levels.

The process of intimal thickening and inflammation associated with HCD may underlie the dramatic increase in the level of proteins from various functional groups, but does not necessarily decrease any particular groups of proteins. This may explain the observed pattern of changes for proteins. Among

the proteins that were significantly different in expression level (p-value < 0.05) between the HCD and control groups, over ten-times more proteins were up-regulated than down-regulated.

More specifically, the net increase in cell numbers during neointima formation fits well with the elevated levels of multiple core histones and nucleosome-associated proteins, ribosomal proteins, mRNA processing proteins, chaperones and proteins involved in intracellular transport and membrane trafficking. Also contributing to the large number of proteins with increased abundance, proteins facilitating the inflammatory response were highly elevated as a group in the ascending aorta of the HCD-treated rabbit.

Our results are also consistent with the presence of altered actin cytoskeletal organisation, induced cell proliferation and migration in the ascending aorta of HCD-treated rabbits, highly likely to be associated with phenotypic change in vascular smooth muscle cells during vascular remodelling. This is also in line with a well-known phenomenon in atherosclerosis; vascular smooth muscle cells are mostly found in the medial layer of normal arteries but migrate from the media towards the intima during progression to atherosclerosis, [185,186]. We also hypothesise severely compromised contractile function of the vascular smooth muscle cells during the course of switching from normal, differentiated cells to the proliferative type as a result of vascular remodelling. The shift in metabolic enzymes indicating increased glycolytic and TCA cycle activity is also likely to be part of the vascular remodelling in response to the diet.

Most of our findings correlated very well with the current understanding of the atherosclerotic process. However, our finding of highly elevated Gpnmb was novel in the context of atherosclerosis. This finding therefore merits further investigation in order to uncover the role of this protein in the pathogenesis of atherosclerosis and explore the potential of Gpnmb as a therapeutic target.

This study demonstrates the successful application of proteomics to provide detailed profiling of protein changes in the arterial tissue. Establishment of such a platform could also play a significant role in monitoring of disease-modifying effects of future treatments of atherosclerosis.

Chapter 3. Molecular Profiling of the Brain in Alzheimer's Disease: a Metabolomics Approach

3.1. Introduction

AD is the most common form of dementia and is clinically characterised by a progression from episodic memory problems to a slow global decline in cognitive function [22]. In the USA, the current estimate of the AD population is 5.2 million and the total estimated prevalence is expected to reach 13.8 million by 2050 [187]. To date, there are no treatments with proven disease-modifying effects and AD remains the largest unmet medical need in neurology [22]. It was pointed out recently that lack of mechanistic grounding is the major cause of failure in AD clinical trials; researchers were urged to prioritise the development of a molecular mechanistic theory that distinguishes AD by the underlying pathogenesis, which can then be used to rigorously test the efficacy of drugs targeting those mechanisms [188].

AD pathology presents a complicated interplay between several biochemical alterations, including changes in APP metabolism, phosphorylation of the tau protein, oxidative stress, energetics and mitochondrial dysfunction, inflammation, membrane lipid dysregulation and neurotransmitter pathway disruption [189]. Despite intensive research in each area of these pathological changes, there is an urgent need for a greater global understanding of the molecular mechanism underlying AD pathologies in an integrative manner. Systemic studies such as proteomics and metabolomics, therefore, would provide an unprecedented and valuable information platform for delineating complicated diseases such as AD.

In AD research, systematic studies on metabolic perturbations in the human brain have been scarce, mainly due to 1) the difficulties in acquiring human brain tissue of high quality; and 2) the lack of reliable metabolic platforms. To date, most human studies investigating metabolic changes associated with AD were performed on cerebral-spinal fluid (CSF) and plasma/serum. The current study aims to elucidate the molecular changes that occur in AD brain by profiling the metabolic perturbations using both gas-chromatography/mass-spectrometry (GC-MS) and liquid-chromatography/mass-spectrometry (LC-MS). The use of two distinct approaches was chosen in order to overcome limitations associated with each technique in respect to mass, volatility, polarity of target compounds, and to extend the total number of metabolites that could be successfully identified and quantified. Since some brain regions are more affected by AD than others [190], we further aimed to examine and compare different regions of the brain.

In my studies, I compared seven functionally distinctive brain regions that are considered to be either severely affected: hippocampus (HP), entorhinal cortex (ENT), middle-temporal gyrus (MTG) [190,191], or moderately affected: sensory cortex (SCx), motor cortex (MCx), cingulate gyrus (CG), along with a control region, cerebellum (CB) that is believed to be relatively spared by AD [28,192].

Through these studies, we expected to gain a better understanding of the molecular basis of AD pathology in the human brain, with the objective of identifying novel biomarkers and processes that can be translated into blood or CSF screening for diagnosis and/or prognosis of AD.

3.2. Methods

3.2.1. Brain sample collection

All brains were kindly provided by the New Zealand Neurological Foundation Human Brain Bank at the University of Auckland Faculty of Medical and Health Sciences (www.fmhs.auckland.ac.nz/sms/anatomy/research/brain_bank.aspx), with the written approval of the Institutional Human Subjects Ethics Committee.

Brain samples were collected from *post-mortem* brains of nine patients with AD, and nine control patients with no brain disease. Patients' details (**Table 3-1**) include the cause of death as determined by *post-mortem* examination, neuro-pathological severity as measured by Braak scores assigned by neuropathologists, according to the Consortium to Establish a Registry for AD (CERAD) criteria [28,193], and the brain weights. To preserve anonymity, the Brain Bank assigned a code name for each brain using an alphanumeric system: for brains obtained from AD and control patients, the codes were AZ (for Alzheimer's) followed by a number, and H (for Healthy) followed by numbers respectively. The overall group characteristics of the sample set were as summarised in **Table 3-2**. The AD and control groups were matched in age, female/male sex ratio, and *post-mortem* delay. The significantly lower brain weight in AD compared to the control group is in line with the severity of brain pathology revealed by their Braak scores [28]. On average, AD brains weighed ~16% less compared to the control brains. The median (range) of brain weights in the AD patients we studied here were 1062 (831~1355) g, compared with 1260 (1094~1461) in the matched control subjects ($p<0.005$) (**Table 3-2**).

Table 3-1: Details of AD and Control brains used in the current study

Case No	Case Code	Group	Age /Sex	Ante-mortem brain/mental state	Cause of death	Braak Stage	Post-mortem delay (h)	Brain Weight (g)
1	AZ42	AD	60/M	Alzheimer's disease & dementia	Alzheimer's disease	VI	7.0	1020
2	AZ71	AD	62/F	Alzheimer's disease & dementia	Alzheimer's disease	VI	6.0	831
3	AZ48	AD	63/F	Alzheimer's disease & dementia	Bronchopneumonia	VI	7.0	1080
4	AZ72	AD	70/F	Alzheimer's disease & dementia	Lung cancer	V	7.0	1044
5	AZ90	AD	73/M	Alzheimer's disease & dementia	Gastrointestinal haemorrhage	IV	4.0	1287
6	AZ96	AD	74/F	Alzheimer's disease & dementia	Metastatic cancer	V	8.5	1062
7	AZ39	AD	74/M	Alzheimer's disease & dementia	Pseudomonas bacteraemia	VI	12.0	1355
8	AZ80	AD	77/M	Alzheimer's disease & dementia	Myocardial infarction	VI	4.5	1180
9	AZ38	AD	80/M	Alzheimer's disease & dementia	Bronchopneumonia/pulmonary oedema	V	5.5	1039
10	H155	Control	61/M	No brain disease or dementia	Ischaemic heart disease	-	7.0	1258
11	H121	Control	64/F	No brain disease or dementia	Pulmonary embolism	-	5.5	1260
12	H132	Control	63/F	No brain disease or dementia	Ruptured aorta	-	12.0	1280
13	H122	Control	72/F	No brain disease or dementia	Emphysema	-	9.0	1230
14	H204	Control	66/M	No brain disease or dementia	Ischaemic heart disease	-	9.0	1461
15	H241	Control	76/F	No brain disease or dementia	Metastatic carcinoma	II	12.0	1094
16	H164	Control	73/M	No brain disease or dementia	Ischaemic heart disease	-	13.0	1315
17	H123	Control	78/M	No brain disease or dementia	Ruptured abdominal aortic aneurysm	-	7.5	1260
18	H150	Control	78/M	No brain disease or dementia	Ruptured myocardial infarction	-	12.0	1416

Brain pathology and Braak stage were analysed by a qualified neuropathologist and cause of death was determined at post-mortem examination. Abbreviations: AD, Alzheimer's disease; F, female; M, male.

Table 3-2: Group characteristics of the brains used for the current study

Variable	Control	Alzheimer's disease
Number	9	9
Age	70.1 (6.7)	70.3 (7.1)
Male sex, n (%)	5 (55.6)	5 (55.6)
Post-mortem delay (h)	9 (5.5-13.0)	7 (4.0-12.0)
Brain weight (g)	1260 (1094-1461)	1062 (831-1355)*

Age is shown as mean (SD); *post-mortem* delay and brain weights are median (range); *p=0.005compared with control; all other differences are non-significant (t-test).

3.2.2. Sub-sampling

Sub-sampling was carried out to dissect brain tissue from the seven brain regions that we aimed to examine and compare: three severely affected regions (including HP, ENT, and MTG), three moderately affected regions (including MCx, SCx and CG), and a relatively spared region (CB) [28,191,192].

All seven areas of the brain were pre-dissected by expert neuroanatomists for accurate identification of the brain regions. Brain tissue for HP and ENT was dissected out from a single block (both regions are on a single block as they are small regions that are anatomically adjacent). Likewise, samples for SCx and MCx were from the same block. Samples for CB, MTG and CG were from 3 separate blocks.

A typical brain block from the human brain bank contains both the grey and white matter. We dissected only the grey matter for all the brain regions except for CB, which had aggregates of grey matter surrounded by deep cerebellar white matter in a tree-like pattern making it impractical to separate the two tissue types. Any superficial blood frozen on the blocks was removed prior to dissection.

For the metabolomics analysis, we dissected 50 ± 5 mg of tissue from each brain region of each donor. Careful handling was required to avoid thawing of the brain tissue; fresh frozen blocks were transferred from -80 ^{o}C to the -20 ^{o}C freezer for 10 to 20 mins, and then transferred onto a metal board placed within a dry ice-filled container. Brain blocks were cut into smaller pieces with scalpel blades (kept cold on dry ice when not in use) and collected materials were kept frozen during weighing on a digital scale. After the desired weight of tissue was obtained, each sample was transferred into Eppendorf Safe-Lock tubes and submerged in a liquid nitrogen container until transferred to a -80 ^{o}C freezer.

For sub-sampling, each brain region was treated as one set of samples. Seven sets of samples were numerically coded (Table 3-3). The examiner and the data interpreter were blinded to the diagnosis of the sample cases. Samples were coded and randomised for chemical analysis, and calculation of relative quantities. Samples were re-grouped into AD and controls for the calculation of fold-changes, thereby breaking the blind, at the final stage.

Table 3-3: Brain samples numbering scheme

Patients	1(HP)	2(MCx)	3(SCx)	4(CB)	5(ENT)	6(MTG)	7(CG)
AZ42	101	201	301	401	501	601	701
AZ71	102	202	302	402	502	602	702
AZ48	103	203	303	403	503	603	703
AZ72	104	204	304	404	504	604	704
AZ90	105	205	305	405	505	605	705
AZ96	106	206	306	406	506	606	706
AZ39	107	207	307	407	507	607	707
AZ80	108	208	308	408	508	608	708
AZ38	109	209	309	409	509	609	709
H155	110	210	310	410	510	610	710
H121	111	211	311	411	511	611	711
H132	112	212	312	412	512	612	712
H122	113	213	313	413	513	613	713
H204	114	214	314	414	514	614	714
H241	115	215	315	415	515	615	715
H164	116	216	316	416	516	616	716
H123	117	217	317	417	517	617	717
H150	118	218	318	418	518	618	718

The first digit refers to a specific brain region as numbered on the top and the last two digits refer to individual brain case numbers as detailed in Table 2.

3.2.3. Materials for metabolomics

Water and methanol were Fluka Chromasolv LC-MS grade (SigmaAldrich, Dorset England). Chloroform ("Pesticide Analysis" grade), Pyridine ("99% extra pure" grade) and Hexane ("Extra dry" grade) were obtained from Acros Organics (Geel, Belgium), as was N-methyltrimethyltrifluoroacetamide (97% grade). Isotopically labelled internal standards (Citric acid-d_4, $^{13}C_6$-D-fructose, L-tryptophan-d_5, L-alanine-d_7, stearic acid-d_{35}, benzoic acid-d_5, and leucine-d_{10}) were purchased from Cambridge Isotopes Inc (Tewksbury, MA).

3.2.4. Sample extraction for metabolomics

Aliquots (50 ± 5 mg wet weight) of tissue in Eppendorf Safe-Lock tubes were subjected to a Folch-style extraction using a Tissuelyser (Qiagen; Manchester, UK). Each sample was extracted in 0.8 mL 50:50 MeOH:$CHCl_3$, to which a solution of the labelled internal standards in MeOH had been added, to achieve a final concentration of 0.016 mg/mL for each internal standard in the extraction solvent. The extraction solvent and tube racks were held at -20 °C overnight, until immediately before use. Following addition of a single 3 mm Tungsten carbide bead to each sample tube, samples were extracted in batches for 10 minutes with the homogeniser set to 25 Hz. All samples obtained from the same brain region were handled as separate batches for this and subsequent procedures. Following tissue disruption, 0.4 mL water was added and the samples vortexed for 10-15 s. Phase separation was accomplished by centrifugation at 2,400 g for 15 min. After separation, tissue debris lay at the interface between the lower phase (non-polar extract in $CHCl_3$) and the upper phase (polar extract in MeOH:H_2O). Extraction blanks were prepared by including two tubes without tissue samples within each batch.

3.2.4.1. To prepare the non-polar extracts for LC-MS

From each sample, 100 µL of the non-polar extract (lower phase) was carefully removed with a pipette, minimising disturbance of the polar extract (upper phase) and debris layer. These non-polar extracts were dispensed into a new set of tubes. A further 100 µL of the non-polar extract was removed from each sample and combined into a single tube to make a pooled quality control (QC) sample of the non-polar extracts. This pooled QC sample was gently mixed and dispensed in 100 µL aliquots to a tube set. Non-polar extracts, along with their pooled QC samples, were then dried at ca 30 °C for 2 h 30 min in a Speedvac centrifugal concentrator (Savant; Thermo Scientific) and stored at 4 °C until analysed by LC-MS. LC-MS samples were reconstituted in 150 µL MeOH and analysed without derivatisation.

3.2.4.2. To prepare the polar extracts for GC-MS

Before proceeding to the polar extract preparation, the remainder of the non-polar extract (residual $CHCl_3$) in the extraction tubes was removed using a 500 µL HPLC syringe. The tubes were then centrifuged at 16,000 × g for 15 min to encourage tissue debris to form a coherent pellet. Without this step, residual $CHCl_3$ was occasionally entrained into the polar fractions, leading to total loss of the extract during vacuum drying.

From each sample, 200 µL of the polar extract (upper phase) was transferred to new set of tubes containing 600 µL MeOH (Before dilution, 50:50 MeOH:H_2O; after dilution, 700 MeOH:100 H_2O (ca 87.5% MeOH)). Higher MeOH content increases efficiency of protein precipitation. A further 200 µL of the polar extract was removed from each sample and combined into a single tube to make a pooled

QC sample of the polar extracts. This pooled sample was then gently mixed, and dispensed into a set of tubes containing 600 µL MeOH. After brief mixing, both the polar extracts and their pooled QC samples were centrifuged once more for 15 min at 16,000 × g. From each tube (800 µl volume), 750 µL aliquot was transferred to a final set of new tubes and dried at ca 30°C for 16-18 h in a Speedvac centrifugal concentrator. Dried residues were then held in sealed tubes at 4 °C until derivatised for GC-MS analysis.

3.2.5. GC-MS

3.2.5.1. Derivatisation

Methoxime/trimethylsilyl derivatives were prepared using a previously described procedure [194]. Briefly, 60 µL of a solution of 20 mg/ml methoxylamine hydrochloride in dry pyridine was added to each sample tube, which was then closed, vortexed for 10-15 s and heated to 80 °C for 20 min using a "Dri-block" heater. Samples were then removed from the heating block and allowed to cool for 1-2 min. After addition of 60 µL N-methyltrimethylsilyltrifluoroacetamide (MSTFA), each sample was briefly vortexed, and heated for a further 20 min at 80 °C. The samples were allowed to cool briefly, and then supplemented with 20 µL of a solution of retention index markers (selected n-alkanes covering the range C12 to C32; 0.3 mg /mL *docosane, nonadecane, decane, dodecane, and pentadecane* in pyridine). After brief mixing, the samples were centrifuged at 16,000 × g for 5 min, and 95 µL aliquots transferred to autosampler vials.

3.2.5.2. GC-MS analysis

GC-MS analysis was carried out using a Gerstel MPS2 autosampler, an Agilent 7890A Gas Chromatograph with Split/Splitless inlet, and a LECO Pegasus HT time-of-flight mass spectrometer. The method used was an adaptation of a previously described method for untargeted metabolomics [194]. Chromatographic conditions were adjusted (and checked with standard reference materials) to ensure adequate separation of glucose, sorbitol and fructose (**Figure 3-1**).

Gas chromatography was conducted using an Agilent/J&W DB-17MS column (30 m × 0.25 mm × 0.25 µm, Agilent Part No 122-4732, Santa Clara, CA) with a 3 m deactivated Fused Silica retention gap (0.25 mm, Agilent Part No 160-2256-10), and Helium carrier gas at 1.4 ml/min in constant flow mode. Injections of 1 µL sample were made in Pulse Splitless mode at an inlet temperature of 270 °C, using an "empty, hot needle" technique. Initial column temperature was 50 °C, held for 6 min then increased to 300 °C at 10 °C/min and held for a further 4 min. This resulted in a total cycle time of 42 min between injections.

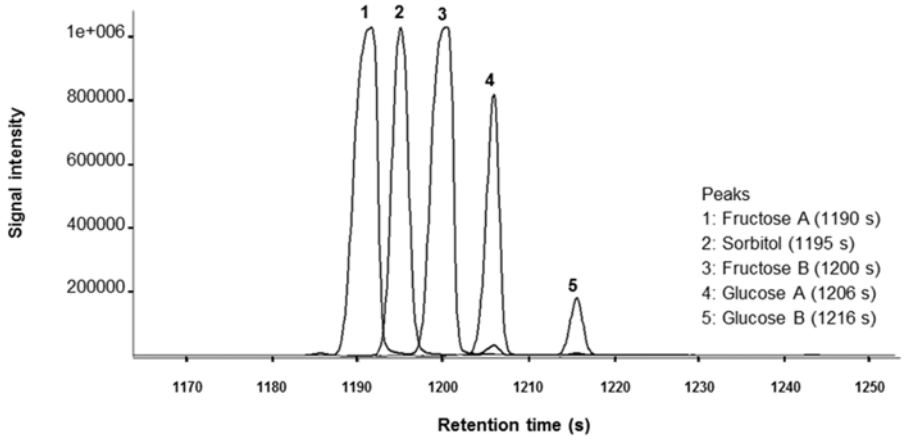

Figure 3-1 Overlaid chromatograms of standard compounds showing resolution of fructose, sorbitol and glucose.

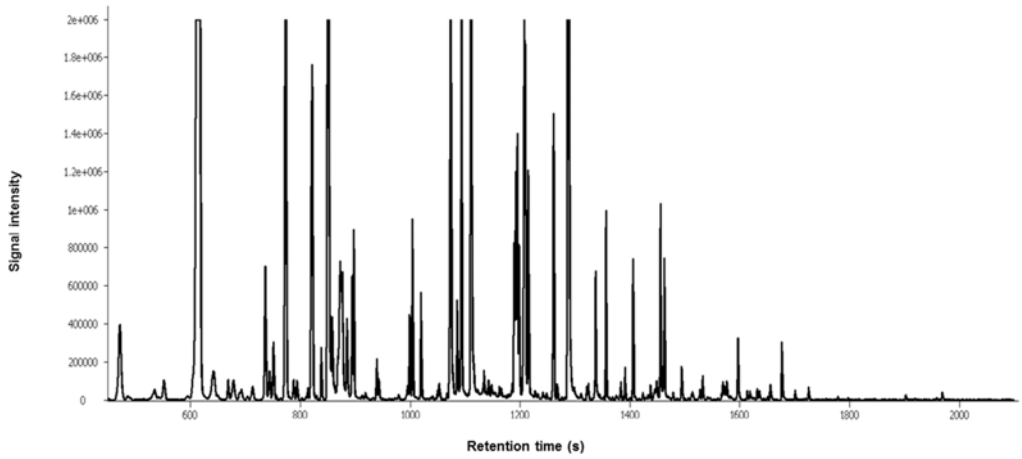

Figure 3-2 Representative mass chromatogram of GC-MS analysis of a human brain tissue extract.

Mass chromatogram for a control group sample from cerebellum (713), m/z 73, indicative of TMS derivatives. The y-axis has been expanded to allow low intensity peaks to be seen – actual full scale was ~1x107 (arb. units) for the most abundant metabolites.

After an initial 450 s solvent delay (to allow solvent and reagents to elute without damaging the detector), mass spectral data were acquired at 10 spectra per second, for the range 45-800 Da. Standard 70 eV electron energy was employed, at a source temperature of 220 °C.

Prior to sample analysis, the following checks and routine maintenance were undertaken to verify correct operation of the instrument: The GC septum and inlet liner were replaced, and the syringe checked for leak-free operation, and replaced if required. Recently acquired data were reviewed, to confirm adequate chromatographic separation and absence of tailing (which would be restored by replacement of either the retention gap or the column). The instrument's Log file was reviewed, to confirm that no "fatal" malfunctions were recorded. The analyser vacuum was checked to be better than

2×10^{-7} Torr with a carrier gas flow of 0.6 mL/min helium. An “air leak test” was carried out using recommended settings (155 °C, 1.4 mL/min He carrier gas, “split” injection mode) and method according to the manufacturer. In the event of failure, column connections and other flow path seals were adjusted until a leak test “pass” was achieved. The supplied “Acquisition System Adjust” and “Instrument Optimisation” methods were then run. “Acquisition System Adjust” applies a standard signal to data collection electronics, and essentially ensures that the two amplifiers used (low gain and high gain) do not have an offset at the signal level where the instrument switches from the high gain to the low gain units. “Instrument Optimisation” focuses the source voltages to optimise response and mass resolution, and carries out a mass calibration. On successful completion of the optimisation procedure, the report (written to the Log file) was reviewed. Successive optimisation reports over a period of weeks or months showed a gradual change in settings for key parameters and performance metrics (e.g. set detector and optics voltages, measured stability, noise and mass resolution). Any sharp change in settings as compared to the preceding optimisation report potentially indicated a fault on the instrument, which would be investigated and corrected prior to use.

The study was treated as a series of single batch experiments, in which a specific brain region constituted a batch. Within a batch, individual cases and controls were randomised, and run in a sequence interleaved with injections of the pooled QC (once per four study samples) and extraction blanks (two per batch). A “lead-in” sequence of six QC injections at the start of each batch was used to condition the chromatographic system. Extraction blanks (containing only the buffer and no brain samples and carried through the entire extraction and analysis procedure) were inspected visually to confirm absence of carryover, but were not included in subsequent data analysis.

3.2.5.3. Data reduction for GC-MS

Data were prepared using the “Reference Compare” method within ChromaTOF 4.5 (LECO; St. Joseph, MI). The software was used to carry out a global peak deconvolution of representative samples, based on user-supplied parameters such as expected chromatographic peak width, required number of co-maximising m/z signals, and required signal-to-noise ratio for the strongest m/z peak in the group. On this basis, the software compiled a list of nominated “metabolites” and searched mass spectral libraries to provide putative identities. Data bases we employed were: the NIST Mass Spectral Reference Library (NIST08/2008; National Institute of Standards and Technology/Environmental Protection Agency/National Institutes of Health Spectral Library; NIST, Gaithersburg, MD, USA); the Golm Metabolome Database (Max Planck Institute of Molecular Plant Physiology, Potsdam-Golm, Germany); and an in-house library developed at the University of Manchester [195]. For a subset of the identified metabolites, chromatographic retention data were available from reference standard materials, and definite identification could be achieved, based on matching both mass spectrum and expected retention time.

From the list of nominated metabolites, a reference table consisting of expected mass spectrum and retention time windows was compiled. This was then applied as a target list of features to be searched across all the study samples. As the pooled QC samples should contain all metabolites encountered in the experiment, these were deemed suitable for compilation of the reference table. However, the automatically-generated list of nominated metabolites included mass spectra of variable quality. For example, low concentration metabolites which eluted in the vicinity of higher concentration components yielded relatively poor spectra, while for some species, extensive fragmentation left little characteristic information in the mass spectrum. In order to provide a robust reference table, the initial list of nominations was edited to remove ambiguous and low quality spectra prior to use. It proved useful to carry out the global deconvolution on several (three to four) pooled QC injections across the entire experiment. By displaying these overlaid during editing of the nomination list, reproducible spectra were more readily distinguished from lower quality candidates.

The resulting target list (**Table 3-4**) consists of a mixture of definitively or putatively identified metabolites, and unidentified metabolites which were sufficiently characteristic to be confidently reported. By reporting unidentified features (i.e. metabolites with no names) it will be possible to use future identifications retrospectively on existing data. However, these unidentified features are not listed in the results section and hence, will not be further discussed in here.

In order to use the edited reference table as a reporting tool, appropriate parameters such as mass spectrum match threshold and tolerable retention time deviation were specified, and the table was initialised using a pooled QC sample (to provide reference m/z peak areas). Although data can be interpreted using these peak areas alone, improved reproducibility was achieved by the use of internal standards. For quantitation purposes, the peak area of each metabolite was compared to that of a non-endogenous chemical added at a constant concentration to each sample, allowing compensation for variation introduced by factors such as the volume of sample injected. In this work, a set of seven isotopically-labelled standards were used. The most suitable standard was assigned to each metabolite by determining which internal standard resulted in the lowest variance for a given metabolite across all the QC injections.

The resulting data for each experiment were compiled into a matrix of metabolite intensity data. This was merged with experimental metadata for visualisation and statistical analysis. Although the automated procedure has a high degree of reliability (estimated to return correct peak areas for more than 95% of features measured), data sets were also curated manually to remove possible integration errors.

Table 3-4: Confidence level of metabolites identified in the GC-MS study

Definitive	Confident Putative	Putative
jxc005 Alanine	jxc004 Lactic acid	jxc002 Styrene
jxc010 Valine	jxc008 Butanediol	jxc003 Hydroxylamine
jxc014 β-Hydroxybutyric acid	jxc020 Oxalic acid	jxc013 2-hydroxy-3-methylbutyric acid
jxc017 Valine	jxc022 Glycerol	jxc018 Ethanolamine
jxc019 Leucine	jxc025 Pyridine, 3-hydroxy-	jxc021 Mono methylphthalate
jxc024 L-Isoleucine	jxc027 4-hydroxybutyric acid	jxc036 Serine
jxc026 Leucine	jxc028 4-Hydroxypyridine	jxc038 Glyceric acid
jxc033 Isoleucine	jxc032 Phosphoric acid, monomethyl ester	jxc063 Erythronic acid
jxc034 Glycine	jxc037 Phosphoric acid	jxc066 4-Aminobutyric acid
jxc039 Threonine	jxc041 Urea	jxc075 2-Hydroxyglutaric acid
jxc042 L-Serine	jxc046 Fumaric acid	jxc076 N-bromosuccinimide
jxc044 L-Threonine	jxc047 Succinic acid	jxc079 Xylitol
jxc053 Threitol	jxc048 Nonanoic Acid	jxc080 Arabic acid
jxc065 l-Aspartic acid,	jxc051 beta-Alanine	jxc087 L-Glutamic acid
jxc068 L-Aspartic acid	jxc055 Uracil	jxc088 Fucose
jxc070 Methionine	jxc060 Benzene, 1-hydroxy-2-(hydroxyoxymethyl)	jxc090 Pentonic acid-1,4-lactone
jxc071 Methionine	jxc064 Malic acid	jxc091 Pentonic acid
jxc072 Cysteine	jxc077 Xylitol	jxc097 Pentonic acid
jxc089 Pyroglutamic acid	jxc078 Creatinine	jxc104 2-Pyrrolidone-5-carboxylic acid
jxc094 Phenylalanine	jxc103 N-acetylglutamic acid	jxc105 Arabinofuranose,
jxc098 Phenylalanine	jxc106 L-Glycerol-2-phosphate	jxc111 Mannitol
jxc100 Proline	jxc107 Ornithine	jxc128 L Ascorbic acid
jxc102 Asparagine	jxc110 Ornithine	jxc138 9H-Purine, 6-hydroxy-
jxc112 Fructose	jxc115 N-acetylaspartic acid	jxc145 Fructose-6-phosphate
jxc113 Glycerol-3-phosphate	jxc122 Myristic acid	jxc161 Glucose-6-phosphate
jxc114 Sorbitol	jxc132 N-acetylglutamic acid	jxc164 Myo-Inositol-1-phosphate
jxc113b Fructose	jxc143 Adenine	jxc166 Guanine
jxc114 Glucose	jxc144 N-acetylglucosamine	jxc172 Disaccaride
jxc117 Glucose	jxc151 Heptadecanoic acid	jxc182 Adenosine
jxc119 Citric acid	jxc155 Uric acid	jxc184 Guanosine
jxc121 L-Lysine	jxc188 Cholesterol	jxc187 Adenosine-5-monophosphate
jxc123 Lysine		
jxc127 Scyllo-inositol		
jxc131 myo-Inositol		
jxc134 Tyrosine		
jxc139 Tyrosine		
jxc141 Hexadecanoic acid		
jxc160 Stearic acid		
jxc162 Glucose-6-phosphate		
jxc168 Tryptophan		

Definitive – mass spectrum and retention time confirmed during this work, Confident Putative – mass spectrum and retention time consistent with reported data, and Putative – mass spectrum matches without retention time confirmation.

In the final statistical analysis, case number 6 (H241 in **Table 3-1**) was excluded due to the reported post-mortem AD pathology (with Braak stage II) albeit lacking in clinical AD symptoms before death.

The data were initially processed with a set of in-house procedures developed in the R programming environment [196]. A principal components analysis (PCA) was performed to visualise the overall integrity of the experiment by confirming closely-grouped QC samples and no identifiable run order or drift effects across the sample set. For the statistical analysis, data were $\log_{10}$-transformed before the analysis and back-transformed for interpretation of fold-changes and confidence intervals. To compare metabolite intensities between AD and control samples, univariate statistical tests were performed to generate mean ratios (AD vs control) with confidence intervals and Kruskal-Wallis p-values. In certain cases, the confidence interval "llim" and/or "ulim" values were uninterpretable or not available (^{NA}) (i.e. the confidence interval in these cases being too large to be calculated). In such cases, the calculated fold-change was not considered significant regardless of the p-value.

More in-depth statistical analysis was carried out for a subset of the metabolites involved in the polyol pathway, including glucose, sorbitol, and fructose. The analysis applied to the polyol pathway metabolites is computationally intense and was therefore not practical for application to all the metabolites reported in the study.

The LECO GC-MS software provided metabolite identification and integrated peak area quantifications. Three metabolites were identified as glucose derivatives, two as fructose, and one as sorbitol. Manual verification of the mass spectra across all samples led to the discounting of two glucose-related metabolites and one fructose-related metabolite due to the occasional appearance of overlapping interferences. In the remaining glucose, fructose and sorbitol signals, a small number of software peak mis-assignments were corrected by manually selecting the correct peak for subsequent quantification.

The raw data were log-transformed, with normality and outliers evaluated by QQ plot and Cook's D statistic respectively. Initial assessment of differential expression between case and control samples was performed with Welch's unequal variance *t*-test on each metabolite from each brain region separately. This process showed that levels of these metabolites were elevated in the case group in every comparison (two-sided test, 5% significance level, with false discovery rate adjustment by the Benjamini-Hochberg method).

3.2.6. LC-MS

3.2.6.1. Sample preparation

Extracted and dried samples stored at 4 ^{o}C were reconstituted in 150 µL of MeOH:H_2O (1:1), vortexed until the pellet was re-suspended and then centrifuged at 16,000 × g for 15 min (room temp). From each individual sample (including QCs and blanks), 100 µL was transferred into vials for Orbitrap loading.

3.2.6.2. LC-MS Analysis

LC-MS analysis was carried out with an Accela UHPLC system coupled to an Orbitrap Velos mass spectrometer equipped with a heated electrospray ionisation source (HESI) (ThermoFisher Scientific, Hemel Hempstead, UK). Aliquots of 10 µL were injected and Chromatographic separations were performed on a Hypersil GOLD column (100 × 2.1 mm, 1.9 µm; ThermoFisher Scientific, Runcorn, UK) operating at a column temperature of 50 °C. Samples were analysed separately in positive ("pos")- and negative ("neg")-ion modes to cover metabolites that preferentially ionise in either mode. Two solvents were applied (solvent A - 0.1% (v/v) formic acid in water (vol/vol) and solvent B - 0.1% (v/v) formic acid in methanol (vol/vol)) at a flow rate of 400 µL/min. Solvent A was held at 100% for 0.5 min followed by an increase to 100% solvent B over 4.5 min, which was then held for a further 15.5 min. A step change to 100% solvent A was performed at 20.5 min and then held to equilibrate for 1.5 min. All column eluent was transferred to the mass spectrometer and full-scan profiling data were acquired in the Orbitrap mass analyser (mass resolution 30,000 at m/z = 400). The source and ion transfer parameters applied were as follows: source heater = 200 °C, sheath gas = 50 (arbitrary units), aux gas = 15 (arbitrary units), capillary temperature = 300 °C, ISpray voltage = 4.5 kV (positive-ion mode) and 3 kV (negative-ion mode), slens = 60% (positive-ion mode) 65% (negative-ion mode) and AGC = 5 x 10^5.

As for GC-MS, the analysis was performed as a series of single batch experiments, in which a specific brain region constituted a batch. Within each batch, individual cases and controls were randomised, and run in a sequence interleaved with injections of the pooled QC (once per three study samples) and extraction blanks (one per batch). Ten "lead-in" injections of QC were performed for LC-MS.

3.2.6.3. Manual removal of PEG-contaminated samples:

Unexpectedly, the LC-MS analysis showed polyethylene glycol (PEG) in some brain tissues, with the HP and ENT groups showing the largest number of PEG-contaminated samples. A retrospective investigation revealed the likely origin of PEG in the samples, brain blocks which had previously been sectioned for histological and/or immuno-histochemical examinations by others; the OCT, containing 4.26% PEG, is commonly used in the Brain Bank for embedding tissue prior to sectioning. Although the OCT was removed after sectioning, it may well have been carried over into some of our samples during collection steps.

Although PEG contamination was not problematic for GC-MS, it caused major effects on the LC-MS data set. We therefore performed manual clean-up of the chromatograms via two steps. The first step was to exclude overtly PEG-contaminated samples; for HP and ENT, heavily-, intermediately-, and lightly-contaminated samples were removed successively from the statistical analysis (**Table 3-5**). SCx and MCx had less PEG-contaminated samples and they were all removed at a single step (**Table 3-5**). MTG, CG, and CB were free of PEG-contaminated samples. The second step was to remove data from

regions of the chromatograms showing residual PEG contamination; all peaks in the region (about 1 min wide) where PEG was observed were removed. Data for corresponding regions were removed for all brain regions.

The above steps were considered likely to have cleared most of the features directly attributable to the PEG-contamination. High levels of PEG in the sample could however affect both the RT and the sensitivity for other metabolites. Such an effect can only be traced by manual examination of various outputs such as the "fold-changes" with and without the contaminated samples for all the metabolites, a labour intensive procedure that was not applied to this study.

Sample 14 was removed from HP due to low response for most of the metabolites detected and sample 10 was automatically removed by the software as an outlier from CB during analysis (Table 3-5).

Table 3-5: Removal of PEG-contaminated samples for LC-MS study

Brain regions	Heavily contaminated samples	Intermediately contaminated samples	Lightly contaminated samples	Outlier	Remaining # of AD samples	Remaining # of control samples
HP	9, 17	7, 12	11	14	7	4
ENT	6, 12	7, 9	None	None	6	7
MTG	None	None	None	None	9	8
SCx	None	11, 12, 18	None	None	9	5
MCx	None	11, 12,	None	None	9	6
CG	None	None	None	None	9	8
CB	None	None	None	10	9	7

With awareness of the confounding effects of PEG contamination, it was decided to clean up the data and carry on further analysis, considering the precious nature of our human brain tissue samples.

3.2.6.4. Data reduction for LC-MS

LC-MS data reduction was carried out by following procedures as described in Dunn *et al*. [195], excluding those aspects related to QC drift correction and alignment of multiple batches of a single experiment, neither of which were shown to be required in this work. Briefly, XCMS was used to identify m/z features and align these across the set of samples for each brain region, using its "Matched filter" algorithm. Tables of aligned m/z features were then submitted to MetAnalyse, an in-house utility running under R [196] which allowed normalisation, PCA visualisations and univariate statistical tests to be generated. Putative Metabolite Identifications were generated using the PutMedID workflow [197]. It should be emphasised that PutMedID generates putative ID's, some of which are of low reliability, and that extensive post-processing inspection and editing is required before ID's generated can be accepted as reasonable.

3.2.6.5. Manual data processing performed for interpretation of LC-MS data

The LC-MS datasets were subjected to manual data reduction to remove any features or IDs made with little confidence. As noted earlier, due to limitations in the available software tool, the analytical process generated substantial numbers of nominated candidate ID's which were evidently unreliable. Before proceeding to attempt biological or clinical interpretation of the resulting data, it was essential to edit out as many of these unlikely "possibilities" as possible, to focus attention on those which were deemed to be more reliable or probable.

First of all, features with retention time < 90 seconds were removed from the dataset since no true separation was occurring during that phase of the chromatogram. The second step of pruning involved removing all the Metgroups that could not be interpreted with confidence. A particular Metgroup number represents a set of m/z features which the software recognises as a mass spectrum for a metabolite. Therefore, features within a particular Metgroup are supposed to be multiple measurements of or related to a single metabolite and should therefore generate similar calculated fold-changes, as long as all the features are of sufficient intensity. A typical Metgroup consists of a set of features with m/z interpreted as [M], [M+Na] (a sodium adduct), and [M+H] (protonated), along with their respective isotopes. Presence of different adducts allows more accurate inference of a molecular formula deduced from multiple signals. A minimum of two features, an M and its corresponding isotope (i.e. M+1), was required for a particular Metgroup to be carried forward for subsequent processing in this study. Metgroup 0 is an exception as it contains all the features that cannot be grouped by the software. In our dataset, Metgroup 0 features typically contain a single feature at a given RT; each m/z signal has been interpreted on its own without support from another signal. Examination of metabolites that were sorted into Metgroup 0 in this study showed a great number of highly questionable identifications of very low confidence. Therefore, all features within Metgroup 0 were removed from the subsequent analysis.

The remaining dataset was then sorted into groups by Metgroup and ion mode and the groups consisting of features with $p \geq 0.05$ (by Kruskal–Wallis test) were removed. Removal of statistically insignificant features in this step was done to minimise the labour-intensive manual processing down-stream. Manual pruning of the remaining data were carried out to remove unreasonable metabolites (e.g. drugs, alkaloids, flavonoids, phytochemicals, pesticides, herbicides, synthetic chemicals, etc.) that were judged to be improbable in the study population. Furthermore, the long list of IDs was manually reduced in cases where the system generated multiple redundant IDs. For example, PC (18:0/18:0) and PC (16:0/20:0) were reduced to PC (36:0) since the mass spectral information available did not allow specificity of fatty acid chain, but did allow compound class and total molecular weight to be inferred. Only one ID was retained for IDs with multiple stereochemical possibilities such as in the case of PC (P-16:0/18:1) and PC (16:0/P-18:0), or isomer-based effects such as for example 2-keto tridecanoic acid and 10-keto tridecanoic acid. Synonyms were also reduced to a single ID (e.g. lauric

acid and dodecanoic acid). Finally, IDs that were detected in the "wrong" ion-mode were removed (e.g. triacylglycerols do not ionise in the negative ion-mode).

Then each group (a Metgroup + an ion-mode) containing multiple features, was reduced to one feature. The feature with the highest MPA value was retained if it was statistically significant and only the IDs that were consistently reported in all the features were retained during this procedure. In rare cases where features within a group had no overlapping IDs, the entire group was deleted.

IDs with unlikely adducts were also removed from the dataset. In both ion-modes, IDs matched to Na_Na, Na_HCOONa, HCOOK, HCOONa, NaCl, NaClx2, NaCl_HCOONa, and KCl adducts were removed. None of these can be absolutely ruled out but they are relatively unlikely for the classes of molecules detected in the chloroform extracts. For example, Na_Na implies that there would be two separate, negatively-polarised regions in the molecule where sodium ions would bind. The primarily lipid molecules we detected in these fractions generally have small polar-regions (for example, the head group on certain classes of lipids, such as phosphatidylcholines), and it was considered unlikely that two Na^+ ions could bind to such compact structures, for example. In the "neg" ion-mode, IDs matched to K^+ and Na^+ adducts were also removed. These are very unlikely to occur in this mode, since the ion measured is negatively charged and invoking either of these two adducts would imply the initial attachment of a positive ion to the molecule.

Features containing IDs belonging to different main classes of metabolites were removed as they provide no specific information with additional interpretational value. Finally, if a metabolite was observed in both the positive and the negative ion-mode, only the feature with the stronger signal was retained and bolded in the result tables to indicate that these are "higher confidence" ID's as the data in both ion modes is supporting the same inference.

3.3. Results

3.3.1. Overview

3.3.1.1. Principal Component Analysis

The change in metabolites was measured by both GC-MS and LC-MS in brain tissues dissected from seven brain regions of nine AD brains and eight control brains. The datasets were used to generate PCA plot to assess the quality of each brain region experiment. A good experiment produces a PCA plot where the following apply: 1) biological variation is greater than technical variation (QCs group together as they are the same, and each biological class covers a larger area on the plot than the QCs); and 2) the biological classes are separated from each other (for example, in this study different

metabolite 'fingerprints' would be apparent between AD and control samples). We also examined the absence of a run-order effect, which would show up with early injected samples in one region; later-injected samples grouped in different regions of the plot. This approach is also an efficient way to identify outliers and to investigate further possibilities.

In this study, PCA analysis was performed after the automatic removal of outliers by the software and manual removal of PEG-contaminated samples for LC-MS.

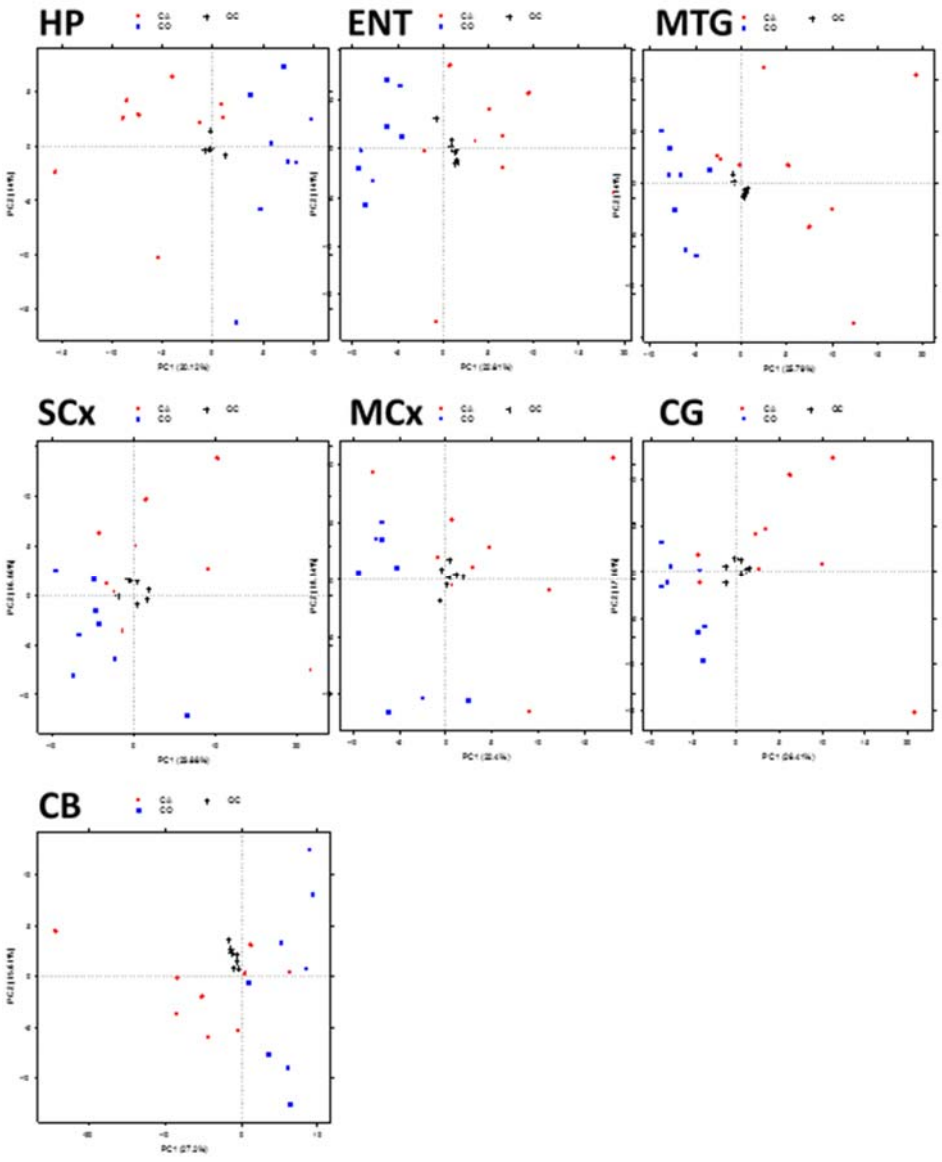

Figure 3-3 PCA scores biplot of seven brain regions in GC-MS study

In the GC-MS study, all seven brain regions exhibited good class separation between AD (red dots) and control (blue dots) samples. Technical variation was small as indicated by the tightly scattered QC samples (black crosses). Each dot in the plot corresponds to an individual sample.

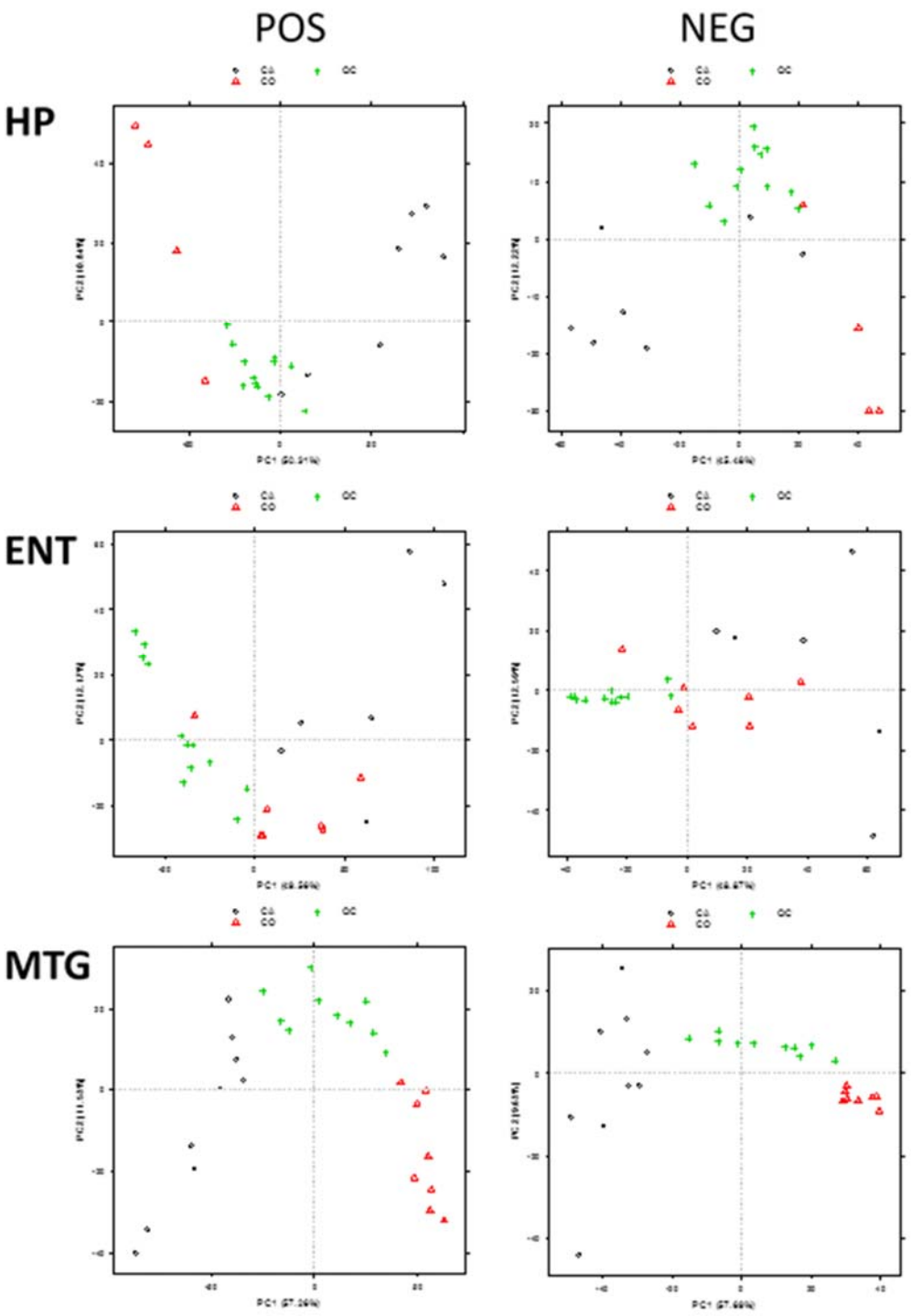

Figure 3-4 PCA scores biplot of HP, ENT, and MTG in LC-MS study

HP, ENT and MTG showed class separation between AD (black circles) and control (red triangles) samples. Technical variation of the LC-MS methodology applied was not ideal as indicated by the scattering QC samples (green crosses). Each dot in the plot corresponds to an individual sample.

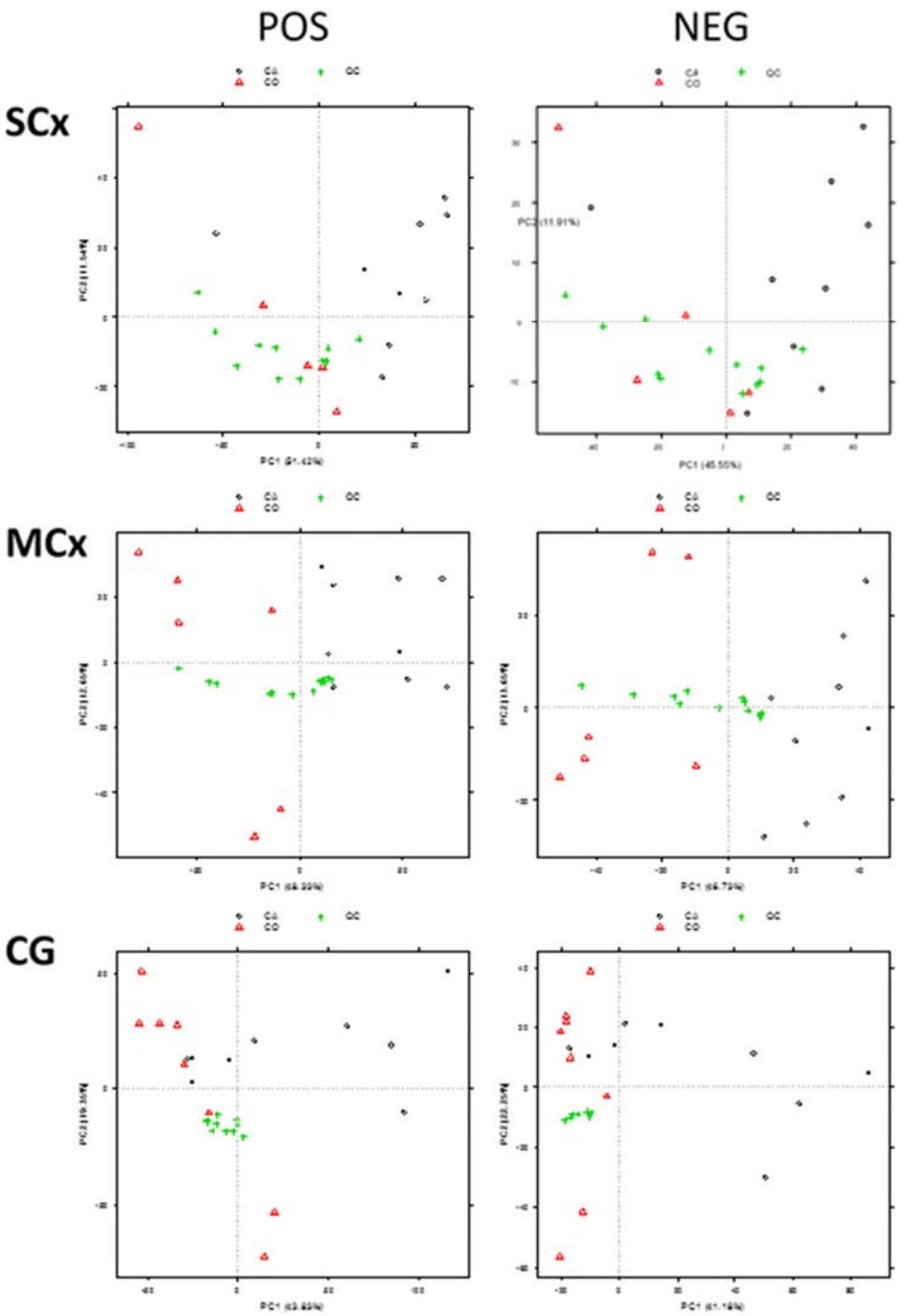

Figure 3-5 PCA scores biplot of SCx, MCx and CG in LC-MS study

SCx, MCx and CG showed class separation between AD (black circles) and control (red triangles) samples. In both SCx and MCx, technical variation was not ideal as indicated by the scattering QC samples (green crosses). Technical variation was small in CG. Each dot in the plot corresponds to an individual sample.

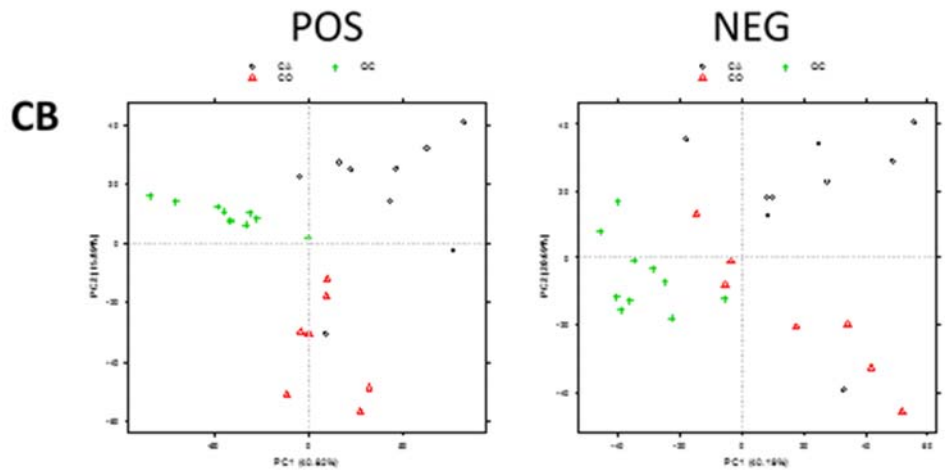

Figure 3-6 PCA scores biplot of CB in LC-MS study

CB showed class separation between AD (black circles) and control (red triangles) samples. Technical variation was not ideal as indicated by the scattering QC samples (green crosses). Each dot in the plot corresponds to an individual sample.

In the GC-MS study, strong group separation was observed in HP, ENT, MTG, SCx, and MCx. Weaker, but still clear separation was observed in CG and CB (**Figure 3-3**).

In the LC-MS study, PCA was performed for both datasets obtained from the positive- and negative-ion modes. Group separation was observed in all brain regions. However, technical variations of the LC-MS methodology was not ideal (**Figure 3-4, Figure 3-5, Figure 3-6**), when compared to that of GC-MS.

After examining the PCA plots to gain confidence that the experiment was successful, statistical analysis was performed for individual metabolites.

3.3.1.2. GC-MS overview

Of the 191 features detected by GC-MS, we report 98 features that were "IDed" with varying levels of confidence (**Table 3-4**). Features that were subject to interference on the chromatogram and those that were considered to be the minor derivatisation products of other metabolites were not reported. This generated a residuum of 68 IDs with good confidence (i.e. definitive/confident putative) and 30 IDs with less confidence (i.e. putative). Finally, 72 metabolites of the 98 measured showed significant ($p < 0.05$) differences between cases and controls in at least one of the studied brain regions (**Table 3-6**).

Table 3-6: Number of metabolites and the confidence level by which they were identified in the GC-MS study summary for GC-MS study

ID	all	p<0.05 in at least 1 brain region
Definitive+Confident putative	68	47
Putative	30	25
Total	98	72

The overall trend across the seven brain regions was that more metabolites were unaltered (range 60~73) than altered (range 25~38). Of the metabolites that showed significant difference between AD and control groups, more were increased (range 18~29) than decreased (range 3~13) in the AD brains (Figure 3-7).

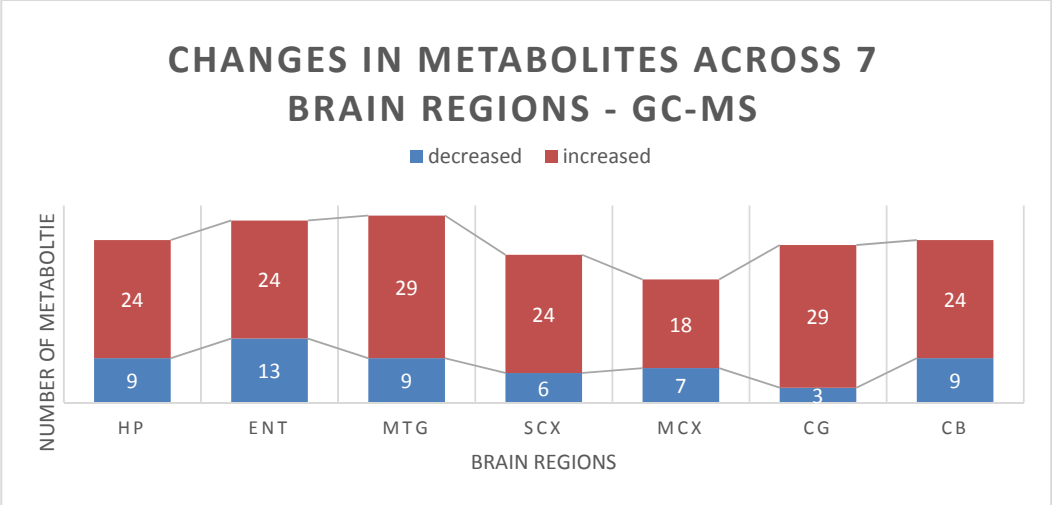

Figure 3-7 Overview of the changes in metabolites in GC-MS study

The distribution of altered metabolites (p-value <0.05) detected in GC-MS study showed similar pattern in all brain regions; more metabolites were increased than decreased. Total numbers of altered metabolites were comparable among brain regions.

The total number of metabolites that were altered in AD was comparable between the brain regions under examination in this study. The high-impact regions (HP, ENT, and MTG) and the low-impact regions (SCx, MCx, and CG) did not exhibit notable differences and surprisingly, CB, conventionally believed to be spared in AD, exhibited a similar degree of changes in metabolites compared to other regions (Figure 3-8).

3.3.1.3. LC-MS overview

In contrast to the GC-MS study, more metabolites were decreased than increased in level according to the LC-MS study (Figure 3-8). Again, CB exhibited a similar degree of metabolite alteration as the rest of the brain regions. Interestingly, unlike the other brain regions, CB was the only region with more metabolites increased than decreased in the LC-MS study. The metabolite IDs identified in LC-MS study have all been considered to be putative, although some features are presented with stronger confidence, having been deduced from multiple observations/detection.

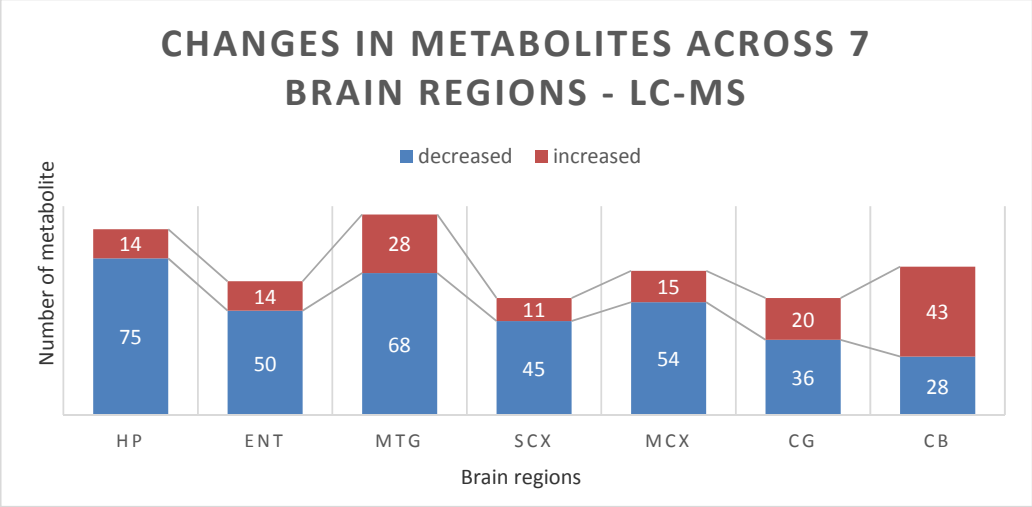

Figure 3-8 Overview of the changes in metabolites in LC-MS study

The distribution of altered metabolites (p-value <0.05) detected in LC-MS study showed similar pattern in all brain regions; more metabolites were decreased than increased. Total numbers of altered metabolites appeared to be slightly greater in HP and MTG compared to the other brain regions.

3.3.2. Specific changes in metabolites – GC-MS

3.3.2.1. Polyol pathway

Free glucose (non-phosphorylated) levels were markedly elevated in AD brains in every region studied. Mean (± 95% CI) fold-elevations in glucose varied from the highest of 17.4 (5.7~53.7) in the MTG, followed by MCx, SCx, HP, CG and ENT in order of magnitude, and the lowest value of 6.9 (2~23.6) in the CB. Sorbitol is the first committed metabolite of the polyol (or sorbitol-aldose reductase) pathway of glucose metabolism, which is usually a minor route of tissue glucose clearance in mammals [198]. Here we found that brain sorbitol levels were markedly elevated in all seven brain regions in AD patients compared with controls. Fold-elevations in sorbitol ranged from the lowest value of 3.4 (1.7~7.0) in MCx to the highest of 5.3 (2.7~10.4) in the ENT. Fructose is the second metabolite in the polyol pathway of

glucose metabolism in mammals [198]. Here, we found that brain fructose levels in AD patients were markedly elevated in all seven brain regions studied compared with controls, consistent with the changes in glucose and sorbitol levels. Mean (± 95% CI) elevations in fold-changes in fructose varied from 4.6 (2.1~10.1) in the MCxto 7.1 (2.8~18.1) in the CB. Variability in sorbitol and fructose values between brain regions tended to be less than that for glucose and there was no evidence of different levels of elevation in sorbitol and fructose between brain regions. Fold-changes in glucose across all regions were markedly higher than those of the other two polyol pathway metabolites, whereas values for sorbitol and fructose did not differ significantly from each other (**Table 3-7**).

Table 3-7: Changes amongst polyol pathway intermediates

	HP	ENT	MTG	SCx	MCx	CG	CB
Polyol pathway							
Glucose/117 (D)	9.9***(3.25/30.2)	8***(2.57/24.88)	17.42***(5.65/53.68)	10.77***(3.5/33.1)	12.3***(3.88/38.99)	9.31***(2.88/30.13)	6.87***(2/23.59)
Sorbitol (D)	5.03***(2.62/9.67)	5.3***(2.71/10.37)	3.86***(1.96/7.61)	4.98***(2.56/9.68)	3.42***(1.68/6.97)	3.84***(1.99/7.38)	4.58***(2.08/10.11)
Fructose/112 (D)	6.98***(3.26/14.93)	7.05***(3.23/15.36)	7.02***(3.44/14.32)	6.8***(3.3/13.99)	4.58***(2.09/10.05)	4.79***(2.24/10.23)	7.14***(2.82/18.09)

Metabolite ID confidence: Definitive (D). Alteration in metabolite levels across seven brain regions shown as AD/control ratio$^{\text{statistical significance}}$ (llim/ulim). Abbreviations: ***, p<0.01; llim, lower limit of detection; ulim, upper limit of detection.

3.3.2.2. Metabolites of the Glycolytic pathway & Pentose-phosphate pathway

Table 3-8: Changes amongst glycolytic and pentose-phosphate pathway intermediates

	HP	ENT	MTG	SCx	MCx	CG	CB
Glycolysis							
Glucose-6-P (D)	19.59***(7.03/46.42	6.35***(NA)	12.96***(4.27/32.77)	5.6***(2.22/22.09)	7.88***(3.12/32.95)	6.51***(2.77/18.2)	4.66**(0.35/23.72)
Fructose-6-P (P)	0.78^{NS}(0.52/1.21)	0.66**(0.47/0.89)	0.78**(0.61/0.98)	1.07^{NS}(0.77/1.48)	1.08^{NS}(0.76/1.59)	0.94^{NS}(0.67/1.35)	0.88^{NS}(0.66/1.2)
Pentose-phosphate pathway							
Pentonic acid-1,4-lactone (P)	1.61**(1.04/2.31)	1.22^{NS}(0.96/1.52)	1.71***(1.26/2.27)	1.25^{NS}(0.92/1.76)	1.86*(1.09/2.84)	2.44***(1.07/3.98)	1.61**(1.15/2.35)
Pentonic acid-91 (P)	0.97^{NS}(0.64/1.69)	1.31**(1.07/1.61)	1.32**(1.05/1.62)	1.11^{NS}(0.75/1.83)	1.31**(0.99/1.81)	1.46***(1.13/1.86)	1.23^{NS}(0.86/1.79)
Pentonic acid-97 (P)	2.01**(1.13/3.91)	2.01***(1.38/2.88)	1.96***(1.34/2.77)	1.66**(1.13/2.62)	1.75**(1.18/2.55)	1.96**(1.25/2.98)	1.79*(0.96/3.36)
Arabinofuranose/Arabinose (P)	3***(1.75/6.76)	2.34*(0.82/5.85)	4.41***(2.11/7.01)	2.75***(1.55/6.88)	5.15***(1.85/166.51)	3.05***(1.4/6.26)	3.06**(1.23/16.37)
Arabic acid (P)	1.4^{NS}(0.88/2.08)	0.8^{NS}(0.55/1.1)	2.03^{NS}(1.09/3.04)	1.3^{NS}(0.82/1.89)	1.29^{NS}(0.82/2.06)	1.56*(0.96/2.46)	2.04**(1.19/3.3)
Erythronic acid (P)	1.56**(1.03/2.5)	1.78***(1.29/2.42)	1.2^{NS}(0.87/1.55)	1.2^{NS}(0.85/1.74)	1.17^{NS}(0.91/1.49)	1.41*(1.01/1.95)	1.58^{NS}(0.97/2.31)

Metabolite ID confidence: Definitive (D) and Putative (P). Alteration in metabolite levels across seven brain regions shown as AD/control ratio$^{\text{statistical significance}}$ (llim/ulim). Abbreviations: *, p <0.1; **, p<0.05; ***, p<0.01; ^{NS}, not significant; NA, not available; llim, lower limit of detection; ulim, upper limit of detection.

Under normal circumstances, brain energy is mainly provided by the oxidation of glucose through glycolysis. The first two steps of glycolysis consist of enzyme-catalysed reactions whereby glucose is converted to glucose-6-P, followed by glucose-6-P to fructose-6-P. Here, levels of glucose-6-P were highly elevated in all AD brain regions, although statistical significance was not reached in ENT and CB by the methods employed. The fold-elevation of glucose-6-P was greater in HP and MTG, 13.0 and 19.6 respectively, compared to SCx, MCx and CG (which ranged from 5.6 to 7.9), showing a pattern resembling that of glucose levels in different brain regions. Interestingly, fructose-6-P (putative ID) levels were significantly lower in ENT and MTG of AD brain compared to that of controls (**Table 3-8**).

The pentose-phosphate pathway, a metabolic pathway that provides a (usually minor) alternative route of glucose metabolism, makes a small contribution to glucose metabolism by converting glucose-6-P to NADPH and pentoses (five-carbon sugars). The levels of pentoses were also elevated in the AD brains, varying from 1.3- to 5.2-fold among different pentoses and different brain regions. Arabinose is an aldopentose and arabic acid is also known as pentonic acid. Erythronic acid has been identified as a major hallmark of pentose-phosphate pathway defects [199]: in our study, erythronic acid levels were significantly higher in HP, ENT and CG, with fold-elevations ranging from 1.4 to 1. 8. However, it should be noted that all IDs within this category were putative and are therefore provided with a lower degree of confidence than those designated otherwise (**Table 3-8**).

3.3.2.3. Alternative fuels

Although glucose is the obligatory energy-generating substrate in the brain, other substrates can also be utilised as alternative fuel sources by the brain, to provide up to half of overall energy requirements under certain physiological circumstances (for example, the ketosis of starvation or the keto-acidosis of type-1 diabetes). Here we found that the levels of butanediol, a precursor for formation of ketone bodies (specifically acetone, acetoacetate and beta-hydroxybutyrate), were increased by more than 3-fold in all brain regions except for MTG. The levels of the ketone body β-hydroxybutyrate were elevated more than 2-fold in all brain regions except for HP, MTG and CB, consistent with up-regulation of the ketone body formation pathway and/or decreased mitochondrial clearance of ketone bodies. Lactic acid was increased by more than 2-fold in HP and MCx. Increased 2-hydroxy-3-methylbutyric acid has previously linked to lactic- and keto-acidosis [200]. Here, the levels of 2-hydroxy-3-methylbutyric acid were also strongly elevated in HP, SCx, and CG, ranging from 3.8 to 7.6-fold, again consistent with increased production or decreased utilization/clearance of ketone body.

The level of threitol was also consistently elevated throughout all seven brain regions, ranging from 1.8- to 3.1-fold. Xylitol was elevated in HP, CG and CB (1.5- to 1.8-fold). N-acetylglucosamine was elevated from 1. 7- to 1.8- fold in MTG, CG, and CB. Although myoinositol was only significantly increased in

ENT (1.3-fold), the derivative myoinositol-1-P was significantly elevated in all brain regions except for SCx, and to a higher degree (1.9- to 4.2-fold) (Table 3-9).

3.3.2.4. Nucleobases, nucleosides and their catabolites

We detected levels of three free nucleobases, adenine, guanine, and uracil (Table 3-10). Adenine and guanine are both purines: adenine was significantly elevated 1.7-fold in the CB, and guanine was significantly increased, by 2.0- and 1.5-fold in MTG and SCx, respectively. Hypoxanthine, which is not incorporated into nucleic acids but is an important intermediate in the synthesis and degradation of purine bases, was decreased (to 0.8-fold of control) in ENT, MTG, SCx, and CB. Uric acid is the final breakdown product of purine catabolism in humans, and, in contrast to hypoxanthine it was significantly elevated in all brain regions except the HP and CG. The fold-elevation of uric acid ranged from 3.0- in CB to 23.7-fold in MTG. Uracil, a pyrimidine component of RNA, was markedly decreased in all brain regions examined, with levels that ranged from 0.5- to 0.7-fold of control values.

Guanosine is a ribonucleoside comprising the purine base guanine attached to a ribose ring: here, its level was increased to 2.3-fold of control values in the MTG. Elevations in levels of purines and pyrimidines and their catabolites are consistent with increased rates of nucleic acid breakdown or turnover.

Table 3-9: Changes amongst metabolites relating to alternative fuels

	HP	ENT	MTG	SCx	MCx	CG	CB
Alternative fuel/ Sugars and alike							
Butanediol (CP)	5.39**(2/16.26)	3.49***(2.06/6.01)	1.92^{NS}(0.71/4.73)	3.32***(1.9/6.82)	4.82***(2.31/27.05)	3.61***(2.69/4.74)	3.76**(1.68/9.04)
β-Hydroxybutyric acid (D)	2.42^{NS}(0.99/4.41)	2.07**(1.21/3.5)	1.7^{NS}(0.9/2.63)	2.81**(1.51/6.4)	2.09*(1.17/3.2)	2.43***(1.62/3.29)	1.98^{NS}(0.78/3.72)
Lactic acid (CP)	2***(1.23/3.77)	0.85^{NS}(0.31/1.45)	1.24^{NS}(0.66/2.23)	1.33**(0.88/2.14)	2.13**(1.03/6.74)	1.34NS(0.84/2.29)	0.78^{NS}(0.21/1.75)
2-hydroxy-3-methylbutyric acid (P)	7.62***(3.16/26.73)	0.83**(NA)	0.69*(NA)	4.28***(1.9/9.33)	1.48^{NS}(NA)	3.84**(1.72/11.05)	1.18**(NA)
Threitol (D)	1.78**(1.09/3.42)	2.18***(1.43/3.08)	1.78**(1.12/2.59)	2.23***(1.58/2.99)	2.1***(1.52/2.79)	2.1***(1.56/2.88)	3.14***(1.52/4.9)
Xylitol-79 (P)	1.68**(1.17/2.37)	1.33^{NS}(0.91/1.88)	1.33^{NS}(0.84/1.92)	1.22^{NS}(0.82/1.72)	1.21^{NS}(0.81/1.74)	1.48**(1.05/1.98)	1.82**(1.16/2.75)
Disaccaride (P)	5.86**(2.34/11.48)	6.42**(-4.13/18.77)	4.9**(0.52/9.89)	8.25^{NS}(-1.63/21.97)	0.88^{NS}(NA)	1.77**(1.05/3.27)	1.01^{NS}(0.48/1.79)
N-acetylglucosamine (CP)	1.13^{NS}(0.55/2.66)	1.19^{NS}(0.67/1.81)	1.83***(1.24/2.46)	1.47**(0.98/2.07)	1.32^{NS}(0.91/1.99)	1.67***(1.22/2.2)	1.71**(1.12/3.28)
Myo-Inositol (D)	1.03^{NS}(0.84/1.28)	1.26**(1.05/1.54)	1.05^{NS}(0.89/1.23)	1.07^{NS}(0.96/1.21)	0.92^{NS}(0.79/1.05)	0.88^{NS}(0.73/1.04)	0.96^{NS}(0.84/1.09)
Myo-Inositol-1P (P)	2.18**(1.16/4.17)	2.03**(1.23/3.23)	4.2***(2.05/8.49)	1.79^{NS}(0.88/3.27)	1.88**(1.08/3.98)	3.53***(1.9/7.77)	3.09**(1.45/10.33)

Metabolite ID confidence: Definitive (D), Confident Putative (CP), and Putative (P). Alteration in metabolite levels across seven brain regions shown as AD/control ratio$^{\text{statistical significance}}$ (llim/ulim). Abbreviations: *, p <0.1; **, p<0.05; ***, p<0.01; ^{NS}, not significant; NA, not available; llim, lower limit of detection; ulim, upper limit of detection.

Table 3-10: Changes amongst nucleobases and nucleosides

	HP	ENT	MTG	SCx	MCx	CG	CB
Nucleobase/nucleoside & metabolites							
Adenine (CP)	0.95^{NS}(0.67/1.36)	1.04^{NS}(0.66/1.56)	0.91^{NS}(0.72/1.13)	0.88^{NS}(0.56/1.55)	0.86^{NS}(0.59/1.31)	0.87^{NS}(0.57/1.43)	1.7***(1.22/2.42)
Guanine (P)	0.7^{NS}(0.31/3.6)	0.89(NA)	2.0**(1.22/3.62)	1.48*(1/2.35)	2.15*(0.99/4.48)	1.36*(0.99/1.89)	1.43^{NS}(0.9/2.35)
Hypoxanthine (P)	0.8^{NS}(0.63/1.04)	0.8***(0.7/0.9)	0.78***(0.66/0.92)	0.79**(0.64/0.96)	0.79^{NS}(0.62/0.99)	0.88^{NS}(0.73/1.04)	0.8**(0.69/0.93)
Uric acid (CP)	3.97^{NS}(1.32/11.52)	9.4**(3.57/39.47)	23.68***(5.42/314.26)	7.48**(2.65/529.15)	4.83*(1.52/36.05)	7.11*(NA)	3.04*(1.31/6.2)
Uracil (CP)	0.58***(0.4/0.81)	0.54***(0.39/0.73)	0.59***(0.4/0.84)	0.64***(0.46/0.85)	0.58***(0.38/0.82)	0.61**(0.44/0.85)	0.69***(0.51/0.91)
Guanosine (P)	0.7^{NS}(0.25/1.81)	0.92^{NS}(0.25/2.3)	2.32**(1.19/4.76)	0.98^{NS}(0.46/2.12)	1.01^{NS}(NA)	2.13*(0.99/5)	1.7^{NS}(0.83/3.7)

Metabolite ID confidence: Confident Putative (CP) and Putative (P). Alteration in metabolite levels across seven brain regions shown as AD/control ratio$^{\text{statistical significance}}$ (llim/ulim). Abbreviations: *, p <0.1; **, p<0.05; ***, p<0.01; ^{NS}, not significant; NA, not available; llim, lower limit of detection; ulim, upper limit of detection.

3.3.2.5. Miscellaneous lipids

The human brain comprises nearly 60% complex lipids, and fatty acids are among the most crucial molecules that determine the integrity and performance of the brain [201]. Two fatty acids, namely myristic acid (or tetradecanoic acid) and heptadecanoic acid were increased in brain regions including MTG, MCx and CG (with significant elevations ranging from 1.2- to 1.4-fold). Cholesterol trended towards decrease in all regions studied, but statistical significance was reached only in MCx.

Glycerol provides the poly-alcohol backbone of triglycerides and glycerophospholipids. Here, levels of glycerol were significantly decreased in HP, ENT, and MCx (from 0.7- to 0.8-fold of control values). Oxidation of glycerol yields glyceric acid, which was significantly increased in MTG, CG, and CB, with fold-elevations ranging from 2.0 to 3.3, consistent with increased glycerol oxidation in AD brain. Glycerol can also be phosphorylated to form glycerol-3-P in the brain [202]. We found significantly elevated levels of glycerol-3-P in all brain regions except MTG, ranging from 1.4 to 2.1-fold.

3.3.2.6. TCA cycle & urea cycle metabolites

TCA cycle metabolites, including citric acid, succinic acid, fumaric acid, and malic acid were all elevated where the fold-changes were statistically significant. Citric acid levels were significantly elevated in brain of AD patients to levels of between 1.6- and 1.9-fold higher than controls in HP and ENT respectively. Significant elevations (to 1.4-fold of control values) in both succinic acid and fumaric acid were measured in MCx and CG, respectively, whereas malic acid levels were 1.8- to 2.4-fold increased in ENT and MTG, respectively.

Urea cycle (also known as the Ornithine cycle) metabolites were decreased in general. Urea levels were significantly lowered, to ~50% of control values in HP, MTG and CG. Consistently, ornithine levels were significantly decreased, to ~60% in HP and ENT, and ~40% in CB. N-acetylglutamic acid is the allosteric effector of carbamoyl phosphate synthetase, which plays a critical role in regulation of the urea cycle. The levels of N-acetylglutamic acid were decreased in general across all brain regions. However, the reduction in N-acetylglutamic acid levels was statistically significant only in ENT and MCx (to 0.8-fold of control values in both).

Table 3-11: Changes amongst simple lipids and related compounds

	HP	ENT	MTG	SCx	MCx	CG	CB
Simple lipids & related compounds							
Myristic acid (CP)	0.73^{NS}(0.52/1.17)	0.91^{NS}(0.7/1.17)	1.17**(1.01/1.38)	1.25^{NS}(0.83/1.94)	0.99^{NS}(0.72/1.38)	0.97^{NS}(0.63/1.35)	0.79^{NS}(0.54/1.09)
Heptadecanoic acid (CP)	1.17*(0.92/1.55)	1.18*(0.98/1.42)	1.36***(1.13/1.63)	1.23**(0.98/1.49)	1.25*(1.06/1.46)	1.32**(1.05/1.64)	1.22^{NS}(0.92/1.54)
Cholesterol (CP)	0.58^{NS}(0.32/2.07)	0.84^{NS}(0.59/1.18)	1.22^{NS}(0.91/1.63)	0.81^{NS}(0.49/1.29)	0.53**(0.35/0.87)	0.97^{NS}(0.69/1.31)	0.6^{NS}(0.28/1.36)
Glycerol metabolism							
Glycerol (CP)	0.73***(0.59/0.89)	0.78***(0.71/0.86)	0.89^{NS}(0.76/1.04)	0.87^{NS}(0.67/1.16)	0.78**(0.61/1)	0.97^{NS}(0.85/1.11)	0.96^{NS}(0.86/1.08)
Glyceric acid (P)	1.19^{NS}(0.68/2.41)	1.09^{NS}(0.55/2.21)	3.31***(1.62/5.36)	0.94^{NS}(0.51/3.08)	0.8^{NS}(0.43/2.4)	2.68***(1.9/3.58)	1.98***(1.27/2.76)
Glycerol-3-P (D)	1.75***(1.25/2.76)	2.08***(1.58/2.8)	1.3*(0.91/1.88)	1.75***(1.25/2.64)	1.75**(1.15/2.95)	1.47**(1.08/2.03)	1.38**(1.07/1.76)

Metabolite ID confidence: Definitive (D), Confident Putative (CP), and Putative (P). Alteration in metabolite levels across seven brain regions shown as AD/control ratio$^{\text{statistical significance}}$ (llim/ulim). Abbreviations: *, p <0.1; **, p<0.05; ***, p<0.01; ^{NS}, not significant; llim, lower limit of detection; ulim, upper limit of detection.

Table 3-12: Changes amongst TCA and urea cycle intermediates

	HP	ENT	MTG	SCx	MCx	CG	CB
TCA cycle							
Citric acid (D)	1.62***(1.16/2.29)	1.94***(1.21/3.67)	1.31^{NS}(0.79/2.79)	1.47**(0.98/2.39)	1.08^{NS}(0.66/1.92)	1.33^{NS}(0.79/2.15)	0.99^{NS}(0.57/1.84)
Succinic acid (CP)	1.29*(0.99/1.65)	0.82^{NS}(0.42/1.26)	1.11^{NS}(0.76/1.51)	1.2^{NS}(0.95/1.53)	1.35*(1.04/1.71)	1.25^{NS}(0.96/1.59)	1.29^{NS}(0.93/1.7)
Fumaric acid (CP)	2.31^{NS}(0.57/4.3)	1.27^{NS}(0.89/1.83)	1.93^{NS}(0.99/3.13)	1.25^{NS}(0.65/1.95)	0.77^{NS}(0.46/1.26)	1.41*(1/1.91)	1.58^{NS}(0.61/2.63)
Malic acid (CP)	1.54^{NS}(1/2.4)	1.8**(1.14/3.21)	2.39**(1.36/4.58)	0.91^{NS}(0.56/1.69)	0.72^{NS}(0.38/1.63)	1.57*(0.94/2.6)	1.06^{NS}(0.57/1.68)
Urea cycle							
Urea (CP)	0.54**(0.31/0.92)	0.77^{NS}(0.38/1.65)	0.45**(0.28/0.95)	0.57**(0.21/1.03)	0.76^{NS}(0.33/1.42)	0.48**(0.28/0.82)	0.79^{NS}(0.42/1.44)
Ornithine (CP)	0.61*(0.41/0.97)	0.61*(0.4/0.99)	1.01^{NS}(0.66/1.59)	0.75^{NS}(0.45/1.28)	0.63^{NS}(0.34/1.67)	0.95^{NS}(0.53/1.6)	0.37**(0.16/0.79)
N-acetylglutamic acid (CP)	0.61*(0.32/1.03)	0.81*(0.64/0.99)	0.91^{NS}(0.7/1.18)	0.88^{NS}(0.69/1.1)	0.75**(0.59/0.95)	0.84^{NS}(0.7/1.04)	0.99^{NS}(0.78/1.22)
Creatinine (CP)	1.08^{NS}(0.96/1.23)	1.01^{NS}(0.91/1.12)	1.26***(1.14/1.39)	1^{NS}(0.88/1.14)	0.99^{NS}(0.85/1.17)	1.09^{NS}(0.97/1.23)	1.11**(1.03/1.2)

Metabolite ID confidence: Definitive (D) and Confident Putative (CP). Alteration in metabolite levels across seven brain regions shown as AD/control ratio$^{\text{statistical significance}}$ (llim/ulim). Abbreviations: *, p <0.1; **, p<0.05; ***, p<0.01; ^{NS}, not significant; llim, lower limit of detection; ulim, upper limit of detection.

3.3.2.7. Amino acids

Table 3-13: Changes amongst amino acids and related metabolites

	HP	ENT	MTG	SCx	MCx	CG	CB
Amino acids							
Leucine (D)	0.81*(0.55/1.26)	0.73*(0.54/0.95)	0.85^{NS}(0.61/1.17)	0.73^{NS}(0.52/1.02)	0.74^{NS}(0.46/1.17)	0.83^{NS}(0.4/1.32)	0.73**(0.54/0.99)
L-Threonine (D)	0.85^{NS}(0.63/1.19)	0.99^{NS}(0.69/1.57)	1.4**(1.11/1.78)	1.12^{NS}(0.7/1.83)	1.42^{NS}(0.74/4.06)	1.3^{NS}(0.94/1.81)	1.13^{NS}(0.75/2.17)
Valine (D)	0.93^{NS}(0.63/1.5)	0.93^{NS}(0.68/1.3)	1.52*(1.01/2.62)	1.03^{NS}(0.75/1.39)	0.84^{NS}(0.43/1.89)	1.3^{NS}(0.82/2.08)	0.71**(0.5/0.97)
Lysine (D)	0.57**(0.36/0.91)	0.74^{NS}(0.48/1.08)	1.13^{NS}(0.73/1.79)	0.89^{NS}(0.47/1.47)	0.99^{NS}(0.46/2.28)	1.09^{NS}(0.65/1.75)	0.54^{NS}(0.21/0.96)
Methionine (D)	0.98^{NS}(0.66/1.45)	0.93^{NS}(0.61/1.34)	1.39^{NS}(0.78/2.39)	0.98^{NS}(0.51/1.64)	1^{NS}(0.58/1.74)	1.48^{NS}(0.77/2.45)	0.64*(0.43/0.98)
l-Aspartic acid (D)	0.69**(0.5/0.93)	0.61***(0.44/0.83)	0.85^{NS}(0.58/1.19)	0.98^{NS}(0.68/1.4)	0.95^{NS}(0.5/1.81)	0.94^{NS}(0.62/1.44)	0.82^{NS}(0.57/1.22)
L-Aspartic acid (D)	0.88^{NS}(0.59/1.3)	0.75**(0.57/0.96)	0.96^{NS}(0.66/1.33)	1.07^{NS}(0.79/1.39)	1.1^{NS}(0.74/1.56)	0.93^{NS}(0.57/1.5)	0.77^{NS}(0.51/1.13)
N-acetylaspartic acid (CP)	0.85^{NS}(0.71/1.05)	0.93^{NS}(0.83/1.03)	0.88***(0.82/0.94)	1.02^{NS}(0.95/1.1)	0.96^{NS}(0.89/1.03)	0.96^{NS}(0.89/1.04)	0.99^{NS}(0.92/1.06)
Cysteine (D)	2.08**(1.29/3.24)	1.41^{NS}(0.84/2.74)	0.75^{NS}(0.53/1.06)	0.89^{NS}(0.56/1.47)	1.02^{NS}(0.62/1.89)	1.43*(1.06/1.89)	0.84^{NS}(0.6/1.23)
Glycine (D)	0.93^{NS}(0.81/1.07)	0.82***(0.75/0.89)	0.85**(0.75/0.97)	0.84*(0.7/0.99)	0.83^{NS}(0.66/1.02)	0.93^{NS}(0.78/1.09)	0.9^{NS}(0.8/1.03)
Proline (D)	0.51**(0.29/0.99)	0.38***(0.23/0.65)	0.47*(0.2/1.66)	0.69^{NS}(0.36/1.34)	0.78^{NS}(0.39/2.15)	0.75^{NS}(0.39/1.6)	0.45*(0.24/1.09)
Serine (P)	0.71**(0.52/0.96)	0.67***(0.54/0.85)	1.02^{NS}(0.72/1.41)	0.79^{NS}(0.54/1.14)	0.81^{NS}(0.54/1.24)	1.02^{NS}(0.72/1.41)	0.71**(0.55/0.95)
Phenylalanine (D)	1.21^{NS}(0.92/1.62)	1.13^{NS}(0.84/1.5)	1.77***(1.26/2.48)	1.41**(0.98/2.19)	1.55*(0.94/2.76)	1.73***(1.19/2.45)	1.23^{NS}(0.92/1.66)
Tyrosine (D)	1.6^{NS}(0.89/3.22)	1.89**(1.11/2.85)	2.8***(1.55/4.66)	1.79^{NS}(1/3.08)	2.34*(1.02/7.12)	2.97***(1.46/5.21)	1.31^{NS}(0.73/2.35)
Tryptophan (D)	2.59**(1.07/6.19)	2.72**(1.25/4.57)	5.67***(2.26/10.64)	2.33*(1.12/3.79)	2.35**(1.22/10.47)	5.03***(1.81/9.47)	1.03^{NS}(0.69/1.65)
L-Glutamic acid (P)	1.21^{NS}(0.99/1.5)	1.03^{NS}(0.87/1.2)	1^{NS}(0.9/1.11)	1.2**(1.02/1.43)	1.25^{NS}(0.9/1.7)	1.16**(1.01/1.35)	1.41^{NS}(0.95/2.66)
Pyroglutamic acid (D)	1.04^{NS}(0.94/1.16)	1.06*(1/1.12)	1.02^{NS}(0.95/1.09)	1.07**(1.01/1.14)	1.1**(1.01/1.2)	1.04^{NS}(0.95/1.13)	1.02^{NS}(0.94/1.1)
4-aminobutyric acid (P)	1.18^{NS}(0.87/1.68)	0.68***(0.57/0.82)	0.64***(0.54/0.75)	0.75**(0.61/0.93)	0.72**(0.52/0.99)	0.8*(0.57/1.19)	0.83^{NS}(0.62/1.09)
4-hydroxybutyric acid (CP)	0.74*(0.47/1.14)	0.65***(0.48/0.86)	1.06^{NS}(0.79/1.44)	0.76*(0.54/1.07)	0.79^{NS}(0.56/1.12)	0.87^{NS}(0.51/1.3)	0.71*(0.49/1.09)

Metabolite ID confidence: Definitive (D), Confident Putative (CP), and Putative (P). Alteration in metabolite levels across seven brain regions shown as AD/control ratio$^{\text{statistical significance}}$ (llim/ulim). Abbreviations: *, p <0.1; **, p<0.05; ***, p<0.01; ^{NS}, not significant; llim, lower limit of detection; ulim, upper limit of detection.

In this study, amino acids were identified with better confidence compared to other categories of metabolites (**Table 3-4**).

The levels of leucine were decreased to ~0.7-fold of control values in ENT and CB whereas threonine was significantly increased in MTG, to around 1.4-fold. Valine showed an increase in MTG (to 1.5-fold), whereas it was decreased in CB to 0.7-fold of control. The levels of lysine and methionine were both decreased to ~0.6-fold of control in HP and CB respectively. Aspartic acid levels were decreased to ~0.7-fold of control in HP and ENT. N-acetylaspartic acid levels were decreased to around 0.9-fold of in MTG. Cysteine levels were increased > 2-fold in HP and 1.4-fold in CG. Glycine, proline, and serine appeared to be globally decreased, although statistical significance was not reached in some brain regions. Glycine was down-regulated to 0.8-~0.9 in ENT, MTG, and SCx, and proline was decreased to ~0.3- to 0.5-fold in HP and ENT, and CB. Serine was significantly decreased to ~0.7-fold of control in HP, ENT, and CB.

The aromatic amino acids, including phenylalanine, tyrosine, and tryptophan, were elevated overall although statistical significance was not reached in some brain regions. Phenylalanine was elevated over 1.7-fold in MTG and CG. Tyrosine levels were increased between 1.9- to 3.0-fold in ENT, MTG, MCx, and CG. Tryptophan was markedly elevated in all brain regions apart from CB, with increments ranging from 2.3- to 5.7-fold.

Glutamic acid was increased to around 1.2-fold in SCx and CG. Pyroglutamic acid is known to form from glutamic acid during the process of GC-MS but may also form spontaneously *in vivo* [203]: here, pyroglutamic acid was slightly increased in ENT, SCx, and MCx. The levels of the neurotransmitter 4-aminobutyric acid (GABA) were significantly decreased in ENT, MTG, SCx, and MCx to ~0.6 to 0.8-fold of control. Gamma-hydroxybutyric acid is a GABA analogue that naturally occurs in the brain, where it is formed primarily from GABA [204]: here, gamma-hydroxybutyric acid was significantly decreased to 0.7-fold of control in EC.

3.3.2.8. Miscellaneous

Table 3-14: Changes amongst miscellaneous low molecular-weight metabolites

	HP	ENT	MTG	SCx	MCx	CG	CB
Miscellaneous low molecular-weight metabiolites							
Ethanolamine (P)	0.63**(0.42/0.9)	0.56***(0.34/0.81)	0.56***(0.4/0.76)	0.51***(0.38/0.72)	0.51**(0.34/0.81)	0.69**(0.49/0.98)	0.62***(0.43/0.87)
2-hydroxyglutaric acid (P)	1.82**(1.22/2.95)	2.02***(1.29/3.66)	1.79***(1.23/2.92)	1.55*(1.02/2.63)	1.51**(1.01/2.54)	1.73**(1.07/3.28)	1.22**(0.64/4.46)
Phosphoric acid, monomethyl ester (CP)	0.74^{NS}(0.53/1.04)	0.52***(0.35/0.74)	0.37***(0.31/0.44)	0.73*(0.49/1.09)	0.59^{NS}(0.35/1.07)	0.65^{NS}(0.38/1.1)	0.81^{NS}(0.63/1.05)
Phosphoric acid (CP)	1.06^{NS}(0.77/1.53)	1.02^{NS}(0.85/1.27)	0.78^{NS}(0.52/1.12)	0.92*(0.77/1.11)	0.86***(0.77/0.95)	0.79^{NS}(0.54/1.09)	0.96^{NS}(0.91/1.01)
N-bromosuccinimide (P)	1.17^{NS}(0.94/1.45)	1.22^{NS}(1.01/1.49)	1.21**(1.03/1.44)	1.18**(1.02/1.37)	1.24^{NS}(0.96/1.6)	1.26***(1.11/1.41)	1.09^{NS}(0.96/1.22)
L(+)-Ascorbic acid (P)	1.77*(1.02/3.49)	1.75**(1.11/2.78)	1.05^{NS}(0.72/1.62)	1.8**(0.92/3.58)	2.07***(1.27/3.37)	1.7*(0.99/2.54)	1.55^{NS}(0.84/2.76)
2-pyrrolidone-5-carboxylic acid (P)	1.48**(0.99/2.01)	1.14^{NS}(0.89/1.41)	1.05^{NS}(0.92/1.19)	1.14^{NS}(0.95/1.38)	1.16^{NS}(0.79/1.58)	1.1^{NS}(0.88/1.37)	1.52***(1.19/1.89)
3-hydroxypyridine (CP)	1.08^{NS}(0.89/1.35)	0.9*(0.78/1.04)	1^{NS}(0.89/1.13)	0.96^{NS}(0.84/1.1)	0.87^{NS}(0.72/1.07)	1.07^{NS}(0.92/1.25)	1.17**(1.02/1.33)
4-hydroxypyridine (CP)	1.1^{NS}(0.95/1.28)	0.98^{NS}(0.84/1.15)	0.91^{NS}(0.65/1.18)	0.95^{NS}(0.81/1.12)	0.91^{NS}(0.74/1.14)	1.15^{NS}(0.99/1.33)	1.19**(1.05/1.34)

Metabolite ID confidence: Confident Putative (CP), and Putative (P). Alteration in metabolite levels across seven brain regions shown as AD/control ratio$^{statistical\ significance}$ (llim/ulim). Abbreviations: *, p <0.1; **, p<0.05; ***, p<0.01; ^{NS}, not significant; llim, lower limit of detection; ulim, upper limit of detection.

Some of the metabolites here grouped as “miscellaneous” have previously been linked to brain disease (**Table 3-14**). Ethanolamine levels were significantly decreased in all brain regions, to 0.5- to 0.7-fold of control. 2-Hydroxyglutaric acid levels were elevated significantly in all brain regions (by 1.5- to 2-fold) except CB. Ascorbic acid (vitamin C) and N-bromosuccinimide levels were both increased in AD brain compared to controls whereas phosphoric acid was decreased significantly in MCx (to 0.9-fold).

3.3.3. Specific changes in metabolites – LC-MS

Definitions of the lipid structural classes referred to in this section and following parts of this thesis are accessible at the following URL: (http://www.lipidmaps.org/data/index.html). This database adopted a classification system in which each class of lipid is given a designated number that represent their position in the classification hierarchy.

In the system of LIPID MAPS, abbreviations such as PE and PC are used to refer to species with one or two radyl side-chains. The ‘O-’prefix is used to indicated the presence of an alkyl-ether substituent e.g. PC(O-16:0/18:1), whereas the ‘P-’ / ‘dm’ prefix is used for the alkenyl-ether (or Plasmalogen) substituents e.g. PC(P-16:0/18:1). For sphingolipids, the ‘d’ prefix is used for a dihydroxy base e.g. Cer(d18:1/18:0). Stereochemistry is also specified in the LIPID MAPS. However, our method does not distinguish the stereochemistry and therefore, is not relevant to the interpretation of our results.

3.3.3.1. Sphingolipids

Only two sphingoid bases were altered significantly in the current study (**Table 3-15**); both were elevated (1.3- to 1.7-fold). Ten species of ceramides were altered significantly in at least one brain region, most of which were found to be decreased. A few species, including Cer (d18:1/18:1), Cer (d18:1/18:0), Cer (d18:1/24:1) and Cer (d18:1/26:1) showed increased levels in CG and CB. By contrast, in HP, ENT, MTG, SCx and MCx, detected ceramides were significantly and consistently decreased. Elevations were observed in CG (2 out of 6) and CB (4 out of 6) for detected ceramides.

The pattern of changes in phosphosphingolipids were very similar to that of ceramides and all the phosphosphingolipids reported herein (**Table 3-16**) belong to the sub-class of ceramide phosphocholines (also termed sphingomyelins) [designated as SP0301]. Sphingomyelins detected in this study were decreased to ~0.2- to 0.8-fold of control in all brain regions except CB, where 4 out of 7 detected species showed an increase (1.2- to1.4-fold).

The changes in neutral glycosphingolipids (**Table 3-17**) were similar to those of ceramides and sphingomyelins. The neutral glycosphingolipids affected by AD were mainly glucosylceramides (GlcCer) and these were consistently decreased (to ~0.2- to 0.7-fold of control) in all brain regions

except for CB, where every detected species with statistical significance was increased (ranging from 1.3- to 1.6-fold).

Of those detected in this study, the only species of acidic glycosphingolipid that changed significantly in the AD brain was the sulphatide, which decreased to 0.3- and 0.4-fold of control in MCx and CG respectively.

Structures of representative sphingolipid species are shown in **Figure 3-9**.

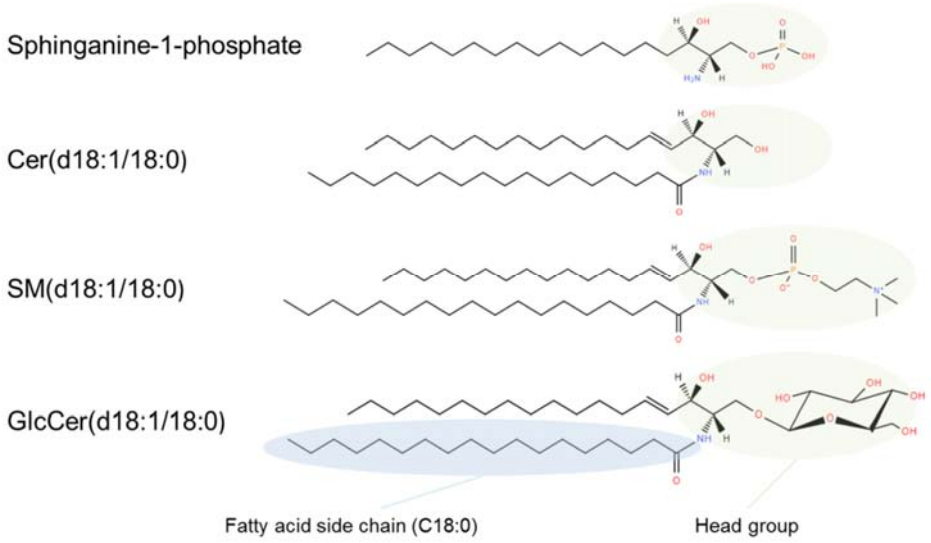

Figure 3-9 Structures of representative sphingolipid species.

The head group (shown in green) defines the lipid class, while differences in the fatty acid chains (highlighted in blue) define members within the class. Abbreviations: Cer, ceramide; SM, sphingomyelin; GlcCer, glucosylceramide; d, dihydroxy. Structures were obtained from http://www.lipidmaps.org/data/.

Table 3-15: Changes amongst sphingoid bases and ceramides

	HP	ENT	MTG	SCX	MCX	CG	CB
Sphingoid bases [SP01]	**Sphingolipids [SP]**						
Hexadecasphinganine	1.72(0.0082)				1.51(0.0047)	1.48(0.0433)	
Sphinganine 1-phosphate	1.27(0.033)						
Ceramides [SP02]	**Sphingolipids [SP]**						
N-Palmitoylsphingosine	0.23(0.033)						
Cer (d18:1/18:1)	**0.22(0.0082)**	**0.47(0.0424)**	0.15(0.0019)			**2.43(0.046)**	**2.07(0.0172)**
Cer (d18:1/18:0)		**1.86(0.0066)**			0.27(0.0015)	2.27(0.0161)	1.88(0.0095)
Cer (d18:1/20:0)	0.63(0.033)		**0.11(0.0012)**		0.28(0.0455)		
Cer (d18:0/22:0)	0.46(0.0339)	0.57(0.0066)				0.53(0.0087)	
Cer (d18:2/23:0)						0.7(0.0357)	
Cer (d18:1/24:1)	0.3(0.014)	0.49(0.0321)	**0.14(0.0066)**	0.4(0.0196)	**0.22(0.0067)**		**1.31(0.0129)**
Cer (d18:0/24:0)		0.75(0.0455)					
N-(24-hydroxytetracosanyl)sphinganine							0.51(0.0026)
Cer (d18:1/24:0)/Cer(d18:0/24:1)						**0.59(0.0433)**	0.6(0.005)
Cer (d18:1/26:1)						0.52(0.0161)	1.31(0.0446)

Alterations in metabolite levels across seven brain regions shown as AD/control ratio (p-value). Elevated levels are shown in red and metabolite IDs detected in both "pos" & "neg" modes are shown in bold.

Table 3-16: Changes amongst phosphosphingolipids

	HP	ENT	MTG	SCx	MCx	CG	CB
Phosphosphingolipids [SP03]	**Sphingolipids [SP]**						
SM(d18:0/0:0)							1.41(0.03)
SM(d18:1/16:0)	**0.28(0.0082)**	0.65(0.0101)	**0.24(0.0005)**	**0.38(0.0136)**	0.25(0.0015)	0.65(0.0161)	0.9(0.0129)
SM(d18:1/18:1)	0.33(0.014)		**0.22(0.0005)**				
SM(d18:1/17:0)/SM(d19:1/16:0)	0.41(0.0105)		0.28(0.0012)				
SM(d18:1/18:0)	0.39(0.0082)			**0.52(0.0136)**	**0.35(0.0015)**		
SM(d18:1/20:0)	0.24(0.0082)					0.45(0.0433)	0.79(0.03)
SM(d18:1/22:0)	0.47(0.0082)					0.74(0.0343)	0.83(0.0229)
SM(d17:1/24:1)SM(d18:2/23:0)		0.7(0.0152)		0.6(0.0136)	0.44(0.0045)		1.18(0.039)
SM(d18:1/24:1)	0.54(0.0082)	0.8(0.0455)	0.49(0.0005)	0.59(0.0136)	0.5(0.0047)	0.56(0.0209)	1.23(0.039)
SM(d18:1/23:0)	0.53(0.0376)		0.36(0.0005)	0.49(0.0136)		0.57(0.0357)	
SM(d17:1/26:1)SM(d18:2/25:0)/SM(d19:1/24:1)		0.71(0.0223)	**0.42(0.0005)**			0.63(0.0167)	
SM(d18:1/24:0)/SM(d18:0/24:1)	0.49(0.0233)		0.31(0.0005)	**0.46(0.0093)**	0.38(0.0032)		
SM(d18:1/26:1)	0.38(0.0082)		0.21(0.0008)	0.47(0.0196)			
SM(d18:1/25:0)	0.39(0.0105)		0.23(0.0008)	0.46(0.0424)	0.32(0.0066)		1.25(0.0066)

Alterations in metabolite levels across seven brain regions shown as AD/control ratio (p-value). Elevated levels are shown in red and metabolite IDs detected in both "pos" & "neg" modes are shown in bold.

Table 3-17: Changes amongst neutral glycosphingolipids and acidic glycosphingolipids

	HP	ENT	MTG	SCx	MCx	CG	CB
Neutral glycosphingolipids [SP05]	**Sphingolipids [SP]**						
GlcCer(d18:0/22:0)		**0.34(0.0152)**		**0.63(0.0281)**	**0.26(0.0045)**		
GlcCer(d18:0/24:0)	**0.19(0.0339)**	**0.45(0.0376)**		0.64(0.0284)		**0.57(0.0157)**	
GlcCer (d18:1/18:0)/GlcCer(d18:0/18:1)		0.63(0.0455)		0.62(0.0388)	0.33(0.0041)		1.64(0.0095)
GlcCer (d18:1/22:0)		0.46(0.0223)		0.35(0.0192)	**0.28(0.0032)**	0.47(0.0343)	
GlcCer (d18:1/23:0)	0.31(0.0082)				0.23(0.0032)	0.45(0.0209)	
GlcCer (d18:1/24:0)/GlcCer (d18:0/24:1)			0.19(0.0005)	0.58(0.0196)		0.51(0.0433)	1.28(0.0095)
GlcCer (d18:1/25:0)	0.4(0.014)	0.71(0.0321)	**0.24(0.0008)**	**0.42(0.0136)**	0.37(0.0032)		1.3(0.007)
GlcCer (d18:1/26:0)/GlcCer(d18:0/26:1)							1.33(0.0229)
GldCer (d18:1/24:1)	**0.24(0.0082)**	**0.48(0.0152)**	**0.18(0.0005)**	0.52(0.0196)	**0.56(0.0095)**	0.61(0.0209)	**1.32(0.007)**
GlcCer (d18:1/26:1)	**0.26(0.0082)**	**0.65(0.0455)**	**0.16(0.0005)**	**0.38(0.0136)**	**0.54(0.0067)**	0.51(0.0161)	1.25(0.039)
GlcCer (d18:2/22:0)	0.23(0.0339)	**0.38(0.0284)**					
GlcCer (d18:2/23:0)	**0.43(0.0143)**	**0.59(0.0321)**	**0.42(0.0016)**	**0.51(0.0424)**	0.32(0.0045)	0.59(0.0209)	
LacCer (d18:1/14:0)					**0.28(0.0066)**		
Acidic glycosphingolipids [SP06]	**Sphingolipids [SP]**						
C24:1 Sulphatide/Cis-tetracosenoyl sulfatide					0.27(0.0389)	0.44(0.0209)	

Alterations in metabolite levels across seven brain regions shown as AD/control ratio (p-value). Elevated levels are shown in red and metabolite IDs detected in both "pos" & "neg" modes are shown in bold.

3.3.3.2. Glycerophosphocholines: Glycerophospholipids

The representative structures of main glycerophospholipid classes are shown in **Figure 3-10**; Lipid classes are defined by the head group (**Figure 3-10**) and the differences in the fatty acid chains define members within the class (**Figure 3-11**).

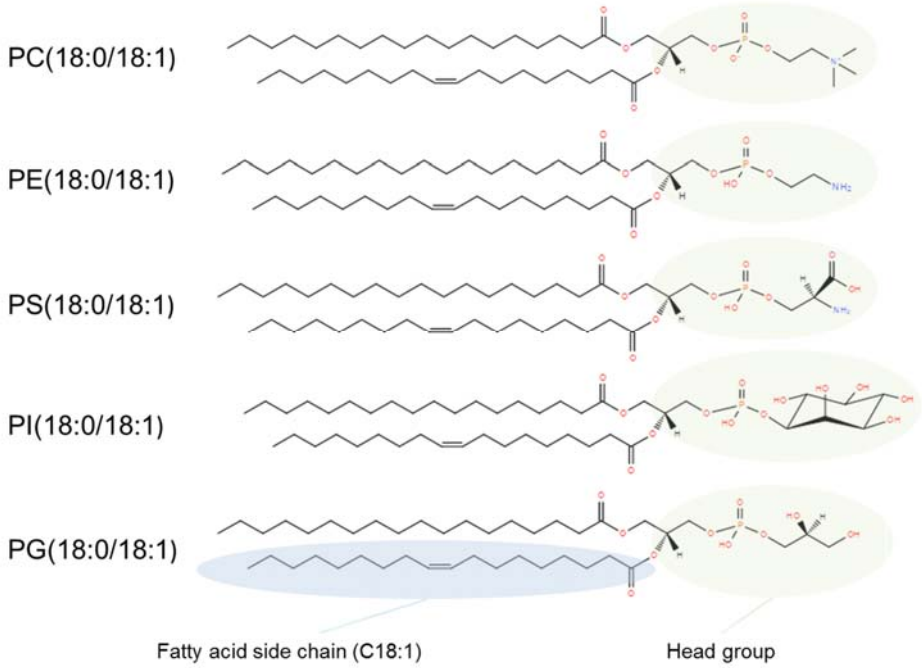

Figure 3-10 Structures of five main glycerophospholipid classes discussed in this study.

The head group (shown in green) defines the lipid class, while differences in the fatty acid chains (shown in blue) define members within the class. Abbreviations: PC, glycerophosphocholines; PE, glycerophosphoethanolamines; PS, glycerophosphoserines; PI, glycerophosphoinositols; PG, glycerophosphoglycerols. Structures were obtained from http://www.lipidmaps.org/data/.

Changes in the levels of glycerophosphocholines (PCs) were variable for those species carrying relatively short-chain fatty-acyl groups (comprising 6 to 22 total carbon-chain length) (**Table 3-18**). The most consistent change was observed in the MTG where all 7 species with statistically significant changes were elevated, to between 1.3- and 3.5-fold. In HP, ENT, and SCx, only one to two species were detected that were statistically significant, and these tended to increase rather than to decrease. In contrast, CG and CB had 1 and 4 species of PCs detected respectively, and the majority of these were decreased (to ~0.6 to 0.8-fold of control values). Species that showed consistent changes over different brain regions include lysoPC(18:2) (~1.2- to 2.5-fold in HP, MTG, SCx, and CB) and PC(17:1) (~0.6- to 0.7-fold in HP and CG) (where lysoPC designates the class of lysoglycerophosphocholine molecules).

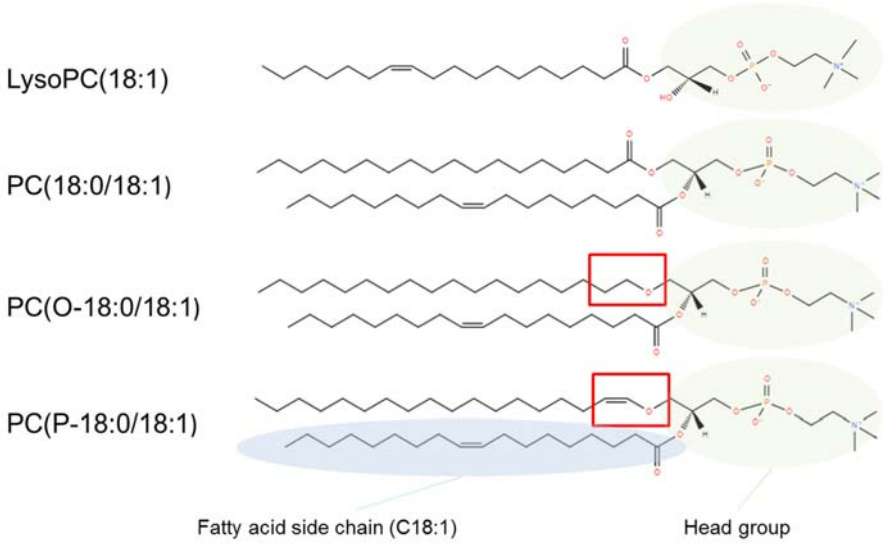

Figure 3-11 Structures of representative glycerophosphocholines species.

Within the same lipid class (i.e. same head group (shown in green)), differences in the fatty acid chains (shown in blue) define members within the class. Abbreviations: Lyso PC, monoacylglycerophosphocholine; PC, glycerophosphocholines; O-, alkyl ether substituent; P-, plasmalogen substituent. Structures were obtained from http://www.lipidmaps.org/data/.

PCs that incorporate long-chain fatty-acyl groups that are listed here (which are composed of 36 or more total carbon chain-lengths in their two component fatty-acyl moieties) (**Table 3-18**), belong either to the diacylglycerophosphocholine class [designated as GP0101], or monoacylglycerophosphocholine class [designated as GP0105]. PCs with long-chain fatty-acyl groups showed consistently lower levels (to ~0.1- to 0.5-fold) in the brain regions including HP, ENT, MTG, SCx, and MCx. Elevation of PCs within this category were observed only in CG and CB, where a mixture of increased (1.2- to 1.4-fold) and decreased (to ~0.3 to 0.8 of control species) where found.

PCs with either an alkyl-ether substituent (subclasses of which include 1-alkyl,2-acylglycerophosphocholines [designated as GP0102]/ 1-acyl,2-alkylglycerophosphocholines [designated as GP0108], monoalkylglycerophosphocholines [designated as GP0106], dialkylglycerophosphocholines [designated as GP0104]) or an 1Z-alkenyl-ether (plasmalogen) substituent (including 1-(1Z-alkenyl), 2-acylglycerophosphocholines [designated as GP0103]/ 1-acyl,2-(1Z-alkenyl)-glycerophosphocholines [GP0109], 1Z-alkenylglycerophosphocholines [GP0107]) showed decreased levels in the AD brain (**Table 3-19**), with the only exception being PC(O-15:0/O-1:0)/PC(O-8:0/O-8:0)/PC(O-16:0/0:0).

Table 3-18: Changes amongst phosphatidyl cholines with short- and long-chain fatty-acyl groups

	HP	ENT	MTG	SCx	MCx	CG	CB
PC [GP01] with short chain fatty-acyls	**Glycerophospholipids [GP]**						
PC(O-6:0/0:0)		1.5(0.0321)					
PC(20:2)			3.5(0.0027)				
LysoPC(14:0)/PC(O-12:0/2:0)			1.46(0.0008)				
LysoPC(22:6)		0.69(0.0321)	1.51(0.0071)				0.65(0.03)
LysoPC(18:2)	1.63(0.014)		2.36(0.0005)	2.54(0.0404)			1.23(0.0455)
LysoPC(16:0)/PC(O-14:0/2:0)			1.25(0.0343)				
LysoPC(18:1)/PC(O-16:1/2:0)/PC(P-16:0/2:0)			1.27(0.0094)				0.81(0.039)
LysoPC(22:4)			**1.3(0.0343)**				
LysoPC(20:2)/PC(O-18:2/2:0)							0.57(0.0389)
PC(17:1)	0.71(0.014)					0.57(0.0015)	
PC [GP01] with long chain fatty-acyls	**Glycerophospholipids [GP]**						
PC(36:2)	0.11(0.0082)				0.16(0.0015)		0.82(0.0129)
PC(36:4)	0.14(0.0143)						
PC(38:2)	0.21(0.0143)	0.46(0.0043)			0.28(0.0019)		0.83(0.039)
PC(38:4)						1.37(0.0343)	
PC(38:6)	0.13(0.0105)		0.11(0.0005)	0.31(0.0136)	0.23(0.0251)		0.67(0.0018)
PC(40:4)/PC(38:1)		0.42(0.0223)	0.25(0.0034)			0.46(0.0357)	
PC(40:8)							0.66(0.0424)
PC(42:1)							1.16(0.03)
PC(42:2)	0.45(0.0339)						1.26(0.005)
PC(42:10)/PC(40:7)							0.39(0.0018)
PC(44:2)	0.31(0.0339)						1.28(0.007)
PC(44:7)							1.43(0.0009)
PC(44:12)						0.33(0.0163)	0.41(0.0018)

Alterations in metabolite levels across seven brain regions shown as AD/control ratios (p-value). Elevated levels are shown in red and metabolite IDs detected in both "pos" & "neg" modes are shown in bold.

Table 3-19: Changes amongst phosphatidyl cholines with substituents

	HP	ENT	MTG	SCx	MCx	CG	CB
PC [GP01] with substituents	**Glycerophospholipids [GP]**						
PC(O-15:0/O-1:0)/PC(O-8:0/O-8:0)/PC(O-16:0/0:0)			1.41(0.0275)				
PC(O-15:0/2:0)/PC(O-16:0/1:0)/PC(17:0)				0.34(0.0008)			
LysoPC(18:0)/ PC(O-16:0/2:0)		0.45(0.0495)				**0.51(0.0343)**	0.76(0.0172)
PC(O-16:0/3:1)	0.33(0.019)	0.44(0.0074)		0.48(0.0278)			
PC(O-16:2/0:0)	0.38(0.0339)			0.71(0.0196)			
PC(O-14:0/18:0)/PC(O-16:0/16:0)	0.22(0.0082)		0.21(0.0034)	0.41(0.0446)			
PC(O-16:0/18:0)/PC(O-17:0/17:0)		0.51(0.0339)	0.22(0.0019)				0.53(0.0009)
PC(O-18:2/0:0)					0.53(0.0047)		
LysoPC(dm18:1)/PC(O-18:2/0:0)		0.66(0.0321)	0.46(0.0005)	0.54(0.0136)			
PC(P-20:0/22:4)	0.31(0.0082)	0.59(0.0223)	0.22(0.0005)	0.44(0.0136)	0.26(0.0015)		
PC(P-20:0/22:6)	0.18(0.0339)	0.43(0.0152)	0.22(0.0019)	0.74(0.0424)	0.21(0.0062)		
PC(16:0/dm18:0/PC(O-16:0/18:1)/PC(O-18:0/16:1)	0.29(0.0209)		0.1(0.0019)		0.23(0.0032)		
PC(18:0/dm18:0)/PC(20:0/dm16:0)/PC(O-16:0/20:1)	0.39(0.0433)		0.24(0.0019)	0.41(0.0045)	0.27(0.0142)	0.52(0.0343)	
PC(18:0/dm18:1)/PC(20:1/dm16:0)/PC(P-18:0/18:1)/PC(18:2/O-18:0)	0.34(0.0339)	0.55(0.033)		0.48(0.0163)	0.23(0.0321)		
PC(20:0/dm18:1)/PC(20:1/dm18:0)/PC(22:1/dm16:0)					0.22(0.0022)		
PC(22:1/dm18:1)/PC(22:2/dm18:0)	0.2(0.0082)						
PC(22:4/dm18:0)/PC(O-18:0/22:5)	0.38(0.0082)	0.61(0.0321)					
PC(22:4/dm18:1)/PC(22:5/dm18:0)/PC(O-18:0/22:6)		0.33(0.0104)				0.57(0.0098)	

Alterations in metabolite levels across seven brain regions shown as AD/control ratio (p-value). Elevated levels are shown in red and metabolite IDs detected in both "pos" & "neg" modes are shown in bold.

3.3.3.3. Glycerophosphoethanolamines: Glycerophospholipids

Glycerophosphoethanolamines (PEs) listed here (Table 3-20) belong either to the class of diacylglycerophosphoethanolamines [designated as GP0201] or monoacylglycerophosphoethanolamines [designated as GP0205]. In all brain regions except CB, the species with greater retention time were decreased while the two species with the least retention time (PE(44:11) & PE(20:4)) were increased. Unlike other brain regions, CB was the only brain region showing increased PEs with greater retention times.

Similar to the PCs with substituents, PEs with akyl/alkenyl substituents had greater retention times (Table 3-21) compared to PEs with simple acyl-chains (Table 3-20), and were consistently decreased in all brain regions with only one exception found, that being the CB. Of additional note, fewer species of PEs with substituents were altered in CG and CB compared to the other brain regions examined in this study.

3.3.3.4. Other Glycerophospholipids

Glycerophosphoserine (PS) species with short-chain fatty acyls (composed of 22 or less total carbon-chain lengths) listed in Table 3-22 are known as lysoPS. All lysoPSs were elevated wherever the changes were statistically significant. The rest of the PSs either had long-chain fatty-acyl moieties (composed of ≥35 total carbon-chain length) or had akyl/alkenyl substituents. These species of PS were, in general, decreased in different regions of AD brain except for CB, which showed 4 out of 5 PSs were increased.

The pattern of changes observed for glycerophosphoinositol groups (PIs) were remarkably similar to that of PSs. PIs with short-chain fatty-acyl groups (Table 3-23) were all lysoPIs. In the AD brain, lysoPIs were consistently elevated in the brain regions where they were found to be altered significantly. Among these, PI(20:2) was the most consistently observed species (elevated by ~1.9- to 2.6-fold). On the other hand, PIs with long-chain fatty-acyl groups (composed of ≥33 total carbon-chain length) were all decreased wherever statistical significance was reached. In CB, the only statistically-significant change was a 1.4-fold-elevation in the level of PI(40:6), which was not detected in any other brain regions in this study.

Glycerophosphoglycerols (PGs) that differed significantly were all increased (in HP, MTG, SCx, and MCx). Among the PGs reported herein, the first three features containing short-chain fatty-acyl groups (composed of ≤22 total carbon-chain length) are also known as lysoPGs. No PGs were found to differ in ENT and CG. PG with alkyl-ether substituents, PG(O-18:0/17:0)/PG(O-20:0/15:0)/PG(O-16:0/19:0), was the only PG detected in CB, and in contrast to other PGs in other brain regions, it was decreased to 0.5-fold of control (Table 3-24).

Four metabolites belonging to other main-classes of GP were found. These were PT(36:1) and 1,2-ditetradecanoyl-sn-glycero-3-phosphosulfocholine belong to the class of 'Other Glycerophospholipids' [designated as GP00]; PA(42:4), which belongs to the class of 'Glycerophosphates' [designated as GP10], and PE(18:0/22:6(4Z,7Z,10Z,12E,16Z,19Z)(14OH)), which belongs to the class of 'Oxidised glycerophospholipids' [designated as GP20].

Due perhaps to the small number of species reported for these main classes, no clear trend was discernible and they have not been further discussed here (**Table 3-24**).

Table 3-20: Changes amongst phosphatidyl ethanolamines with simple acyl-chains

	HP	ENT	MTG	SCx	MCx	CG	CB
PE [GP02] with simple acyl-chains	**Glycerophospholipids [GP]**						
PE(44:11)		1.27(0.0455)	2.06(0.0005)			1.46(0.0343)	
PE(20:4)		1.59(0.0176)	1.33(0.0094)	1.31(0.0196)		1.41(0.0029)	
LysoPE(22:6)							**0.68(0.007)**
LysoPE(20:2)							1.4(0.0339)
LysoPE(22:4)	0.64(0.0376)	0.7(0.0101)					
LysoPE(22:2)	0.47(0.014)	0.6(0.0027)	0.31(0.0008)	0.51(0.0389)		0.68(0.03)	1.48(0.0054)
PE(36:6)							0.73(0.0172)
PE(38:6)	0.37(0.0082)		**0.23(0.0005)**	0.55(0.0278)	0.4(0.0184)	0.62(0.0161)	0.74(0.0012)
PE(42:7)	0.49(0.014)						
PE(40:7)			0.34(0.0005)				
PE(34:2)	0.49(0.0376)	0.64(0.0321)	0.42(0.0012)		0.4(0.0067)		
PE(44:12)							0.44(0.0009)
PE(46:5)							1.34(0.0095)

Alterations in metabolite levels across seven brain regions shown as AD/control ratio (p-value). Elevated levels are shown in red and metabolite IDs detected in both "pos" & "neg" modes are shown in bold.

Table 3-21: Changes amongst phosphatidyl ethanolamines with substituent

	HP	ENT	MTG	SCx	MCx	CG	CB
PE [GP02] with substituent	**Glycerophospholipids [GP]**						
PE(O-16:1/22:6)/PE(20:5/dm18:1)/PE(22:6/dm16:0)	**0.53(0.0233)**		**0.33(0.0005)**	**0.42(0.0278)**	0.5(0.0451)		0.76(0.0009)
PE(14:0/dm18:1)/PE(14:1/dm18:0)/PE(16:1/dm16:0)			0.59(0.0285)				
PE(22:6/dm18:1)	**0.28(0.0105)**		0.3(0.0005)		0.44(0.0282)		0.83(0.0095)
PE(16:1/dm18:1)/PE(18:2/dm16:0)			0.47(0.0008)				
PE(20:4/dm18:1)/PE(20:5/dm18:0)/PE(22:5/dm16:0)	**0.35(0.0339)**	0.72(0.0152)	**0.43(0.0005)**	0.67(0.0093)	0.44(0.0022)	0.83(0.0209)	
PE(22:5/dm18:1)/PE(22:6/dm18:0)	0.51(0.0082)						0.65(0.0009)
PE(34:1)/PE(16:0/dm18:1)/PE(16:1/dm18:0)	0.56(0.0233)						
PE(O-18:1/20:4)/PE(20:3/dm18:1)/PE(20:4/dm18:0)/ PE(22:4/dm16:0)/PE(O-16:0/22:5)/PE(O-18:0/20:5)	0.63(0.0233)		0.37(0.0005)		0.56(0.0067)		
PE(22:4/dm18:1)	**0.32(0.0082)**	0.64(0.0066)	0.32(0.0005)	**0.73(0.0136)**	**0.55(0.0015)**	0.71(0.0117)	
PE(18:1/dm18:1)/PE(20:2/dm16:0)	0.47(0.0082)	0.65(0.0223)	0.55(0.0011)	0.56(0.0136)	**0.58(0.0032)**		
PE(22:4/dm18:0)	**0.35(0.0082)**	**0.67(0.0101)**	**0.31(0.0005)**	0.68(0.0278)	**0.52(0.0067)**	0.53(0.0071)	
PE(20:1/dm18:1)/PE(20:2/dm18:0)				0.72(0.0136)			
PE(P-20:0/22:4)/PE(22:0/dm18:1)/PE(22:1/dm18:0)/PE(24:1/dm16:0)		0.77(0.0376)				0.67(0.0053)	
PE(20:0/dm18:1)/PE(20:1/dm18:0)/PE(22:1/dm16:0)	0.62(0.0376)			0.73(0.0388)	0.51(0.0047)		
PE(22:1/dm18:1)	0.49(0.014)						1.3(0.0229)
PE(O-20:0/22:4)	0.44(0.0433)	0.59(0.0233)				0.7(0.0357)	

Alterations in metabolite levels across seven brain regions shown as AD/control ratio (p-value). Elevated levels are shown in red and metabolite IDs detected in both "pos" & "neg" modes are shown in bold.

Table 3-22: Changes amongst phosphatidyl serines

	HP	ENT	MTG	SCx	MCx	CG	CB
PS [GP03] with short-chain fatty acyls		**Glycerophospholipids [GP]**					
PS(20:4)		2.23(0.0062)				4.52(0.003)	
PS(22:6)		1.82(0.0118)	2.81(0.0005)	1.99(0.0063)	**2.93(0.0015)**	2.36(0.0124)	
PS(21:0)			1.49(0.0011)				
PS(18:1)				1.52(0.0388)			
PS [GP03] with long-chain fatty acyls/substituent		**Glycerophospholipids [GP]**					
PS(36:3)		2.35(0.0209)					
PS(P-18:0/17:2)							1.46(0.03)
PS(39:4)							0.53(0.0018)
PS(O-16:0/O-16:0)			0.03(0.0367)				
PS(38:9)			0.51(0.0253)				
PS(41:5)	0.29(0.0082)		0.16(0.0005)	0.54(0.0388)			
PS(35:0)	0.41(0.0082)	0.6(0.0455)	0.23(0.0005)	0.51(0.0196)	0.27(0.0015)		
PS(39:3)	0.36(0.0082)		0.19(0.0005)	0.48(0.0196)	0.28(0.0184)		2.14(0.0012)
PS(41:4)	0.28(0.0082)	0.51(0.0455)	0.16(0.0005)				
PS(39:2)	0.35(0.0082)				0.25(0.0095)		1.29(0.03)
PS(37:2)							1.71(0.007)
PS(37:0)					0.53(0.0022)		
PS(41:3)		0.58(0.0321)	0.18(0.0005)				
PS(39:1)		0.55(0.0066)	0.26(0.0005)	0.55(0.0136)	0.3(0.0015)		
PS(39:0)		0.62(0.0152)	0.27(0.0005)	0.6(0.0136)	0.4(0.0047)	0.72(0.0161)	
PS(O-16:0/21:0)/PS(O-18:0/19:0)/PS(O-20:0/17:0)	0.55(0.0233)						
PS(O-16:0/20:5)/PS(P-18:0/18:4)/PS(P-16:0/20:4)	1.49(0.033)						

Alterations in metabolite levels across seven brain regions shown as AD/control ratio (p-value). Elevated levels are shown in red and metabolite IDs detected in both "pos" & "neg" modes are shown in bold.

Table 3-23: Changes amongst phosphatidylinositols

	HP	ENT	MTG	SCx	MCx	CG	CB
PI [GP06] with short-chain fatty acyls	**Glycerophospholipids [GP]**						
PI(18:0)			2.1(0.0054)				
PI(18:3)				1.42(0.0278)			
PI(20:2)	2.54(0.0376)	1.89(0.0101)	2.48(0.0021)	2.4(0.0196)	2.3(0.0251)	2.56(0.0029)	
PI(20:4)			1.89(0.0021)				
PI [GP06] with long-chain fatty acyls	**Glycerophospholipids [GP]**						
PI(33:1)		0.35(0.0082)					
PI(34:1)		0.65(0.0101)				0.65(0.0209)	
PI(36:1)	0.35(0.014)	0.34(0.0043)			0.35(0.0022)		
PI(36:2)					0.62(0.025)		
PI(36:4)/PI(34:1)			0.6(0.0011)				
PI(38:5)		0.67(0.0455)	0.55(0.0015)			0.71(0.0343)	
PI(40:4)		0.4(0.0185)					
PI(40:6)							1.38(0.0206)

Alterations in metabolite levels across seven brain regions shown as AD/control ratio (p-value). Elevated levels are shown in red and metabolite IDs detected in both "pos" & "neg" modes are shown in bold.

Table 3-24: Changes amongst glycerophosphoglycerol and other glycerophospholipids

	HP	ENT	MTG	SCx	MCx	CG	CB
PG [GP04]	**Glycerophospholipids [GP]**						
PG(22:6)			2.43(0.0039)		1.75(0.0451)		
PG(20:3)	1.94(0.014)		6.65(0.0005)	2.08(0.0278)	2.45(0.0095)		
PG(20:4)					2.01(0.0184)		
PG(33:5)	2.25(0.0082)						
PG(36:8)			1.38(0.0071)				
PG(O-18:0/17:0)/PG(O-20:0/15:0)/PG(O-16:0/19:0)							0.53(0.0012)
Other GP	**Glycerophospholipids [GP]**						
PT(36:1)	0.42(0.0082)		0.24(0.0005)	0.56(0.0136)	0.29(0.0022)		
PA(42:4)	0.82(0.014)						
1,2-ditetradecanoyl-sn-glycero-3-phosphosulfocholine						3.44(0.0019)	
PE(18:0/22:6(4Z,7Z,10Z,12E,16Z,19Z)(14OH))			0.15(0.0143)				

Alterations in metabolite levels across seven brain regions shown as AD/control ratio (p-value). Elevated levels are shown in red and metabolite IDs detected in both "pos" & "neg" modes are shown in bold.

3.3.3.5. Glycerolipids

Only one species of monoradylglycerol [the general lipidomic class designation of which is GL01] was found to be significantly altered here: MG(18:0) was decreased to 0.7-fold of control in the ENT (**Table 3-25**). All the diradylglycerols [lipidomic class designation GL02] detected belonged to the sub-class of diacylglycerols [lipidomic class designation GL0201]. Diacylglycerols (DGs) were listed in the order of increasing retention time. The first three DGs (those with the least retention time) were increased wherever significance was reached. For the rest of the DGs, the levels were mostly diminished in HP, ENT, MTG, SCx, and MCx, and increased in CG and CB (**Table 3-25**).

Triradylglycerols [designated as GL03] were the least consistent metabolite group as there was very little overlap in metabolites when examined across different brain regions. All the triradylglycerols found herein belong to the sub-class triacylglycerols [designated as GL0301] and these have been listed in the order of increasing retention time (**Table 3-26**).

There was no significant change in the level of triacylglycerols (TGs) detected in ENT and CG. TG(34:2), the only species that was altered significantly in more than one brain region, decreased in both HP and MTG. The rest of the TGs in HP showed increases ranging from 1.3- to 1.7-fold. All three TGs that were significantly altered in MTG showed a decrease to ~0.3- to 0.7-fold of control. SCx and MCx showed elevation in the same set of TGs, ranging from 1.2- to 1.4-fold. Of the four TGs that were significantly different in CB, one was increased and three were decreased. The only glycosyldiradylglycerols [designated as GL05] altered in this study, decreased to 50% in HP.

Table 3-25: Changes amongst monoradylglycerol and diradylglycerols

	HP	ENT	MTG	SCx	MCx	CG	CB
Monoradylglycerols [GL01]		**Glycerolipids [GL]**					
MG(18:0)		0.72(0.0223)					
Diradylglycerols [GL02]		**Glycerolipids [GL]**					
DG(30:2)			2.19(0.0005)				
DG(42:10)	1.83(0.0082)	1.32(0.0455)	2.19(0.0005)	1.28(0.0136)	1.57(0.0015)	1.57(0.0161)	
DG(38:1)					1.56(0.0022)		1.49(0.0095)
DG(38:9)	0.56(0.0275)						
DG(30:1)			0.3(0.0005)			0.58(0.0279)	
DG(34:2)	0.68(0.0233)						
DG(36:3)			2.7(0.0005)		0.71(0.0126)	2.43(0.0094)	1.41(0.004)
DG(34:1)	0.48(0.0082)			0.76(0.0063)	0.6(0.0015)	1.62(0.0269)	1.34(0.0129)
DG(38:4)	0.34(0.014)			0.4(0.0128)	0.28(0.0015)		
DG(38:3)	0.4(0.0433)		0.17(0.0066)		0.31(0.0062)		
DG(34:0)			0.27(0.0005)				
DG(36:1)	0.28(0.0082)	0.57(0.0223)	0.33(0.0005)	0.44(0.0136)	0.34(0.0015)		
DG(42:6)/DG(40:3)							1.61(0.0278)

Alterations in metabolite levels across seven brain regions shown as AD/control ratio (p-value). Elevated levels are shown in red and metabolite IDs detected in both "pos" & "neg" modes are shown in bold.

Table 3-26: Changes amongst triradylglycerols

	HP	ENT	MTG	SCx	MCx	CG	CB
Triradylglycerols [GL03]	**Glycerolipids [GL]**						
TG(34:2)	0.58(0.0082)		0.29(0.0005)				
TG(56:5)/TG(54:2)							2.5(0.0376)
TG(42:0)							0.58(0.0095)
TG(50:3)							0.4(0.0009)
TG(56:10)/TG(54:7)							0.8(0.039)
TG(54:5)	1.65(0.0167)						
TG(52:3)			0.56(0.0209)				
TG(54:4)	1.28(0.0376)						
TG(56:7)				1.2(0.0196)	1.35(0.0047)		
TG(52:2)			0.65(0.0433)				
TG(54:3)	1.34(0.0233)						
TG(56:6)				1.16(0.0278)	1.39(0.0015)		
Glycosyldiradylglycerols [GL05]	**Glycerolipids [GL]**						
SQDG(32:0)	0.52(0.0339)						

Alterations in metabolite levels across seven brain regions shown as AD/control ratio (p-value). Elevated levels are shown in red and metabolite IDs detected in both "pos" & "neg" modes are shown in bold.

3.3.3.6. Fatty Acids and their derivatives and Sterol Lipids

Numerous species corresponding to the main classes of Fatty Acyl species [FA] were detected, including Fatty Acids and Conjugates [designated as FA01], Fatty alcohols [FA05], Fatty aldehydes [FA06], Fatty amides [FA08], and Fatty acyl glycosides [FA13]. All Fatty Acyls that reached significance were increased across all brain regions except for MTG, in which four species of fatty acyls were decreased. The observed increase in fatty acids is in line with the increased FAs in our corresponding GC-MS study (**Table 3-27**).

All the Sterol Lipids [ST] were increased except for Cholesteryl esters [ST0102] (**Table 3-28**). The observed decrease in cholesterol esters correlates well with the decrease in cholesterol (**Table 3-11**). There was no significant change in sterol lipid level detected in SCx and MCx.

Table 3-27: Changes amongst fatty acids

Metabolites	HP	ENT	MTG	SCx	MCx	DG	CB
Fatty Acids and Conjugates [FA01]	**Fatty Acyls [FA]**						
Suberic acid/Ethyladipic acid						1.92(0.0015)	
3,9-hexadecadiynoic acid							1.48(0.005)
4,7,10-hexadecatrienoic acid/Hiragonic acid							1.75(0.0253)
10-methyl-heptadecanoic acid/2,6-dimethyl-hexadecanoic acid					1.52(0.0015)		
2,3-Dihydroxycyclopentaneundecanoic acid/Hexadecanedioic acid		1.6(0.0152)	3.05(0.0015)		1.68(0.0095)		1.2(0.03)
Tricosanedioic acid						1.76(0.0039)	
8(R)-hydroxy-hexadeca-2E,4E,6E,10Z-tetraenoate			2.62(0.0005)			1.75(0.0343)	
Methyl 9-butylperoxy-10,12-octadecadienoate					2.39(0.0281)		
15-oxo-18Z-tetracosenoic acid							1.3(0.0026)
2-hydroxytetracosanoate	1.68(0.0082)			1.29(0.0136)			
Fatty alcohols [FA05]/Fatty aldehydes [FA06]							
13-methyl-1,2-nonadecanediol/1,2-eicosanediol		1.42(0.0185)	3.1(0.0005)				
2,4-hexadienal							1.22(0.039)
2,5-undecadienal			7.3(0.0008)				
5,8-tetradecadienal	1.8(0.0082)						
Hexadecanal			0.32(0.0005)				
Octadecanal			0.11(0.0005)				
11Z-ecosenal			1.71(0.0005)				
Fatty amides [FA08]/Fatty acyl glycosides [FA13]							
Linoleamide					1.45(0.0451)		
Palmitic amide			1.86(0.0005)				
Octadecanamide			1.86(0.0005)				
N-arachidonoyl alanine/N-palmitoyl proline/N-oleoyl alanine			0.65(0.0078)				
1-(O-alpha-D-glucopyranosyl)-3-keto-(1,25R)-hexacosanediol			0.74(0.0274)		1.17(0.0285)		

Alterations in metabolite levels across seven brain regions shown as AD/control ratio (p-value). Elevated levels are shown in red and metabolite IDs detected in both "pos" & "neg" modes are shown in bold.

Table 3-28: Changes amongst sterol lipids

Metabolites	HP	ENT	MTG	SCx	MCx	CG	CB
	Sterol Lipids [ST]						
17beta-Hydroxy-4-mercaptoandrost-4-en-3-one 4-acetate 17-propionate	1.78(0.014)						
17beta-Hydroxy-3-methoxyestra-1,3,5(10)-triene-17-carbonitrile		3.26(0.0374)				2.48(0.0304)	
1'H-5alpha-Androst-2-eno[3,2-b]indol-17beta-ol			1.31(0.0124)				
3-sulfodeoxycholic acid						1.46(0.0029)	1.17(0.0129)
11beta,21-Dihydroxypregn-4-ene-3,20-dione 21-acetate/ 6beta,17beta-Dihydroxyandrost-4-en-3-one diacetate						1.54(0.0209)	
3-(acetyloxy)-9-mercaptoandrosta-3,5-diene-11,17-dione							2.44(0.0415)
CE(18:1)	0.15(0.0275)		0.15(0.0143)				
CE(18:2)							**0.38(0.0095)**
	Miscellaneous						
3-(4-Hydroxyphenyl)pyruvate/2-Hydroxy-3-(4-hydroxyphenyl)propenoate/ 4-Hydroxyphenylpyruvic acid		1.32(0.0455)					
Dimethylprotoporphyrin IX dimethyl ester			0.47(0.0012)				
3-oxo-8(R)-hydroxy-hexadeca-6E,10Z-dienoate							1.23(0.0229)
Ubiquinone-9							1.71(0.007)
Vaccenyl carnitine						2.64(0.0071)	1.88(0.0095)

Alterations in metabolite levels across seven brain regions shown as AD/control ratio (p-value). Elevated levels are shown in red and metabolite IDs detected in both "pos" & "neg" modes are shown in bold.

3.4. Discussion

Metabolomics is used to detect perturbations in the metabolome, a pool of metabolites that reflects changes downstream of the genome, transcriptome and proteome [205]. Metabolites are not only the building blocks for biological macromolecules such as proteins, complex lipids, DNA and RNA, but are also central to intermediary metabolism, and also provide many necessities for life such as chemical energy. Furthermore, metabolites can act as signalling molecules with regulatory functions in a biological system [195]. Therefore, metabolomics can provide accurate biochemical profiles representative of biological status, with proximity to other aspects of the phenotype of the system.

Recent developments in the field have enabled two modes of approach: targeted and untargeted metabolomics. While the targeted approach profiles only a set of predesignated metabolites (often with enhanced probability of the individual molecules being detected), the untargeted approach can provide a global examination of disease-specific signatures of perturbations in all the metabolites that are detected within a study, some of which can then be followed in subsequent studies by targeted methods.

Recently, metabolomics has been applied in numerous AD-focused human studies, mostly carried out using CSF and/or plasma samples [206-212] and in relatively rare cases, using human brain tissue [213,214]. To date, there has not been to our knowledge a comprehensive description of the AD-associated changes in metabolites carried out by applying both GC-MS and LC-MS in human brain. Furthermore, examination of seven brain regions in a comparative manner at the multi-omics level has never been reported in the literature.

In this study, we applied an untargeted metabolomics approach to determine global changes in the metabolites from seven brain regions of AD patients compared to controls. The use of an untargeted approach provided an unbiased set of data which reflects changes in multiple pathways affected in the disease. To our knowledge, this is the first study that examines and compares multiple brain regions, which are known to be affected by AD to different extents, in AD patients by comprehensive metabolic profiling through combination of both GC-MS and LC-MS.

3.4.1. Findings from GC-MS

3.4.1.1. Glucose metabolism: Polyol and Pentose-phosphate pathways

Defects in energy metabolism are a fundamental component of AD pathogenesis [215]. Altered cerebral glucose metabolism manifests years before the onset of clinical symptoms of AD [216] and AD brains show defects in both glucose uptake [217] and regional cerebral perfusion [192]. These defects are generally worse in regions that show greater histological [218,219], functional [220] and molecular [221] evidence of damage, consistent with the operation of a specific disease process [220,222,223]. However, the exact underlying molecular mechanism is unknown.

One potential explanation for abnormal *in vivo* brain glucose uptake in AD patients could be reduced glucose transporter (GLUT1 and GLUT3) activity [224], leading to low brain glucose levels and consequential cerebral hypometabolism. This is believed to be the cause of cognitive decline in the sporadic AD [225], but direct measurements of glucose in AD brain have hitherto been lacking.

On the contrary, in this study glucose levels were found to be markedly elevated in all AD brain regions examined (**Table 3-7**). This finding suggests that diminished glucose transporter activity is unlikely to play a significant role in the observed decrease in brain glucose uptake that is characteristic of AD. Rather, our findings point to a different mechanism, whereby cerebral glucose uptake could be depressed as a consequence of the elevations in brain glucose, through the effects of a decreased trans-cell-membrane concentration gradient that lowers the drive for uptake via facilitated diffusion.

The presence of elevated brain glucose levels in AD is consistent with defective glucose clearance, perhaps via the effects of insulin resistance in the AD brain [226]. Recently, an *in vivo* study carried out in a murine model of AD has shown that acute induction of locally elevated cerebral glucose levels increased Aβ production in the hippocampus [36]. Combined with the previously reported finding that individuals with elevated blood glucose levels (even without diabetes) have increased risk of developing dementia [48], accumulation of glucose and abnormal glucose metabolism in the brain could well play a causal role in AD pathogenesis.

In addition to increases in glucose, we found markedly elevated levels of sorbitol and fructose in all seven brain regions studied (**Table 3-7**). Both are free sugars and components of the polyol pathway (**Figure 2-9**). A gradient in the severity of these metabolic defects could also be discerned. In general, the perturbation in glucose levels was greater in tissues that are more severely damaged in AD. Taken together, these metabolic derangements are consistent with insufficient glucose clearance via glycolysis and glycogenesis in AD brain, with consequent increases in the activity of the polyol pathway, which normally plays only a minor role in cellular glucose clearance [227].

Elevated flux through the polyol pathway is known to occur in the tissues of diabetic mammals, where it has been linked to accelerated formation of advanced glycation endproducts (AGEs) and consequent increases in damage to cellular proteins, nucleic acids and lipids via generation of reactive oxygen species (ROS) [227]. Our findings of elevated polyol pathway flux in the AD brain provide substantive evidence for a close metabolic link between the tissue damage in the brain in AD and diabetes, and indicate that processes which damage tissues in diabetes probably also contribute to tissue damage in AD brain.

High intracellular free-glucose levels can induce polyol pathway activity which leads to increased conversion of glucose to sorbitol, and sorbitol to fructose (**Figure 3-12**): all three sugars are non-phosphorylated, in contrast to those catabolised via the main route of glycolysis. The net effects of these reactions are: 1) decreased levels of NADPH; and 2) increased reduction of NAD^+ to NADH [228]. The rise in the cytosolic NADH:NAD^+ ratio has been suggested to inhibit glycolysis at the level of the glyceraldehyde 3-phosphate dehydrogenase (GAPDH)-catalysed reaction, which increases the pool of

triose phosphate [229]. In the cytosol, NADH can be oxidised to NAD^+ by lactate dehydrogenase (LDH) (coupled to reduction of pyruvate to lactate), and by glycerol-3-phosphate dehydrogenase (GAPDH) (coupled to reduction of dihydroxyacetone phosphate to glycerol-3-P), also known as the glycerol-phosphate shuttle [229]. Our study showed significant increases in the levels of both lactic acid and glycerol-3-P (most consistently in HP and MCx), which may be a consequence of increased NADH oxidation in the cytosol. It has to be noted however, that many cells and tissues have limited capacity to oxidise cytosolic NADH by the above mechanisms [229]. Hence the increased lactic acid and glycerol-3-P levels may not be directly related to presumptive increase in activity of the polyol pathway and its downstream corollaries.

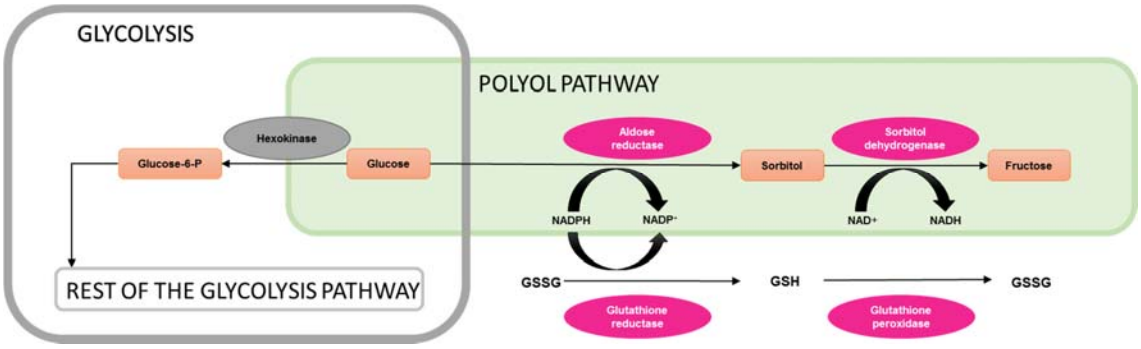

Figure 3-12 Polyol pathway in the AD brain.

The normal fate of intracellular glucose is degradation via glycolysis and/or incorporation into glycogen in glycogenic tissues such as liver and skeletal muscle. When high glucose levels saturate hexokinase, glucose can be diverted to the polyol pathway. Aldose reductase and sorbitol dehydrogenase are the key enzymes of the polyol pathway and, since these were found to be elevated according to our parallel iTRAQ study (Chapter Four), could be responsible for the elevation in both sorbitol and fructose in AD. Increased consumption of NADPH (e.g. as a result of polyol pathway activation) may compromise the recycling of glutathione disulphide (GSSG) to glutathione (GSH), which in turn may compromise the conversion of hydrogen peroxide to water. Two enzymes governing these reactions, glutathione reductase and glutathione peroxidase were also elevated in AD brain (Chapter Four).

In line with the proposed inhibition of glycolysis, we observed strong elevation in the levels of glucose-6-P across all brain regions examined. However, the levels of fructose-6-P (putative ID) were decreased in ENT and MTG (**Table 3-8**). This finding is consistent with the iTRAQ result showing decrease in phosphofructokinase levels (explained in further detail in Chapter Four).

Elevated glucose-6-P levels provide increased substrate for the pentose-phosphate pathway, a minor pathway of glucose metabolism. Depletion in NADPH levels (a consequence of elevated polyol pathway activity) can in turn activate the pentose-phosphate pathway to replenish NADPH, which in turn can be utilised in glutathione formation as part of the pathway by which ROS are detoxified in concert with glutathione peroxidase [230].

Significant up-regulation of the pentose-phosphate pathway has been reported in patients with mild cognitive impairment that later progressed to AD and it is known that more glucose is metabolised *via* the pentose-phosphate pathway under hypoxic conditions in the brain [211]. The general trend of increase in 5-carbon metabolites observed by us here may thus reflect altered pentose-phosphate pathway

activity in AD brain, especially considering the increase in pentose-phosphate pathway enzymes in the iTRAQ study (detailed in Chapter Four). The elevation in erythronic acid has previously been identified as a major hallmark of pentose-phosphate pathway defects and transaldolase (TALDO) deficiency [199]. Therefore, the observed increase in erythronic acid is further consistent with defects in pentose-phosphate pathway activity in AD brain. Although 5-carbon sugars are an important substrate of the pentose-phosphate pathway, those that we observed in this metabolomic study (**Table 3-8**) are putative IDs with a lower confidence level. Further studies with authentic internal standards will be required to cement this finding.

3.4.1.2. Alternative fuel sources

The brain uses glucose as its principal metabolic substrate but is also capable of utilising other substrates including glutamate, lactate, and ketone bodies as substrates for energy production [231]. The use of alternative fuel sources plays a critical role in energy production in the brain during starvation, or when glucose utilisation is impaired in neurodegenerative diseases such as AD [232]. When glucose is in short supply, ketone bodies constitute the brain's principal alternative fuel [233]. During a prolonged fast, ketosis takes place whereby ketone bodies provide ~60% of the energy requirement of the brain [234]. Ketosis, therefore, is a very important biological state that compensates for energy shortage in the human brain; indeed, the level of β-hydroxybutyrate and lactate are known to increase during fasting-induced ketosis [235]. Our observation of increased β-hydroxybutyrate and lactic acid levels is suggestive of a ketotic environment in AD brain. Furthermore, 2-hydroxy-3-methylbutyric acid (also termed 2-hydroxyisovaleric acid) was strongly elevated in AD brain in our study. This metabolite has previously been associated with lactic acidosis and ketoacidosis (which comprise pathological acidotic states in which ketosis, mainly caused by elevated β-hydroxybutyrate but also acetoacetate, is accompanied by lowered systemic pH values; note that lactic acidosis is primarily caused by low pH generated by increased lactate levels with decompensation of metabolic defence mechanisms and is also usually accompanied by a significant component of ketoacidosis) in humans [200]. This finding provides further supportive evidence for the presence of ketoacidosis in the AD brain. 2-Hydroxy-3-methylbutyric acid can also originate from the catabolism of valine, leucine or isoleucine [236]. However, the changes in the levels of these amino acids were either inconsistent in their pattern of alteration or non-significant; I interpret these findings to indicate that altered levels of these may not account for the observed strong elevation in the level of 2-hydroxy-3-methylbutyric acid, although further work would be required to confirm this postulate.

We have also observed strong elevations of butanediol in the AD brain, which can act as precursor for formation of ketone bodies. Elevation in ketone bodies could result from the following processes: 1) increased dietary intake of ketone body-generating nutrients, for example ketogenic amino acids, since transport of ketone bodies remain intact in AD [233]; 2) increased local, endogenous ketogenesis (that is, within the brain), for example in astrocytes; or 3) decreased metabolism of ketone bodies in the brain. We have no information on whether the patients we studied had increased dietary intake of ketogenic nutrients such as ketogenic amino acids before death. Therefore, we cannot correlate the observed

increase in ketone bodies in the AD brain with a dietary source. The group of ketogenic amino acids includes the following: leucine, isoleucine, lysine, phenylalanine, tyrosine, and tryptophan. While leucine and lysine are purely ketogenic, the rest are also glucogenic. Levels of the exclusively ketogenic amino acids leucine and lysine were decreased in brain regions showing statistically significant differences between AD and controls. Conversely, phenylalanine, tyrosine and tryptophan were mainly increased. Therefore, our data cannot be used to infer whether or not ketogenesis was activated. The AD brain however, has a reduced capability to break down ketone bodies resulting from reduction in activity of 3-oxoacid CoA transferase 1, an enzyme that plays a central role in extra-hepatic ketone-body catabolism (see details in Chapter Four). Regardless of the underlying mechanism for the build-up in ketone bodies, this perturbation is likely to have profound effects on fuel metabolism in the brain. Unlike glucose, transport and metabolism of ketone bodies is not diminished in the AD brain [237], and ketone bodies produced by astrocytes have been suggested to act as substrates for neuronal metabolism *in situ*, and may also have a neuroprotective effect [233]. Supporting this theory, oral administration of ketogenic compounds has been associated with cognitive improvement in both AD patients [225,238], and in a mouse model of AD [239]. The neuroprotective effect of ketone bodies has been attributed to its ability to reduce glutamate-induced free radical formation by lowering the NADH:NAD^+ ratio and also by enhancing mitochondrial respiration in neocortical neurons, which may in turn restore normal bioenergetic function in the face of oxidative stress [240]. Furthermore, β-hydroxybutyrate has been shown to preserve neuronal integrity and stability during glucose deprivation [241]. However, the compensatory shift from the glycolysis pathway to the ketogenic/fatty acid β-oxidation pathway was suggested to eventually lead to white matter degeneration [232].

3.4.1.3. Other sugars and derivatives

Xylitol is a key molecule in the interconversion of L-xylulose and D-xylulose that takes part in the glucuronate-xylulose pathway. The glucuronate-xylulose pathway, along with the pentose-phosphate pathway, is known to be activated in diabetic tissue when glucose is over-utilised [242].

The build-up in xylitol seen in this study may be linked to elevated levels of L-xylulose reductase in the AD brain (details in Chapter 4). It has been demonstrated that xylitol metabolism in the presence of glucose induces lactate formation and accumulation of dihydroxyacetone phosphate in erythrocytes [243]. The highly elevated glucose levels found in this study may have caused the down-stream build-up of xylitol, lactate and glycerol-3-P (hypothetical metabolic environment as shown in **Figure 3-13**).

Xylitol is converted to D-xylulose by xylitol dehydrogenase, followed by conversion to xylulose-5-P before entering the pentose-phosphate pathway. Although we suspect that the pentose-phosphate pathway may have been activated in the AD brain, we detected neither xylulose-5-P nor xylitol dehydrogenase as supportive evidence.

We also observed increased levels of threitol, a sugar alcohol that can be regarded as the main end-product of xylose (which can be converted to xylitol or D-xylulose) metabolism in man [244]. We speculate

that there is a connection between the build-up of xylitol and threitol arising from altered xylitol metabolism in the AD brain.

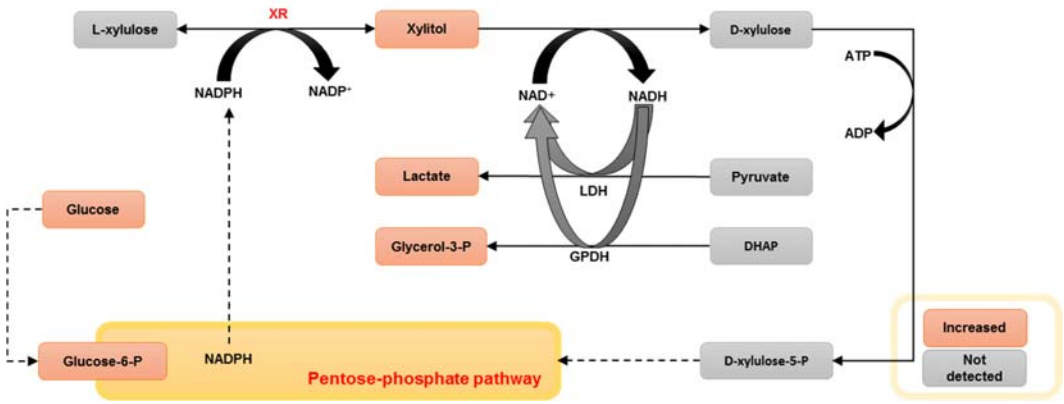

Figure 3-13 Xylitol metabolism in AD brain (hypothetical)

The increase in xylitol observed in this study is consistent with the observation of increased xylulose reductase (XR) level in the AD brain (as per iTRAQ study, Chapter Four). Xylitol metabolism in the presence of glucose was suggested to induce lactate and dihydroxyacetone phosphate (DHAP) formation. This is consistent with the increased levels of lactate and glycerol-3-P. Xylitol can be converted to xylulose-5-P, which is a substrate for the pentose-phosphate pathway. Elevated glucose-6-P can also be shunted to the pentose-phosphate pathway. Increased pentose-phosphate pathway activity may enhance the supply NADPH for xylitol metabolism. Abbreviations: DHAP, dihydroxyacetone phosphate; XR, xylulose reductase; LDH, lactate dehydrogenase; GPDH, Glycerol-3-phosphate dehydrogenase.

A change that may be directly related to the high brain-glucose levels was the increased level of N-acetylglucosamine (GlcNAc), a monosaccharide derived from glucose. Excess glucose can lead to synthesis of UDP-N-acetylglucosamine (UDP-GlcNAc), which is used by O-linked N-acetylglucosamine transferase (OGT) to catalyse the addition of O-linked N-acetylglucosamine (O-GlcNAc) to target proteins. This modification was proposed to serve as a signalling modification analogous to protein phosphorylation [245]. This is a dynamic modification occurring in the nucleus and cytoplasm, and sustained increases in O-GlcNAc have been associated with the pathogenesis of diseases such as AD [245,246]. In the iTRAQ results (Chapter Four), OGT was significantly decreased in CB.

In this study, the level of myoinositol-1-P was significantly elevated in all brain regions apart from SCx. A possible explanation is the observed up-regulation of myo-inositol 1-phosphate synthase, a key enzyme in the myo-inositol biosynthesis pathway; this enzyme catalyses the conversion of glucose 6-phosphate to 1-myo-inositol 1-phosphate in an NAD-dependent manner (see Chapter Four). Myo-inositol-1-P can be hydrolysed by myo-inositol monophosphatase (IMPase) to form free myo-inositol. In ENT, we detected a 1.3-fold-elevation of MI and the level of IMPase enzyme also trended towards an elevation (Chapter Four). These findings are consistent with a previous study demonstrating that both IMPase activity and protein levels were significantly higher in AD than in control brains [247]. Myo-inositol is presumed to act as an osmolyte within astrocytes and its level is known to be raised in a number of neurological and psychiatric disorders, including AD, and often increases with disease progression [248]. Myo-inositol is a key precursor of membrane phospho-inositides (PI) and phospholipids

and it is also involved in cell-membrane and myelin-sheet structures. Increased membrane turnover or damage to myelin sheets in AD may be the underlying cause of increased concentrations of free myo-inositol. Arguing against the above hypothesis, it has also been shown that activation of the polyol pathway decreased the levels of NADPH and oxidised NAD^+, which in turn leads to decreased synthesis of myo-inositol (along with glutathione, nitric oxide, and taurine). In addition, inhibition of the polyol pathway in the tissues of STZ-diabetic rats resulted in preservation of myo-inositol level in nerves [249]. Intriguingly, our results suggest both increased polyol pathway activity and myo-inositol levels, at least in the ENT of the AD brain. Taken together, elevation of both myo-inositol-1-P and myo-inositol could therefore reflect compensatory mechanisms concerned with phospholipid metabolism and membrane turnover in AD.

3.4.1.4. Nucleobase, nucleosides and nucleotides

Genomic stability in the brain is of particular interest because neurons are terminally differentiated and have a high level of metabolic activity, which results in high amounts of ROS [250]. Therefore, the level of nucleosides is an important aspect of the physiological status of the brain. Furthermore, some nucleosides and nucleotides can act as neuromodulators and co-transmitters in the brain and were suggested to play a role in neurodegenerative diseases such as AD [251].

We detected changes in three nucleobases, adenine, guanine, and uracil. Adenine and guanine are purines. Adenine was significantly elevated in the CB while guanine was increased in MTG and SCx. Hypoxanthine, an important intermediate in both the synthesis and degradation of purine nucleotides, was decreased by about 20% in the AD brain. In contrast, the hypoxanthine derivative uric acid showed extreme elevation in the AD brain. Uric acid is a powerful antioxidant and radical scavenger in humans whose generation is increased during oxidative stress [252]. The neuroprotective effect of uric acid has been associated with its ability to suppress oxidative stress and lipid peroxidation [253]. Uric acid is also the final breakdown product of purine metabolism in humans (not of amino acids) and its immediate precursor is hypoxanthine. The elevated uric acid levels observed in this study may also reflect increased purine catabolism, possibly in response to polyol pathway-induced oxidative stress.

Patients with mild cognitive impairment and AD have been reported to have lower levels of uric acid in their plasma [254-256] and serum [257]. Nevertheless, patients with presenile and senile dementia of the Alzheimer type, and multi-infarct dementia showed significantly elevated levels of uric acid in the CSF [258], which is consistent with our findings in the AD brain.

One of the most dramatic changes observed consistently across all brain regions is the decreased levels of the pyrimidine, uracil. The direct effect of reduced uracil levels in the brain has not been previously demonstrated; however, impaired uracil repair induced by folate deficiency was suggested to participate in neurodegeneration and neuropsychiatric dysfunction [259]. The ribonucleoside guanosine was significantly elevated in MTG, which coincides with the increase of guanine in that brain region (note: both guanine and guanosine IDs were classified as ‘putative’).

3.4.1.5. Lipids

The saturated fatty acids myristic acid (tetradecanoic acid) and margaric acid (heptadecanoic acid) were both up-regulated in AD (consistently in MTG). A general increase in fatty acids was also observed in the LC-MS study, which will be discussed further in Section 3.4.2.4.

The brain is highly enriched in cholesterol compared with other tissues. Nearly all cholesterol in the brain is synthesised *in situ* as plasma lipoproteins do not cross the intact blood-brain barrier [260]. It has been suggested that profound alterations in cholesterol metabolism occur in AD although whether these contribute to neurodegeneration remains unclear [261]. Reduction in the levels of cholesterol in hippocampal neurons caused by statin treatment not only reduced synaptic density but also impaired synaptic vesicle release [262] which is critical for brain function. Consistent with the observed decrease in cholesterol levels, we also found the levels of the esters of cholesterol significantly decreased in AD brain (see Section 3.4.2.4).

Interconversion between glycerol and glucose can occur via the following pathway: glycerol↔glycerol-3-P↔ dihydroxyacetone phosphate ↔glycerlaldehyde-3-P↔glucose. Increased levels of glycerol-3-P and glucose, combined with decreased levels of glycerol, suggests that the glycerol to glucose conversion may be favoured in the AD brain. Glycerol can be released through the degradation of phospholipids (plasma membranes) and TGs, which may be consistent with the altered levels of both phospholipids and TGs (see Section3.4.2.2 and 3.4.2.3).

3.4.1.6. TCA cycle and urea cycle

Appropriate mitochondrial function is critical in brain energetics due to the central role of these organelles in ATP generation. Normal TCA-cycle function is important for complete oxidation of the pyruvate generated by glycolysis. The TCA cycle is initiated by condensation of acetyl-CoA, provided by oxidative decarboxylation of pyruvate through the action of the pyruvate dehydrogenase complex (PDHC). According to our iTRAQ data (see details in Chapter Four), the protein levels of PHDC subunits, isocitrate dehydrogenase, alpha-ketoglutarate dehydrogenase complex (KGDHC), and succinyl CoA synthetase were all decreased significantly in the AD brain. These changes in the early TCA cycle enzymes may in part, explain the alterations in TCA cycle metabolites. While the changes were not consistent in all brain regions, all the statistically significant observations showed increases in citrate, succinate, fumarate, and malate.

Taken together, these results are consistent with defective activity ofthe TCA cycle. Specifically, decreased enzymes with accumulation in metabolites associated with the cycle may lead to glucose hypometabolism and oxidative stress, as well as mitochondrial dysfunction in the brain of AD patients.

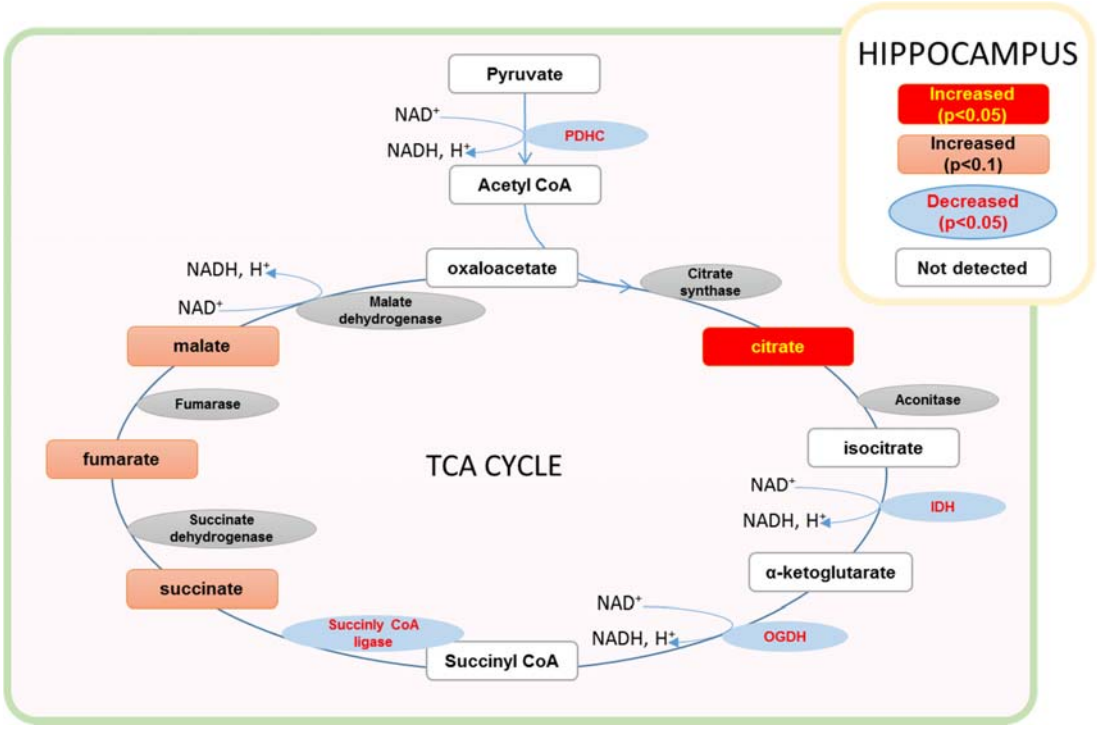

Figure 3-14 TCA cycle in HP of AD brain

Altered metabolites of TCA cycle all showed increased abundance. This observation may be associated with the change in TCA cycle enzymes; altered enzymes of TCA cycle all showed decreased abundance in the AD brain (as per iTRAQ results, Chapter Four). Abbreviations: PDHC, Pyruvate dehydrogenase complex; IDH, isocitrate dehydrogenase; OGDH, 2-oxoglutarate dehydrogenase.

3.4.1.7. Urea cycle and amino acid metabolism

The urea cycle removes neurotoxic ammonia by converting it to non-toxic urea. When the urea cycle is defective, ammonia can build up in the circulation and readily enter the brain across the blood brain barrier. The brain is very sensitive to excessive ammonia as marked by brain damage in patients with carbamoyl phosphate synthetase deficiency [263]. However, whether or not the urea cycle exists in human brain is still being debated. While some argue that urea can be synthesised from arginine within the brain as shown in rat [264], others believe that carbamoyl phosphate synthetase is absent in the CNS [265], hence supporting the opposing view that the urea cycle is absent from the brain. In our iTRAQ study, we detected peptides derived from carbamoyl phosphate synthetase in HP but not in ENT or CB. We found the level of carbamoyl phosphate synthetase to be reduced to ~60% in the HP of AD brain (see Chapter Four).

The urea cycle is critical for amino-acid metabolism. Nitrogen from catabolism of amino acids can enter the cycle in the form of ammonium ions or glutamate, by the transdeamination or the transamination route (**Figure 3-15**). In the transdeamination route, α-ketoglutarate accepts an amino group from the donor amino acid to form glutamate in the cytosol, which is then transported into the mitochondrion for deamination. The ammonium ion is incorporated into carbamoyl phosphate, which in turn reacts with ornithine to enter the urea cycle as citrulline. The formation of carbamoyl phosphate is catalysed by

carbamoyl phosphate synthetase, which is only active in the presence of its allosteric effector N-Acetylglutamic acid. The decrease in the levels of N-acetylglutamic acid in the AD brain is in line with the lower level of carbamoyl phosphate synthetase (present in HP according to our iTRAQ study). Reduced carbamoyl phosphate synthetase activity may compromise the transdeamination route and result in the buildup of glutamate. In the HP, where carbamoyl phosphate synthetase was found to be lowered to ~0.6-fold, N-acetylglutamic acid was also trended downwards to ~0.6-fold of control ($p<0.1$) while glutamate was increased 1.2-fold (but not signficantly $p>0.1$).

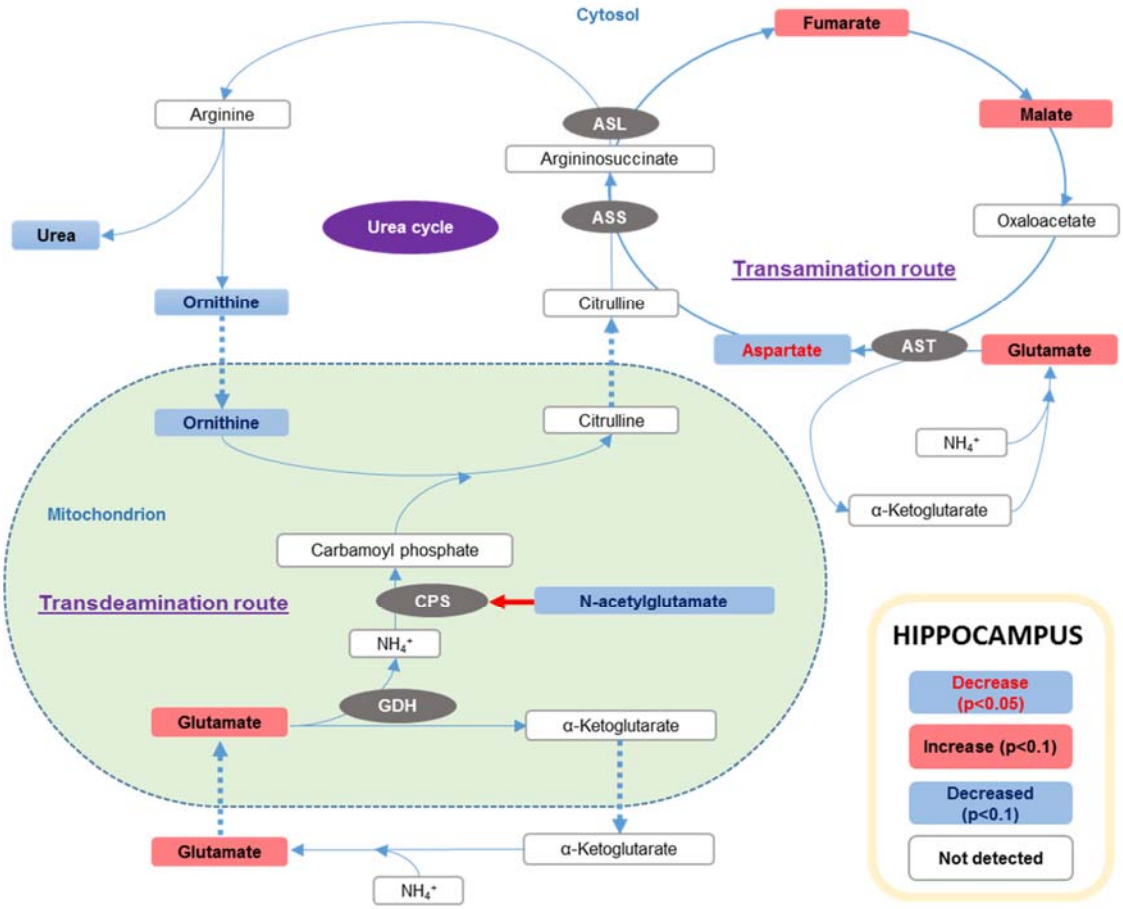

Figure 3-15 Urea cycle and nitrogen homeostasis in HP of AD brain

Homeostasis of nitrogen (generated from amino acid catabolism) is maintained through the urea cycle in conjuction with transdeamination/transamination routes. The decrease in N-acetylglutamate, an allosteric effector of the carbomoyl-phosphate synthase (CPS, rate-limiting enzyme of urea cycle), likely impaired the transdeamination route and the urea cycle. Despite the increased levels of fumarate, malate, and glutamate, levels of aspartate were decreased, indicating inefficient transamination route function. Accumulation of glutamate may be associated with blockage in the transamination and the transdeamination routes. Abbreviations: ASL, argininosuccinate lyase; ASS, argininosuccinate synthetase; AST, aspartate transaminase; CPS, carbomoyl-phosphate synthase; GDH, glutamate dehydrogenase.

The transamination route consists of two transamination reactions. The initial step is identical to the transdeamination route, and the second transamination involves oxaloacetate accepting an amino

group from glutamate to form aspartate, catalysed by aspartate amino transferase, which in turn condenses with citrulline to form argininosuccinate. Argininosuccinate is then cleaved into fumarate and arginine. Arginine is hydrolysed to ornithine and urea (**Figure 3-15**). The observed build-up of glutamate and concomitant decrease in aspartate may reflect defects in this route. In line with the marked elevation in glutamate, we also observed an elevation in pyroglutamate, which is reported to form from glutamate and/or glutamine during derivatisation and GC injection. Moreover, a decrease in the levels of both ornithine and urea also indicate a defect in the urea cycle in the AD brain. (It has to be noted that ornithine is reported to form from arginine during derivatisation and GC injection, in which case, less arginine in the samples may be the cause of less ornithine).

Although the main function of the urea cycle is to produce urea, a small but significant quantity of arginine is diverted to form creatine, which is ultimately used for ATP production. The breakdown product of creatine, creatinine, has been shown to increase in the CSF of presenile and senile dementia of Alzheimer type and mild cognitive impairment patients [258]. Creatinine levels were significantly increased in the MTG of AD brains compared to the controls in our study.

3.4.1.8. Amino acids

Amino acids are highly concentrated in the brain where they are of particular importance since their derivatives can not only subserve structural functions and provide an energy source, but also participate in synaptic transmission as neurotransmitters and neuromodulators. The metabolism of amino acids in the brain is similar to that in other tissues with the exception of ongoing uncertainty concerning the status of the urea cycle.

Glycine, proline, and serine were consistently decreased in AD across most of the brain regions in this study. Both serine and glycine are glucogenic, and can be synthesised from intermediates formed by glycolysis. The lower levels of these amino acids may be related to compromised glycolysis in AD brain.

Changes in the levels of free amino acids may also have profound effects in the brain through alterations in neurotransmitter function. In our study, the levels of leucine were decreased in ENT and CB, while valine was decreased in CB but increased in MTG. The branched-chain amino acids leucine and valine are ideal candidates as the amino donors for brain glutamate synthesis as glutamate does not cross the blood brain barrier. Experimental evidence shows that up to approximately 25% of the nitrogen present in brain glutamate is derived from leucine alone [266]. Therefore, our observation of decreased leucine may be a direct consequence of increased glutamate formation in the AD brain.

Glutamate not only plays a critical role in the urea cycle (as discussed in earlier), but also act as the main excitatory neurotransmitter. It can also cause excitotoxicity upon excessive accumulation. Previously reported changes in glutamate levels in AD brain are contradictory, possibly due to general differences in the measurements performed in *ante-* and *post-mortem* tissue [267,268]. Glutamate is also the precursor of GABA, a predominant inhibitory CNS neurotransmitter. GABA is formed by the enzyme glutamic acid decarboxylase which has been reported to be decreased in AD [269]. The observed increase

in glutamate and concomitant reduction in GABA in our study is consistent with defective glutamic acid decarboxylase function in AD. Gamma-hydroxybutyric acid is a GABA analogue that occurs naturally in the brain, where it is formed primarily from GABA [204]. Therefore, our observation of decreased gamma-hydroxybutyric acid may be a direct consequence of reduced levels of GABA.

N-acetylaspartate (a derivative of aspartic acid) is the second-most concentrated molecule in the brain after glutamate and is known to decrease in numerous neuropathological conditions, including AD [270]. Consistently, lower levels of N-acetylaspartate were found in MTG of AD brain in the current study.

We also observed an overall elevation in the levels of phenylalanine, tyrosine, and tryptophan, although statistical significance was not reached in all brain regions. Apart from their roles as constituents of protein, the only other known functions of these aromatic amino acids in the brain are as precursors for the monoamine (serotonin) and catecholamine (dopamine, norepinephrine, and epinephrine) neurotransmitters. The biosynthesis of these neurotransmitters is sensitive to local substrate concentrations [271]. Therefore, altered levels of these amino acids likely influence their rates of conversion to neurotransmitter products, presumably with functional consequences in the brain. Serotonin levels have been shown to be significantly lower in AD brains [272,273]. However tryptophan was reported to be unaltered [273]. Interestingly, we found tryptophan consistently elevated in most brain regions. Phenylalanine is the precursor for tyrosine, which is a precursor of dopamine, norepinephrine and epinephrine (collectively known as the catecholamines). Lower levels of dopamine have been reported in AD brains and were negatively associated with the level of its precursor, tyrosine [273]. Significant reduction in norepinephrine has also been previously reported in AD patients [274]. Our observation of increased levels of phenylalanine and tyrosine in the AD brain is consistent with previously reported increases in levels of these amino acids in the CSF of AD patients [275]. Overall, it is intriguing to observe such consistent increases in precursors of neurotransmitters when the actual neurotransmitters are known to be decreased in AD. Neuropsychiatric symptoms seen in AD are not simply a consequence of neurodegeneration, but probably result from differential neurotransmitter alterations [272]. The altered levels of neurotransmitter precursors found in this study ae consistent with possible defects in neurotransmitter synthetic pathways in the brains of AD patients.

3.4.1.9. Other significant findings of GC-MS

We observed several other alterations in metabolites that may have implications in the pathology of AD brain. Ascorbate (vitamin C) is a vital antioxidant molecule in the brain, and its regional asymmetry in distribution within different brain areas is believed to be associated with its role as a neuromodulator. Neurodegenerative diseases typically involve high levels of oxidative stress and thus ascorbate has been proposed to have potential therapeutic roles against AD [276]. Our data showed a general increase in ascorbate levels in the AD brain. However, we cannot exclude that the AD patients were subjected to ascorbate treatment prior to death.

We also observed significantly elevated 2-hydroxyglutaric acid levels in the AD brain. Increased 2-hydroxyglutaric acid (in serum, urine and CSF) is the biochemical hallmark of a genetic disorder called

hydroxyglutaric aciduria, wherein the central nervous system is exclusively affected [277]. It has been suggested that 2-hyroxyglutaric acid may cause the observed neuropathology in hydroxyglutaric aciduria via induction of oxidative stress in the brain [278]. 2-Hydroxyglutaric acid is normally metabolised to α-ketoglutarate by L-2-hydroxyglutarate dehydrogenase (L2HGDH) [279], which we found to be decreased in CB of AD brain (see Chapter Four). The significant alteration in 2-hydroxyglutaric acid may be associated with changed glutamate metabolism in the AD brain (discussed in 3.3.2.6).

3.4.2. Findings from LC-MS

3.4.2.1. Sphingolipids

Accumulating evidence suggests that disrupted lipid homeostasis plays an important role in the pathogenesis/pathology of AD. Not only does neuronal lipid composition regulate the trafficking and activity of the membrane-bound proteins that control Aβ levels and their propensity to aggregate, but the toxicity of Aβ is exerted through perturbation of cellular membranes, in part by modulating phospholipase activities [214]. More specifically, deregulation of sphingolipid metabolism has been linked to the accumulation of Aβ peptides in AD. Furthermore, Aβ has been shown to induce apoptosis via the sphingomyelin/ceramide pathway in various brain cells, *in vitro* [280].

Ceramide is the core constituent of most sphingolipids. It can be produced by hydrolysis of sphingomyelin via sphingomyelinases, or synthesised *de novo* from fatty acyl CoA and sphingosine. Sphingomyelin degradation is the probable source of most ceramide in cells [281]. Ceramide is also an important second messenger molecule that regulates diverse cellular processes and it has been suggested that elevated ceramide levels induce neuronal death in AD via: 1) involvement in apoptotic signalling in neurons; and/or 2) stabilising the APP cleaving enzyme 1 (BACE1) thereby promoting Aβ biogenesis [280]. Previously, increases in the level of acid ceramidase in AD brain [282] have been suggested to account for the increase ceramide levels in the CSF [283]. Elevated levels of acid sphingomyelinase and ceramidase expression in AD may also lead to a reduction in sphingomyelin and elevation of ceramide [280]. In line with this, we found levels of sphingomyelins consistently decreased in all the brain regions examined in current study (except for CB, where some species of sphingomyelin were increased). However, the change in ceramides trended the same way as sphingomyelins and contradicted previously reported results. Ceramides in the heavily affected brain regions (including HP, ENT, MTG, SCx and MCx) were decreased whereas in the less affected brain regions (CG and CB), elevations were observed in some of the species. According to our proteomics study (see details in Chapter Four), there was no significant change in sphingomyelinase protein but the levels of ceramidase protein were significantly increased in HP. This profile may reflect steady hydrolysis of sphingomyelin to ceramide but increased ceramide conversion to sphingosine. Sphingosine is an important product of ceramide hydrolysis by ceramidases and can be phosphorylated by sphingosine kinase to form sphingosine-1P. In contrast to ceramide and sphingosine, sphingosine-1P can antagonise apoptosis and has been suggested to act as a potent neuroprotective factor against Aβ-induced neuronal apoptosis through inhibiting sphingomyelinase activation [284-286]. Contradictory to the

previously reported reduction in sphingosine-1P and elevated ceramide [280], we found here elevated sphingosine-1P with lowered ceramide. However, this finding is consistent with our parallel proteomics result: increased levels of ceramidase may have increased conversion of ceramide to sphingosine, which may have led to the elevation in the sphingosine-1P receptor 1 (S1PR1) level in the HP in our study (Chapter Four) (**Figure 3-16**).

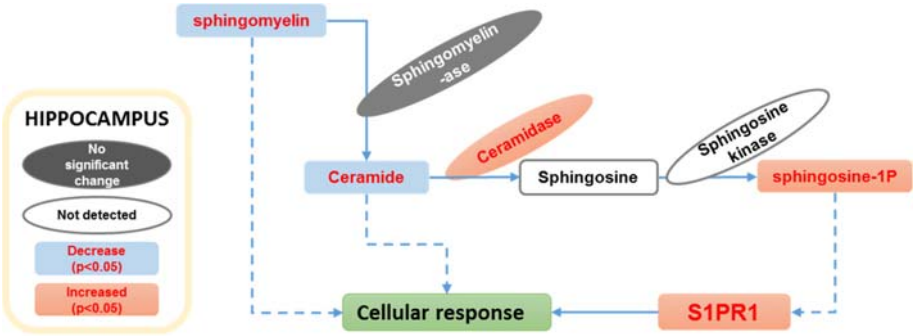

Figure 3-16 Sphingolipid perturbation in HP of AD brain.

Hydrolysis of sphingomyelin by sphingomyelinase generates ceramide, a core constituent of most sphingolipids. Sphingomyelin and ceramide levels were both decreased in the AD brain but no significant change in sphingomyelinase was observed (Chapter Four). Ceramidase, increased according to our iTRAQ study, may increase the hydrolysis of ceramide to sphingosine, which in turn, is phosphorylated to form sphingosine-1P by sphingosine kinase. Increased levels of sphingosine-1P and its receptor, sphingosine-1P receptor 1 (as per iTRAQ study), may take part in a diverse cellular processes. Abbreviations: S1PR1, sphingosine-1P receptor 1; SM, sphingomyelin.

Ceramide can also be converted to GlcCer by glucosylceramide synthase activity. The pattern of change in GlcCer species was very similar to those of sphingomyelin and ceramide, indicating that the conversion between sphingomyelin, ceramide, and GlcCer may be at a steady rate. Taken together, levels of glycolipids were generally reduced in all the brain regions except for CB. In line with this, glycolipid transfer protein was only found to be significantly up-regulated in CB (see Chapter Four), possibly induced by the increased level of glycolipids in CB.

3.4.2.2. Glycerophospholipids

Glycerophospholipids are lipids that constitute a diverse group of molecules with important functions in the brain. The PCs are the main component of cell membranes and lipoproteins, precursors of signalling molecules, inflammatory molecules (e.g. platelet-activating factor), and neurotransmitters [287]. Hydrolysis of PCs by phospholipases generates the signalling and inflammatory molecules [288]. In this study, PCs are reported in three separate tables. PCs with smaller retention times (<400) were summarised into one table and the rest (retention time >400) into two other tables depending on the whether the side-chains consisted of acyl groups only or also contained alkyl-ether/plasmalogen substituents. Levels of PCs with smaller retention times were quite variable in all the brain regions except MTG, wherein all of those with statistical significance were elevated. All the PCs with only acyl chains were strongly decreased (to ~0.1- to 0.5-fold of control) in the heavily affected brain regions (including HP, ENT, MTG, SCx and MCx). In CG and CB, elevated species were also present. All except one of the PCs with substituents that reached statistical significance were decreased (to ~0.1- to 0.8-

fold). The number of species that were significantly altered was greater in the more heavily affected brain regions in CG and CB.

Among the PEs that were altered significantly in this study, only the two with the smallest retention times (PE(44:11) and PE(20:4)) were increased while the remainder were decreased in all brain regions except CB. The CB not only had fewer altered PEs compared to the heavily affected brain regions but was also the only region with a mixture of increased and decreased PEs.

Reduction in both PCs and PEs has previously been reported in human AD brain [289,290], and in the brain of a transgenic mouse model with mutated human APP/tau protein [291]. A recent data-mining study where 29 neurolipidomic datasets were investigated for changes in neuronal membrane phospholipid metabolism in AD, suggested that the hydrolysis of platelet-activating factor precursors and ethanolamine-containing plasmalogens was increased whereas the regeneration of rare alkyl-acyl and alkenyl-acyl structural phospholipids were compromised [292].

In this study, the increased species of PCs and PEs were mostly lysophosphatidylcholine (lysoPCs) and PEs with smaller retention times, possibly consistent with a role as bioactive metabolites belonging to the platelet-activating factor-like lipids that include oxidised phospholipids (oxPL) and lysoPC. Accumulation of these metabolites could possibly arise from increased hydrolysis of platelet-activating factor precursors and they have been associated with aggravating tau pathology, enhancing vesicular release, and signalling neuronal loss [292]. Our finding is also consistent with the observed increase in the lysoPC to PC ratio that accompanies the GP decrease in late onset AD [287]. Supporting the changes described above, our study also showed various alterations in the enzymes involved in the metabolism of phospholipids; significant changes were detected in numerous phospholipases, lysophospholipases, and also annexins that suppress phospholipase activity (see details in Chapter Four).

Consistent with the current literature, our study showed that PCs and PEs were in general depleted in more heavily affected brain regions in AD. For example, our study identified a large number of PCs and PEs with alky-acyl and alkenyl-acyl structures that were greatly diminished in the heavily affected brain regions (that is, with the exception of CB). Reduction of plasmalogen-containing PEs in grey matter has previously been correlated to the severity of AD and considering that that synaptic vesicles are comprised of over 60% of plasmalogen in total PE, plasmalogen deficiency was proposed to affect synaptic function and structure adversely in AD [293]. We believe that the reduction in plasmalogen-containing PEs and PCs as detected in our study could play a significant role in AD neuropathology/pathogenesis, especially in aspects of neuronal integrity.

Changes in PSs and PIs showed similar pattern to PCs and PEs; lyso-species were increased and the rest were decreased in all brain regions except for CB. The majority of the PSs reported here were decreased, consistent with previously shown progressive reduction of PS (together with PC and PE) content from healthy to mild cognitive impairment, and from mild cognitive impairment to AD in the CSF [287]. Reduction in overall PI content has been documented before in the *post-mor*tem brain of AD patients [294]. Metabolism of structural-membrane PIs can generate powerful lipid-based second messengers.

Therefore, a decrease in PIs as observed in this study could possibly imply impaired neurotransmitter release. For example, depletion in species such as PI(16:0/20:4), PI(16:0/22:6), and PI(18:0/22:6) has been implicated in accelerating Aβ42 biogenesis in AD [292]. All the PGs reported here (half of which were lysoPGs), were increased in most of the heavily affected brain regions whereas in the less affected regions (CG and CB), they were either unaltered or decreased.

With the exception of CB, all the brain regions exhibited overwhelmingly consistent features of up-regulated lysophospholipids (including species of lysoPC, lysoPS, lysoPI, and lysoPG) and various fatty acids, with concomitant reductions in phospholipid-containing long-acyl chains or alkyl/plasmalogen substituents. This profile fits well with the idea of increased hydrolysis of phospholipids, in particular those that contain long-acyl chains or alkyl/plasmalogen substituents.

Intriguingly, this pattern of lipid-compositional change in AD brain is similar to that observed in the brain after being exposed to snake venom toxin with phospholipase activity. A snake venom component known as snake presynaptic phospholipase A2 neurotoxins (SPANs) was shown to stimulate membrane-lipid hydrolysis to generate lyso-phospholipids and fatty acids [295]. Addition of lyso-phospholipids and fatty acids into neuronal cultures has also been shown to initiate a similar response to that of SPANs, including neurotransmitter release and vesicular depletion that leads to synaptic failure [295].

Our observations in this study provide further support for the hypothesis that compositional changes in lipids might increase vesicular release and precipitate vesicular depletion over the course of AD progression [292].

3.4.2.3. Glycerolipids

DG and TG make up only a small portion of the entire brain lipidome. Many species of signalling DGs (eg DG(38:4)) have been shown to be up-regulated in the AD brain [214]. In our study, species of DG were only increased in CG and CB whereas HP, MTG, SCx and MCx presented a general decrease in DG species (including DG(38:4)) with few exceptions (e.g. DG(42:10)).

TG is considered to act as a store for fatty acids, as well as a precursor for DG and phospholipids. TG metabolism (both synthesis and degradation) can generate intermediates such as lysoPA, PA, and DG that are modulators of signalling pathways involving peroxisome proliferator-activated receptor-γ (PPARγ), the mammalian target of rapamycin (mTOR), and protein kinase C (PKC) isoforms [296]. In the current study, only a few TGs were altered and none of these species was consistently detected across the different brain regions. In general, altered TGs were increased in HP, SCx, and MCx but decreased in MTG and CB. Glycerol-3-P acyltransferases are the rate-limiting enzymes of TG biosynthesis [297]. Our proteomic data indicate a reduction in these enzymes (1-acyl-sn-glycerol-3-phosphate acyltransferase) in CB but not in HP and ENT (Chapter Four). Decreased levels of TGs may be a consequence of reduced TG biosynthesis in CB (glycerol-3-P was increased in CB according to GC-MS studies). On the other hand, this finding could also result from increased TG degradation,

considering the increased levels of breakdown intermediates such as DG and fatty acid in the CB. The build-up of DG may also result from decreased breakdown of DG itself. Here, the enzyme that catalyses the hydrolysis of DG (diacylglycerol lipase α) was decresased in CB, but not in HP and ENT (Chapter Four). Therefore, at least in CB, both the synthesis of TG and degradation of DG were likely defective, which may account for the observed accumulation of DGs and reduction of TGs.

DG is a lipid second messenger involved in modulating a variety of neurological functions such as synaptic activity, neuronal plasticity, and neurotransmitter release [298,299]. Protein levels of the enzyme DG kinase β which converts DG to PA, trended toward an increase in CB and HP (Chapter Four). While the level of DGs were increased in CB and decreased in HP, PA was found only in HP and the level was reduced. DG is also a precursor for PC, PE and PS [297] and elevation of DG may account for increased down-stream phospholipids. In line with this, elevation in species of PC, PE, and PS were only seen in CB, opposite to the general trend of reduction in all other brain regions.

3.4.2.4. Fatty acyls and Sterol lipids

Fatty acids serve as an energy source that can be mobilised via TG hydrolysis. Free fatty acids are utilised through oxidation in three consecutive processes: β-oxidation, the TCA cycle, and respiratory chain. Circulating fatty acids do not enter the brain and it has been suggested that the brain endogenously synthesises and degrades its constituent fatty acids [300]. Elevated fatty acids were not consistent across all brain regions examined, although those with significant changes were increased in abundance. HP, ENT and SCx showed no more than two species with significant change. In comparison, MTG, MCx, CG, and CB showed more species with increased abundance. According to our parallel iTRAQ study, enzymes involved in β-oxidation were increased in abundance in HP and ENT, while decreased in CB. On the other hand, fatty-acid synthesising enzymes were decreased in HP, ENT, and CB (Chapter Four).

Among the sterol lipids that were detected with significant alteration, steroids were increased while sterols (specifically cholesterol esters) were decreased. Steroids comprise of a variety of hormones (e.g. sex steroids) with profound effects on brain function [301]. Current understanding of the effects of steroids support the notion that they can modulate neurological function and altered steroid function may possibly explain the reduction in AD risk associated with hormone replacement therapy [302]. Although we detected only a few species of putative steroid molecules, the results showed an unambiguous trend of elevation in the AD brain, which may be indicative of a general status of steroid perturbation in the disease state.

Brain cholesterol is primarily derived by *de novo* synthesis as the blood brain barrier prevents the uptake of cholesterol-containing lipoproteins from the circulation. In regard to AD, both the generation and clearance of Aβ are apparently regulated by cholesterol. Acyl-CoA cholesterol acyltransferase (ATAT) is responsible for cholesterol esterification and is also essential for the regulation of intracellular cholesterol homeostasis [303]. In humans, there are two isoforms of ACAT, known as ACAT1 and ACAT2. According to our iTRAQ study, both isoforms are present in significant amounts in human brain. ACTA1

was not altered in any of the brain regions examined (CB, HP, and ENT) while ACAT2 was up-regulated in CB only (Chapter Four). Previously, accumulation of cholesterol esters has been reported in the ENT of AD brain [214]. In contrast, we have detected a reduction in cholesterol ester in HP, MTG, and CB in our current study. However, only two species of cholesterol ester were inconsistently observed in different brain regions and therefore, no conclusive trend can be deduced regarding cholesterol ester alteration in the AD brain from the current study.

3.5. Conclusion

We have performed a comprehensive analysis of the metabolite changes in seven brain regions of post-mortem brain from nine AD and eight control patients. The changes in metabolites with functional implications in the brain were supported by our parallel proteomics dataset derived from the same samples (discussed in Chapter Four).

In summary, AD brains exhibited defective energy production; specifically, the glycolytic pathway may be compromised with subsequent effects on activation of the polyol pathway and the pentose-phosphate pathway. The change in levels of alternative fuel sources including amino acids may be a result of disrupted TCA and urea cycle activity, which may also be associated with defects in glycolytic pathway function. The observed perturbations in the levels of phospholipids and fatty acids may represent a response to impaired fuel metabolism, with catastrophic effects on the integrity and function of neurons and related structures. We hypothesise that physiological manifestation of AD could also be closely linked to the loss of brain sphingolipid content and build-up of neurotransmitter precursors. These interpretations do not take into account the possibility that various causes of death and pre-mortem treatments that are common in AD patients could influence metabolite levels. This is due to the unavailablity of established correlation between these factors and metabolite levels through systematic examination. Brain regions including HP, ENT, MTG, MCx and SCx appear to carry more severe metabolite alterations than CG and CB. The intriguing difference between brain regions, especially in the CB, may represent the difference between the early and late–stage responses to the underlying disease process.

Chapter 4. Molecular Profiling of the Brain in Alzheimer's Disease: a Proteomics Approach

4.1. Introduction

AD is a multifactorial disease with many pathophysiological characteristics. Definitive diagnosis of AD requires *post-mortem* examination confirming sufficient numbers of plaques and tangles [304,305]. Accumulation of Aβ peptide and microtubule-associated protein tau which exhibit hyperphosphorylation, and oxidative modifications are considered to be central to the pathology of AD [306]. Defects in axonal transport are closely linked to these central pathological features of AD: disturbances in axonal transport participate in plaque biogenesis, as APP is axonally transported to synaptic terminals in brain regions affected in AD [307]. Furthermore, microtubules are an intrinsic part of the axonal transport system and deficits therein are intertwined with abnormalities of microtubule-associated protein tau [308].

Other prominent features of AD include decreased energy metabolism and increased oxidative damage in the brain; early region-specific decline in glucose utilisation and mitochondrial dysfunction are also characteristic of AD brain. These defects consequently deplete ATP production and increase ROS production in neurons [309]. In an environment of such disturbed cellular homeostasis and energy metabolism, oxidative stress not only renders neurons vulnerable to excitotoxicity but also activates the cascade of apoptotic cell death [306]. Excitotoxicity in the AD brain arises from altered glutamatergic signalling [310], and dysregulation in other neurotransmitters has also been documented, including abnormalities of adrenergic, serotonergic and dopaminergic neurotransmission [311]. In response to pathological stimuli (such as ROS) associated with AD, inflammatory events mediated through both innate and cell-mediated immune mechanisms are also present in AD brain [306].

Proteomics is a relatively recent technique currently undergoing rapid development. A sub-discipline of proteomics, “neuroproteomics”, investigates protein-driven molecular mechanisms and functions of the CNS (and CNS disorders) through examination of proteomes, and aids discovery of novel protein biomarkers for diagnosis, treatment monitoring and prognosis [312]. Mass spectrometry based proteomics has been recognised as a powerful tool with the potential to accelerate biomarker discovery [313].

In the study of neurodegenerative disease, CNS tissue is an ideal source for biomarker discovery; *post-mortem* proteomics analysis of brain is also important for understanding the complexity of neurodegenerative disease as it allows for examination of protein changes in the tissue where the degenerative process occurs [312]. However, with the difficulty in studying brain tissue directly, the neuroproteomic approach was most commonly applied to CSF and blood (serum/plasma). To date, there are only a few proteomics studies of AD carried out using whole tissue extraction of brain tissue. Typically examining a single AD affected brain region, these studies identified 800 to1400 of proteins of which 10 to 200 were changed significantly in the pathological state (**Table 4-1**).

Table 4-1: Overview of proteomics studies of human AD brain, whole tissue extraction

Brain tissue	Method	Identified proteins, total (altered)	Reference
Temporal neocortex	DML, LC MS/MS	1096 (62)	314
Temporal neocortex	DML, LC MS/MS	827 (69)	315
Hippocampus, parietal cortex, cerebellum	iTRAQ 2D LC MS/MS	950 (31)	316
Temporal cortex	AMT, LC MS/MS	1400 (197)	317
Substantia nigra	Nano-UPLC MS/MS	not specified (19)	318

DML; dimethyl labelling, iTRAQ; Isobaric tag for relative and absolute quantitation, AMT; accurate mass and time tag.

In this study, we aimed to carry out iTRAQ-based proteomics analysis of three regions of *post-mortem* brains of AD patients, HP, ENT, and CB, which are known to undergo different degrees of damage in the disease process. We aimed to generate and compare molecular profiles that represents global disturbance in these brain regions and gain insight into the different molecular mechanisms underlying AD pathogenesis in a brain-region specific manner.

4.2. Methods

Human brain tissue samples for the proteomics study were collected at the same time as those for the metabolomics study, as per Chapter Three.

4.2.1. Protein extraction and preparation for iTRAQ

To each 2-mL safelock tube containing 50-100 µg human brain tissue, 500 µL 1 M Triethyl ammonium bicarbonate buffer (TEAB) + 0.1% (w/v) SDS were added. One 3-mm tungsten bead was added into the tube and samples were homogenised with a Qiagen tissuelyser, 2 × 3 min at 25 Hz. The tubes were then vortexed for 10 s and centrifuged at 4 ^{o}C for 5 min at 13,400 × g. The supernatants were transferred into a new set of tubes.

Protein concentration was measured with Bio-Rad reagent (Bio-Rad Protein Assay Dye Reagent Concentrate (500-0006)) and a SpectraMax M5 plate-reader (Molecular Devices). From each sample, a volume equivalent to 100-µg protein was transferred into a new set of tubes for further processing. Identical reference-pool samples (total of 100-µg protein per reference sample) were made by

combining portions from four representative individual samples from each group, AD and control. All samples were equalised for final volume using 1 M TEAB.

Protein samples were reduced by addition of DTT to a final concentration of 59 mM, followed by incubation at 60 °C for 30 min. The samples were then vortexed and spun briefly. Alkylation was carried out by addition of iodoacetamide to a final concentration of 11 mM, followed by incubation in the dark at room temperature for 10-15 min, and subsequently vortexed and spun briefly.

Protein digestion was carried out by adding trypsin (Promega, V511A) at 10:1 substrate:enzyme ratio (ie. 10 µg trypsin for each 100 µg protein sample aliquot). Lyophilised trypsin was first reconstituted in 0.2 M TEAB to 0.5 µg/µL concentration. To each protein sample, 20 µL of this trypsin solution was added to ensure the final concentration of SDS in the protein sample (from the extraction buffer) was brought down to 0.05% (w/v) or lower. Samples were incubated overnight at 37 °C after vortexing and a pulse spin. After digestion, the samples were dried completely in an Eppendorf concentrator, and re-suspended in 30 µL 1 M TEAB to achieve equal volume across all samples before iTRAQ labelling. Samples were vortexed after re-suspension.

4.2.2. iTRAQ

4.2.2.1. iTRAQ labelling

The iTRAQ labelling was carried out according to the manufacturer's instruction using the 8-plex iTRAQ kit (AB Sciex, ITRAQ REAGENT 8PLEX MULTI-PLEX KIT Product Number: 4390812). Briefly, vials containing iTRAQ reagent were taken out of the freezer and thawed on the bench for 2-3 min. After spinning the samples down, 70 µL isopropanol was added to each vial, followed by a pulse spin. The content of the vials was then transferred to the protein samples according to the labelling scheme below (**Table 4-2**). Protein samples containing the iTRAQ labels were then incubated on the bench for 2-3 h followed by a further pulse spin.

Table 4-2: iTRAQ labelling scheme

	HP			ENT			CB		
LABEL	**Run 1**	**Run 2**	**Run 3**	**Run 1**	**Run 2**	**Run 3**	**Run 1**	**Run 2**	**Run 3**
113	RP1	RP1	RP1	RP1	RP1	RP1	RP1	RP1	RP1
114	RP2	RP2	RP2	RP2	RP2	RP2	RP2	RP2	RP2
115	101	102	104	504	501	502	401	403	404
116	103	106	105	505	503	508	406	402	408
117	107	109	108	506	507	509	407	405	409
118	112	113	111	514	512	510	412	413	410
119	117	115	114	515	513	511	417	414	411
121	110	118	116	516	517	518	418	415	416

Abbreviation: RP; reference pool sample

All the iTRAQ-labelled samples destined for the same LC-MS/MS run were pooled, followed by a spin at 13,400 × g for 5 min. Each pooled sample was then divided into 2 equal aliquots which were

completely dried using an Eppendorf concentrator. One pooled aliquot from each 8-plex experiment was subjected to High-pH reverse-phase (HpHRP) for peptide fractionation. Remaining dried-pool aliquots were stored in -80 ^{o}C for repeated analysis if required.

4.2.2.2. High-pH reversed-phase fractionation (HpHRP) and Nano UPLC

HpHRP was performed using an Agilent HPLC 1200 system controlled with Mercury software (Agilent, Santa Clara, California). Reversed-phase chromatography buffers (loading buffer (A2) (0.1% (v/v) ammonium hydroxide in HPLC-grade water) and elution buffer (B2) (0.1% (v/v) ammonium hydroxide in acetonitrile)) were made fresh daily.

A high-pH reversed-phase column (Agilent ZORBAX 300Extend-C18 4.6 × 150mm 3.5micron, Agilent) was used for liquid chromatography separation. The system was tested using a quality control sample (digest of bovine serum albumin) before and after each iTRAQ sample pool to ensure good fractionation.

Dried iTRAQ-labelled pools were re-suspended in 900 µL of a mixture of 97% (v/v) loading buffer (A2) and 3% (v/v) elution buffer (B2). The sample were then vortexed, centrifuged at 13,400 g for 2 min, and transferred to LC glass vials from which 880 µL was injected into the HPLC system. Each sample was first loaded onto the column using a 40-min run with a flow of 1mL/min at 3% (v/v) B2. The peptides were then eluted using the gradient described in **Table 4-3**. A total of 86 fractions were collected in a 96-well plate, which was dried in a concentrator (Eppendorf) and stored at –20 ˚C prior to 2D-LC-MS/MS analysis.

Table 4-3: HpHRP fractionation & nano UPLC gradient

HpHRP		**nano UPLC**			
TIME	% B2	TIME	FLOW (µL/min)	% A	% B
0	3	0	0.3	97	3
5	3	3	0.3	97	3
30	27	91	0.3	60	40
35	50	93	0.3	10	90
36	100	108	0.3	10	90
41	100	109	0.3	97	3
42	3	130	0.3	97	3

A nano-Acquity UPLC system (Waters) was used to separate the peptides before electrospray ionisation. Samples were re-suspended in 20 µL (97% water + 3% can + 0.1% trifluoroacetic acid (TFA; v/v/v)) and 5 µL was injected into the system. Peptides were trapped on a nanoAcquity 2G-V/M Trap Sym C18 5 µm 180 µm × 20 mm (Part #: 763973-902, Waters) and washed at a flow rate of 7.5 µL/min for 10 min. Peptides were then eluted and chromatographed using a nanoACQUITY BEH300 C18 1.7

µm 75 µm × 250 mm (Part #: 186003815, Waters) at 300 nL/min using the gradient shown in Table 4-3. The buffers used for nano-separation were : loading buffer (A) : 97% water + 3% acetonitrile + 0.1% formic acid and elution buffer (B) (v/v/v) : 100% acetonitrile + 0.1% formic acid (v/v). Gradients used for each fraction were as shown in (Table 4-3).

4.2.2.3. MS/MS

The eluent was directed into an ESI microionspray II source of a QSTAR Elite Q-TOF spectrometer (AB SCIEX) scanning in MS from 400 to 1200 m/z. Multiply-charged peptides (2+ to 4+) were selected for MS/MS analysis (110–1200 m/z). The information-dependent acquisition (IDA) settings were: 4 precursors per cycle and cycle times (MS 0.75 s, MS/MS1 0.75 s, MS/MS2 0.75 s, MS/MS3 1 s and MS/MS4 1 s). Selected peptides were fragmented twice and then dynamically excluded for 90 s. The resulting data were searched against the uniprot_sprot2013 database using Protein-Pilot v4.0 (AB SCIEX). Search parameters were: iTRAQ 8plex, trypsin; cys alkylation, iodoacetamide; search effort, thorough.

4.2.3. Data processing

4.2.3.1. Manual processing

Raw proteomic data exported as peptide summaries from each ProteinPilot search were processed manually. Specifically, all spectra matched with an “unused” below the 1% FDR threshold were discarded (Table 4-4), as were any spectra labelled “0” in the “Used” column (indicating that they failed on either confidence, level of iTRAQ label, were shared between more than one identified proteins or were otherwise deemed inappropriate for use by the matching software). Any remaining spectra matched to a reversed (decoy) sequence were also discarded.

The remaining, pruned datasets were then normalised as follows. All spectra were grouped in terms of the matched sequence being correctly cleaved or containing missed cleavages, as well as sequences containing a PQ motif (known to interfere with the 115 m/z iTRAQ label) or ending with a P (known to interfere with the 116 m/z iTRAQ label). The raw iTRAQ areas associated with each spectrum and each label was then converted to their natural logs (after addition of 1 to each value, to avoid excluding data for which no signal was detected for certain iTRAQ labels) and normalised to adjust for unequal loading. Separate correction factors were calculated for spectra matched to correctly cleaved peptides and peptides containing a missed tryptic cleavage site. In order to avoid interference from PQ-containing peptides and peptides ending with a P, the two sets of correction factors were calculated on data excluding these motifs. Correction factors were, however, applied to the entire dataset, including spectra matched to peptides containing the PQ motif or ending with a P. Corrected data were then back-transformed to linear space and the 1 added to each value for the purpose of normalisation was subtracted to give the final, corrected areas.

Table 4-4: Peptide summaries from all 8Plex runs

Brain region and run number		Unused score corresponding to the 1% FDR cut-off	Number of proteins above FDR cut-off		Number of matched spectra above FDR cut-off	
			Before pruning	After pruning	Before pruning	After pruning
HP	**Run 1**	0.84	3,509	3,115	449,019	29,373
HP	**Run 2**	0.70	3,857	3,374	636,015	36,873
HP	**Run 3**	0.84	4,220	3,651	442,599	53,035
ENT	**Run 1**	1.03	3,686	3,239	548,970	34,109
ENT	**Run 2**	1.15	3,473	2,994	448,223	32,830
ENT	**Run 3**	0.84	3,720	3,230	515,276	29,624
CB	**Run 1**	0.83	4,713	4,237	641,468	42,593
CB	**Run 2**	0.89	4,466	4,085	671,215	41,639
CB	**Run 3**	0.87	4,363	4,016	614,609	38,903

For each brain region, protein data from three runs were combined and aligned. Because most databases contain multiple entries for the same protein, as well as isoforms of proteins, the identical protein can be matched with the same probability to more than one specific entry in a sequence database. For investigations involving more than one run, this phenomenon leads to scattering of some data across multiple similar or identical database entries in a manner which weakens statistical power and hence compromises the quality of the results, unless precautions are taken to align identical peptides to the identical database entry in each run. To address this issue, a “combined search” is usually conducted in addition to the individual searches. The combined search involves asking ProteinPilot to perform an additional search, using the mass spectrometry output from all runs conducted for a tissue type (in this case, all three runs conducted for a specific brain region). While the data from the individual searches is used specifically to track iTRAQ label intensity for each protein in each sample, the combined search output is used to determine the “true” protein identity for each matched spectrum (based on a larger amount of data than is available from a single run).

This approach was applied for the brain samples of this study; however because of the very large amounts of data generated for these samples, the combined search result was too large to handle with the available computing equipment and so had to be abandoned. Instead, the alignment had to be done in a semi-manual fashion where the pruned peptide summaries from all three runs performed for each brain region were evaluated at the level of each matched peptides. Briefly, any peptide matched to a specific protein ID in two runs (but not three) was assigned to the same protein also in the third run. Any peptides matched to distinct proteins in all three runs were manually examined to determine the most likely “true identity”. Through this procedure, a customised ‘backbone’ database was created for each brain region and this was then used to append comparable protein names and accession numbers to each peptide matched in the individual runs.

After the alignment, all iTRAQ areas matched to the same protein were combined for each label. This generated raw sums for each protein for each of the eight iTRAQ labels. In conjunction with this, each spectrum matched to a peptide with a C-terminal P or containing a PQ motif was either removed from the data (if additional, non-compromised matches were available for the same protein) or retained in the data-set (if no other matches to the same protein were made). For spectra compromised in this manner that were retained, the data were managed manually at the pivot-table step. At that point, the sum for the 115 m/z label was removed for all proteins that were only identified by peptides containing a PQ motif and replaced with a letter code (to prevent calculations from the corresponding cells). Similarly, sums for the 116 m/z label were removed for any protein that was exclusively identified by peptides ending with a P.

The calculated raw sums were then exported to a master file, where data from all three runs conducted for each brain region were assembled and aligned. Following conversion to their natural logarithms, ratios were obtained for each protein in each sample, relative to the same protein in the region-specific reference sample (made from pooling of aliquots of all included samples from the region under study) that was repeated between runs. The resulting ratios were then scaled to let the average of the control group be 0 for each protein, and two-tailed t tests used to evaluate statistically significant differences between the groups. Correction for multiple comparisons was not applied as we consider this study a screening proteomics study designed for hypothesis generation. The resulting dataset is to be treated as preliminary only with validation through targeted studies. Cut-off for significance was set to $p<0.05$ and statistical analysis was limited to proteins detected in at least three samples per group.

The region-specific master files generated for each of the three regions were first aligned and then organised according to protein function/structure or, in the case of less well-researched proteins, according to common sequence motifs. This enabled immediate recognition of differences occurring within specific metabolic pathways, protein clusters or biological processes. However, the manual organisation is time-consuming as it was largely done by literature search for each identified protein. Due to the enormity of this task, pathway analysis was also performed to guide the progress of manual editing.

4.2.4. Pathway analysis

4.2.4.1. Go-enrichment

Simple enrichment analysis of the proteomic data were performed using the web-based GO Enrichment Analysis tool that is freely available on http://www.geneontology.org/page/go-enrichment-analysis. This tool uses GO annotations to calculate if the entered data (accessions only, no values) are enriched for any of the thousands of annotations available. There are three different parameters for the analysis; biological process, molecular function and cellular compartment.

Data format correction for Go-enrichment: a typical Protein Pilot entry shows an accession number such as “sp|P19367|HXK1_HUMAN” and this had to be converted to “HXK1_HUMAN” (ie. remove the prefix

"sp" and the |SWISSPROT_NUMBER|) in order to be recognised by the Go-enrichment analysis tool. Entries with multiple accessions were simplified. After correction, the full set of entries was first copied and pasted to analyse biological process, to get an overall look at overrepresented annotations in the dataset without focusing on the proteins that were significantly elevated or decreased in AD. This process was then repeated twice, for significantly increased and decreased subsets of the proteins respectively. The returned annotations from each analysis were then aligned and the p-values for the increased and decreased subsets were coupled to those returned for all proteins. Specifically, for any annotation that was found to be enriched ($p<0.05$) in a subset (increased or decreased), only those for which p was smaller in the subset than in the entire dataset were accepted as significant. This was to accommodate the fact that the brain samples were clearly enriched for many hundreds of annotations typical for brain tissue, but in a manner unrelated to disease. Also, the annotations for which the subsets were both significantly elevated and decreased were eliminated. Finally, all significantly altered annotations were aligned for all three brain regions.

4.2.4.2. IPA

Ingenuity Pathway Analysis (IPA) software (Qiagen) was used to generate a list of significantly altered canonical pathways. Unlike GO Enrichment Analysis, IPA uses all the changed proteins in a pathway, i.e. both increased and decreased proteins, to infer the significance of change for each pathway.

IPA provides p-values calculated by Fisher's Exact Test for detected pathways. The null hypothesis is the proportion of significant proteins from each dataset (p-value<0.05, FC>1.1) that map to a function that is similar to the proportion that map to the function in the entire population (i.e. when the entire dataset was used as the reference set). In this way, pathways that are enriched in the subset (p-value<0.05, FC>1.1) over and above those identified in the entire dataset were flagged as significantly altered in disease. Finally, pathways were aligned for all three brain regions.

It has to be noted that pathway analysis in this study was performed for the purpose of guiding the manual process and to obtain general comparisons between brain regions. Some of the pathways detected are very generic and neither GO Enrichment Analysis, nor IPA took into account the magnitude of changes in protein abundance. Therefore, detailed interpretation of the data generated in this study was heavily based on manual editing.

4.3. Results

4.3.1. Overall changes

The overall protein changes in three brain regions are summarised in **Table 4-5**. A total of 4138 unique proteins were identified in the HP, 3859 in the ENT and 4893 in CB. A marginally larger proportion of

the proteins were found to be significantly different in the HP (21.3% of all detected) and ENT (19.2% of all detected) compared to CB (18.2% of all detected).

Table 4-5: iTRAQ result summary

	HP	ENT	CB
Total proteins	4138	3859	4893
Higher abundance (p<0.05)	355 (8.6%)	256 (6.6%)	232 (4.7%)
Trending higher (p<0.1)	125 (3.0%)	119 (3.1%)	118 (2.4%)
Lower abundance (p<0.05)	527 (12.7 %)	485 (12.6%)	660 (13.5%)
Trending lower (p<0.1)	194 (4.7%)	200 (5.2%)	226 (4.6%)

The number of proteins differing between the AD and controls was comparable across all three brain regions.

Of the total amount of proteins identified in each brain region, 4.7~8.6% were increased (p<0.05) and 12.6~13.5% were decreased (Table 4-5). However, at the level of the specific proteins, there was much less consistency; only about half of the significantly altered proteins were consistent between brain regions and only about 30% of them were consistent across all three brain regions (Table 4-6). HP shared more significantly altered proteins with ENT than with CB. There was a similar amount of mutual, significantly altered proteins between HP and CB as between ENT and CB. Of the 3362 proteins that were found in all three brain regions, 60 were significantly increased and 169 were significantly decreased in all three brain regions (Table 4-6).

Table 4-6: Mutual changes among different brain regions

	HP & ENT	HP & CB	ENT & CB	All regions
Total proteins	3486	3747	3598	3362
Higher abundance (p<0.05)	144	107	84	60
Lower abundance (p<0.05)	294	239	255	169

To visualise the shared changes, the magnitude of changes was plotted for individual proteins in compared brain regions. The response was quite comparable between HP and ENT (Figure 4-1), whereas, both HP (Figure 4-2) and ENT (Figure 4-3) showed more dramatic response when compared to CB for most of the proteins plotted (i.e. proteins significantly increased/decreased in both brain regions). For those proteins that were significantly changed in all three brain regions, the magnitude of change was again smaller in CB compared to HP and ENT (Figure 4-4).

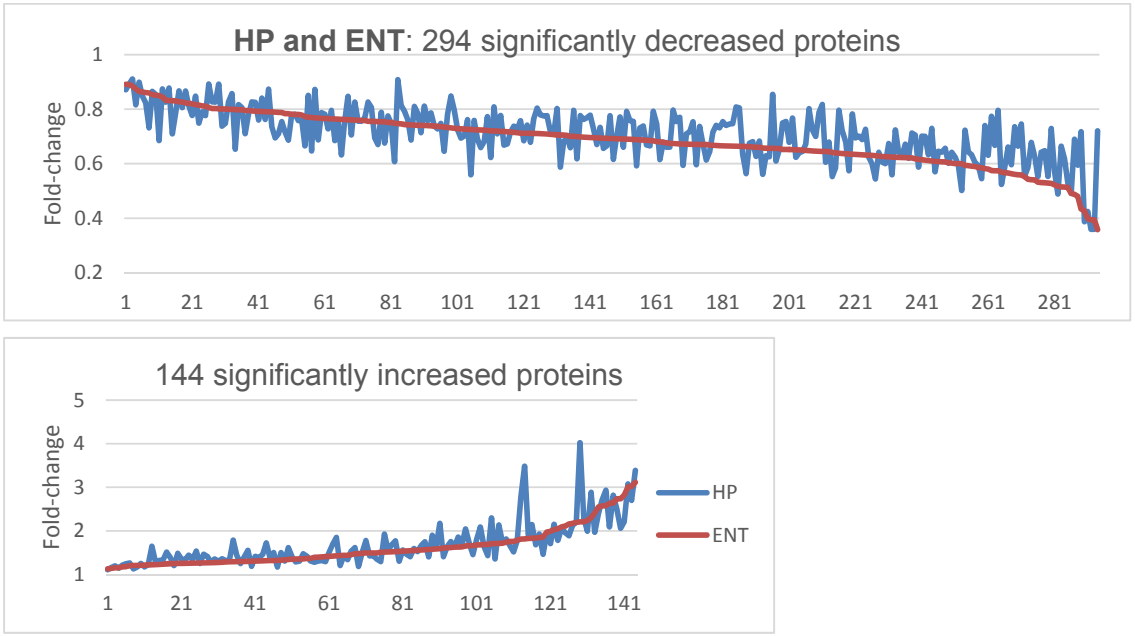

Figure 4-1 Proteins significantly changed in both HP and ENT

Magnitude of change was plotted for individual proteins in HP (blue line) and ENT (red line) and sorted from weakest to strongest fold-change in ENT. Differences in individual protein fold-changes between HP and ENT generate the variability in the blue line. The responses of each protein to the effect of AD were comparable between HP and ENT, in both decreased (top graph) and increased (bottom graph) proteins.

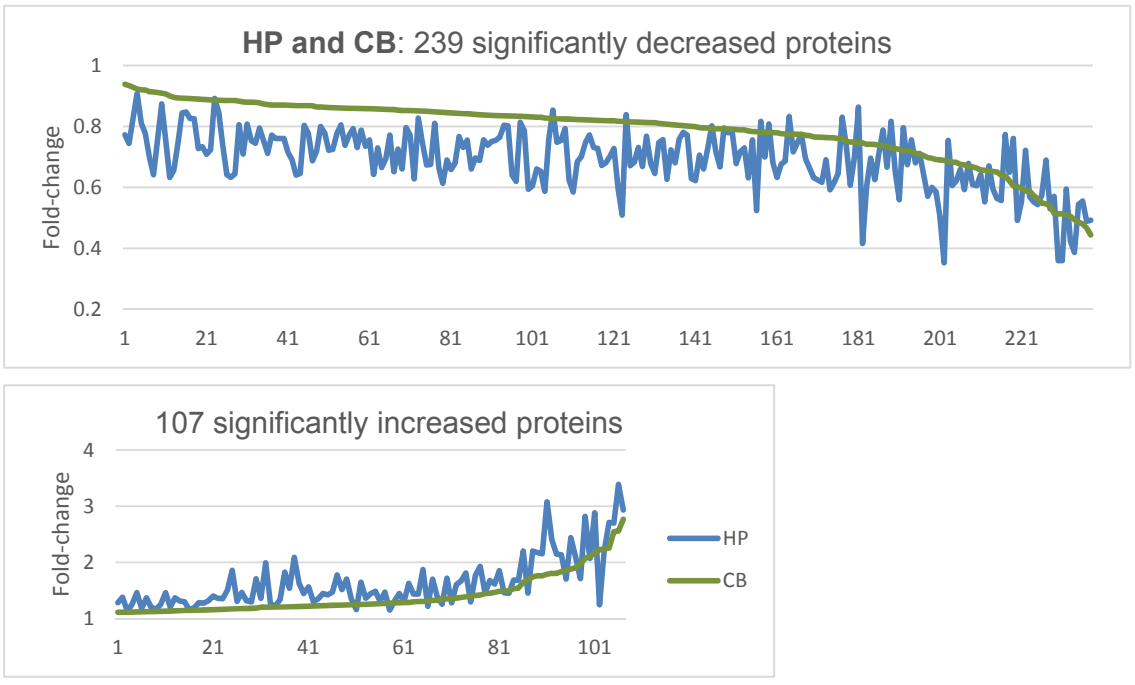

Figure 4-2 Proteins significantly changed in both HP and CB

Magnitude of change was plotted for individual proteins in HP (blue line) and CB (green line) and sorted from weakest to strongest fold-change in CB. Differences in individual protein fold-changes between HP and CB generate the variability in the blue line. The responses of each protein to the effect of AD appeared to be greater in HP when compared to CB, in both decreased (top) and increased (bottom) proteins.

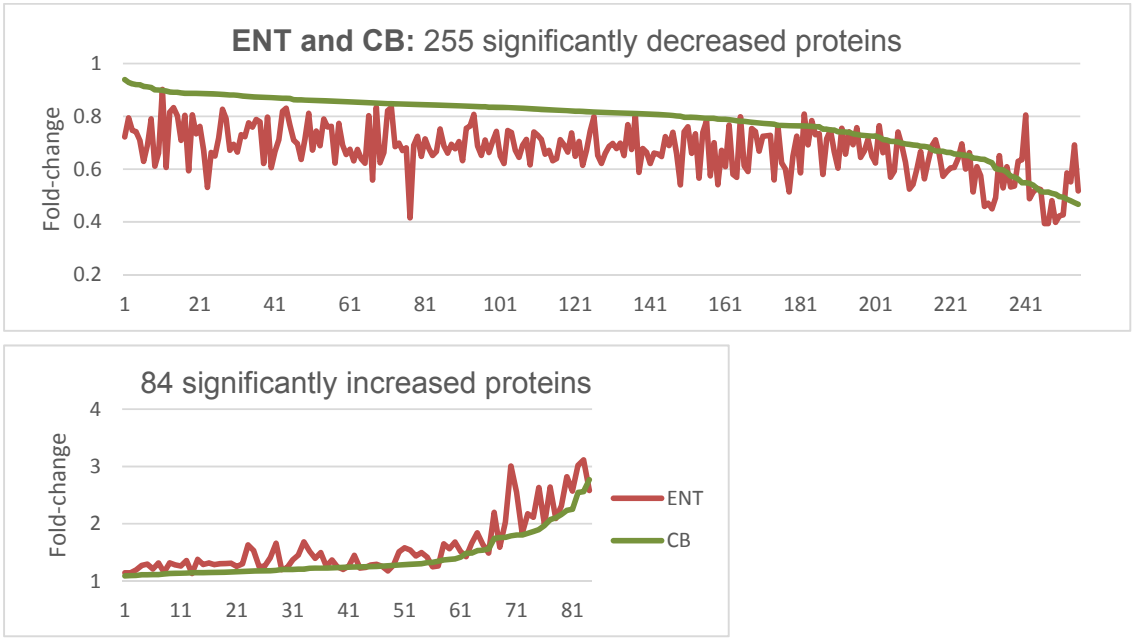

Figure 4-3 Proteins significantly changed in both ENT and CB

Magnitude of change was plotted for individual proteins in ENT (red line) and CB (green line) and sorted from weakest to strongest fold-change in CB. Differences in individual protein fold-changes between ENT and CB generate the variability in the red line. The responses of each protein to the effect of AD appeared to be greater in ENT when compared to CB, in both decreased (top) and increased (bottom) proteins.

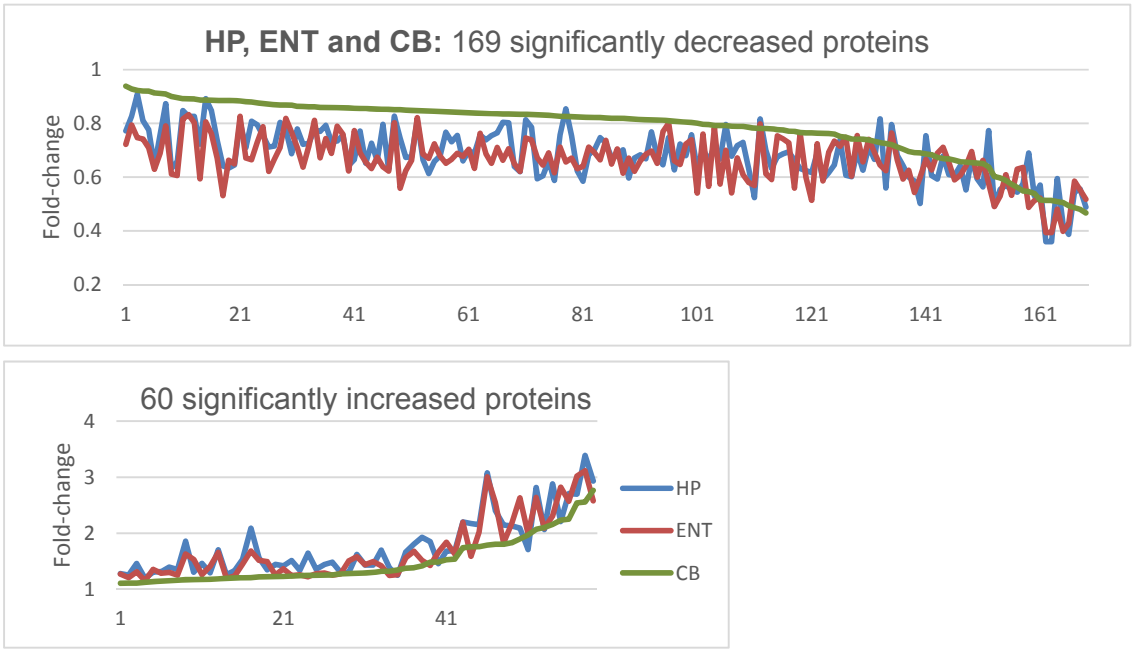

Figure 4-4 Proteins significantly changed in HP, ENT, and CB

Magnitude of change was plotted for individual proteins in HP (blue line), ENT (red line) and CB (green line), and sorted from weakest to strongest fold-change in CB. Differences in individual protein fold-changes between HP/ENT and CB generate the variability in the blue/red line. The responses of each protein to the effect of AD appeared to be greater in HP and ENT when compared to CB, in both decreased (top) and increased (bottom) proteins.

4.3.2. Pathway alterations

4.3.2.1. Pathways altered in all three brain regions

The most consistent features across all three brain regions can be categorised into the following pathways: 1) immune response, 2) signalling, 3) mitochondrial function, 4) protein processing, and 5) cell cycle regulation. Acute phase response was detected by both pathway-analysis methods.

Go-enrichment generated more specific changes in immune-related processes including increased complement activation, defence response, and humoral response, as well as decreased antigen processing and presentation of peptide antigen via MHC class II, which is likely to be associated with immunodeficiency signalling (detected by IPA).

Table 4-7: Pathways altered in all three brain regions

	Go-enrichment (HP, ENT, & CB)	IPA (HP, ENT, & CB)	HP	ENT	CB
Immune-related	Acute-phase response	Acute Phase Response Signalling	<0.0001	<0.0001	0.0177
	Complement activation	Primary Immunodeficiency Signalling	0.0013	0.0005	0.0109
	Complement activation, classical pathway	Haematopoiesis from Pluripotent Stem Cells	0.0063	0.0006	0.0207
	Defence response				
	Humoral immune response mediated by circulating immunoglobulin				
	Antigen processing & presentation of exogenous peptide antigen via MHC class II				
	Antigen processing & presentation of peptide antigen via MHC class II				
	Antigen processing & presentation of peptide or polysaccharide antigen via MHC class II				
Signalling	Protein-activation cascade	FXR/RXR Activation	<0.0001	0.0017	0.0034
	Regulation of mitochondrial outer membrane permeabilisation involved in apoptotic signalling pathway	LXR/RXR Activation	<0.0001	0.0313	0.0121
	Regulation of protein insertion into mitochondrial membrane involved in apoptotic signalling pathway	HIPPO signalling	<0.0001	0.0044	0.0009
		PI3K/AKT Signalling	0.0003	0.0002	0.0192
	Positive regulation of protein insertion into mitochondrial membrane involved in apoptotic signalling pathway	IGF-1 Signalling	0.0007	0.0182	0.0279
		Clathrin-mediatedEndocytosis Signalling	0.0251	0.0274	0.029
Mitotic cell cycle		Cell Cycle: G2/M DNA Damage Checkpoint Regulation	0.0001	0.0271	0.0009
Mitochondria	Regulation of mitochondrion organisation	Acetyl-CoA Biosynthesis I (PDHC)	0.0004	0.0088	0.0002
Protein processing		Protein Ubiquitination Pathway	0.0195	<0.0001	0.023
		Amyloid Processing	0.0452	0.0365	0.0207

Go-enrichment: pathways enriched with proteins that were increased or decreased in abundance were highlighted as pink or blue respectively.

Signalling pathways were also consistently detected by both analyses. Activation and alteration in signalling via FXR/RXR, LXR/RXR, HIPPO, PI3K/AKT, IGF-1, and clathrin-mediated endocytosis signalling as detected by IPA may correspond to the reported decrease in regulation of mitochondrial membrane integrity involved in apoptotic signalling pathways reported by Go-enrichment (Table 4-7).

These alterations in signalling may be associated with cell-cycle change; Cell cycle G2/M phase-transition-related pathways were altered in all three brain regions (Table 4-7).

Adult neurons are fully differentiated post-mitotic cells; however, they may reactivate cell-cycle activity when triggered by apoptotic signals [319]. Such inappropriate re-entry into the cell cycle with interrupted mitotic processes is suggested to play a role in neuronal degeneration in AD [319,320].

In all three brain regions, processes that maintain mitochondrial integrity and function were found to be affected. Mitochondrial organization was altered, as well as Acetyl-Co-A biosynthesis via pyruvate dehydrogenase complex (PDHC) which is localised in the mitochondria.

IPA but not Go-enrichment identified significant alteration in protein degradation and amyloid processing pathways.

4.3.2.2. Pathways altered in HP and ENT

Both analyses identified pathway alterations that are shared between two brain regions only. Pathway alterations restricted to HP and ENT are listed in Table 4-8.

Table 4-8: Pathways altered in HP and ENT

	Go-enrichment (HP & ENT)	IPA (HP & ENT)	HP	ENT	CB
Immune-related	Inflammatory response				
	Humoral immune response				
DNA/protein	Chromatin assembly				
	Chromatin assembly or disassembly				
	Nucleosome organisation				
	Protein-DNA complex subunit organisation				
Signalling	Negative regulation of apoptotic signalling pathway	Myc Mediated Apoptosis Signalling	0.0174	0.0204	0.1387
		14-3-3-mediated Signalling	0.0307	0.0013	0.1765
		Prostate Cancer Signalling	0.0305	0.0472	0.4132
Cell cycle	Cell cycle G2/M phase transition				
	G2/M transition of mitotic cell cycle				
Protein modification	de novo' post-translational protein folding	Protein Ubiquitination Pathway	0.0195	<0.0001	0.023
	Protein modification by small protein removal				
	Cullin deneddylation				
	Protein deneddylation				
Oxidative stress	Response to hydrogen peroxide				
	Hydrogen peroxide metabolic process				
	Response to transition metal nanoparticle				
Mitochondrial	Positive regulation of mitochondrion organisation				
β-oxidation		Fatty Acid β-oxidation III (Unsaturated, Odd Number)	0.0455	0.0462	1
Miscellaneous	Homotypic cell-cell adhesion				

Go-enrichment: pathways enriched with proteins that were increased or decreased in abundance were highlighted as pink or blue respectively.

In addition to the immune-response-related pathways identified in all three brain regions, Go-enrichment analysis identified increased inflammatory response and humoral immune response in HP and ENT (Table 4-8). Processes associated with transcription were increased, including chromatin assembly/disassembly, nucleosome organisation, and protein-DNA complex subunit organisation. Both Go-enrichment and IPA also identified apoptosis-related signalling processes to be altered: negative regulation of apoptotic signalling was increased and apoptosis-related signalling processes mediated by Myc and 14-3-3 were significantly affected in HP and ENT. G2/M phase-transition in the cell cycle was decreased in HP and ENT according to Go-enrichment (Table 4-8), whereas the same process was highlighted as altered in all three brain regions by IPA. Protein folding/modification processes were decreased according to Go-enrichment and IPA indicated changes in protein degradation in HP and ENT.

Increased processes that play a role in oxidative stress included response to hydrogen peroxide, hydrogen peroxide metabolism, and response to transition metal nanoparticles. Positive regulation of mitochondrial organisation was diminished and homotypic cell-cell adhesion was increased, according to Go-enrichment. IPA also identified significantly altered fatty acid oxidation process in both HP and ENT (Table 4-8).

4.3.2.3. Pathways altered in HP and CB

Pathway alterations restricted to HP and CB are listed in Table 4-9. Both analyses identified immune-related pathways in HP and CB. Go-enrichment reported increased regulation of immune system process and regulation of inflammatory response, while IPA identified more specific pathways (lipid antigen presentation by CD1 and CTLA4 signalling in cytotoxic T lymphocytes). An altered coagulation system was identified by both analyses.

According to the Go-enrichment analysis, nucleosome assembly was increased in HP and CB. This appears to be similar to the increased nucleosome organisation (along with other DNA-related processes) reported for HP and ENT (Table 4-8). In contrast to the DNA related process, formation of translation pre-initiation complex was decreased in HP and ENT.

IPA identified alterations in cyclins and cell cycle regulations. There was also change in dopamine receptor signalling, ERK/MAPK and Wnt/ β-catenin signalling, and the biosynthesis of heparin, dermatan, chondroitin–sulphate in HP and CB. Processes associated with the TCA cycle were decreased in HP and CB (Table 4-9).

Table 4-9 Pathways altered in HP and CB

	Go-enrichment (HP & CB)	IPA (HP & CB)	HP	ENT	CB
Immune-related	Regulation of immune system process	Lipid Antigen Presentation by CD1	0.0262	1	0.0099
	Regulation of inflammatory response	CTLA4 Signalling in Cytotoxic T Lymphocytes	0.001	0.2033	0.0121
Coagulation	Regulation of response to wounding	Coagulation System	0.0029	0.1065	0.0434

	Platelet degranulation				
DNA, protein	Nucleosome assembly				
	Formation of translation pre-initiation complex				
Cell cycle		Cyclins and Cell Cycle Regulation	0.0008	0.2942	0.0115
Neurotransmitter		Dopamine Receptor Signalling	0.0041	0.2898	0.0001
Signalling		ERK/MAPK Signalling	0.0132	0.2586	0.004
		Wnt/β-catenin Signalling	0.001	0.0555	0.0357
Biosynthesis		Heparan Sulfate Biosynthesis (Late Stages)	0.0455	0.215	0.0305
		Dermatan Sulfate Biosynthesis (Late Stages)	0.0326	0.1187	0.0185
		Chondroitin Sulfate Biosynthesis (Late Stages)	0.0455	0.215	0.0305
TCA cycle	TCA cycle	TCA Cycle II (Eukaryotic)	0.0235	0.0532	0.0016
		Branched-chain α-keto acid Dehydrogenase Complex	0.0021	0.2042	0.0009
Go-enrichment: pathways enriched with proteins that were increased or decreased in abundance were highlighted as pink or blue respectively.					

4.3.2.4. Pathways altered in ENT and CB

CB shared fewer pathways in common with ENT (Table 4-10) than HP. Response to ROS was increased and microtubule-based movement was decreased in ENT and CB according to Go-enrichment analysis. Processes involved in response to oxidative stress were also found to differ in both HP and CB (Table 4-9). Therefore, oxidative stress-related processes are spread across all three brain regions. The process of tRNA charging was identified to be affected in both ENT and CB by IPA. This change may parallel the decreased translation process reported for HP and CB (Table 4-9).

Table 4-10 Pathways altered in ET and CB

	Go-enrichment (ENT & CB)	IPA (ENT & CB)	HP	ENT	CB
tRNA charging		tRNA Charging	0.0875	0.0058	<0.0001
Oxidative stress	Response to reactive oxygen species				
Microtubule	Microtubule-based movement				
Go-enrichment: pathways enriched with proteins that were increased or decreased in abundance were highlighted as pink or blue respectively.					

4.3.2.5. Pathways altered in HP

Pathways that were specifically altered in the HP of AD brain are summarised in Table 4-11. Immune-related response was detected by both pathway analyses; complement system and coagulation were enhanced in the HP in AD.

Go-enrichment also suggested increased expression of proteins involved in regulation of response to oxidative stress and IPA specifically identified altered proteins that are responsible for production of nitric oxide and ROS in macrophages. Numerous signalling pathways were altered according to IPA and these may correspond to the increased regulation of signalling and response to stress and/or

various stimuli, as detected by Go-enrichment analysis. In the HP, protein-folding was decreased although DNA and chromatin-related processes, as well as DNA-protein complex assembly, were enhanced. Changes in pathways involved in cell-cycle regulation were detected by both analyses in the HP in AD.

Table 4-11 Pathways altered in HP only

	Go-enrichment (HP)	IPA (HP)	HP	ENT	CB
Immune-related	Regulation of complement activation	Complement System	0.0029	0.1266	0.1051
	Regulation of humoral immune response	B Cell Development (bone marrow)	0.0021	0.1187	0.5361
	Regulation of acute inflammatory response	Dendritic Cell Maturation (adaptive immune response)	0.0082	0.1529	1
	Blood coagulation, fibrin clot formation	Intrinsic Prothrombin Activation Pathway	0.0088	0.2368	0.1095
		Extrinsic Prothrombin Activation Pathway	0.0415	0.118	0.1072
Oxidative stress	Regulation of response to oxidative stress	Production of Nitric Oxide and Reactive Oxygen Species in Macrophages	0.0112	0.1582	0.1489
Signalling	Enzyme linked receptor protein signalling pathway	Cardiac β-adrenergic Signalling	0.0254	1	0.0729
	Positive regulation of signalling	Ovarian Cancer Signalling	0.0457	0.1772	0.2548
	Negative regulation of extrinsic apoptotic signalling pathway	Huntington's Disease Signalling	0.0325	0.2678	0.411
	Regulation of protein activation cascade	Granzyme A Signalling	0.0423	0.1956	0.5975
	Positive regulation of cell communication	Altered T Cell and B Cell Signalling in Rheumatoid Arthritis	0.0326	0.5164	1
	Regulation of response to stress	LPS/IL-1 Mediated Inhibition of RXR Function	0.0258	1	0.2585
	Regulation of response to external stimulus	Xenobiotic Metabolism Signalling	0.0059	0.2329	0.504
	Response to lipid	IL-6 Signalling	0.0181	0.0943	1
	Response to other organism	IL-8 Signalling	0.0317	1	1
	Response to biotic stimulus	IL-17A Signalling in Airway Cells	0.0368	0.1083	0.3366
	Response to external biotic stimulus	Gαs Signalling	0.0321	1	0.1856
	Response to alcohol	Ceramide Signalling	0.0181	0.344	1
	Response to selenium ion	Telomerase Signalling	0.0258	0.0813	0.2745
		Protein Kinase A Signalling	0.0032	0.4205	0.1574
		Sonic Hedgehog Signalling	0.0088	1	0.0557
DNA & protein	DNA conformation change				
	DNA packaging				
	Chromatin organisation				
	Protein-DNA complex assembly				
	'de novo' protein folding				
Cell cycle	Epithelial cell differentiation	Mitotic Roles of Polo-Like Kinase	0.0065	0.1384	0.1725
	Organ development	Cell Cycle Regulation by BTG Family Proteins	0.0057	0.2464	0.0607
Neurotransmitter and AA related		Serotonin Degradation	0.0023	0.1637	0.3876
		Noradrenaline and Adrenaline Degradation	0.0064	0.1637	0.3444
		Dopamine Degradation	0.016	0.3678	0.1426
		Tryptophan Degradation X (Mammalian, via Tryptamine)	0.0088	0.1485	0.299
		Lysine Degradation II	0.0097	0.6204	0.4379
		Leucine Degradation I	0.0063	1	1

Degradation		**Histamine Degradation**	0.0138	0.54	1
		Putrescine Degradation III	0.0256	0.3678	0.5432
		Glycogen Degradation III	0.0423	0.54	1
		Ethanol Degradation II	0.0368	0.1083	0.3876
		Formaldehyde Oxidation II (Glutathione-dependent)	0.0455	1	1
Metabolic	**Regulation of coenzyme metabolic process**				
	Regulation of cofactor metabolic process				
	Regulation of acetyl-CoA biosynthetic process from pyruvate				
	Regulation of acyl-CoA biosynthetic process				
Go-enrichment: pathways enriched with proteins that were increased or decreased in abundance were highlighted as pink or blue respectively.					

One of the most significant categories of pathways that IPA reported was degradation of different substrates, including neurotransmitters (serotonin, noradrenaline/adrenaline, and dopamine), amino acids (lysine and leucine), and metabolites (including histamine, putrescine, glycogen, and ethanol).

According to Go-enrichment analysis, regulation of metabolic processes was decreased, as was regulation of both acetyl-CoA and acyl-CoA biosynthesis.

4.3.2.6. Pathways altered in ENT

Table 4-12 Pathways altered in ENT only

	Go-enrichment (ENT)	IPA (ENT)	HP	ENT	CB
Immune related	Immunoglobulin mediated immune response	4-1BB Signalling in T Lymphocytes	0.1042	0.0263	1
	B cell mediated immunity	B Cell Receptor Signalling	0.2648	0.0486	1
		Role of IL-17A in Psoriasis	0.3814	0.0462	0.1747
Signalling		PCP pathway (Wnt pathway?)	0.0643	0.0165	1
		Neuregulin Signalling (synaptic plasticity)	1	0.0099	1
		Sertoli Cell-Sertoli Cell Junction Signalling	0.4069	0.0342	1
Cell cycle	Cell cycle process	Role of MAPK Signalling in the Pathogenesis of Influenza	0.2421	0.0414	0.259
	Mitotic cell cycle				
	Mitotic cell cycle process	RAN Signalling (mitosis)	0.2036	0.0471	1
Oxidative stress	Cellular response to reactive oxygen species				
	Cellular response to oxidative stress				
	Reactive oxygen species metabolic Process				
	Hydrogen peroxide catabolic process				
	Transition metal ion homeostasis				
ECM & Cell adhesion	Extracellular matrix organization				
	Extracellular structure organization				
	Positive regulation of cell adhesion				
	Positive regulation of heterotypic cell-cell adhesion				
Carbohydrate	Cellular carbohydrate biosynthetic process	Superpathway of D-myo-inositol (1,4,5)-trisphosphate Metabolism	0.1455	0.0435	0.3511
		D-myo-inositol (1,4,5)-trisphosphate Degradation	0.2333	0.0263	0.2473
		D-myo-inositol (1,3,4)-trisphosphate Biosynthesis	0.1718	0.0219	0.4203
		1D-myo-inositol Hexakisphosphate Biosynthesis II (Mammalian)	0.2333	0.0219	0.4203
Nucleotide		Purine Nucleotides De Novo Biosynthesis II	0.3631	0.0435	0.484
		Pyridoxal 5'-phosphate Salvage Pathway	0.0773	0.0225	0.556
Protein modification	Cellular protein modification process				
	Protein modification process				
	macromolecule modification				
	Protein modification by small protein conjugation or removal				
Microtubule	Microtubule-based process				
	Organelle transport along microtubule				

Go-enrichment: pathways enriched with proteins that were increased or decreased in abundance were highlighted as pink or blue respectively.

Pathways that were specifically altered in the ENT of AD brain are summarised in Table 4-12. In the ENT of AD brain, immune-related processes were detected by both Go-enrichment and IPA. Specifically, immunoglobulin and B-cell-mediated immune responses were increased.

Signalling processes were also detected by IPA, including Neuregulin Signalling and Ran signalling. Mitotic cell-cycle processes were consistently decreased in ENT according to the Go-enrichment analysis.

Go-enrichment also reported an up-regulation in response towards oxidative stress, as well as ECM organization and cell adhesion. Cellular carbohydrate metabolism was increased in ENT according to Go-enrichment and IPA reported significant alteration in metabolism, degradation and biosynthesis of myo-inositol.

Nucleotide synthesis and utilisation was also altered in ENT in AD according to IPA. Go-enrichment detected decreased protein modification processes in ENT, as well as microtubule-related processes.

4.3.2.7. Pathways altered in CB

Pathways that were specifically altered in the CB of AD brain are summarised in**Table 4-13**. In CB of AD brain, the neuroprotective role of THOP1 in AD was found to be significantly altered.

In CB, metabolism-related disturbance was most frequently reported in terms of the number of altered processes by Go-enrichment. First of all, processes for nucleotide/nucleobase metabolism were increased. Proteins involved in NADP and NADPH-related processes and the pentose-phosphate shunt were up-regulated, as well as those involved in carbohydrate metabolism in general. Interestingly, cellular and aerobic respiration was decreased, as well as pyruvate metabolism. Furthermore, processes related to oxidative phosphorylation (OxPhos) and ATP synthesis in the mitochondria were decreased.

The mevalonate pathway was identified as compromised in CB of AD brain. This is an important metabolic pathway that synthesises sterol isoprenoids such as cholesterol, and non-sterol isoprenoids such as dolichol, haeme-A, isopentenyl tRNA, and ubiquinone [321].

Proteins involved in processes related to DNA and RNA were down-regulated, as well as tRNA-related processes. However, proteins involved in regulation of protein processing and proteolysis were increased in AD.

Regulation of neurotransmitters and amino acids was altered in CB. Amino acid activation was decreased according to Go-enrichment. Pathways of glutamate and serotonin receptor signalling, glutamate and valine degradation, and tetrahydrobiopterin (BH4) biosynthesis were altered according to IPA. BH4 is an essential cofactor for dopamine and serotonin synthesis in the brain. In addition, BH4 is also an essential cofactor for all isoforms of nitric oxide synthase (NOS) [322]. In line with this, IPA also identified altered pathways involving oxidative stress associated with nitric oxide.

Cytoskeleton organisation and vesicle-facilitated transport were decreased in CB in AD, and cell activation was increased. The only signalling pathway that was flagged in this brain region was Gαq Signalling.

Table 4-13 Pathways altered in CB only

	Go-enrichment (CB)	IPA (CB)	HP	ENT	CB
		Neuroprotective Role of THOP1 in Alzheimer's Disease	0.06	0.4618	0.026
Nucleotide	Pyridine-containing compound metabolic process				
	Pyridine nucleotide metabolic process				
	Nicotinamide nucleotide metabolic process				
	Nucleobase metabolic process				
NADP/ NADPH	NADP metabolic process				
	NADPH regeneration				
Pentose metabolism	Pentose-phosphate shunt				
	Pentose metabolic process				
Carbohydrate metabolism	Single-organism carbohydrate catabolic process	2-oxobutanoate Degradation I	0.2905	0.2936	0.0402
	Carbohydrate catabolic process				
	Oxidoreduction coenzyme metabolic process				
	Monosaccharide catabolic process				
Metabolism	Cellular respiration	Mevalonate Pathway I	1	1	0.0109
	Aerobic respiration	Superpathway of Geranylgeranyldiphosphate Biosynthesis I (via Mevalonate)	1	1	0.0295
	Pyruvate metabolic process				
	Regulation of sulfur metabolic process				
Mitochondria	Oxidative phosphorylation	Oxidative Phosphorylation	1	1	0.0025
	Mitochondrial ATP synthesis coupled electron transport	Mitochondrial Dysfunction	1	1	0.0016
	ATP synthesis coupled electron transport				
	Mitochondrial electron transport, NADH to ubiquinone	2-ketoglutarate Dehydrogenase Complex	0.1172	0.5164	0.0185
DNA/RNA	Transcription, DNA-templated	Assembly of RNA Polymerase I Complex	0.2135	1	0.0305
	Nucleobase-containing compound biosynthetic process				
	RNA biosynthetic process				
tRNA	tRNA aminoacylation for protein translation				
	tRNA aminoacylation				
	tRNA metabolic process				
Protein	Regulation of protein processing				
	Regulation of proteolysis				
Neurotransmitters & AA	Amino acid activation	Glutamate Receptor Signalling	0.2337	1	0.0407
		Glutamate Dependent Acid Resistance	1	1	0.0305
		Glutamate Degradation III (via 4-aminobutyrate)	1	1	0.0402
		Serotonin Receptor Signalling	0.3631	0.3678	0.0058
		Tetrahydrobiopterin Biosynthesis I	0.2135	0.215	0.0305
		Tetrahydrobiopterin Biosynthesis II	0.2135	0.215	0.0305
		Valine Degradation I	0.2003	0.4618	0.0186
Nitric oxide Oxidative stress		Glutathione Redox Reactions I	0.1042	0.1065	0.0109
		Nitric Oxide Signalling in the Cardiovascular System	0.0578	0.2261	0.0395
		eNOS (nitric oxide synthase) Signalling	0.2322	1	0.0394
	Cortical cytoskeleton organization				

Cytoskeletal and vesicle	**Cortical actin cytoskeleton organization**				
	Single-organism membrane budding				
	Golgi vesicle budding				
	Vesicle targeting, to, from or within Golgi				
	Retrograde vesicle-mediated transport, Golgi to ER				
Miscellaneous	**Cell activation**	**Gαq Signalling (apoptosis?)**	0.1538	1	0.0459
		Breast Cancer Regulation by Stathmin1	0.1751	1	0.0187
		Heparan Sulfate Biosynthesis (found in ECM)	0.0687	0.2042	0.0402
Go-enrichment: pathways enriched with proteins that were increased or decreased in abundance were highlighted as pink or blue respectively.					

In summary, general AD-related features identified across all three brain regions include: major alterations in processes involved in immune function, apoptosis-related signalling and the mitotic cell cycle, mitochondrial function and oxidative stress, and also protein processing. Transcription-related processes appeared to be increased in ENT and HP but decreased in CB. CB also showed profound deficit in tRNA charging pathways. Amino acid and neurotransmitter-associated processes were disturbed in HP and CB, but not detected in ENT. Although metabolism-related alteration was detected in all brain regions, it was most prominent in the CB with increased NADP/NADPH, pentose-phosphate pathway, and carbohydrate metabolism and decreased respiration and mitochondrial ATP production.

4.3.3. Specific changes in protein levels

Changes in individual proteins are reported in this section to examine the details of the altered pathways. Pathway analysis is a helpful tool for generating overall descriptions of global changes in the proteome. However, it should be complemented by details of protein changes in order to understand the exact defects in each of the altered pathways.

4.3.3.1. Glucose metabolism

In this study, enzymes involved in glycolysis showed differing patterns of change across HP, ENT and CB (**Table 4-14**). The level of hexokinase was not significantly changed in the AD brain. However, the enzymes governing the first two steps of glycolysis, glucose-6-phosphate isomerase and phosphofructokinases, were decreased in abundance. Enzymes that catalyse subsequent steps of glycolysis were not altered in HP and ENT, but significantly increased in CB (**Table 4-14**). Proteins involved in gluconeogenesis and transporters of glucose showed significant changes with no brain-region-specific pattern (**Table 4-14**).

In the AD brain significantly altered enzymes involved in the pentose-phosphate pathway showed increased abundance in those cases where statistical significance was reached, as well as those that are shared between glycolysis and the pentose-phosphate pathway. We also observed changes in polyol pathway proteins; aldose reductase was significantly increased in the CB and sorbitol dehydrogenase was up-regulated in all three brain regions (**Table 4-15**).

Although glycogenin 1 levels were increased, enzymes involed in glycogen synthesis were decreased, e.g. glycogen-branching enzyme (**Table 4-16**).

Table 4-14: Proteomic findings relating to glucose metabolism

	HP				ENT				CB			
General name	Abundance (C)	Abundance (AD)	p	N_C,N_{AD}	Abundance (C)	Abundance (AD)	p	N_C,N_{AD}	Abundance (C)	Abundance (AD)	p	N_C,N_{AD}
Glycolysis												
Hexokinase-1	1(0.77-1.29)	0.87(0.71-1.07)	0.34	(8,9)	1(0.85-1.18)	1.02(0.82-1.27)	0.86	(8,9)	1(0.96-1.04)	1.02(0.96-1.08)	0.54	(8,9)
Glucose-6-phosphate isomerase	1(0.95-1.05)	0.66(0.55-0.78)	0.0004	(8,9)	1(0.9-1.11)	0.7(0.55-0.89)	0.009	(8,9)	1(0.96-1.05)	0.94(0.87-1.01)	0.11	(8,9)
6-phosphofructokinase, liver type	1(0.79-1.26)	0.83(0.68-1.02)	0.19	(8,9)	1(0.87-1.15)	0.71(0.57-0.88)	0.008	(8,9)	1(0.94-1.07)	0.91(0.82-1.02)	0.13	(8,9)
6-phosphofructokinase type C	1(0.8-1.25)	0.81(0.66-0.98)	0.11	(8,9)	1(0.81-1.24)	0.76(0.63-0.92)	0.04	(8,9)	1(0.94-1.06)	0.87(0.82-0.93)	0.003	(8,9)
Fructose-2,6-bisphosphatase	1(0.73-1.38)	0.72(0.6-0.85)	0.05	(8,9)	1(0.79-1.27)	0.55(0.39-0.77)	0.005	(8,9)	1(0.73-1.37)	0.75(0.55-1.01)	0.14	(8,9)
Fructose-bisphosphate aldolase A	1(0.94-1.06)	1(0.9-1.11)	0.96	(8,9)	1(0.85-1.18)	0.98(0.85-1.13)	0.84	(8,9)	1(0.95-1.06)	1.08(1.03-1.13)	0.02	(8,9)
Fructose-bisphosphate aldolase C	1(0.91-1.1)	1.02(0.91-1.16)	0.73	(8,9)	1(0.89-1.12)	1.05(0.93-1.18)	0.53	(8,9)	1(0.95-1.05)	1.1(1.04-1.16)	0.01	(8,9)
Triosephosphate isomerase	1(0.83-1.21)	0.95(0.89-1.01)	0.57	(8,9)	1(0.79-1.26)	0.98(0.9-1.06)	0.82	(8,9)	1(0.88-1.14)	1.13(1.07-1.19)	0.07	(8,9)
Glyceraldehyde-3-phosphate dehydrogenase	1(0.94-1.06)	1.11(1-1.23)	0.06	(8,9)	1(0.86-1.16)	1.1(0.97-1.24)	0.26	(8,9)	1(0.91-1.1)	1.18(1.09-1.27)	0.007	(8,9)
Phosphoglycerate kinase 1	1(0.89-1.13)	1.03(0.95-1.12)	0.65	(8,9)	1(0.87-1.14)	1.05(0.96-1.15)	0.5	(8,9)	1(0.94-1.06)	1.19(1.1-1.3)	0.002	(8,9)
Phosphoglycerate mutase 1	1(0.92-1.08)	0.7(0.59-0.84)	0.002	(8,9)	1(0.89-1.12)	0.73(0.61-0.86)	0.003	(8,9)	1(0.92-1.08)	0.89(0.79-1)	0.08	(8,9)
Phosphoglycerate mutase 2	1(0.66-1.52)	2.3(1.52-3.48)	0.005	(8,9)	1(0.73-1.37)	1.71(1.15-2.53)	0.03	(8,9)	1(0.86-1.17)	1.29(1.02-1.63)	0.05	(8,9)
Alpha-enolase	1(0.9-1.11)	1.2(1.09-1.33)	0.009	(8,9)	1(0.84-1.19)	1.09(0.97-1.24)	0.35	(8,9)	1(0.92-1.08)	1.13(1.06-1.21)	0.01	(8,9)
Gamma-enolase / Neuron-specific enolase	1(0.89-1.13)	0.97(0.86-1.08)	0.63	(8,9)	1(0.9-1.11)	1.04(0.9-1.21)	0.58	(8,9)	1(0.93-1.08)	1.11(1.01-1.21)	0.06	(8,9)
Pyruvate kinase isozymes M1/M2	1(0.91-1.09)	1.14(1-1.31)	0.08	(8,9)	1(0.88-1.14)	1.08(0.91-1.27)	0.45	(8,9)	1(0.93-1.08)	1.17(1.07-1.29)	0.007	(8,9)
Gluconeogenesis												
Fructose-1,6-bisphosphatase 1	1(0.7-1.42)	1.4(1.04-1.89)	0.11	(8,9)	1(0.82-1.22)	2.16(1.55-3)	0.0008	(6,6)	1(0.89-1.12)	0.91(0.82-1.02)	0.07	(3,3)
Phosphoenolpyruvate carboxykinase [GTP], mitochondrial	1(0.42-2.36)	0.79(0.36-1.75)	0.43	(3,3)	1(0.49-2.02)	0.37(0.03-5.36)	0.25	(3,3)	1(0.71-1.42)	0.6(0.48-0.77)	0.02	(8,9)
Regulators and transporters												
Glucose 1,6-bisphosphate synthase	1(0.85-1.18)	0.69(0.58-0.83)	0.003	(8,9)	1(0.86-1.17)	0.79(0.73-0.86)	0.009	(8,9)	1(0.93-1.07)	0.98(0.91-1.04)	0.58	(8,9)
Solute carrier family 2, facilitated glucose transporter member 1 (GLUT1)	1(0.88-1.14)	0.97(0.81-1.16)	0.72	(8,9)	1(0.67-1.49)	0.89(0.72-1.11)	0.57	(8,9)	1(0.88-1.14)	0.83(0.74-0.94)	0.03	(8,9)
Solute carrier family 2, facilitated glucose transporter member 3 (GLUT3)	1(0.68-1.48)	0.8(0.61-1.05)	0.29	(8,9)	1(0.73-1.37)	1.07(0.87-1.3)	0.69	(8,9)	1(0.88-1.14)	0.93(0.81-1.06)	0.37	(8,9)
Pro low-density lipoprotein receptor-related protein 1	1(0.85-1.17)	1.01(0.91-1.13)	0.86	(8,9)	1(0.91-1.1)	1.14(1.06-1.23)	0.03	(8,9)	1(0.93-1.07)	0.9(0.85-0.95)	0.01	(8,9)

Table 4-15: Proteomic findings relating to pentose-phosphate pathway and polyol pathway

	HP				ENT				CB			
General name	Abundance (C)	Abundance (AD)	p	N_C,N_{AD}	Abundance (C)	Abundance (AD)	p	N_C,N_{AD}	Abundance (C)	Abundance (AD)	p	N_C,N_{AD}
Pentose-phosphate pathway												
Glucose-6-phosphate 1-dehydrogenase	1(0.89-1.12)	1.15(0.93-1.44)	0.2	(8,9)	1(0.89-1.12)	1.15(0.99-1.34)	0.11	(8,9)	1(0.86-1.16)	1.08(0.85-1.36)	0.55	(8,9)
6-phosphogluconolactonase	1(0.93-1.07)	1.17(1.03-1.32)	0.03	(8,9)	1(0.9-1.12)	1.07(0.94-1.22)	0.35	(8,9)	1(0.95-1.05)	1.12(1.01-1.25)	0.04	(8,9)
6-phosphogluconate dehydrogenase	1(0.9-1.11)	1.25(1.08-1.46)	0.01	(8,9)	1(0.92-1.09)	1.21(1.04-1.4)	0.02	(8,9)	1(0.95-1.05)	1.11(1.05-1.17)	0.005	(8,9)
Transketolase	1(0.87-1.15)	1.11(0.96-1.28)	0.26	(8,9)	1(0.9-1.12)	0.98(0.87-1.1)	0.73	(8,9)	1(0.91-1.1)	1.13(1.05-1.22)	0.03	(8,9)
Ribulose-phosphate 3-epimerase	1(0.77-1.3)	1.11(1.01-1.24)	0.33	(5,6)	1(0.85-1.17)	1.17(1.04-1.33)	0.07	(6,6)	1(0.74-1.36)	1.26(1.11-1.43)	0.1	(5,6)
Transaldolase 1	1(0.79-1.27)	1.25(1.05-1.49)	0.1	(8,9)	1(0.82-1.21)	1.01(0.8-1.27)	0.96	(8,9)	1(0.94-1.06)	1.36(1.19-1.54)	0.0004	(8,9)
Glycolysis/ Pentose-phosphate pathway												
Glucose phosphomutase 1	1(0.93-1.07)	1.12(1.01-1.24)	0.05	(8,9)	1(0.91-1.1)	1.12(1.05-1.19)	0.04	(8,9)	1(0.92-1.09)	1.04(0.98-1.1)	0.42	(8,9)
Phosphoglucomutase-2	1(0.89-1.13)	1.31(1.19-1.44)	0.001	(8,9)	1(0.81-1.23)	1.36(1.14-1.62)	0.02	(8,9)	1(0.92-1.08)	1.14(1.06-1.22)	0.01	(8,9)
Putative deoxyribose-phosphate aldolase	1(0.87-1.15)	1.17(1.01-1.35)	0.09	(8,9)	1(0.57-1.76)	0.91(0.71-1.16)	0.72	(8,9)	1(0.82-1.22)	0.98(0.77-1.25)	0.86	(5,6)
L-xylulose reductase	1(0.88-1.13)	1.13(1.03-1.23)	0.09	(8,9)	1(0.92-1.09)	1.19(1.05-1.34)	0.02	(8,9)	1(0.92-1.09)	1.07(0.98-1.17)	0.21	(8,9)
Polyol pathway												
Aldose reductase	1(0.92-1.09)	1.08(1.02-1.14)	0.11	(8,9)	1(0.89-1.13)	1.05(0.94-1.17)	0.51	(8,9)	1(0.93-1.07)	1.19(1.11-1.28)	0.0009	(8,9)
Sorbitol dehydrogenase	1(0.78-1.27)	1.4(1.19-1.64)	0.02	(8,9)	1(0.88-1.13)	1.3(1.07-1.59)	0.02	(8,9)	1(0.91-1.1)	1.15(1.09-1.22)	0.01	(8,9)

Table 4-16: Proteomic findings relating to glycogen

	HP				ENT				CB			
General name	Abundance (C)	Abundance (AD)	p	N_C,N_{AD}	Abundance (C)	Abundance (AD)	p	N_C,N_{AD}	Abundance (C)	Abundance (AD)	p	N_C,N_{AD}
Glycogen												
Glycogenin-1	1(0.93-1.08)	1.52(1.36-1.69)	<0.0001	(8,9)	1(0.84-1.18)	1.49(1.22-1.81)	0.003	(8,9)	1(0.94-1.06)	1.12(0.99-1.27)	0.07	(8,9)
Glycogen synthase, muscle	1(0.88-1.14)	0.95(0.79-1.14)	0.57	(8,9)	1(0.7-1.43)	0.77(0.53-1.14)	0.23	(5,6)	1(0.92-1.08)	0.82(0.7-0.96)	0.02	(8,9)
1,4-alpha-glucan-branching enzyme	1(0.73-1.38)	0.87(0.65-1.15)	0.41	(6,6)	1(0.81-1.23)	0.5(0.3-0.84)	0.02	(3,3)	1(0.86-1.16)	0.91(0.73-1.14)	0.43	(8,9)
Glycogen synthase kinase-3 alpha	1(0.83-1.21)	0.69(0.6-0.79)	0.002	(8,9)	1(0.88-1.13)	0.78(0.7-0.88)	0.005	(8,9)	1(0.94-1.07)	1.02(0.95-1.09)	0.61	(8,9)
Glycogen synthase kinase-3 beta	1(0.81-1.23)	0.65(0.54-0.79)	0.003	(8,9)	1(0.63-1.6)	1.06(0.76-1.48)	0.82	(8,9)	1(0.9-1.11)	0.83(0.77-0.9)	0.005	(8,9)
Glycogen phosphorylase, brain form	1(0.91-1.1)	1.13(1.03-1.24)	0.05	(8,9)	1(0.94-1.06)	1.1(0.96-1.27)	0.17	(8,9)	1(0.96-1.04)	1.11(1.05-1.18)	0.004	(8,9)

4.3.3.2. Lipid metabolism

Another aspect of energy metabolism is fatty acid oxidation (FAO)/β-oxidation in which fatty acids are broken down in the mitochondria to generate acetyl-CoA, which in turn enters the TCA cycle.

In this study, we observed differential changes in proteins involved in FAO across different brain regions. Proteins involved in the transport of fatty acids and acetyl-CoA into mitochondria were decreased in the AD brain (**Table 4-17**).

Four steps in FAO are catalysed respectively by acyl-CoA dehydrogenases, enoyl-CoA hydratase, hydroxyacyl-CoA dehydrogenase, and thioesterases. Of the proteins involved in FAO, all those which were changed significantly in CB were down-regulated. In sharp contrast, all those changed significantly in HP and ENT were up-regulated, except cytosolic acyl coenzyme A thioester hydrolase (**Table 4-17**). Unsaturated fatty acid oxidation is facilitated by enoyl CoA isomerases to reconfigure the double bond. In this study, enoyl-CoA delta isomerase 1 and 2 were significantly elevated in HP and ENT (**Table 4-17**).

Across all brain regions, decreased abundance was observed for proteins involved in fatty acid biosynthesis (**Table 4-18**).

Glycerolipid is glycerol esterified with one, two, or three fatty acids, corresponding to mono-, di- and tri-acylglycerols. Only four proteins directly involved in glycerolipid metabolism were changed, and no trend was seen (**Table 4-18**).

We also found altered levels of enzymes involved in the metabolism of phospholipids, the major class of membrane lipid. Proteins involved in glycerol-3-phosphate metabolism were affected mainly in the CB, showing decreased levels of dehydrogenases and acyltransferases for glycerol-3-phosphate. It was mainly phosphatidylethanolamines (PE) and/or phosphatidylcholines (PC)-regulating proteins which were also most severely affected in the CB, with three up-regulated, four down-regulated and a further three trending to be decreased (**Table 4-19**).

Proteins involved in phospholipid scrambling, including phospholipid scramblase (3 and 4) and anoctamin-6, were significantly increased and trending to increase in HP and ENT respectively. Probable phospholipid-transporting ATPase IA and cell cycle control protein 50A, both components of P4-ATPase flippase complex [323], were significantly increased in CB (**Table 4-19**).

We here observed significant increase in proteins involved in sphingosine metabolism and signalling in the HP of AD brain (**Table 4-19**).

Table 4-17: Proteomic findings relating to fatty acid oxidation

	HP				ENT				CB			
General name	Abundance (C)	Abundance (AD)	p	N_C,N_{AD}	Abundance (C)	Abundance (AD)	p	N_C,N_{AD}	Abundance (C)	Abundance (AD)	p	N_C,N_{AD}
Membrane transport												
Carnitine O-palmitoyltransferase 2	1(0.65-1.54)	1.05(0.74-1.48)	0.85	(8,9)	1(0.77-1.3)	0.89(0.64-1.22)	0.46	(5,6)	1(0.85-1.17)	0.73(0.67-0.8)	0.002	(8,9)
Carnitine O-acetyltransferase	1(0.88-1.14)	0.61(0.49-0.75)	0.0004	(8,9)	1(0.88-1.13)	0.63(0.47-0.84)	0.006	(8,9)	1(0.9-1.11)	0.68(0.56-0.84)	0.002	(8,9)
Even-numbered saturated FAO												
Acyl-CoA-binding protein	1(0.83-1.21)	1.39(1.19-1.62)	0.007	(8,9)	1(0.8-1.24)	1.09(0.91-1.31)	0.49	(8,9)	1(0.89-1.12)	1.12(0.98-1.29)	0.15	(8,9)
Long-chain-fatty-acid--CoA ligase 3	1(0.83-1.21)	1.03(0.87-1.21)	0.8	(8,9)	1(0.83-1.21)	0.96(0.75-1.23)	0.78	(8,9)	1(0.92-1.09)	0.83(0.73-0.94)	0.01	(8,9)
Long-chain-fatty-acid--CoA ligase 6	1(0.82-1.23)	0.87(0.72-1.04)	0.24	(8,9)	1(0.88-1.14)	1.21(1.03-1.41)	0.05	(8,9)	1(0.88-1.13)	0.87(0.81-0.94)	0.05	(8,9)
Very-long-chain acyl-CoA dehydrogenase VLCAD homolog isoform 1	1(0.85-1.18)	0.83(0.72-0.94)	0.05	(8,9)	1(0.84-1.2)	0.92(0.8-1.06)	0.42	(8,9)	1(0.93-1.08)	0.74(0.68-0.81)	<0.0001	(8,9)
Very-long-chain acyl-CoA dehydrogenase	1(0.92-1.08)	1.2(1.05-1.36)	0.02	(8,9)	1(0.9-1.12)	1.16(1.02-1.33)	0.06	(8,9)	1(0.91-1.1)	0.92(0.86-1)	0.16	(8,9)
Long-chain specific acyl-CoA dehydrogenase, mitochondrial	1(0.51-1.96)	0.61(0.45-0.81)	0.08	(3,2)	1(0.46-2.18)	2.46(1.57-3.88)	0.03	(5,6)	1(0.14-7.11)	1.34(0.57-3.16)	0.6	(3,3)
Medium-chain specific acyl-CoA dehydrogenase, mitochondrial	1(0.84-1.19)	1.23(1.13-1.34)	0.03	(8,9)	1(0.85-1.17)	1.22(1.08-1.38)	0.04	(8,9)	1(0.84-1.19)	0.96(0.87-1.07)	0.67	(8,9)
Trifunctional enzyme subunit alpha	1(0.91-1.1)	0.96(0.82-1.11)	0.57	(8,9)	1(0.86-1.16)	0.84(0.69-1.02)	0.12	(8,9)	1(0.9-1.11)	0.86(0.78-0.94)	0.02	(8,9)
Trifunctional enzyme subunit beta	1(0.88-1.14)	0.99(0.87-1.12)	0.9	(8,9)	1(0.85-1.18)	0.8(0.66-0.97)	0.06	(8,9)	1(0.91-1.1)	0.9(0.82-0.98)	0.07	(8,9)
Enoyl-CoA hydratase domain-containing protein 2, mitochondrial									1(0.63-1.58)	0.42(0.25-0.69)	0.008	(8,6)
Hydroxyacyl-coenzyme A dehydrogenase, mitochondrial	1(0.91-1.1)	1.12(1.04-1.22)	0.04	(8,9)	1(0.85-1.17)	1.12(1-1.24)	0.21	(8,9)	1(0.94-1.07)	1.04(0.96-1.13)	0.38	(8,9)
Acyl-coenzyme A thioesterase 8					1(0.79-1.26)	0.75(0.58-0.97)	0.07	(8,9)	1(0.7-1.42)	1.04(0.88-1.22)	0.82	(5,6)
Acyl-coenzyme A thioesterase 13	1(0.91-1.1)	0.96(0.82-1.12)	0.59	(8,9)	1(0.91-1.1)	1.15(0.99-1.35)	0.09	(8,9)	1(0.9-1.11)	1.05(0.9-1.23)	0.55	(8,9)
Cytosolic acyl coenzyme A thioesterase	1(0.92-1.09)	0.79(0.7-0.89)	0.002	(8,9)	1(0.95-1.06)	0.93(0.88-0.99)	0.05	(8,9)	1(0.94-1.06)	1.04(1-1.08)	0.22	(8,9)
Odd-numbered saturated FAO												
Methylmalonyl-CoA epimerase	1(0.89-1.12)	1.15(0.92-1.44)	0.23	(8,9)	1(0.9-1.11)	1.2(1.06-1.37)	0.02	(8,9)	1(0.86-1.16)	1.24(1.06-1.44)	0.03	(8,9)
Methylmalonyl-CoA mutase	1(0.76-1.31)	0.59(0.46-0.76)	0.005	(8,9)	1(0.76-1.31)	0.48(0.37-0.63)	0.0005	(8,9)	1(0.86-1.17)	0.51(0.37-0.71)	0.001	(8,9)
unsaturated FAO												
Delta(3,5)-Delta(2,4)-dienoyl-CoA isomerase, mitochondrial	1(0.9-1.12)	1.18(1-1.39)	0.07	(8,9)	1(0.8-1.24)	1.03(0.88-1.2)	0.81	(8,9)	1(0.94-1.07)	1.13(0.97-1.3)	0.11	(8,9)
Enoyl-CoA delta isomerase 1, mitochondrial	1(0.9-1.11)	1.2(1.03-1.41)	0.04	(8,9)	1(0.84-1.19)	1.25(1.06-1.47)	0.04	(8,9)	1(0.86-1.17)	1.11(0.96-1.27)	0.28	(8,9)
Enoyl-CoA delta isomerase 2, mitochondrial	1(0.9-1.12)	1.17(1.09-1.26)	0.01	(8,9)	1(0.87-1.15)	1.21(1.09-1.35)	0.02	(8,9)	1(0.89-1.12)	1.1(1-1.21)	0.16	(8,9)

Table 4-18: Proteomic findings relating to fatty acid synthesis and glycerolipid metabolism

	HP				ENT				CB			
General name	Abundance (C)	Abundance (AD)	p	N_C,N_{AD}	Abundance (C)	Abundance (AD)	p	N_C,N_{AD}	Abundance (C)	Abundance (AD)	p	N_C,N_{AD}
Fatty acid synthesis												
Fatty acid synthase	1(0.9-1.11)	0.69(0.58-0.84)	0.002	(8,9)	1(0.92-1.09)	0.63(0.52-0.78)	0.0007	(8,9)	1(0.92-1.09)	0.98(0.88-1.1)	0.74	(8,9)
L-aminoadipate-semialdehyde dehydrogenase-phosphopantetheinyl transferase	1(0.93-1.07)	0.73(0.62-0.85)	0.001	(8,9)	1(0.86-1.17)	0.74(0.63-0.87)	0.006	(8,9)	1(0.94-1.07)	0.82(0.77-0.87)	0.0001	(8,9)
Acetyl-CoA carboxylase	1(0.7-1.43)	0.82(0.61-1.11)	0.31	(6,6)	1(0.76-1.32)	0.74(0.62-0.89)	0.06	(8,9)	1(0.83-1.21)	0.79(0.61-1.04)	0.13	(8,9)
Acyl-CoA synthetase family member 3, mitochondrial	1(0.7-1.43)	0.82(0.61-1.1)	0.31	(6,6)	1(0.8-1.25)	0.65(0.49-0.86)	0.01	(8,9)	1(0.89-1.13)	0.73(0.61-0.86)	0.003	(8,9)
ATP-citrate synthase	1(0.93-1.08)	0.71(0.62-0.81)	0.0002	(8,9)	1(0.93-1.08)	0.79(0.66-0.94)	0.02	(8,9)	1(0.92-1.08)	0.94(0.84-1.05)	0.32	(8,9)
Glycerolipid metabolism												
Diacylglycerol kinase beta	1(0.84-1.19)	1.08(0.88-1.34)	0.46	(5,6)	1(0.73-1.38)	1.32(1.06-1.65)	0.09	(5,6)	1(0.87-1.15)	1.2(1-1.44)	0.08	(8,9)
sn1-specific diacylglycerol lipase alpha	1(0.74-1.36)	1.36(0.93-1.99)	0.16	(8,9)	1(0.62-1.62)	1.16(0.84-1.6)	0.53	(6,6)	1(0.96-1.04)	0.9(0.82-0.99)	0.04	(8,9)
Monoglyceride lipase	1(0.81-1.24)	0.76(0.67-0.87)	0.03	(8,9)	1(0.85-1.18)	0.94(0.82-1.08)	0.5	(8,9)	1(0.92-1.09)	0.94(0.87-1.03)	0.27	(8,9)
Acylglycerol kinase, mitochondrial	1(0.74-1.35)	1(0.88-1.15)	0.99	(5,6)	1(0.82-1.22)	0.94(0.75-1.18)	0.62	(5,6)	1(0.85-1.17)	0.72(0.65-0.79)	0.001	(8,9)

Table 4-19: Proteomic findings relating to phospholipid and sphingosine

	HP				ENT				CB			
General name	Abundance (C)	Abundance (AD)	p	N_C,N_{AD}	Abundance (C)	Abundance (AD)	p	N_C,N_{AD}	Abundance (C)	Abundance (AD)	p	N_C,N_{AD}
Phospholipid metabolism												
Glycerol-3-phosphate dehydrogenase [NAD^+], cytoplasmic	1(0.75-1.33)	1.07(0.92-1.26)	0.62	(8,9)	1(0.76-1.31)	0.82(0.57-1.16)	0.31	(8,9)	1(0.82-1.22)	1.19(1.14-1.24)	0.08	(8,9)
Glycerol-3-phosphate dehydrogenase, mitochondrial	1(0.79-1.26)	1.1(0.91-1.34)	0.46	(8,9)	1(0.84-1.2)	1.15(0.85-1.54)	0.38	(8,9)	1(0.9-1.11)	0.8(0.65-1)	0.06	(8,9)
Glycerol-3-phosphate dehydrogenase 1-like protein	1(0.88-1.14)	0.83(0.77-0.89)	0.01	(8,9)	1(0.8-1.26)	0.95(0.82-1.11)	0.69	(8,9)	1(0.93-1.08)	0.99(0.93-1.06)	0.85	(8,9)
1-acyl-sn-glycerol-3-phosphate acyltransferase alpha	1(0.81-1.23)	0.9(0.67-1.2)	0.49	(8,9)	1(0.7-1.42)	0.96(0.78-1.16)	0.8	(8,9)	1(0.9-1.11)	0.87(0.77-0.98)	0.05	(8,9)
1-acyl-sn-glycerol-3-phosphate acyltransferase gamma	1(0.85-1.17)	0.87(0.29-2.62)	0.63	(3,3)	1(0.74-1.35)	0.76(0.66-0.86)	0.06	(5,6)	1(0.94-1.07)	0.76(0.65-0.9)	0.004	(8,9)
Lysophosphatidylglycerol acyltransferase 1	1(0.78-1.29)	1.05(0.86-1.28)	0.72	(6,6)	1(0.69-1.44)	0.85(0.7-1.03)	0.32	(5,6)	1(0.8-1.25)	0.81(0.69-0.94)	0.09	(8,9)
Ethanolamine-phosphate cytidylyltransferase	1(0.86-1.16)	0.86(0.75-0.98)	0.1	(8,9)	1(0.89-1.13)	0.81(0.66-1.01)	0.08	(8,9)	1(0.94-1.07)	0.89(0.8-0.98)	0.04	(8,9)

Choline/ethanolaminephosphotransferase 1	1(0.77-1.29)	1.13(0.9-1.42)	0.41	(8,9)	1(0.68-1.47)	1.17(0.77-1.76)	0.48	(5,6)	1(0.83-1.2)	1.24(1.11-1.39)	0.04	(8,9)
N-acyl-phosphatidylethanolamine-hydrolyzing phospholipase D	1(0.89-1.13)	1.24(1.02-1.52)	0.04	(5,6)	1(0.69-1.45)	1.37(1.21-1.55)	0.09	(8,9)	1(0.63-1.6)	2.22(1.52-3.26)	0.007	(5,6)
Phosphatidylethanolamine-binding protein 1	1(0.93-1.07)	1.09(0.97-1.22)	0.17	(8,9)	1(0.86-1.16)	1.05(0.91-1.22)	0.56	(8,9)	1(0.93-1.08)	1.19(1.1-1.29)	0.002	(8,9)
Lysophospholipase-like protein 1	1(0.83-1.2)	0.78(0.66-0.93)	0.04	(8,9)	1(0.88-1.14)	0.81(0.2-3.36)	0.59	(3,3)	1(0.83-1.2)	0.79(0.67-0.94)	0.05	(8,9)
Abhydrolase domain-containing protein 4					1(0.26-3.84)	1(0.74-1.33)	0.99	(3,3)	1(0.93-1.07)	0.8(0.6-1.06)	0.07	(3,3)
Acyl-protein thioesterase 2	1(0.87-1.15)	0.96(0.84-1.09)	0.63	(8,9)	1(0.76-1.31)	0.62(0.52-0.74)	0.004	(8,9)	1(0.92-1.09)	0.81(0.69-0.94)	0.02	(8,9)
Phospholipase A-2-activating protein	1(0.54-1.85)	0.85(0.75-0.97)	0.52	(5,6)	1(0.77-1.31)	0.69(0.52-0.91)	0.04	(8,9)	1(0.86-1.16)	0.8(0.71-0.92)	0.02	(8,9)
Phospholipase D3	1(0.79-1.27)	0.95(0.78-1.15)	0.71	(8,9)	1(0.86-1.17)	1.03(0.91-1.17)	0.71	(8,9)	1(0.91-1.09)	0.79(0.66-0.94)	0.02	(8,9)
Scrambling												
Phospholipid scramblase 3					1(0.33-3)	2.55(2.08-3.12)	0.09	(8,9)				
Phospholipid scramblase 4	1(0.88-1.14)	1.55(1.29-1.88)	0.0006	(8,9)	1(0.86-1.17)	1.3(1.03-1.64)	0.05	(8,9)	1(0.78-1.29)	0.98(0.87-1.11)	0.9	(8,9)
Anoctamin-6	1(0.6-1.66)	2.18(1.35-3.51)	0.009	(3,3)	1(0.7-1.43)	1.43(0.9-2.28)	0.06	(3,3)	1(0.74-1.35)	0.97(0.6-1.58)	0.91	(5,6)
Probable phospholipid-transporting ATPase IA	1(0.7-1.42)	0.78(0.56-1.08)	0.24	(8,9)	1(0.82-1.22)	0.99(0.75-1.29)	0.93	(8,9)	1(0.92-1.08)	1.34(1.24-1.44)	<0.0001	(8,9)
Cell cycle control protein 50A	1(0.8-1.25)	0.78(0.62-0.98)	0.09	(8,9)	1(0.78-1.29)	1.28(1.05-1.56)	0.07	(5,6)	1(0.86-1.16)	1.24(1.11-1.38)	0.02	(8,9)
Sphingosine metabolism & signalling												
Serine palmitoyltransferase 1	1(0.86-1.16)	0.88(0.86-0.9)	0.06	(3,3)	1(0.44-2.26)	0.65(0.5-0.85)	0.14	(3,3)	1(0.54-1.87)	0.82(0.41-1.63)	0.42	(3,3)
3-ketodihydrosphingosine reductase	1(0.84-1.2)	1.26(1.06-1.5)	0.05	(8,9)	1(0.67-1.49)	1.05(0.59-1.86)	0.79	(3,3)	1(0.91-1.1)	0.99(0.93-1.04)	0.75	(8,9)
Acid ceramidase; N-acylsphingosine amidohydrolase	1(0.9-1.11)	1.26(1.04-1.53)	0.03	(8,9)	1(0.87-1.15)	1.23(0.95-1.58)	0.12	(8,9)	1(0.92-1.08)	1.2(0.98-1.46)	0.08	(8,9)
Prosaposin	1(0.92-1.08)	1.19(1.05-1.36)	0.02	(8,9)	1(0.81-1.23)	1.14(0.91-1.43)	0.33	(8,9)	1(0.89-1.12)	1.15(0.99-1.35)	0.1	(8,9)
Prosaposin receptor GPR37L1	1(0.75-1.34)	1.09(0.94-1.25)	0.56	(8,9)	1(0.82-1.21)	1.21(1.1-1.33)	0.06	(8,9)	1(0.89-1.12)	0.87(0.76-0.99)	0.08	(8,9)
Fatty aldehyde dehydrogenase	1(0.82-1.22)	1.14(0.99-1.32)	0.23	(8,9)	1(0.82-1.22)	1.13(0.99-1.29)	0.24	(8,9)	1(0.92-1.08)	0.85(0.78-0.92)	0.005	(8,9)
Sphingosine 1-phosphate receptor 1	1(0.75-1.33)	1.67(1.29-2.17)	0.007	(6,6)					1(0.72-1.4)	0.95(0.73-1.23)	0.76	(5,6)
Arylsulfatase A	1(0.85-1.17)	1.18(1.03-1.36)	0.08	(8,9)	1(0.75-1.34)	0.86(0.69-1.08)	0.37	(8,9)	1(0.92-1.09)	1(0.87-1.15)	0.99	(8,9)

4.3.3.3. Pyruvate dehydrogenase and TCA cycle

Pyruvate dehydrogenase serves as a bridge between anaerobic and aerobic cerebral energy metabolism by linking the glycolysis pathway to the TCA cycle. The pyruvate dehydrogenase complex (PDHC) contains multiple copies of each of three subunits, pyruvate dehydrogenase (E1) and dihydrolipoyl transacetylase (E2) that generate acetyl-CoA and dihydrolipoamide dehydrogenase (E3) which perform redox recycling [324]. There are also two regulatory components, pyruvate dehydrogenase kinase (PDHK) and pyruvate dehydrogenase phosphatase (PDHP). Various components of PDHC were detected in this study and those that were altered in AD showed decreased abundance.

Several enzymes detected in this study take part in pyruvate metabolism through catalysing the conversion/interconversion between other metabolites and pyruvate, namely malic enzyme, malate dehydrogenase, isocitrate dehydrogenase (cytoplasmic) and lactate dehydrogenase. All four enzymes were found to be increased in abundance in CB of AD brain, but not in HP and ENT (**Table 4-20**). This may represent a compensatory mechanism for defective mitochondrial energy production.

Acetyl-CoA enters the TCA cycle and via series of enzymatic reactions, generates NADH that feeds into OxPhos for ATP production. All TCA enzymes that were significantly altered in AD brain were decreased in abundance. The most consistent changes include the decreased abundance of isocitrate dehydrogenase, 2-oxoglutarate dehydrogenase, and succinyl-CoA ligase in all three brain regions (**Table 4-21**). These findings concerning decreases in abundance of TCA enzymes are consistent with reported decreases in mitochondrial numbers and increased mitochondrial damage in AD brain [325].

Table 4-20: Proteomic findings relating to priming for degradation via the TCA cycle

	HP				ENT				CB			
General name	Abundance (C)	Abundance (AD)	p	N_C,N_{AD}	Abundance (C)	Abundance (AD)	p	N_C,N_{AD}	Abundance (C)	Abundance (AD)	p	N_C,N_{AD}
Pyruvate dehydrogenase												
Pyruvate dehydrogenase E1 alpha 1	1(0.8-1.25)	0.72(0.61-0.83)	0.01	(8,9)	1(0.81-1.23)	0.78(0.7-0.88)	0.03	(8,9)	1(0.94-1.06)	0.79(0.72-0.88)	0.0006	(8,9)
Pyruvate dehydrogenase E1 beta	1(0.8-1.25)	0.68(0.56-0.82)	0.008	(8,9)	1(0.82-1.22)	0.75(0.64-0.89)	0.02	(8,9)	1(0.93-1.07)	0.78(0.71-0.85)	0.0002	(8,9)
Dihydrolipoamide S-acetyltransferase	1(0.81-1.23)	0.57(0.46-0.71)	0.0006	(8,9)	1(0.87-1.15)	0.61(0.47-0.79)	0.002	(8,9)	1(0.93-1.07)	0.59(0.47-0.74)	0.0005	(8,9)
PDH E3 (dihydrolipoamide dehydrogenase)	1(0.86-1.16)	0.76(0.64-0.9)	0.01	(8,9)	1(0.83-1.21)	0.92(0.8-1.07)	0.45	(8,9)	1(0.96-1.04)	0.87(0.82-0.93)	0.0008	(8,9)
PDH, component X	1(0.85-1.18)	0.61(0.54-0.67)	<0.0001	(8,9)	1(0.84-1.18)	0.59(0.48-0.72)	0.0003	(8,9)	1(0.9-1.11)	0.66(0.56-0.78)	0.0003	(8,9)
[Pyruvate dehydrogenase [lipoamide]] kinase isozyme 1, mitochondrial	1(0.07-14.54)	1.29(0.64-2.61)	0.44	(2,3)	1(0.1-9.72)	0.87(0.39-1.96)	0.83	(3,3)	1(0.69-1.45)	0.72(0.58-0.9)	0.1	(8,9)
[Pyruvate dehydrogenase [lipoamide]] kinase isozyme 2	1(0.84-1.19)	0.96(0.83-1.11)	0.69	(8,9)	1(0.42-2.39)	0.94(0.6-1.48)	0.88	(5,6)	1(0.88-1.14)	0.78(0.67-0.9)	0.009	(8,9)
[Pyruvate dehydrogenase [lipoamide]] kinase isozyme 3	1(0.8-1.25)	0.79(0.62-1.01)	0.12	(8,9)	1(0.59-1.7)	1.01(0.88-1.17)	0.95	(8,9)	1(0.75-1.33)	0.93(0.85-1.02)	0.59	(8,9)
Pyruvate dehydrogenase phosphatase regulatory subunit									1(0.69-1.46)	0.81(0.52-1.28)	0.39	(6,6)
[Pyruvate dehydrogenase [acetyl-transferring]]-phosphatase 1	1(0.85-1.17)	0.6(0.49-0.75)	0.0008	(6,6)	1(0.71-1.41)	0.56(0.3-1.05)	0.07	(6,6)	1(0.78-1.28)	0.86(0.36-2.05)	0.53	(3,3)
Pyruvate carboxylase, mitochondrial	1(0.76-1.31)	0.75(0.6-0.95)	0.08	(8,9)	1(0.66-1.51)	0.53(0.38-0.73)	0.01	(8,9)	1(0.71-1.42)	0.53(0.39-0.71)	0.005	(8,9)
Pyruvate interconversion												
NADP-dependent malic enzyme	1(0.85-1.18)	1.09(0.9-1.31)	0.44	(8,9)	1(0.84-1.18)	1.14(0.95-1.37)	0.24	(8,9)	1(0.91-1.1)	1.12(1.07-1.18)	0.02	(8,9)
Malate dehydrogenase, cytoplasmic	1(0.95-1.05)	0.96(0.84-1.08)	0.46	(8,9)	1(0.85-1.18)	1.03(0.88-1.21)	0.76	(8,9)	1(0.94-1.06)	1.13(1.05-1.22)	0.008	(8,9)
Isocitrate dehydrogenase [NADP] cytoplasmic	1(0.86-1.16)	1.16(1.01-1.32)	0.1	(8,9)	1(0.84-1.19)	1.1(0.96-1.27)	0.32	(8,9)	1(0.93-1.08)	1.11(1.03-1.19)	0.04	(8,9)
L-lactate dehydrogenase B chain	1(0.94-1.06)	1.14(1-1.3)	0.06	(8,9)	1(0.85-1.18)	1.09(0.94-1.25)	0.4	(8,9)	1(0.92-1.09)	1.19(1.08-1.31)	0.007	(8,9)

Table 4-21: Proteomic findings relating to TCA cycle

	HP				ENT				CB			
General name	Abundance (C)	Abundance (AD)	p	N_C,N_{AD}	Abundance (C)	Abundance (AD)	p	N_C,N_{AD}	Abundance (C)	Abundance (AD)	p	N_C,N_{AD}
TCA (all detected proteins)												
Citrate synthase, mitochondrial	1(0.84-1.19)	0.9(0.76-1.07)	0.34	(8,9)	1(0.83-1.21)	1.08(0.9-1.29)	0.5	(8,9)	1(0.94-1.07)	1(0.93-1.08)	0.95	(8,9)
Aconitase 2, mitochondrial	1(0.88-1.14)	0.88(0.78-1.01)	0.14	(8,9)	1(0.85-1.18)	0.95(0.83-1.07)	0.53	(8,9)	1(0.93-1.08)	0.9(0.84-0.97)	0.03	(8,9)
Isocitrate dehydrogenase [NADP], mitochondrial	1(0.86-1.17)	0.64(0.49-0.84)	0.005	(8,9)	1(0.85-1.18)	0.59(0.4-0.88)	0.02	(8,9)	1(0.91-1.1)	0.7(0.52-0.96)	0.03	(8,9)
Isocitrate dehydrogenase [NAD] subunit alpha	1(0.82-1.22)	0.65(0.5-0.83)	0.007	(8,9)	1(0.84-1.19)	0.73(0.61-0.88)	0.01	(8,9)	1(0.95-1.06)	0.76(0.64-0.9)	0.006	(8,9)
Isocitrate dehydrogenase [NAD] subunit beta	1(0.82-1.23)	0.65(0.51-0.84)	0.009	(8,9)	1(0.8-1.25)	0.76(0.61-0.95)	0.07	(8,9)	1(0.92-1.08)	0.73(0.57-0.92)	0.02	(8,9)
Isocitrate dehydrogenase [NAD] subunit gamma	1(0.83-1.21)	0.59(0.46-0.76)	0.002	(8,9)	1(0.84-1.19)	0.69(0.56-0.85)	0.007	(8,9)	1(0.92-1.08)	0.67(0.53-0.86)	0.005	(8,9)
2-oxoglutarate dehydrogenase E1 component	1(0.84-1.18)	0.67(0.58-0.77)	0.0008	(8,9)	1(0.77-1.3)	0.7(0.58-0.83)	0.02	(8,9)	1(0.87-1.15)	0.65(0.52-0.82)	0.002	(8,9)
2-oxoglutarate dehydrogenase-like, mitochondrial	1(0.79-1.27)	0.55(0.48-0.63)	0.0003	(8,9)	1(0.76-1.31)	0.53(0.41-0.69)	0.001	(8,9)	1(0.84-1.19)	0.57(0.47-0.7)	0.0002	(8,9)
Probable 2-oxoglutarate dehydrogenase E1 component DHKTD1, mitochondrial									1(0.68-1.46)	0.48(0.24-0.95)	0.04	(6,6)
Dihydrolipoyllysine-residue succinyltransferase component of 2-oxoglutarate dehydrogenase complex	1(0.81-1.24)	1.07(0.92-1.24)	0.58	(8,9)	1(0.81-1.24)	1.2(0.98-1.47)	0.17	(8,9)	1(0.83-1.21)	1.05(0.94-1.18)	0.6	(8,9)
Dihydrolipoyl dehydrogenase, mitochondrial	1(0.86-1.16)	0.76(0.64-0.9)	0.01	(8,9)	1(0.83-1.21)	0.92(0.8-1.07)	0.45	(8,9)	1(0.96-1.04)	0.87(0.82-0.93)	0.0008	(8,9)
Succinyl-CoA ligase [ADP/GDP-forming] subunit alpha	1(0.8-1.25)	0.42(0.33-0.55)	<0.0001	(8,9)	1(0.74-1.35)	0.4(0.27-0.6)	0.0008	(8,9)	1(0.86-1.16)	0.51(0.39-0.65)	0.0001	(8,9)
Succinyl-CoA ligase [ADP-forming] subunit beta	1(0.85-1.17)	0.39(0.3-0.5)	<0.0001	(8,9)	1(0.75-1.34)	0.43(0.31-0.59)	0.0004	(8,9)	1(0.86-1.16)	0.49(0.38-0.64)	0.0001	(8,9)
Succinyl-CoA ligase [GDP-forming] subunit beta	1(0.72-1.4)	0.78(0.56-1.09)	0.24	(8,9)	1(0.8-1.25)	0.6(0.34-1.05)	0.08	(8,9)	1(0.86-1.16)	0.56(0.42-0.74)	0.001	(8,9)
Succinate dehydrogenase [ubiquinone] flavoprotein	1(0.77-1.29)	0.85(0.71-1.02)	0.25	(8,9)	1(0.83-1.2)	0.85(0.71-1.03)	0.18	(8,9)	1(0.94-1.07)	0.95(0.85-1.06)	0.39	(8,9)
Succinate dehydrogenase Ip subunit	1(0.78-1.28)	0.82(0.67-1.01)	0.17	(8,9)	1(0.76-1.32)	0.9(0.74-1.1)	0.49	(8,9)	1(0.93-1.07)	1(0.89-1.12)	0.95	(8,9)
Succinate dehydrogenase [ubiquinone] cytochrome b small subunit	1(0.61-1.64)	1.47(0.88-2.46)	0.08	(3,3)								
Succinate dehydrogenase assembly factor 2, mitochondrial	1(0.35-2.83)	0.86(0.77-0.95)	0.29	(2,3)					1(0.56-1.79)	1.13(0.85-1.5)	0.62	(5,6)
Fumarate hydratase, mitochondrial	1(0.86-1.16)	0.87(0.75-1.02)	0.17	(8,9)	1(0.82-1.22)	1.02(0.89-1.16)	0.88	(8,9)	1(0.91-1.09)	0.97(0.91-1.02)	0.47	(8,9)
Malate dehydrogenase, mitochondrial	1(0.8-1.24)	0.9(0.7-1.14)	0.45	(8,9)	1(0.83-1.21)	1.05(0.86-1.28)	0.67	(8,9)	1(0.95-1.06)	1.05(0.96-1.14)	0.29	(8,9)

4.3.3.4. Electron Transport Chain and oxidative stress

The mitochondrial electron transport chain (ETC) is a series of protein complexes which mediates ATP production through OxPhos. At the mitochondrial inner membrane, electrons from NADH and $FADH_2$ produced by TCA cycle (and other pathways such as FAO) enter the ETC via complex I (NADH dehydrogenase) and complex II (succinate dehydrogenase) respectively. The electrons are then passed on to coenzyme Q, which then passes the electrons onto complex III (cytochrome bc1 complex), then cytochrome C, and subsequently to complex IV (cytochrome c oxidase), and onto the terminal electron acceptor oxygen (O_2) (which is reduced to H_2O) through a series of redox reactions. These reactions create a proton gradient across the mitochondrial inner membrane as complex I, III, and IV all act as proton pumps. The proton gradient is used to make ATP via complex V (ATP synthase) [326].

In this study, the most distinct changes in ETC-related proteins were found in CB. Among all detected complex I proteins (37 in HP, 36 in ENT, and 43 in CB), only five and three proteins were significantly decreased in HP and ENT respectively, while 32 proteins were decreased in CB. None of the detected complex I proteins were increased in abundance (**Table 4-22**). All four proteins of complex II were detected and none of them showed any significant change in AD brain (**Table 4-23**).

Proteins of complex III and complex IV showed no change in HP and ENT. However, two complex III proteins and three complex IV proteins were significantly decreased in CB. A further few proteins from both complex III and IV showed a trend ($p<0.1$) of decreased abundance in CB (**Table 4-23**).

Complex V was the only complex where subunits showed increased abundance. In HP, there were two proteins of complex V with increased abundance. In ENT, there were two complex V proteins with significant alteration, one increased and one decreased. There was only one protein with significant change in CB, with decreased abundance. All detected coenzyme Q-related proteins with statistical significance were decreased in abundance. No change was observed in the level of cytochrome C protein (**Table 4-24**).

Mitochondrial respiration is closely linked to ROS generation. We found a general increase in superoxide and hydrogen peroxide-metabolising redox enzymes, including superoxide dismutases (SOD1, SOD2, and SOD3) catalase, and glutathione peroxidase-1, in the AD brain. Along with redox-active proteins such as SH3 domain-binding glutamic acid-rich-like proteins, redox sensors implicated in hydrogen peroxide-dependent intracellular signalling were also increased in the AD brain. On the other hand, proteins involved in down-regulating ROS production and protection against oxidative damage (NmrA-like family domain-containing protein 1 and oxidation resistance protein 1) were decreased in AD brain, as well as antioxidant enzyme (**Table 4-25**).

Table 4-22: Proteomic findings relating to ETC complex I

	HP				ENT				CB			
General name	Abundance (C)	Abundance (AD)	p	N_C,N_{AD}	Abundance (C)	Abundance (AD)	p	N_C,N_{AD}	Abundance (C)	Abundance (AD)	p	N_C,N_{AD}
Complex I												
NADH dehydrogenase subunit 1									1(0.93-1.08)	0.72(0.58-0.9)	0.01	(8,9)
NADH dehydrogenase subunit 4									1(0.66-1.51)	0.85(0.55-1.3)	0.53	(8,9)
NADH dehydrogenase subunit 5					1(0.78-1.29)	1.21(0.83-1.78)	0.3	(5,6)	1(0.93-1.08)	1.15(0.99-1.34)	0.05	(2,3)
NADH dehydrogenase subunit 6									1(0.6-1.67)	1(0.9-1.13)	0.97	(3,3)
NADH dehydrogenase [ubiquinone] 1 alpha subcomplex subunit 2	1(0.9-1.11)	0.86(0.79-0.94)	0.02	(8,9)	1(0.79-1.27)	0.74(0.54-1.03)	0.11	(8,9)	1(0.91-1.1)	0.75(0.62-0.9)	0.008	(8,9)
NADH dehydrogenase [ubiquinone] 1 alpha subcomplex subunit 3	1(0.61-1.63)	1.09(0.96-1.24)	0.52	(3,3)					1(0.87-1.15)	0.82(0.67-1.01)	0.07	(5,6)
NADH dehydrogenase [ubiquinone] 1 alpha subcomplex subunit 4	1(0.83-1.2)	0.93(0.85-1.02)	0.42	(8,9)	1(0.8-1.24)	0.94(0.77-1.15)	0.64	(8,9)	1(0.92-1.08)	0.83(0.73-0.94)	0.01	(8,9)
NADH dehydrogenase [ubiquinone] 1 alpha subcomplex subunit 5	1(0.88-1.14)	0.96(0.91-1.02)	0.54	(8,9)	1(0.82-1.23)	0.93(0.78-1.1)	0.5	(8,9)	1(0.9-1.12)	0.74(0.65-0.85)	0.001	(8,9)
NADH dehydrogenase [ubiquinone] 1 alpha subcomplex subunit 6	1(0.9-1.11)	0.89(0.79-1.02)	0.14	(8,9)	1(0.85-1.18)	0.81(0.63-1.05)	0.14	(8,9)	1(0.89-1.13)	0.7(0.59-0.83)	0.001	(8,9)
NADH dehydrogenase [ubiquinone] 1 alpha subcomplex subunit 7	1(0.89-1.12)	1.21(0.98-1.5)	0.09	(8,9)	1(0.79-1.27)	1.19(0.96-1.47)	0.23	(8,9)	1(0.89-1.12)	0.85(0.71-1.01)	0.08	(8,9)
NADH dehydrogenase [ubiquinone] 1 alpha subcomplex subunit 8	1(0.88-1.14)	1.11(0.97-1.28)	0.21	(8,9)	1(0.85-1.18)	0.96(0.76-1.23)	0.77	(8,9)	1(0.89-1.13)	0.85(0.74-0.97)	0.05	(8,9)
NADH dehydrogenase [ubiquinone] 1 alpha subcomplex subunit 9	1(0.88-1.13)	0.98(0.88-1.1)	0.83	(8,9)	1(0.86-1.16)	0.91(0.8-1.04)	0.3	(8,9)	1(0.91-1.1)	0.77(0.68-0.88)	0.002	(8,9)
NADH dehydrogenase [ubiquinone] 1 alpha subcomplex subunit 10	1(0.81-1.23)	0.59(0.5-0.71)	0.0005	(8,9)	1(0.83-1.21)	0.6(0.49-0.74)	0.0007	(8,9)	1(0.95-1.05)	0.65(0.56-0.76)	0.0002	(8,9)
NADH dehydrogenase [ubiquinone] 1 alpha subcomplex subunit 11	1(0.79-1.26)	1.06(0.74-1.52)	0.73	(5,6)	1(0.73-1.38)	1.18(1.09-1.27)	0.23	(5,6)	1(0.86-1.17)	0.84(0.7-1)	0.1	(8,9)
NADH dehydrogenase [ubiquinone] 1 alpha subcomplex subunit 12	1(0.81-1.23)	1.04(0.95-1.13)	0.71	(8,9)	1(0.82-1.23)	0.94(0.82-1.08)	0.55	(8,9)	1(0.91-1.1)	0.77(0.69-0.87)	0.002	(8,9)
NADH dehydrogenase [ubiquinone] 1 alpha subcomplex subunit 13	1(0.9-1.11)	0.99(0.91-1.08)	0.83	(8,9)	1(0.76-1.31)	1.01(0.82-1.26)	0.93	(8,9)	1(0.89-1.12)	0.76(0.67-0.86)	0.002	(8,9)
Acyl carrier protein, mitochondrial	1(0.85-1.18)	0.71(0.61-0.84)	0.004	(8,9)	1(0.75-1.34)	0.74(0.69-0.79)	0.05	(8,9)	1(0.89-1.12)	0.74(0.63-0.87)	0.003	(8,9)
NADH dehydrogenase [ubiquinone] 1 beta subcomplex subunit 1	1(0.9-1.11)	1(0.86-1.16)	0.98	(8,9)	1(0.77-1.29)	0.97(0.79-1.19)	0.84	(8,9)	1(0.89-1.12)	0.82(0.72-0.93)	0.02	(8,9)
NADH dehydrogenase [ubiquinone] 1 beta subcomplex subunit 2									1(0.67-1.49)	0.73(0.49-1.08)	0.14	(5,4)
NADH dehydrogenase [ubiquinone] 1 beta subcomplex subunit 3	1(0.68-1.47)	1.06(0.92-1.23)	0.69	(5,6)	1(0.83-1.2)	0.73(0.64-0.83)	0.006	(5,6)	1(0.89-1.13)	0.87(0.74-1.02)	0.13	(8,9)
NADH dehydrogenase [ubiquinone] 1 beta subcomplex subunit 4	1(0.93-1.07)	1(0.89-1.12)	0.98	(8,9)	1(0.9-1.11)	0.9(0.73-1.1)	0.3	(8,9)	1(0.88-1.13)	0.84(0.75-0.95)	0.03	(8,9)
NADH dehydrogenase [ubiquinone] 1 beta subcomplex subunit 5									1(0.87-1.15)	0.81(0.69-0.95)	0.03	(8,9)

Complex I - continued												
NADH dehydrogenase [ubiquinone] 1 beta subcomplex subunit 6	1(0.55-1.81)	0.85(0.67-1.07)	0.5	(5,6)	1(0.69-1.44)	0.82(0.57-1.17)	0.33	(5,6)	1(0.9-1.11)	0.83(0.73-0.95)	0.02	(8,9)
NADH dehydrogenase [ubiquinone] 1 beta subcomplex subunit 7	1(0.73-1.38)	0.99(0.83-1.17)	0.93	(8,9)	1(0.58-1.74)	1.15(1.03-1.28)	0.53	(5,6)	1(0.84-1.18)	0.89(0.78-1.02)	0.23	(8,9)
NADH dehydrogenase [ubiquinone] 1 beta subcomplex subunit 8	1(0.9-1.11)	0.99(0.87-1.12)	0.86	(8,9)	1(0.87-1.15)	0.88(0.66-1.17)	0.38	(8,9)	1(0.87-1.15)	0.8(0.7-0.92)	0.02	(8,9)
NADH dehydrogenase [ubiquinone] 1 beta subcomplex subunit 9	1(0.91-1.1)	0.98(0.91-1.06)	0.76	(8,9)	1(0.88-1.13)	0.88(0.67-1.18)	0.38	(8,9)	1(0.9-1.12)	0.82(0.74-0.91)	0.008	(8,9)
NADH dehydrogenase [ubiquinone] 1 beta subcomplex subunit 10	1(0.92-1.09)	1.03(0.92-1.15)	0.64	(8,9)	1(0.83-1.2)	0.94(0.74-1.2)	0.67	(8,9)	1(0.89-1.13)	0.8(0.68-0.93)	0.02	(8,9)
NADH dehydrogenase [ubiquinone] 1 beta subcomplex subunit 11	1(0.88-1.14)	1.09(1.02-1.18)	0.19	(8,9)	1(0.83-1.21)	0.98(0.81-1.2)	0.89	(8,9)	1(0.9-1.11)	0.86(0.77-0.95)	0.03	(8,9)
NADH dehydrogenase 75 kDa subunit	1(0.85-1.18)	0.9(0.82-0.99)	0.23	(8,9)	1(0.85-1.18)	0.87(0.76-1)	0.16	(8,9)	1(0.91-1.1)	0.74(0.64-0.86)	0.002	(8,9)
NADH dehydrogenase [ubiquinone] iron-sulfur protein 2	1(0.9-1.11)	0.91(0.86-0.97)	0.09	(8,9)	1(0.8-1.25)	0.86(0.74-1)	0.2	(8,9)	1(0.88-1.13)	0.81(0.71-0.91)	0.01	(8,9)
NADH dehydrogenase [ubiquinone] iron-sulfur protein 3	1(0.92-1.09)	1.05(0.98-1.13)	0.34	(8,9)	1(0.81-1.23)	1.07(0.95-1.2)	0.52	(8,9)	1(0.91-1.1)	0.78(0.69-0.87)	0.002	(8,9)
NADH dehydrogenase [ubiquinone] iron-sulfur protein 4	1(0.9-1.11)	1.04(0.97-1.11)	0.48	(8,9)	1(0.85-1.17)	1.01(0.89-1.14)	0.93	(8,9)	1(0.88-1.14)	0.81(0.71-0.92)	0.02	(8,9)
NADH dehydrogenase [ubiquinone] iron-sulfur protein 5	1(0.87-1.15)	1.16(1.05-1.28)	0.07	(8,9)	1(0.43-2.34)	1.91(1.47-2.47)	0.12	(8,9)	1(0.87-1.15)	0.88(0.76-1.01)	0.15	(8,9)
NADH dehydrogenase [ubiquinone] iron-sulfur protein 6	1(0.9-1.11)	0.73(0.65-0.82)	0.0003	(8,9)	1(0.79-1.26)	1.01(0.87-1.18)	0.93	(8,9)	1(0.9-1.11)	0.82(0.71-0.95)	0.02	(8,9)
NADH dehydrogenase [ubiquinone] iron-sulfur protein 7	1(0.79-1.27)	1.13(1-1.28)	0.32	(8,9)	1(0.75-1.33)	0.8(0.66-0.96)	0.14	(8,9)	1(0.91-1.1)	0.8(0.7-0.92)	0.008	(8,9)
NADH dehydrogenase [ubiquinone] iron-sulfur protein 8	1(0.79-1.26)	0.98(0.81-1.18)	0.86	(8,9)	1(0.8-1.26)	1.16(1.04-1.29)	0.2	(8,9)	1(0.88-1.14)	0.77(0.65-0.92)	0.01	(8,9)
NADH dehydrogenase [ubiquinone] flavoprotein 1	1(0.9-1.12)	0.94(0.89-0.99)	0.24	(8,9)	1(0.92-1.09)	0.9(0.83-0.98)	0.06	(8,9)	1(0.9-1.11)	0.77(0.69-0.86)	0.001	(8,9)
NADH dehydrogenase [ubiquinone] flavoprotein 2	1(0.9-1.11)	0.9(0.81-1.01)	0.14	(8,9)	1(0.81-1.23)	0.95(0.79-1.14)	0.66	(8,9)	1(0.9-1.11)	0.78(0.7-0.87)	0.002	(8,9)
NADH dehydrogenase [ubiquinone] 1 subunit C2	1(0.82-1.22)	0.96(0.74-1.24)	0.75	(5,6)	1(0.78-1.28)	1.15(0.99-1.35)	0.28	(8,9)	1(0.89-1.13)	0.78(0.68-0.9)	0.007	(8,9)
NADH dehydrogenase [ubiquinone] 1 alpha subcomplex assembly factor 2	1(0.87-1.15)	1(0.78-1.28)	1	(8,9)	1(0.7-1.43)	0.89(0.75-1.04)	0.48	(8,9)	1(0.92-1.09)	0.99(0.94-1.04)	0.8	(8,9)
NADH dehydrogenase [ubiquinone] 1 alpha subcomplex assembly factor 3	1(0.73-1.36)	1.16(0.88-1.51)	0.37	(5,6)					1(0.91-1.1)	1.21(0.9-1.63)	0.16	(5,6)
NADH dehydrogenase [ubiquinone] 1 alpha subcomplex assembly factor 4					1(0.66-1.52)	0.81(0.62-1.06)	0.28	(5,6)	1(0.86-1.16)	0.82(0.72-0.94)	0.04	(8,9)
FAD-dependent oxidoreductase domain-containing protein 1	1(0.83-1.2)	0.63(0.5-0.8)	0.003	(8,9)								

Table 4-23: Proteomic findings relating to ETC complex II & III &IV

	HP				ENT				CB			
General name	Abundance (C)	Abundance (AD)	p	N_C,N_{AD}	Abundance (C)	Abundance (AD)	p	N_C,N_{AD}	Abundance (C)	Abundance (AD)	p	N_C,N_{AD}
ETC complex II												
Succinate dehydrogenase [ubiquinone] flavoprotein	1(0.77-1.29)	0.85(0.71-1.02)	0.25	(8,9)	1(0.83-1.2)	0.85(0.71-1.03)	0.18	(8,9)	1(0.94-1.07)	0.95(0.85-1.06)	0.39	(8,9)
Succinate dehydrogenase Ip subunit	1(0.78-1.28)	0.82(0.67-1.01)	0.17	(8,9)	1(0.76-1.32)	0.9(0.74-1.1)	0.49	(8,9)	1(0.93-1.07)	1(0.89-1.12)	0.95	(8,9)
Succinate dehydrogenase [ubiquinone] Cytochrome b small subunit	1(0.61-1.64)	1.47(0.88-2.46)	0.08	(3,3)								
Succinate dehydrogenase assembly factor 2	1(0.35-2.83)	0.86(0.77-0.95)	0.29	(2,3)					1(0.56-1.79)	1.13(0.85-1.5)	0.62	(5,6)
ETC complex III												
Cytochrome b-c1 complex subunit 1	1(0.85-1.18)	1.06(0.96-1.17)	0.47	(8,9)	1(0.87-1.15)	1.08(0.91-1.28)	0.44	(8,9)	1(0.91-1.1)	0.83(0.72-0.97)	0.03	(8,9)
Cytochrome b-c1 complex subunit 2	1(0.91-1.1)	1.05(0.96-1.14)	0.44	(8,9)	1(0.87-1.15)	0.94(0.79-1.12)	0.55	(8,9)	1(0.9-1.11)	0.84(0.74-0.96)	0.03	(8,9)
Cytochrome b-c1 complex subunit 6	1(0.86-1.16)	1.14(1-1.31)	0.15	(8,9)	1(0.35-2.87)	2.27(1.83-2.82)	0.11	(8,9)	1(0.77-1.3)	1.21(1.1-1.33)	0.15	(8,9)
Cytochrome b-c1 complex subunit 7	1(0.88-1.14)	1.11(0.97-1.27)	0.2	(8,9)	1(0.84-1.19)	1.08(0.93-1.25)	0.46	(8,9)	1(0.92-1.09)	0.85(0.73-0.99)	0.06	(8,9)
Cytochrome b-c1 complex subunit 8	1(0.9-1.11)	1.02(0.92-1.12)	0.79	(8,9)	1(0.85-1.17)	1(0.85-1.17)	0.98	(8,9)	1(0.91-1.1)	0.83(0.69-0.99)	0.05	(8,9)
Cytochrome b-c1 complex subunit 9					1(0.53-1.9)	1.21(0.99-1.48)	0.46	(5,6)	1(0.84-1.19)	0.87(0.74-1.01)	0.17	(8,9)
Cytochrome b-c1 complex subunit 10	1(0.75-1.33)	0.8(0.55-1.17)	0.12	(2,3)					1(0.87-1.15)	0.85(0.57-1.26)	0.36	(6,6)
Cytochrome b-c1 complex subunit Rieske	1(0.86-1.16)	0.98(0.9-1.08)	0.82	(8,9)	1(0.85-1.18)	1.03(0.83-1.27)	0.82	(8,9)	1(0.89-1.13)	0.84(0.71-1.01)	0.09	(8,9)
Cytochrome c-1	1(0.9-1.11)	1.05(0.93-1.2)	0.46	(8,9)	1(0.84-1.19)	1.08(0.89-1.31)	0.51	(8,9)	1(0.9-1.11)	0.92(0.77-1.08)	0.32	(8,9)
Ubiquinol-cytochrome c reductase complex chaperone CBP3	1(0.81-1.24)	0.9(0.8-1.01)	0.27	(5,6)					1(0.93-1.07)	1.01(0.92-1.12)	0.8	(8,9)
ETC complex IV												
Cytochrome c oxidase subunit 1 (MT)									1(0.73-1.38)	0.81(0.5-1.31)	0.37	(5,6)
Cytochrome c oxidase subunit 2 (MT)	1(0.82-1.22)	1.06(0.9-1.24)	0.62	(8,9)	1(0.84-1.19)	1.1(0.92-1.32)	0.38	(8,9)	1(0.86-1.16)	0.84(0.73-0.97)	0.07	(8,9)
Cytochrome c oxidase subunit 4 isoform 1	1(0.89-1.13)	0.97(0.86-1.1)	0.7	(8,9)	1(0.79-1.26)	0.96(0.78-1.19)	0.76	(8,9)	1(0.91-1.1)	0.85(0.72-1)	0.07	(8,9)
Cytochrome c oxidase subunit 5A	1(0.88-1.14)	1(0.9-1.12)	0.96	(8,9)	1(0.85-1.17)	1.05(0.85-1.29)	0.68	(8,9)	1(0.9-1.11)	0.84(0.7-1)	0.07	(8,9)
Cytochrome c oxidase subunit 5B	1(0.89-1.12)	0.93(0.84-1.03)	0.3	(8,9)	1(0.8-1.24)	0.96(0.86-1.07)	0.68	(8,9)	1(0.9-1.11)	0.85(0.72-0.99)	0.06	(8,9)
Cytochrome c oxidase subunit 6B1	1(0.87-1.15)	1.01(0.91-1.13)	0.9	(8,9)	1(0.83-1.2)	1.04(0.89-1.2)	0.74	(8,9)	1(0.91-1.1)	0.87(0.78-0.98)	0.05	(8,9)
Cytochrome c oxidase subunit 6C	1(0.86-1.16)	0.96(0.82-1.13)	0.7	(8,9)	1(0.84-1.19)	1.02(0.79-1.33)	0.87	(8,9)	1(0.89-1.12)	0.89(0.75-1.06)	0.2	(8,9)
Cytochrome c oxidase subunit 7A2	1(0.84-1.18)	1.04(0.93-1.17)	0.63	(8,9)	1(0.84-1.19)	0.94(0.82-1.08)	0.53	(8,9)	1(0.93-1.08)	0.83(0.7-0.99)	0.04	(8,9)
Cytochrome c oxidase subunit 7A-related protein	1(0.66-1.52)	0.85(0.66-1.09)	0.09	(2,3)	1(0.74-1.35)	0.76(0.41-1.39)	0.18	(2,3)	1(0.86-1.16)	0.76(0.61-0.96)	0.04	(8,9)
Cytochrome c oxidase subunit 7B	1(0.89-1.13)	1.03(0.88-1.21)	0.73	(8,9)	1(0.71-1.4)	0.9(0.72-1.12)	0.56	(8,9)	1(0.85-1.18)	0.88(0.66-1.18)	0.35	(5,6)
Cytochrome c oxidase subunit 7C	1(0.82-1.22)	0.95(0.81-1.11)	0.63	(8,9)	1(0.86-1.16)	0.86(0.69-1.07)	0.2	(8,9)	1(0.89-1.12)	0.84(0.73-0.96)	0.04	(8,9)
Cytochrome C oxidase assembly factor 3	1(0.82-1.22)	1.17(1.01-1.35)	0.17	(8,9)	1(0.64-1.56)	1.45(0.97-2.17)	0.06	(3,3)	1(0.88-1.13)	0.85(0.7-1.03)	0.13	(8,9)
Cytochrome c oxidase protein 20									1(0.66-1.52)	1.28(1.05-1.55)	0.19	(5,6)
Cytochrome c oxidase assembly protein COX11									1(0.71-1.41)	0.71(0.51-0.99)	0.11	(8,9)
Cytochrome c oxidase assembly protein COX15									1(0.79-1.27)	1.32(1.09-1.58)	0.05	(8,9)

Table 4-24: Proteomic findings relating to ETC complex V

	HP				ENT				CB			
General name	Abundance (C)	Abundance (AD)	p	N_C,N_{AD}	Abundance (C)	Abundance (AD)	p	N_C,N_{AD}	Abundance (C)	Abundance (AD)	p	N_C,N_{AD}
ETC complex V												
ATP synthase subunit alpha	1(0.77-1.3)	0.91(0.74-1.12)	0.54	(8,9)	1(0.79-1.27)	1(0.82-1.23)	0.98	(8,9)	1(0.92-1.09)	0.97(0.9-1.05)	0.59	(8,9)
ATP synthase subunit beta	1(0.76-1.31)	0.94(0.74-1.2)	0.7	(8,9)	1(0.78-1.28)	1.11(0.88-1.4)	0.48	(8,9)	1(0.92-1.09)	1.01(0.93-1.09)	0.88	(8,9)
ATP synthase subunit gamma	1(0.85-1.17)	1.02(0.91-1.15)	0.82	(8,9)	1(0.85-1.18)	0.96(0.83-1.1)	0.64	(8,9)	1(0.89-1.12)	0.94(0.82-1.07)	0.42	(8,9)
ATP synthase subunit delta	1(0.79-1.27)	1(0.82-1.24)	0.98	(8,9)	1(0.74-1.35)	1(0.76-1.3)	0.99	(8,9)	1(0.9-1.11)	0.98(0.84-1.16)	0.85	(8,9)
ATP synthase subunit epsilon									1(0.87-1.14)	1.03(0.89-1.18)	0.77	(8,9)
ATP synthase subunit epsilon-like protein, mitochondrial	1(0.76-1.31)	0.99(0.86-1.15)	0.95	(8,9)	1(0.85-1.17)	1.01(0.85-1.2)	0.94	(8,9)				
ATP synthase lipid-binding protein	1(0.1-9.78)	1.05(0.65-1.68)	0.84	(2,3)	1(0.69-1.45)	0.27(0.16-0.47)	0.002	(3,3)	1(0.02-61.81)	0.99(0.38-2.57)	0.98	(2,3)
6.8 kDa mitochondrial proteolipid									1(0.64-1.56)	0.91(0.36-2.33)	0.73	(3,3)
ATP synthase subunit a	1(0.68-1.47)	1.1(1.04-1.17)	0.52	(5,6)	1(0.92-1.08)	1.15(1.06-1.25)	0.009	(5,6)	1(0.86-1.16)	0.92(0.78-1.09)	0.41	(8,9)
ATP synthase subunit b	1(0.91-1.1)	1.08(0.95-1.24)	0.28	(8,9)	1(0.87-1.15)	1.04(0.86-1.27)	0.68	(8,9)	1(0.88-1.14)	0.93(0.83-1.05)	0.36	(8,9)
ATP synthase subunit d	1(0.89-1.13)	1.17(1.04-1.32)	0.05	(8,9)	1(0.87-1.15)	0.99(0.82-1.2)	0.94	(8,9)	1(0.88-1.13)	0.93(0.77-1.11)	0.44	(8,9)
ATP synthase subunit e	1(0.89-1.12)	1.12(0.99-1.26)	0.15	(8,9)	1(0.49-2.03)	1.19(0.84-1.68)	0.62	(8,9)	1(0.88-1.14)	0.88(0.77-1.01)	0.14	(8,9)
ATP synthase subunit f, isoform 2	1(0.79-1.26)	1.41(1.23-1.61)	0.01	(8,9)	1(0.72-1.39)	1.29(1.07-1.56)	0.14	(8,9)	1(0.87-1.14)	1.05(0.89-1.23)	0.62	(8,9)
ATP synthase subunit g	1(0.84-1.19)	0.94(0.83-1.07)	0.52	(8,9)	1(0.86-1.16)	0.93(0.75-1.16)	0.55	(8,9)	1(0.84-1.18)	0.9(0.77-1.05)	0.28	(8,9)
ATP synthase-coupling factor 6	1(0.87-1.15)	1.25(1.1-1.42)	0.01	(8,9)	1(0.86-1.16)	1.06(0.86-1.32)	0.6	(8,9)	1(0.83-1.21)	0.96(0.81-1.14)	0.72	(8,9)
ATP synthase subunit O	1(0.89-1.13)	1.06(0.98-1.15)	0.34	(8,9)	1(0.79-1.27)	0.93(0.8-1.08)	0.54	(8,9)	1(0.9-1.11)	0.94(0.82-1.09)	0.45	(8,9)
ATPase inhibitor	1(0.76-1.32)	0.92(0.67-1.26)	0.64	(8,9)	1(0.79-1.27)	1.19(0.97-1.46)	0.22	(8,9)	1(0.84-1.2)	1.23(1.07-1.43)	0.05	(8,9)
ATP synthase protein 8									1(0.68-1.46)	0.77(0.28-2.11)	0.38	(3,3)
ATP synthase subunit s	1(0.67-1.49)	0.87(0.77-0.98)	0.26	(3,3)					1(0.58-1.73)	0.68(0.25-1.81)	0.23	(3,3)
ATP synthase subunit s-like protein									1(0.77-1.3)	0.56(0.3-1.05)	0.06	(2,3)
ATP synthase mitochondrial F1 complex assembly factor 1	1(0.88-1.14)	1.01(0.85-1.2)	0.93	(8,9)	1(0.68-1.48)	1.1(1.04-1.17)	0.15	(2,3)	1(0.88-1.14)	0.81(0.74-0.88)	0.008	(8,9)
ATP synthase mitochondrial F1 complex assembly factor 2					1(0.51-1.97)	1.33(0.85-2.08)	0.21	(3,3)	1(0.79-1.27)	0.95(0.79-1.15)	0.68	(5,6)
Q and C												
Ubiquinone biosynthesis protein COQ9, mitochondrial	1(0.85-1.17)	0.88(0.79-0.97)	0.13	(8,9)	1(0.85-1.17)	0.89(0.78-1.01)	0.2	(8,9)	1(0.92-1.09)	0.77(0.73-0.81)	<0.0001	(8,9)
Coenzyme Q10 homolog A					1(0.74-1.36)	0.69(0.52-0.92)	0.04	(5,6)				
Coenzyme Q-binding protein COQ10 homolog B	1(0.67-1.5)	0.7(0.4-1.22)	0.21	(6,6)					1(0.89-1.12)	0.86(0.76-0.96)	0.04	(8,9)
ES1 protein homolog, mitochondrial	1(0.92-1.09)	0.64(0.54-0.75)	0.0001	(8,9)	1(0.83-1.2)	0.65(0.54-0.78)	0.002	(8,9)	1(0.95-1.06)	0.83(0.7-0.99)	0.05	(8,9)
Cytochrome c	1(0.82-1.22)	0.8(0.63-1.02)	0.12	(8,9)	1(0.8-1.26)	0.9(0.74-1.09)	0.4	(8,9)	1(0.93-1.07)	1.02(0.94-1.1)	0.73	(8,9)

Table 4-25: Proteomic findings relating to oxidative stress

	HP				ENT				CB			
General name	Abundance (C)	Abundance (AD)	p	N_C,N_{AD}	Abundance (C)	Abundance (AD)	p	N_C,N_{AD}	Abundance (C)	Abundance (AD)	p	N_C,N_{AD}
Superoxide/peroxide/nitric oxide related												
NADPH oxidase 2-NOX2	1(0.61-1.63)	1.71(1.35-2.16)	0.04	(5,6)	1(0.48-2.09)	1.68(0.98-2.88)	0.08	(3,3)	1(0.89-1.12)	1.16(1.02-1.32)	0.05	(6,6)
Superoxide dismutase [Cu-Zn]-SOD1	1(0.92-1.08)	1.15(1.02-1.3)	0.04	(8,9)	1(0.79-1.27)	1(0.87-1.16)	0.98	(8,9)	1(0.92-1.08)	1.27(1.19-1.36)	0.0001	(8,9)
Superoxide dismutase [Mn]-SOD2	1(0.9-1.12)	1.31(1.1-1.56)	0.01	(8,9)	1(0.86-1.16)	1.4(1.18-1.67)	0.004	(8,9)	1(0.85-1.18)	1.12(0.88-1.44)	0.38	(8,9)
Extracellular superoxide dismutase [Cu-Zn]-SOD3	1(0.85-1.17)	0.99(0.88-1.12)	0.94	(8,9)	1(0.81-1.23)	1.33(1.17-1.5)	0.02	(8,9)	1(0.87-1.14)	1(0.88-1.13)	0.99	(8,9)
Catalase	1(0.91-1.1)	1.32(1.09-1.61)	0.01	(8,9)	1(0.89-1.12)	1.4(1.14-1.72)	0.006	(8,9)	1(0.83-1.2)	1.09(0.86-1.38)	0.52	(8,9)
Glutathione peroxidase 1	1(0.86-1.16)	1.35(1.21-1.5)	0.002	(8,9)	1(0.87-1.15)	1.5(1.3-1.73)	0.0003	(8,9)	1(0.88-1.14)	1.23(1.11-1.35)	0.01	(8,9)
Monoamine oxidase B-like-MAO-B	1(0.79-1.26)	1.91(1.53-2.37)	0.0003	(8,9)	1(0.87-1.16)	1.83(1.54-2.17)	<0.0001	(8,9)	1(0.89-1.12)	1.1(0.99-1.23)	0.17	(8,9)
Hydroxyacylglutathione hydrolase, mitochondrial	1(0.91-1.1)	0.91(0.78-1.06)	0.23	(8,9)	1(0.83-1.2)	0.91(0.79-1.06)	0.39	(8,9)	1(0.94-1.06)	1.12(1.03-1.22)	0.02	(8,9)
Protein DJ-1	1(0.95-1.05)	1.16(1.02-1.32)	0.04	(8,9)	1(0.79-1.27)	1.07(0.92-1.23)	0.6	(8,9)	1(0.93-1.08)	1.24(1.13-1.36)	0.0007	(8,9)
Nitric oxide synthase-interacting protein									1(0.77-1.3)	1.31(1.08-1.58)	0.03	(3,3)
N(G),N(G)-dimethylarginine dimethylaminohydrolase 1	1(0.88-1.13)	1.21(1.03-1.43)	0.04	(8,9)	1(0.8-1.25)	1.08(0.94-1.25)	0.5	(8,9)	1(0.93-1.08)	1.06(0.99-1.13)	0.22	(8,9)
SH3 domain-binding glutamic acid-rich-like protein	1(0.8-1.26)	1.35(1.13-1.61)	0.03	(8,9)	1(0.89-1.13)	1.25(1.04-1.52)	0.04	(8,9)	1(0.9-1.11)	1.16(1.05-1.28)	0.03	(8,9)
SH3 domain-binding glutamic acid-rich-like protein 2	1(0.76-1.31)	1.21(1.04-1.41)	0.18	(8,9)	1(0.84-1.19)	1.24(1.1-1.39)	0.03	(8,9)	1(0.87-1.15)	1.25(1.15-1.35)	0.007	(8,9)
Peroxiredoxin-1	1(0.8-1.25)	1.51(1.25-1.83)	0.005	(8,9)	1(0.86-1.17)	1.25(1.07-1.46)	0.03	(8,9)	1(0.94-1.06)	1.24(1.14-1.34)	0.0002	(8,9)
Peroxiredoxin-2	1(0.95-1.05)	1.1(0.97-1.25)	0.14	(8,9)	1(0.88-1.13)	1.12(0.96-1.3)	0.21	(8,9)	1(0.92-1.09)	1.22(1.08-1.38)	0.009	(8,9)
Peroxiredoxin 3	1(0.87-1.15)	0.96(0.81-1.14)	0.68	(8,9)	1(0.82-1.22)	0.98(0.81-1.18)	0.83	(8,9)	1(0.92-1.08)	1.11(1-1.23)	0.08	(8,9)
Peroxiredoxin-4	1(0.87-1.15)	1.29(1.07-1.54)	0.02	(8,9)	1(0.78-1.28)	1.01(0.86-1.19)	0.94	(8,9)	1(0.89-1.13)	1.13(0.97-1.31)	0.18	(8,9)
Peroxiredoxin 6	1(0.83-1.21)	1.62(1.46-1.81)	0.0002	(8,9)	1(0.9-1.11)	1.58(1.37-1.82)	<0.0001	(8,9)	1(0.94-1.07)	1.28(1.21-1.36)	<0.0001	(8,9)
Peroxiredoxin-5	1(0.94-1.06)	0.75(0.62-0.91)	0.009	(8,9)	1(0.93-1.08)	0.79(0.62-1)	0.05	(8,9)	1(0.97-1.03)	0.87(0.77-0.99)	0.04	(8,9)
Thioredoxin 1	1(0.88-1.14)	1.12(1-1.24)	0.15	(8,9)	1(0.94-1.07)	1.11(0.98-1.26)	0.1	(8,9)	1(0.93-1.08)	1.2(1.08-1.33)	0.006	(8,9)
Thioredoxin 2, mitochondrial	1(0.85-1.17)	0.61(0.5-0.74)	0.0004	(8,9)	1(0.8-1.25)	0.75(0.62-0.91)	0.04	(8,9)	1(0.93-1.07)	0.75(0.67-0.84)	0.0002	(8,9)
Thioredoxin reductase 2, mitochondrial					1(0.62-1.62)	0.69(0.55-0.86)	0.1	(5,6)	1(0.8-1.25)	0.68(0.57-0.8)	0.006	(8,9)
Thioredoxin-like protein 1	1(0.89-1.12)	0.88(0.78-1)	0.1	(8,9)	1(0.9-1.11)	0.87(0.8-0.93)	0.02	(8,9)	1(0.94-1.07)	1.01(0.94-1.09)	0.84	(8,9)
NmrA-like family domain-containing protein 1					1(0.58-1.74)	0.59(0.34-1.01)	0.04	(3,3)				
Oxidation resistance protein 1, mitochondrial	1(0.88-1.13)	0.79(0.75-0.84)	0.002	(8,9)	1(0.88-1.13)	0.86(0.76-0.98)	0.07	(8,9)	1(0.93-1.07)	0.93(0.87-0.99)	0.09	(8,9)

4.3.3.5. Amino acid metabolism and neurotransmitters

Brain amino acid metabolism is critical for maintaining the homeostasis of neurotransmitters such as glutamate [327]. The branched-chain amino acids (BCAA), particularly leucine, act as amino group donors for glutamate synthesis in the brain [328]. We found major alterations in proteins involved in BCAA catabolism and synthesis, mostly decreased in the AD brain, including components of branched-chain alpha-ketoacid dehydrogenase complex (**Table 4-26**).

Enzymes involved in the metabolism of glycine, serine, and threonine were consistently decreased in the CB only (**Table 4-26**). Enzymes of the saccharopine pathway, aminoadipate-semialdehyde synthase, saccharopine dehydrogenase, and aldehyde dehydrogenase family 7 (member A1), were significantly elevated in HP. Tryptophan-metabolising enzymes, including kynurenine pathway enzymes, were decreased in the AD brain, most significantly in ENT.

Aromatic amino acid (phenylalanine, tyrosine, and tryptophan) metabolising enzymes, including tetrahydrobiopterin (BH4) synthesizing enzymes, were generally increased in the AD brain. Enzymes involved in the generation and degradation of GABA were mainly altered in the CB, including glutamate decarboxylase 1 and 2 (**Table 4-26**).

Enzymes involved in urea cycle and nitrogen homeostasis via transamination and transdeamination routes showed variable changes. Ornithine aminotransferase, carbamoyl-phosphate, and glutaminase kidney isoform (GLS) showed decreased abundance while alanine and glycine aminotransferases were increased in AD (**Table 4-27**).

Numerous GABA receptor subunits and GABA receptor-associated proteins were detected in this study, 9 in HP, 8 in ENT and 12 in CB. However, there was neither a pattern nor observable consistency in the changes across different brain regions (**Table 4-28**). Ten or more glutamate receptor-related proteins were detected in the brain regions examined in this study. However, only CB exhibited notable changes in glutamate receptors, four being decreased and two near-significantly decreased (**Table 4-28**).

Table 4-26: Proteomic findings relating to amino acid metabolism

	HP				ENT				CB			
General name	Abundance (C)	Abundance (AD)	p	N_C,N_{AD}	Abundance (C)	Abundance (AD)	p	N_C,N_{AD}	Abundance (C)	Abundance (AD)	p	N_C,N_{AD}
Branched-chain amino acid (valine, leucine and isoleucine)												
Branched-chain-amino-acid aminotransferase, cytosolic	1(0.95-1.05)	0.89(0.8-0.99)	0.05	(8,9)	1(0.78-1.28)	0.85(0.7-1.04)	0.26	(8,9)	1(0.87-1.15)	1.18(1.01-1.37)	0.08	(8,9)
3-methyl-2-oxobutanoate dehydrogenase [lipoamide] kinase	1(0.63-1.59)	0.76(0.55-1.05)	0.22	(5,6)	1(0.44-2.27)	1.09(0.65-1.85)	0.71	(3,3)	1(0.72-1.38)	0.67(0.52-0.88)	0.04	(8,9)
Lipoamide acyltransferase	1(0.85-1.18)	0.69(0.6-0.8)	0.001	(8,9)	1(0.71-1.4)	0.49(0.32-0.74)	0.007	(5,6)	1(0.8-1.25)	0.55(0.41-0.72)	0.001	(8,9)
Dihydrolipoyl dehydrogenase, mitochondrial	1(0.86-1.16)	0.76(0.64-0.9)	0.01	(8,9)	1(0.83-1.21)	0.92(0.8-1.07)	0.45	(8,9)	1(0.96-1.04)	0.87(0.82-0.93)	0.0008	(8,9)
2-oxoisovalerate dehydrogenase subunit alpha	1(0.91-1.09)	0.79(0.68-0.91)	0.007	(8,9)	1(0.84-1.19)	0.9(0.71-1.14)	0.43	(8,9)	1(0.91-1.1)	0.74(0.63-0.87)	0.003	(8,9)
2-oxoisovalerate dehydrogenase subunit beta	1(0.92-1.09)	0.82(0.7-0.95)	0.02	(8,9)	1(0.79-1.27)	0.64(0.52-0.8)	0.006	(8,9)	1(0.9-1.11)	0.73(0.58-0.92)	0.01	(8,9)
Short/branched chain specific acyl-CoA dehydrogenase, mitochondrial	1(0.8-1.24)	0.85(0.75-0.96)	0.16	(8,9)	1(0.83-1.2)	0.84(0.73-0.96)	0.09	(8,9)	1(0.89-1.12)	0.8(0.69-0.94)	0.02	(8,9)
Methylcrotonoyl-Coenzyme A carboxylase 1	1(0.8-1.24)	0.49(0.35-0.69)	0.001	(8,9)	1(0.78-1.28)	0.66(0.43-0.99)	0.06	(8,9)	1(0.68-1.47)	0.44(0.3-0.65)	0.003	(8,9)
Methylcrotonoyl-Coenzyme A carboxylase 2	1(0.94-1.06)	1.14(1.01-1.27)	0.04	(8,9)	1(0.87-1.15)	1.12(0.96-1.32)	0.21	(8,9)	1(0.97-1.03)	1.03(0.93-1.13)	0.52	(8,9)
3-hydroxy-3-methylglutaryl-Coenzyme A lyase	1(0.7-1.43)	1.6(1.39-1.83)	0.02	(8,9)	1(0.65-1.5	1.48(1.21-1.81)	0.08	(8,9)	1(0.92-1.09)	1.01(0.92-1.1)	0.92	(8,9)
3-hydroxyisobutyrate dehydrogenase, mitochondrial	1(0.93-1.08)	1.15(0.97-1.36)	0.11	(8,9)	1(0.9-1.11)	1.32(1.11-1.56)	0.007	(8,9)	1(0.94-1.06)	1.15(1.02-1.29)	0.03	(8,9)
Methylmalonate semialdehyde dehydrogenase	1(0.85-1.18)	0.94(0.8-1.11)	0.58	(8,9)	1(0.84-1.19)	0.85(0.69-1.06)	0.19	(8,9)	1(0.87-1.14)	0.78(0.6-1.01)	0.07	(8,9)
Glycine/Serine/Threonine												
Aminomethyltransferase	1(0.41-2.47)	1.13(0.64-2)	0.64	(3,3)	1(0.88-1.13)	1.07(0.93-1.25)	0.36	(6,6)	1(0.89-1.13)	0.84(0.75-0.93)	0.02	(8,9)
Serine hydroxymethyl transferase 2	1(0.82-1.23)	0.56(0.48-0.65)	0.0001	(8,9)	1(0.88-1.14)	0.62(0.54-0.72)	0.0001	(8,9)	1(0.87-1.15)	0.72(0.57-0.92)	0.02	(8,9)
Phosphoserine aminotransferase isoform 1	1(0.85-1.17)	1.33(1.18-1.5)	0.004	(8,9)	1(0.88-1.13)	1.14(1.01-1.29)	0.11	(8,9)	1(0.89-1.12)	1.1(1.01-1.2)	0.15	(8,9)
Threonine synthase-like 1					1(0.64-1.57)	0.68(0.3-1.54)	0.17	(3,3)	1(0.86-1.16)	0.58(0.47-0.7)	0.0001	(8,9)
Lysine/Tryptophan/Phenylalanine/Tyrosine												
Aminoadipate-semialdehyde synthase	1(0.87-1.15)	1.33(1.13-1.58)	0.007	(8,9)	1(0.71-1.4)	0.9(0.65-1.24)	0.6	(8,9)	1(0.82-1.22)	0.97(0.81-1.16)	0.8	(8,9)
Saccharopine dehydrogenase	1(0.92-1.09)	1.17(1.09-1.25)	0.005	(8,9)	1(0.81-1.23)	1.32(1.14-1.52)	0.02	(8,9)	1(0.92-1.09)	1.02(0.96-1.08)	0.67	(8,9)
Aldehyde dehydrogenase family 7, member A1	1(0.9-1.12)	1.27(1.08-1.49)	0.01	(8,9)	1(0.85-1.17)	1.13(0.96-1.33)	0.22	(8,9)	1(0.9-1.11)	1.11(0.98-1.26)	0.16	(8,9)
Kynurenine aminotransferase III	1(0.72-1.39)	0.6(0.5-0.72)	0.009	(8,9)	1(0.76-1.31)	0.63(0.53-0.73)	0.004	(8,9)	1(0.87-1.15)	0.7(0.61-0.8)	0.0005	(8,9)
Kynurenine--oxoglutarate transaminase 1, mitochondrial	1(0.83-1.2)	0.94(0.63-1.4)	0.75	(8,8)	1(0.82-1.22)	0.76(0.65-0.89)	0.03	(8,9)	1(0.78-1.28)	0.87(0.71-1.07)	0.33	(8,9)

N-acetylserotonin O-methyltransferase-like protein	1(0.79-1.27)	0.81(0.69-0.94)	0.1	(8,9)	1(0.82-1.22)	0.72(0.59-0.87)	0.01	(8,9)	1(0.82-1.22)	0.9(0.83-0.99)	0.3	(8,9)
Glutaryl-CoA dehydrogenase, mitochondrial	1(0.94-1.07)	1.11(0.98-1.26)	0.11	(8,9)	1(0.84-1.2)	1.42(1.25-1.63)	0.002	(8,9)	1(0.89-1.13)	1.08(0.96-1.22)	0.3	(8,9)
Glutathione transferase zeta 1	1(0.81-1.23)	1.3(1.13-1.48)	0.03	(8,9)	1(0.78-1.28)	1.51(1.08-2.11)	0.03	(6,6)	1(0.87-1.14)	1.28(1.1-1.5)	0.01	(8,9)
6-pyruvoyl tetrahydrobiopterin synthase									1(0.8-1.26)	0.69(0.47-1.01)	0.03	(3,3)
Sepiapterin reductase	1(0.9-1.11)	1.29(1.18-1.42)	0.0008	(8,9)	1(0.77-1.3)	1.41(1.27-1.56)	0.02	(8,9)	1(0.91-1.1)	1.18(1.12-1.24)	0.004	(8,9)
Dihydropteridine reductase	1(0.83-1.21)	1.15(0.99-1.34)	0.2	(8,9)	1(0.8-1.25)	0.92(0.75-1.14)	0.55	(8,9)	1(0.83-1.2)	1.29(1.17-1.41)	0.02	(8,9)
Pterin-4-alpha-carbinolamine dehydratase	1(0.9-1.11)	1.43(1.18-1.75)	0.003	(8,9)	1(0.74-1.35)	1.5(1.27-1.76)	0.02	(8,9)	1(0.91-1.1)	1.3(1.17-1.45)	0.0007	(8,9)
Pterin-4-alpha-carbinolamine dehydratase 2	1(0.56-1.78)	1.73(1.3-2.29)	0.06	(6,6)	1(0.35-2.88)	1.53(1.37-1.71)	0.22	(3,3)	1(0.83-1.21)	1.06(1-1.12)	0.48	(6,6)
Glutamate decarboxylase 1	1(0.46-2.19)	0.61(0.51-0.75)	0.16	(5,6)	1(0.35-2.9)	1.04(0.34-3.19)	0.92	(3,3)	1(0.95-1.05)	0.74(0.65-0.85)	0.0007	(8,9)
Glutamate decarboxylase 2	1(0.75-1.33)	0.76(0.64-0.9)	0.08	(8,9)	1(0.8-1.25)	0.8(0.63-1.01)	0.13	(8,9)	1(0.95-1.06)	0.78(0.71-0.86)	0.0002	(8,9)
4-aminobutyrate aminotransferase, mitochondrial	1(0.86-1.16)	1.05(0.95-1.17)	0.52	(8,9)	1(0.86-1.16)	1.19(1.06-1.35)	0.05	(8,9)	1(0.93-1.07)	1.1(1.03-1.16)	0.03	(8,9)
Amine oxidase [flavin- containing] A	1(0.83-1.2)	1.01(0.88-1.15)	0.94	(8,9)	1(0.87-1.14)	1.22(0.98-1.53)	0.09	(8,9)	1(0.91-1.1)	1.21(1.07-1.37)	0.01	(8,9)

Table 4-27: Proteomic findings relating to nitrogen homeostasis

	HP				ENT				CB			
General name	Abundance (C)	Abundance (AD)	p	N_C,N_{AD}	Abundance (C)	Abundance (AD)	p	N_C,N_{AD}	Abundance (C)	Abundance (AD)	p	N_C,N_{AD}
Nitrogen metabolism/Urea cycle												
Ornithine aminotransferase, mitochondrial	1(0.89-1.13)	0.62(0.51-0.76)	0.0004	(8,9)	1(0.27-3.77)	0.96(0.78-1.19)	0.95	(8,9)	1(0.87-1.15)	0.68(0.61-0.77)	0.0002	(8,9)
Carbamoyl-phosphate synthase [ammonia], mitochondrial	1(0.88-1.13)	0.61(0.39-0.95)	0.03	(3,3)								
Argininosuccinate synthase (ASS)	1(0.96-1.05)	1.01(0.84-1.23)	0.88	(8,9)	1(0.86-1.16)	0.92(0.76-1.11)	0.43	(8,9)	1(0.92-1.09)	0.99(0.94-1.05)	0.89	(8,9)
Argininosuccinate lyase (ASL)	1(0.87-1.15)	1.11(0.92-1.34)	0.32	(8,9)	1(0.71-1.4)	1.13(0.85-1.51)	0.49	(6,6)	1(0.93-1.08)	1.13(1.04-1.23)	0.02	(8,9)
Alanine aminotransferase 1	1(0.86-1.16)	1.51(1.1-2.06)	0.02	(8,9)	1(0.86-1.16)	1.42(1.08-1.87)	0.02	(8,9)	1(0.89-1.12)	1.16(1.01-1.34)	0.07	(8,9)
Glycine amidinotransferase, mitochondrial precursor	1(0.91-1.1)	1.29(1.14-1.46)	0.002	(8,9)	1(0.94-1.06)	1.35(1.2-1.53)	0.0003	(8,9)	1(0.9-1.11)	1.11(1.02-1.22)	0.09	(8,9)
Glutamine synthetase 1	1(0.8-1.25)	0.92(0.78-1.08)	0.49	(8,9)	1(0.76-1.31)	1.13(0.89-1.43)	0.45	(8,9)	1(0.94-1.06)	1.07(0.88-1.31)	0.47	(8,9)
Glutaminase kidney isoform (GLS) mitochondrial	1(0.66-1.53)	0.56(0.47-0.66)	0.01	(8,9)	1(0.7-1.43)	0.55(0.42-0.72)	0.008	(8,9)	1(0.78-1.27)	0.48(0.36-0.65)	0.0005	(8,9)
Glutamate dehydrogenase 1 (GDH)	1(0.84-1.19)	1.14(1-1.3)	0.18	(8,9)	1(0.89-1.12)	1.23(1.1-1.37)	0.008	(8,9)	1(0.9-1.11)	1.12(1.02-1.23)	0.07	(8,9)

Table 4-28: Proteomic findings relating to GABA and glutamate receptor-related proteins

	HP				ENT				CB			
General name	Abundance (C)	Abundance (AD)	p	N_C,N_{AD}	Abundance (C)	Abundance (AD)	p	N_C,N_{AD}	Abundance (C)	Abundance (AD)	p	N_C,N_{AD}
GABA receptor												
GABA receptor subunit alpha-1	1(0.76-1.31)	0.95(0.79-1.15)	0.71	(5,6)	1(0.64-1.56)	0.89(0.76-1.04)	0.51	(5,6)	1(0.86-1.16)	0.92(0.83-1.01)	0.26	(8,9)
GABA receptor subunit alpha-6									1(0.84-1.19)	0.76(0.7-0.83)	0.007	(8,9)
GABA receptor subunit beta-2									1(0.88-1.13)	0.88(0.78-0.98)	0.09	(8,9)
GABA receptor subunit beta-3	1(0.74-1.36)	1.07(0.9-1.28)	0.6	(5,6)								
GABA receptor subunit gamma-2	1(0.7-1.44)	0.82(0.58-1.18)	0.39	(8,9)	1(0.7-1.44)	1.22(0.95-1.56)	0.31	(8,9)	1(0.79-1.27)	0.88(0.77-1)	0.26	(6,6)
GABA receptor subunit delta									1(0.77-1.3)	0.83(0.72-0.96)	0.18	(8,9)
GABA receptor-associated protein-like 1					1(0.81-1.23)	1.23(1.05-1.44)	0.09	(8,9)	1(0.19-5.29)	1.03(0.67-1.57)	0.89	(2,3)
GABA receptor-associated protein-like 2	1(0.8-1.25)	1.04(0.93-1.15)	0.75	(8,9)	1(0.9-1.11)	1.11(0.98-1.26)	0.15	(8,9)	1(0.9-1.1)	1.18(1.13-1.24)	0.005	(8,9)
GABA type B receptor subunit 1	1(0.72-1.38)	1.06(0.85-1.31)	0.75	(8,9)	1(0.73-1.37)	1.01(0.77-1.34)	0.94	(8,9)	1(0.92-1.09)	0.89(0.82-0.96)	0.03	(8,9)
GABA type B receptor subunit 2	1(0.84-1.19)	0.8(0.65-0.99)	0.08	(8,9)	1(0.65-1.54)	0.82(0.58-1.17)	0.43	(8,9)	1(0.85-1.17)	0.92(0.82-1.04)	0.36	(8,9)
GABA receptor-associated protein	1(0.91-1.1)	1.1(0.96-1.26)	0.21	(8,9)					1(0.93-1.07)	1.09(1.02-1.18)	0.06	(8,9)
Inactive phospholipase C-like protein 1	1(0.7-1.43)	0.98(0.81-1.2)	0.92	(8,9)	1(0.84-1.18)	0.61(0.47-0.79)	0.002	(8,9)	1(0.9-1.11)	0.89(0.74-1.07)	0.22	(8,9)
BTB/POZ domain-containing protein KCTD12	1(0.79-1.27)	1.41(1.17-1.69)	0.02	(8,9)	1(0.83-1.21)	1.58(1.41-1.77)	0.0005	(8,9)	1(0.86-1.17)	1.06(0.97-1.16)	0.44	(8,9)
Glutamate receptor												
Glutamate receptor 1	1(0.35-2.82)	0.77(0.33-1.81)	0.65	(8,9)					1(0.75-1.33)	0.63(0.53-0.74)	0.006	(8,9)
Glutamate receptor 2	1(0.58-1.72)	0.71(0.45-1.12)	0.28	(8,9)	1(0.65-1.54)	0.72(0.56-0.94)	0.16	(8,9)	1(0.93-1.07)	0.86(0.77-0.97)	0.03	(8,9)
Glutamate receptor 3	1(0.63-1.59)	1.13(0.67-1.93)	0.65	(5,6)	1(0.52-1.91)	0.88(0.7-1.11)	0.64	(5,6)	1(0.7-1.43)	1.18(0.88-1.59)	0.37	(5,6)
Glutamate receptor 4	1(0.56-1.79)	1.12(0.69-1.82)	0.69	(5,6)	1(0.59-1.69)	0.99(0.72-1.38)	0.98	(5,6)	1(0.83-1.2)	0.89(0.76-1.05)	0.3	(8,9)
Glutamate receptor, ionotropic kainate 2	1(0.66-1.52)	1.69(1.35-2.11)	0.004	(2,3)					1(0.8-1.25)	0.78(0.64-0.96)	0.08	(8,9)
Glutamate receptor, ionotropic kainate 3									1(0.32-3.14)	1.13(0.67-1.9)	0.49	(2,3)
Metabotropic glutamate receptor 1									1(0.73-1.37)	0.85(0.6-1.21)	0.44	(8,9)
Metabotropic glutamate receptor 2	1(0.75-1.33)	0.85(0.68-1.06)	0.32	(8,9)	1(0.77-1.29)	0.92(0.73-1.15)	0.56	(8,9)	1(0.86-1.16)	1.14(1.02-1.28)	0.12	(8,9)
Metabotropic glutamate receptor 3	1(0.5-1.99)	1.4(0.59-3.32)	0.49	(8,9)	1(0.88-1.14)	1.05(0.9-1.24)	0.56	(8,9)	1(0.81-1.24)	0.94(0.78-1.13)	0.55	(5,6)
Metabotropic glutamate receptor 4									1(0.83-1.21)	0.84(0.71-1)	0.13	(8,9)
Metabotropic glutamate receptor 5	1(0.5-2)	1.46(1.18-1.79)	0.21	(5,6)	1(0.44-2.26)	1.04(0.74-1.46)	0.74	(2,3)	1(0.68-1.48)	0.81(0.46-1.41)	0.25	(3,3)
Neurochondrin	1(0.78-1.29)	0.73(0.56-0.95)	0.06	(8,9)	1(0.85-1.18)	0.78(0.62-0.99)	0.07	(8,9)	1(0.95-1.05)	0.92(0.86-0.99)	0.04	(8,9)
Metabotropic glutamate receptor 7	1(0.26-3.8)	0.84(0.54-1.29)	0.74	(5,6)	1(0.32-3.17)	0.94(0.22-4.05)	0.9	(3,3)				
Glutamate [NMDA] receptor subunit epsilon-1									1(0.55-1.82)	0.51(0.26-0.98)	0.03	(3,3)
Glutamate [NMDA] receptor subunit zeta-1	1(0.62-1.61)	0.73(0.48-1.12)	0.24	(6,6)	1(0.56-1.79)	1.14(0.72-1.81)	0.48	(3,3)	1(0.58-1.72)	0.76(0.43-1.35)	0.38	(5,6)
Glutamate receptor delta-1 subunit	1(0.83-1.2)	1.03(0.9-1.18)	0.75	(5,6)	1(0.81-1.23)	0.96(0.43-2.14)	0.84	(2,3)	1(0.76-1.31)	1.22(0.71-2.1)	0.26	(3,3)
Glutamate receptor delta-2 subunit									1(0.83-1.21)	0.78(0.62-0.98)	0.07	(8,9)

4.3.3.6. Transcription and mRNA processing

Histones are the basic chromosomal proteins that package and order the DNA into nucleosomes and play roles in gene regulation. Among the detected histone proteins, all of those showing significant change in abundance were increased in the AD brain (15, eight, and nine, in HP, ENT, and CB respectively) (**Table 4-29**).

Chromosomes are made of nucleosomes that consist of DNA wrapped around histones. Although there is a significant increase in the abundance of histone proteins, the protein level of nucleosome assembly protein was decreased in the AD brain. Interestingly, multiple proteins that interact with nucleosome and chromatin structure, and may be involved in regulation of DNA transcription, were increased (High-mobility group protein HMG-I/HMG-Y, Non-histone chromosomal protein HMG-14 and HMG-17, Methyl-CpG-binding protein 2 and parathymosin (**Table 4-30**).

Proteins that modify histones epigenetically (e.g. SETD3, SETD7, and histone deacetylase 6) were decreased in the AD brain, most consistently in CB. Proteins that facilitate transcription activation (e.g. Non-POU domain-containing octamer-binding protein, transcriptional activator protein Pur-alpha) were decreased in AD, along with transcription elongation factors. Interestingly, proteins that act as repressors of transcriptional activation were generally increased in AD (e.g. TSC22 domain family protein 1 and Far upstream element-binding proteins) (**Table 4-31**).

We also found generally decreased levels of RNA helicases (**Table 4-32**) and pre-mRNA processing proteins in the AD brain (**Table 4-33**). On the other hand, of the spliceosome components detected in this study, those altered in AD were all increased in abundance (6, 6, and 4 in HP, ENT, and CB respectively (numbers including near-significant proteins)). Consistent with the change of spliceosome components, splicing factors also showed a general trend of elevation in the AD brain (**Table 4-34**). However, in contrast to the general increase in the abundance of spliceosome components and splicing factors, proteins that are involved in spliceosome assembly were decreased in abundance (**Table 4-34**).

Table 4-29: Proteomic findings relating to histones

	HP				ENT				CB			
General name	Abundance (C)	Abundance (AD)	p	N_C,N_{AD}	Abundance (C)	Abundance (AD)	p	N_C,N_{AD}	Abundance (C)	Abundance (AD)	p	N_C,N_{AD}
Histones												
Histone H1x	1(0.8-1.25)	1.45(1.13-1.86)	0.02	(8,9)	1(0.72-1.39)	1.17(0.91-1.5)	0.4	(8,9)	1(0.88-1.14)	1.21(1.07-1.38)	0.03	(8,9)
Histone H1.0	1(0.82-1.22)	1.72(1.47-2.02)	0.0002	(8,9)	1(0.81-1.23)	1.32(1.13-1.54)	0.03	(8,9)	1(0.78-1.28)	1.26(0.95-1.66)	0.17	(8,9)
Histone H1.2	1(0.8-1.24)	1.87(1.43-2.45)	0.0008	(8,9)	1(0.74-1.36)	1.32(1.11-1.57)	0.09	(8,9)	1(0.83-1.21)	1.3(1.1-1.54)	0.03	(8,9)
Histone H1.3	1(0.5-1.99)	1.86(1.19-2.92)	0.1	(8,9)	1(0.74-1.34)	1.42(1.19-1.69)	0.03	(6,6)	1(0.79-1.26)	1.36(1.06-1.75)	0.05	(8,9)
Histone H1.4	1(0.76-1.31)	1.7(1.2-2.42)	0.01	(8,9)	1(0.73-1.36)	1.21(0.96-1.53)	0.27	(8,9)	1(0.84-1.18)	1.24(1.07-1.43)	0.04	(8,9)
Histone H1.5	1(0.79-1.26)	1.75(1.35-2.27)	0.002	(8,9)	1(0.66-1.51)	1.61(1.22-2.13)	0.03	(5,6)	1(0.73-1.38)	1.24(0.99-1.55)	0.23	(8,9)
Core histone macro-H2A.1	1(0.81-1.24)	1.41(1.14-1.75)	0.02	(8,9)	1(0.72-1.4)	1.54(1.42-1.68)	0.02	(8,9)	1(0.9-1.11)	1(0.9-1.11)	1	(8,9)
Histone H2A type 1-C									1(0.75-1.33)	1.07(0.9-1.28)	0.63	(8,9)
Histone H2A type 2-A	1(0.85-1.18)	1.74(1.46-2.07)	0.0001	(6,6)	1(0.73-1.37)	1.72(1.42-2.07)	0.005	(8,9)	1(0.71-1.41)	1.26(0.94-1.68)	0.25	(8,9)
Histone H2A type 2-B	1(0.79-1.27)	1.43(1.09-1.86)	0.04	(8,9)	1(0.84-1.19)	1.5(1.3-1.72)	0.0009	(8,9)	1(0.78-1.28)	1.12(0.84-1.49)	0.48	(6,6)
Histone H2A type 2-C									1(0.73-1.37)	1.56(1.12-2.19)	0.03	(5,6)
Histone H2A type 3									1(0.65-1.53)	1.19(0.69-2.05)	0.34	(3,3)
Histone H2A.x	1(0.78-1.28)	1.33(1.07-1.66)	0.06	(8,9)	1(0.8-1.25)	1.09(0.89-1.34)	0.5	(8,9)	1(0.88-1.14)	0.97(0.84-1.11)	0.69	(8,9)
Histone H2A.Z	1(0.72-1.38)	1.77(1.3-2.43)	0.01	(8,9)	1(0.7-1.42)	1.02(0.79-1.32)	0.91	(8,9)	1(0.89-1.13)	1.24(1.05-1.45)	0.03	(8,9)
Histone H2B type 1-C/E/F/G/I									1(0.86-1.16)	1.18(0.83-1.69)	0.18	(2,3)
Histone H2B type 1-K	1(0.86-1.16)	1.36(1.14-1.63)	0.008	(8,9)								
Histone H2B type 1-L					1(0.85-1.18)	1.16(0.99-1.34)	0.15	(8,9)				
Histone H2B type 1-M									1(0.88-1.14)	1.15(1-1.32)	0.1	(8,9)
Histone H2B type 2-E					1(0.81-1.23)	1.13(0.91-1.39)	0.36	(8,9)	1(0.48-2.08)	1.36(0.85-2.17)	0.21	(3,3)
Histone H2B type 3-B	1(0.58-1.73)	1.99(1.65-2.4)	0.02	(3,3)					1(0.91-1.1)	1.2(1.04-1.38)	0.03	(8,9)
Histone H2B type 3-B	1(0.83-1.21)	1.62(1.24-2.11)	0.004	(5,6)								
Histone H2B type F-S									1(0.81-1.23)	0.98(0.63-1.55)	0.9	(3,3)
Histone H3.1	1(0.61-1.63)	1.83(1.47-2.26)	0.02	(8,9)	1(0-891.58)	1.46(0.54-4)	0.6	(2,3)	1(0.88-1.14)	1.2(1.11-1.31)	0.02	(8,9)
Histone H3.2									1(0.45-2.22)	1.33(1.05-1.68)	0.06	(2,3)
Histone H3.3	1(0.77-1.3)	1.65(1.49-1.82)	0.002	(8,9)	1(0.86-1.16)	1.23(1.07-1.4)	0.03	(8,9)	1(0.89-1.13)	1.25(1.08-1.44)	0.02	(8,9)
Histone H4	1(0.85-1.17)	1.46(1.31-1.64)	0.0005	(8,9)	1(0.81-1.23)	1.26(1.13-1.41)	0.04	(8,9)	1(0.93-1.07)	1.18(1.07-1.3)	0.007	(8,9)

Table 4-30: Proteomic findings relating to nucleosome

	HP				ENT				CB			
General name	Abundance (C)	Abundance (AD)	p	N_C,N_{AD}	Abundance (C)	Abundance (AD)	p	N_C,N_{AD}	Abundance (C)	Abundance (AD)	p	N_C,N_{AD}
Nucleosome and chromatin metabolism												
Nucleosome assembly protein 1-like 1	1(0.91-1.1)	0.7(0.59-0.84)	0.001	(8,9)	1(0.82-1.22)	0.62(0.49-0.78)	0.002	(8,9)	1(0.91-1.1)	0.91(0.81-1.03)	0.2	(8,9)
High mobility group protein HMG-I/HMG-Y	1(0.79-1.26)	1.79(1.51-2.12)	0.0004	(8,9)	1(0.86-1.17)	1.29(1.11-1.51)	0.02	(8,9)	1(0.76-1.32)	0.93(0.79-1.1)	0.58	(5,6)
Non-histone chromosomal protein HMG-14									1(0.89-1.13)	1.24(1.07-1.43)	0.02	(8,9)
Non-histone chromosomal protein HMG-17					1(0.52-1.92)	1.42(0.9-2.24)	0.14	(3,3)	1(0.79-1.26)	1.24(1-1.53)	0.1	(5,6)
Methyl-CpG-binding protein 2	1(0.86-1.16)	1.26(1.09-1.46)	0.02	(8,9)	1(0.87-1.14)	1.2(1.11-1.3)	0.02	(8,9)	1(0.91-1.1)	1.2(1.08-1.34)	0.009	(8,9)
Parathymosin	1(0.89-1.12)	1.2(0.97-1.49)	0.1	(8,9)	1(0.83-1.2)	1.48(1.2-1.82)	0.005	(8,9)	1(0.89-1.13)	1.11(0.99-1.25)	0.17	(8,9)

Table 4-31: Proteomic findings relating to transcription

	HP				ENT				CB			
General name	Abundance (C)	Abundance (AD)	p	N_C,N_{AD}	Abundance (C)	Abundance (AD)	p	N_C,N_{AD}	Abundance (C)	Abundance (AD)	p	N_C,N_{AD}
Transcription related												
Histone-lysine N-methyltransferase setd3	1(0.86-1.16)	0.76(0.59-0.98)	0.02	(3,3)					1(0.74-1.35)	0.6(0.44-0.83)	0.02	(8,9)
Histone-lysine N-methyltransferase SETD7	1(0.11-8.89)	1.31(1.03-1.67)	0.34	(2,3)	1(0.64-1.56)	0.67(0.42-1.05)	0.13	(5,6)	1(0.88-1.14)	0.76(0.63-0.92)	0.01	(8,9)
Protein arginine N-methyltransferase 1	1(0.87-1.14)	0.67(0.55-0.8)	0.0009	(8,9)	1(0.79-1.26)	0.77(0.7-0.85)	0.04	(8,9)	1(0.88-1.13)	0.86(0.77-0.95)	0.04	(8,9)
Histone deacetylase 6	1(0.79-1.27)	0.94(0.83-1.07)	0.58	(5,6)	1(0.75-1.33)	0.82(0.47-1.45)	0.43	(5,5)	1(0.88-1.13)	0.82(0.73-0.91)	0.01	(8,9)
Non-POU domain-containing octamer-binding protein	1(0.84-1.19)	0.71(0.55-0.92)	0.02	(8,9)	1(0.86-1.16)	0.71(0.56-0.9)	0.01	(8,9)	1(0.91-1.1)	0.97(0.88-1.07)	0.61	(8,9)
Paraspeckle component 1	1(0.92-1.09)	0.78(0.69-0.89)	0.003	(8,9)	1(0.81-1.23)	0.63(0.49-0.83)	0.007	(8,9)	1(0.89-1.13)	0.86(0.74-1.01)	0.1	(8,9)
CCR4-NOT transcription complex subunit 1	1(0.88-1.13)	0.99(0.9-1.1)	0.9	(5,6)	1(0.35-2.84)	0.99(0.74-1.33)	0.98	(3,3)	1(0.94-1.07)	0.81(0.77-0.86)	<0.0001	(8,9)
Transcriptional activator protein Pur-alpha	1(0.89-1.12)	0.87(0.78-0.96)	0.05	(8,9)	1(0.84-1.19)	0.73(0.64-0.84)	0.006	(8,9)	1(0.94-1.07)	0.89(0.81-0.97)	0.02	(8,9)
Nucleolar transcription factor					1(0.77-1.31)	0.81(0.6-1.1)	0.09	(3,3)	1(0.82-1.22)	0.72(0.6-0.86)	0.01	(8,9)
Myb-binding protein 1A	1(0.44-2.28)	0.63(0.5-0.78)	0.13	(3,3)					1(0.82-1.22)	0.82(0.72-0.95)	0.09	(8,9)
Transcription elongation factor A protein-like 6	1(0.82-1.22)	1.09(0.86-1.37)	0.48	(5,6)	1(0.79-1.27)	1.6(1.22-2.1)	0.008	(5,6)	1(0.89-1.12)	1.06(0.96-1.17)	0.38	(8,9)
Transcription elongation factor A protein-like 2									1(0.83-1.21)	0.71(0.55-0.92)	0.03	(8,9)
Transcription elongation factor B polypeptide 1	1(0.8-1.25)	0.62(0.52-0.75)	0.002	(6,6)	1(0.86-1.16)	0.65(0.53-0.8)	0.002	(5,6)	1(0.88-1.14)	0.92(0.82-1.02)	0.2	(5,6)
Transcription elongation factor B polypeptide 2	1(0.83-1.2)	0.72(0.61-0.84)	0.006	(8,9)	1(0.84-1.2)	0.67(0.55-0.8)	0.002	(8,9)	1(0.94-1.07)	0.87(0.8-0.94)	0.007	(8,9)
Transcription intermediary factor 1-beta	1(0.68-1.48)	1.01(0.79-1.29)	0.96	(8,9)	1(0.9-1.11)	0.78(0.66-0.92)	0.01	(8,9)	1(0.96-1.04)	0.96(0.89-1.05)	0.38	(8,9)

TSC22 domain family protein 1	1(0.88-1.13)	0.8(0.63-1.01)	0.07	(8,8)	1(0.78-1.28)	1(0.73-1.36)	0.98	(5,6)	1(0.65-1.54)	1.63(1.28-2.06)	0.03	(5,6)
Pre-B-cell leukaemia transcription factor-interacting protein 1	1(0.86-1.16)	1.64(1.29-2.09)	0.001	(8,9)	1(0.85-1.17)	1.61(1.45-1.8)	0.0001	(8,9)	1(0.87-1.15)	1.05(0.93-1.19)	0.55	(8,9)
Far upstream element-binding protein 1	1(0.87-1.15)	1.05(0.92-1.2)	0.55	(8,9)	1(0.86-1.17)	1.21(1.06-1.39)	0.04	(8,9)	1(0.95-1.06)	0.99(0.91-1.08)	0.83	(8,9)
Far upstream element-binding protein 2	1(0.91-1.1)	1.17(1.08-1.27)	0.009	(8,9)	1(0.91-1.1)	1.21(1.12-1.3)	0.002	(8,9)	1(0.95-1.06)	1.05(0.98-1.12)	0.25	(8,9)

Table 4-32: Proteomic findings relating to RNA helicase

	HP				ENT				CB			
General name	Abundance (C)	Abundance (AD)	p	N_C,N_{AD}	Abundance (C)	Abundance (AD)	p	N_C,N_{AD}	Abundance (C)	Abundance (AD)	p	N_C,N_{AD}
RNA helicase												
ATP-dependent RNA helicase DDX1	1(0.88-1.13)	0.73(0.62-0.87)	0.004	(8,9)	1(0.82-1.22)	0.69(0.55-0.88)	0.02	(8,9)	1(0.94-1.06)	0.97(0.89-1.07)	0.6	(8,9)
Probable ATP-dependent RNA helicase DDX5	1(0.85-1.18)	0.93(0.79-1.1)	0.49	(8,9)	1(0.88-1.14)	0.68(0.49-0.95)	0.03	(8,9)	1(0.9-1.11)	0.81(0.74-0.89)	0.003	(8,9)
Probable ATP-dependent RNA helicase DDX17	1(0.91-1.1)	0.88(0.76-1.03)	0.13	(8,9)	1(0.9-1.11)	0.86(0.75-1)	0.09	(8,9)	1(0.91-1.1)	1(0.9-1.12)	0.98	(8,9)
Probable ATP-dependent RNA helicase DDX47									1(0.76-1.32)	1.39(1.17-1.66)	0.02	(3,3)
Putative ATP-dependent RNA helicase DHX30	1(0.5-2.02)	1.38(1.02-1.88)	0.29	(5,6)	1(0.84-1.2)	0.96(0.79-1.17)	0.7	(5,6)	1(0.93-1.08)	0.75(0.65-0.87)	0.002	(8,9)
ATP-dependent RNA helicase DHX36	1(0.85-1.18)	1.43(0.87-2.34)	0.13	(6,6)					1(0.9-1.11)	0.78(0.62-0.97)	0.04	(8,9)

Table 4-33: Proteomic findings relating to pre-mRNA processing

	HP				ENT				CB			
General name	Abundance (C)	Abundance (AD)	p	N_C,N_{AD}	Abundance (C)	Abundance (AD)	p	N_C,N_{AD}	Abundance (C)	Abundance (AD)	p	N_C,N_{AD}
pre-mRNA processing												
Heterogeneous nuclear ribonucleoprotein A1	1(0.85-1.18)	0.87(0.71-1.06)	0.23	(8,9)	1(0.93-1.08)	0.68(0.55-0.85)	0.004	(8,9)	1(0.9-1.11)	0.98(0.88-1.09)	0.72	(8,9)
Heterogeneous nuclear ribonucleoprotein H2	1(0.69-1.46)	0.93(0.71-1.23)	0.74	(8,9)	1(0.59-1.69)	1.11(0.83-1.49)	0.69	(8,9)	1(0.87-1.15)	0.82(0.71-0.93)	0.03	(8,9)
Heterogeneous nuclear ribonucleoprotein K	1(0.9-1.11)	0.89(0.8-1)	0.1	(8,9)	1(0.87-1.14)	0.85(0.78-0.93)	0.04	(8,9)	1(0.94-1.06)	0.94(0.88-1.01)	0.14	(8,9)
Heterogeneous nuclear ribonucleoprotein L	1(0.9-1.11)	0.89(0.8-1)	0.11	(8,9)	1(0.88-1.14)	0.81(0.7-0.94)	0.03	(8,9)	1(0.92-1.09)	0.97(0.88-1.08)	0.65	(8,9)
Heterogeneous nuclear ribonucleoprotein Q	1(0.92-1.09)	0.9(0.83-0.97)	0.04	(8,9)	1(0.95-1.05)	0.86(0.78-0.96)	0.01	(8,9)	1(0.95-1.05)	0.95(0.9-1.01)	0.16	(8,9)
Poly(rC)-binding protein 1	1(0.87-1.15)	1.01(0.9-1.13)	0.89	(8,9)	1(0.83-1.21)	0.93(0.79-1.08)	0.48	(8,9)	1(0.93-1.08)	0.89(0.84-0.95)	0.02	(8,9)
Poly(rC)-binding protein 2	1(0.87-1.15)	0.96(0.86-1.07)	0.58	(8,9)	1(0.87-1.15)	0.97(0.83-1.14)	0.73	(8,9)	1(0.91-1.1)	0.87(0.77-0.98)	0.06	(8,9)
Pre-mRNA-processing factor 6	1(0.83-1.2)	0.79(0.73-0.87)	0.02	(5,6)					1(0.72-1.4)	0.99(0.77-1.27)	0.96	(8,9)
Pre-mRNA-processing factor 40 homolog A	1(0.1-10.29)	2.23(1.18-4.23)	0.06	(2,3)	1(0.66-1.52)	1.02(0.81-1.3)	0.85	(3,3)	1(0.88-1.14)	0.99(0.83-1.18)	0.91	(8,9)
Pre-mRNA-processing factor 40 homolog B									1(0.8-1.25)	0.74(0.62-0.89)	0.03	(8,9)

Table 4-34: Proteomic findings relating to pre-mRNA splicing

	HP				ENT				CB			
General name	Abundance (C)	Abundance (AD)	p	N_C,N_{AD}	Abundance (C)	Abundance (AD)	p	N_C,N_{AD}	Abundance (C)	Abundance (AD)	p	N_C,N_{AD}
Spliceosome component												
Small nuclear ribonucleoprotein Sm D1	1(0.91-1.1)	1.15(1-1.34)	0.08	(8,9)	1(0.79-1.27)	1.34(1.12-1.6)	0.04	(8,9)	1(0.92-1.09)	1.06(0.94-1.19)	0.39	(8,9)
Small nuclear ribonucleoprotein Sm D2	1(0.94-1.07)	1.14(1.01-1.28)	0.05	(8,9)	1(0.91-1.1)	1.14(0.99-1.3)	0.09	(8,9)	1(0.92-1.09)	1.06(0.95-1.2)	0.34	(8,9)
Small nuclear ribonucleoprotein-associated protein N					1(0.6-1.68)	1.66(1.31-2.09)	0.05	(5,6)				
U1 small nuclear ribonucleoprotein A	1(0.81-1.24)	1.11(0.9-1.38)	0.43	(8,9)	1(0.71-1.41)	1.46(1.05-2.01)	0.08	(8,9)	1(0.78-1.28)	1.07(0.91-1.26)	0.59	(8,9)
U1 small nuclear ribonucleoprotein 70 kDa	1(0.83-1.2)	1.22(1.09-1.37)	0.05	(8,9)	1(0.8-1.25)	1.03(0.83-1.27)	0.84	(8,9)	1(0.9-1.11)	1.16(1.03-1.31)	0.05	(8,9)
U4/U6.U5 tri-snRNP-associated protein 2	1(0.53-1.88)	1.32(0.74-2.35)	0.38	(5,4)	1(0.17-5.89)	2.04(1.5-2.77)	0.35	(6,6)	1(0.88-1.14)	1.19(1.06-1.33)	0.03	(8,9)
U6 snRNA-associated Sm-like protein LSm2	1(0.86-1.16)	1.26(1.14-1.39)	0.01	(8,9)	1(0.85-1.18)	1.19(1.05-1.35)	0.07	(8,9)	1(0.91-1.1)	1.09(0.98-1.21)	0.17	(8,9)
U6 snRNA-associated Sm-like protein LSm3	1(0.92-1.09)	1.18(1-1.39)	0.06	(8,9)	1(0.9-1.11)	1.14(0.98-1.34)	0.12	(8,9)	1(0.9-1.11)	1.1(0.95-1.29)	0.23	(8,9)
U6 snRNA-associated Sm-like protein LSm4	1(0.72-1.39)	1.36(1.09-1.71)	0.09	(8,9)	1(0.81-1.24)	1.31(1.14-1.5)	0.03	(8,9)	1(0.89-1.12)	1.16(1.07-1.25)	0.03	(8,9)
U6 snRNA-associated Sm-like protein LSm7	1(0.77-1.3)	1.24(1.01-1.52)	0.15	(8,9)	1(0.71-1.41)	1.1(0.9-1.34)	0.59	(8,9)	1(0.92-1.08)	1.1(1.02-1.18)	0.06	(8,9)
Pre-mRNA-splicing factor 38B									1(0.78-1.28)	1.3(1.14-1.48)	0.05	(8,9)
Splicing factor 1	1(0.93-1.08)	1.13(1.05-1.23)	0.02	(8,9)	1(0.77-1.29)	1.15(0.93-1.42)	0.35	(8,9)	1(0.85-1.18)	1.02(0.9-1.17)	0.79	(8,9)
Serine/arginine-rich splicing factor 1	1(0.89-1.13)	1.27(1.16-1.4)	0.003	(8,9)	1(0.85-1.17)	1.23(1.08-1.39)	0.03	(8,9)	1(0.93-1.07)	1.11(0.98-1.26)	0.11	(8,9)
Serine/arginine-rich splicing factor 2	1(0.91-1.09)	1.12(1.01-1.25)	0.06	(8,9)	1(0.9-1.11)	1.23(1.16-1.31)	0.002	(8,9)	1(0.94-1.06)	1.11(1.01-1.23)	0.05	(8,9)
Serine/arginine-rich splicing factor 3	1(0.9-1.12)	1.16(1-1.33)	0.08	(8,9)	1(0.9-1.11)	1.14(0.99-1.31)	0.1	(8,9)	1(0.86-1.16)	1.15(0.97-1.37)	0.18	(8,9)
Serine/arginine-rich splicing factor 5	1(0.77-1.31)	0.68(0.51-0.9)	0.01	(3,3)	1(0.76-1.32)	0.71(0.47-1.06)	0.1	(6,6)	1(0.84-1.18)	0.72(0.61-0.86)	0.006	(8,9)
Serine/arginine-rich splicing factor 7	1(0.85-1.18)	1.13(1.04-1.24)	0.14	(8,9)	1(0.83-1.2)	1.23(1.09-1.38)	0.05	(8,9)	1(0.92-1.08)	1.06(0.95-1.18)	0.32	(8,9)
Serine/arginine-rich splicing factor 10	1(0.89-1.12)	1.03(0.93-1.15)	0.64	(8,9)	1(0.79-1.26)	1.37(1.22-1.54)	0.02	(8,9)	1(0.88-1.14)	1.2(1.05-1.38)	0.04	(8,9)
Thioredoxin-like protein 4A	1(0.76-1.31)	1.05(0.61-1.81)	0.76	(3,3)	1(0.64-1.57)	1.66(0.9-3.05)	0.12	(6,6)	1(0.78-1.28)	1.36(1.07-1.74)	0.05	(8,9)
N-alpha-acetyltransferase 38, NatC auxiliary subunit	1(0.89-1.13)	1.13(1.02-1.26)	0.09	(8,9)	1(0.9-1.11)	1.28(1.09-1.51)	0.01	(8,9)	1(0.95-1.05)	1.13(1.01-1.27)	0.04	(8,9)
Spliceosome assembly												
Serine-threonine kinase receptor-associated protein	1(0.89-1.13)	0.77(0.69-0.84)	0.001	(8,9)	1(0.9-1.11)	0.71(0.63-0.81)	0.0002	(8,9)	1(0.96-1.05)	0.84(0.77-0.91)	0.0007	(8,9)
Pre-mRNA-processing-splicing factor 8	1(0.81-1.24)	0.86(0.74-0.99)	0.18	(8,9)	1(0.83-1.21)	0.73(0.58-0.92)	0.03	(8,9)	1(0.93-1.08)	0.97(0.9-1.05)	0.56	(8,9)
U5 small nuclear ribonucleoprotein 200 kDa helicase	1(0.87-1.14)	0.93(0.74-1.17)	0.55	(8,9)	1(0.89-1.12)	0.85(0.74-0.98)	0.05	(8,9)	1(0.93-1.07)	0.99(0.9-1.08)	0.79	(8,9)

4.3.3.7. Translation

Ribosomes are specialised complexes composed of nucleic acids and proteins that are responsible for mediating all protein synthesis. Specialised nucleic acids, ribosomal RNA (rRNA) and transfer RNA (tRNA) molecules, are essential for ribosomes to translate mRNA into proteins. A group of proteins known as initiation factors regulates the rate and specificity of ribosome function [329].

The levels of tRNA synthesising enzymes were mostly down-regulated in all three brain regions in AD (**Table 4-35, Table 4-36**). The most heavily affected region in this regard was CB, with the most number of proteins altered significantly (of 37 detected, 23 decreased & 2 increased). In the HP and ENT, 12 and 15 (out of 33) tRNA synthesising enzymes were decreased respectively.

Mitochondrial ribosomal proteins that were significantly altered in the AD brain (all three regions) were decreased in abundance (**Table 4-37**). Consistent with the changes observed for mitochondrial tRNA synthesising proteins, the disturbance was most severe in the CB where 17 out of 45 mitochondrial ribosomal proteins were significantly decreased in abundance. Eight (of 22) and seven (of 33) mitochondrial ribosomal proteins were decreased in HP and ENT respectively.

On the other hand, 40S and 60S ribosomal proteins, and Ribosomal protein S6 kinases detected in this study showed less statistical significance than tRNA synthetase/ligase or mitochondrial ribosomal proteins. For 40S ribosomal proteins, none (of 32) changed in HP, only one (of 31) increased in ENT, and only one (of 32) decreased in CB. For 60S ribosomal proteins, three (of 40) were decreased in HP, two (of 41) were increased in ENT, and only one (of 41) was decreased in CB. Of all ribosomal protein S6 kinases detected, only one showed significant change, increased in CB (**Table 4-38**).

Various subunits of eukaryotic translation initiation factors 1 to 5 were detected in this study and all those with statistically significant changes were decreased in abundance (**Table 4-39**).

In line with the above described decrease in the level of translation initiation factors, the elongation factors detected in this study were significantly decreased in abundance in AD (**Table 4-40**).

Table 4-35: Proteomic findings relating to cytoplasmic tRNA synthetases

	HP				ENT				CB			
General name	Abundance (C)	Abundance (AD)	p	N_C,N_{AD}	Abundance (C)	Abundance (AD)	p	N_C,N_{AD}	Abundance (C)	Abundance (AD)	p	N_C,N_{AD}
tRNA synthetase (cytoplasmic)												
Alanyl-tRNA synthetase	1(0.79-1.27)	0.81(0.68-0.96)	0.11	(8,9)	1(0.91-1.1)	0.66(0.56-0.78)	0.0002	(8,9)	1(0.93-1.07)	0.8(0.72-0.88)	0.0007	(8,9)
Aminoacyl tRNA synthetase complex-interacting multifunctional protein 2					1(0.88-1.13)	1.06(0.89-1.27)	0.48	(5,6)	1(0.8-1.25)	1.08(0.86-1.36)	0.58	(8,9)
Aminoacyl tRNA synthase complex-interacting multifunctional protein 1	1(0.85-1.18)	0.86(0.75-0.99)	0.13	(8,9)	1(0.82-1.22)	0.73(0.61-0.87)	0.01	(8,9)	1(0.89-1.13)	0.77(0.67-0.88)	0.005	(8,9)
Arginine--tRNA ligase, cytoplasmic	1(0.9-1.12)	0.82(0.66-1.03)	0.1	(8,9)	1(0.84-1.19)	0.74(0.58-0.95)	0.04	(8,9)	1(0.89-1.12)	0.8(0.72-0.88)	0.003	(8,9)
Asparagine--tRNA ligase, cytoplasmic	1(0.92-1.09)	0.87(0.81-0.94)	0.02	(8,9)	1(0.9-1.11)	0.79(0.7-0.89)	0.004	(8,9)	1(0.97-1.03)	0.91(0.84-0.99)	0.03	(8,9)
Aspartyl-tRNA synthetase, cytoplasmic	1(0.89-1.13)	1.03(0.89-1.19)	0.74	(8,9)	1(0.87-1.15)	0.8(0.67-0.94)	0.03	(8,9)	1(0.94-1.06)	0.87(0.79-0.96)	0.02	(8,9)
Bifunctional glutamate/proline--tRNA ligase	1(0.91-1.1)	0.96(0.88-1.03)	0.42	(8,9)	1(0.76-1.31)	0.87(0.8-0.94)	0.28	(8,9)	1(0.94-1.07)	0.84(0.76-0.92)	0.003	(8,9)
Cysteine--tRNA ligase, cytoplasmic	1(0.94-1.06)	0.82(0.76-0.89)	0.0003	(8,9)	1(0.91-1.1)	0.86(0.81-0.91)	0.01	(8,9)	1(0.87-1.16)	1(0.89-1.13)	0.98	(8,9)
Glutamine--tRNA ligase isoform 1	1(0.92-1.09)	1.02(0.92-1.13)	0.74	(8,9)	1(0.83-1.2)	0.91(0.71-1.16)	0.46	(8,9)	1(0.95-1.05)	0.8(0.73-0.89)	0.0007	(8,9)
Glycine--tRNA ligase	1(0.96-1.04)	0.92(0.89-0.95)	0.001	(8,9)	1(0.95-1.06)	0.95(0.89-1.01)	0.17	(8,9)	1(0.95-1.05)	1.06(1.02-1.1)	0.03	(8,9)
Histidine--tRNA ligase, cytoplasmic	1(0.87-1.15)	0.71(0.62-0.81)	0.0009	(8,9)	1(0.77-1.3)	0.62(0.5-0.77)	0.005	(8,9)	1(0.91-1.09)	0.87(0.78-0.97)	0.04	(8,9)
Isoleucine--tRNA ligase, cytoplasmic	1(0.77-1.3)	0.87(0.72-1.06)	0.34	(8,9)	1(0.65-1.54)	0.84(0.67-1.04)	0.41	(8,9)	1(0.93-1.07)	0.77(0.71-0.84)	0.0001	(8,9)
Leucine--tRNA ligase, cytoplasmic	1(0.78-1.28)	0.84(0.69-1.03)	0.23	(8,9)	1(0.7-1.44)	0.84(0.64-1.1)	0.37	(8,9)	1(0.94-1.06)	0.76(0.65-0.89)	0.004	(8,9)
Lysine--tRNA ligase	1(0.74-1.34)	0.81(0.7-0.93)	0.13	(6,6)	1(0.84-1.19)	0.89(0.74-1.08)	0.32	(8,9)	1(0.95-1.06)	0.82(0.74-0.9)	0.001	(8,9)
Methionine--tRNA ligase, cytoplasmic	1(0.9-1.11)	0.86(0.69-1.07)	0.18	(8,9)	1(0.65-1.53)	1.06(0.87-1.3)	0.78	(8,9)	1(0.93-1.08)	0.83(0.76-0.9)	0.001	(8,9)
Phenylalanine--tRNA ligase alpha	1(0.84-1.18)	0.76(0.68-0.85)	0.007	(8,9)	1(0.86-1.17)	0.78(0.68-0.9)	0.01	(8,9)	1(0.87-1.15)	0.89(0.77-1.02)	0.18	(8,9)
Phenylalanine--tRNA ligase beta	1(0.81-1.23)	0.62(0.52-0.74)	0.001	(8,9)	1(0.82-1.21)	0.63(0.51-0.78)	0.002	(8,9)	1(0.93-1.08)	0.82(0.74-0.92)	0.004	(8,9)
Probable threonine--tRNA ligase 2, cytoplasmic	1(0.47-2.15)	1(0.57-1.77)	1	(3,3)	1(0.62-1.62)	1(0.85-1.17)	0.98	(5,6)	1(0.64-1.55)	1.21(0.91-1.62)	0.35	(5,6)
Serine--tRNA ligase, cytoplasmic	1(0.87-1.15)	0.84(0.78-0.91)	0.03	(8,9)	1(0.89-1.13)	0.9(0.83-0.98)	0.12	(8,9)	1(0.95-1.06)	1.1(1.02-1.18)	0.04	(8,9)
Threonine--tRNA ligase, cytoplasmic	1(0.9-1.11)	1.1(1.02-1.19)	0.1	(8,9)	1(0.91-1.1)	1.12(1.02-1.23)	0.08	(8,9)	1(0.93-1.07)	1.07(0.99-1.15)	0.17	(8,9)
Tryptophan--tRNA ligase, cytoplasmic	1(0.89-1.12)	0.93(0.79-1.09)	0.39	(8,9)	1(0.79-1.26)	0.83(0.73-0.94)	0.12	(8,9)	1(0.95-1.06)	1.01(0.94-1.09)	0.76	(8,9)
Tyrosine--tRNA ligase, cytoplasmic	1(0.91-1.1)	0.67(0.57-0.79)	0.0003	(8,9)	1(0.82-1.23)	0.62(0.51-0.77)	0.002	(8,9)	1(0.95-1.06)	0.85(0.76-0.95)	0.01	(8,9)
Valine--tRNA ligase	1(0.88-1.14)	0.93(0.86-1.01)	0.29	(8,9)	1(0.88-1.14)	0.81(0.69-0.94)	0.03	(8,9)	1(0.92-1.09)	0.76(0.7-0.83)	0.0001	(8,9)

Table 4-36: Proteomic findings relating to mitochondrial tRNA synthesis

	HP				ENT				CB			
General name	Abundance (C)	Abundance (AD)	p	N_C,N_{AD}	Abundance (C)	Abundance (AD)	p	N_C,N_{AD}	Abundance (C)	Abundance (AD)	p	N_C,N_{AD}
Mitochondrial												
Proline--tRNA ligase, mitochondrial	1(0.33-3)	0.51(0.27-0.94)	0.1	(3,3)	1(0.49-2.06)	1.12(0.55-2.28)	0.57	(2,3)	1(0.83-1.2)	0.61(0.49-0.76)	0.001	(8,9)
Aspartate--tRNA ligase, mitochondrial	1(0.74-1.34)	0.8(0.72-0.89)	0.11	(5,6)	1(0.56-1.8)	1.31(1.03-1.68)	0.34	(8,9)	1(0.86-1.17)	0.85(0.7-1.02)	0.13	(8,9)
Methionine--tRNA ligase, mitochondrial	1(0.3-3.32)	0.99(0.43-2.25)	0.97	(3,3)	1(0.75-1.34)	0.88(0.73-1.04)	0.19	(3,3)	1(0.69-1.46)	1.1(0.52-2.32)	0.77	(5,6)
Tyrosine--tRNA ligase, mitochondrial	1(0.77-1.31)	0.96(0.74-1.25)	0.82	(8,9)	1(0.83-1.21)	0.6(0.39-0.94)	0.03	(5,6)	1(0.87-1.16)	0.66(0.48-0.91)	0.02	(8,9)
Isoleucine--tRNA ligase, mitochondrial	1(0.71-1.4)	0.57(0.48-0.69)	0.006	(8,9)	1(0.83-1.21)	0.64(0.54-0.75)	0.0008	(8,9)	1(0.82-1.22)	0.55(0.43-0.71)	0.0006	(8,9)
Probable glutamyl-tRNA synthetase, mitochondrial					1(0.63-1.59)	1.08(0.52-2.23)	0.73	(3,3)	1(0.78-1.28)	0.74(0.63-0.87)	0.03	(5,6)
Probable histidyl-tRNA synthetase, mitochondrial	1(0.61-1.64)	0.94(0.6-1.48)	0.71	(3,3)					1(0.7-1.42)	0.59(0.43-0.83)	0.03	(8,9)
Seryl-tRNA synthetase, mitochondrial	1(0.83-1.2)	0.53(0.41-0.68)	0.0003	(8,9)	1(0.74-1.35)	0.51(0.4-0.66)	0.001	(8,9)	1(0.91-1.1)	0.54(0.42-0.69)	0.0003	(8,9)
Probable asparaginyl-tRNA synthetase, mitochondrial									1(0.75-1.33)	0.71(0.38-1.31)	0.12	(3,3)
Probable cysteinyl-tRNA synthetase, mitochondrial	1(0.48-2.07)	0.93(0.48-1.82)	0.78	(3,3)	1(0.51-1.96)	1.5(0.82-2.75)	0.13	(3,3)	1(0.62-1.6)	1.03(0.74-1.43)	0.91	(8,9)
Probable leucyl-tRNA synthetase, mitochondrial	1(0.78-1.28)	0.75(0.63-0.9)	0.05	(8,9)	1(0.62-1.62)	1.33(0.49-3.63)	0.53	(6,6)	1(0.67-1.49)	0.82(0.36-1.9)	0.6	(6,6)
Tryptophanyl-tRNA synthetase, mitochondrial									1(0.25-3.97)	0.68(0.62-0.74)	0.35	(3,2)
Mitochondrial ribonuclease P protein 1	1(0.82-1.21)	0.35(0.2-0.61)	0.008	(3,3)					1(0.66-1.51)	0.69(0.49-0.96)	0.04	(3,3)
3-hydroxyacyl-CoA dehydrogenase type-2	1(0.9-1.11)	0.63(0.48-0.82)	0.004	(8,9)	1(0.9-1.11)	0.66(0.48-0.9)	0.02	(8,9)	1(0.94-1.06)	0.74(0.58-0.95)	0.02	(8,9)

Table 4-37: Proteomic findings relating to mitochondrial ribosomal proteins

	HP				ENT				CB			
General name	Abundance (C)	Abundance (AD)	p	N_C,N_{AD}	Abundance (C)	Abundance (AD)	p	N_C,N_{AD}	Abundance (C)	Abundance (AD)	p	N_C,N_{AD}
Ribosomal protein (mitochondrial)												
28S ribosomal protein S2, mitochondrial									1(0.01-122.49)	2.05(0.19-21.96)	0.36	(2,3)
28S ribosomal protein S7									1(0.5-2)	0.77(0.48-1.23)	0.26	(3,3)
Mitochondrial ribosomal protein S9					1(0.41-2.43)	0.83(0.31-2.22)	0.58	(3,3)	1(0.36-2.76)	1.06(0.29-3.92)	0.92	(5,6)
28S ribosomal protein S12, mitochondrial									1(0.73-1.38)	0.76(0.56-1.03)	0.05	(3,3)
28S ribosomal protein S14, mitochondrial									1(0.84-1.18)	0.72(0.43-1.21)	0.1	(3,3)
28S ribosomal protein S21, mitochondrial	1(0.66-1.52)	0.87(0.75-1.02)	0.44	(5,6)					1(0.39-2.58)	0.6(0.29-1.23)	0.14	(3,3)
Mitochondrial ribosomal protein S23	1(0.55-1.83)	0.58(0.54-0.62)	0.03	(2,3)					1(0.82-1.23)	0.68(0.01-85.29)	0.5	(3,2)
Mitochondrial ribosomal protein S27	1(0.74-1.35)	0.61(0.47-0.79)	0.01	(8,9)	1(0.74-1.34)	0.66(0.55-0.79)	0.01	(8,9)	1(0.74-1.35)	0.67(0.52-0.85)	0.03	(8,9)
28S ribosomal protein S30, mitochondrial	1(0.71-1.41)	0.54(0.39-0.77)	0.009	(5,6)	1(0.67-1.5)	0.59(0.4-0.85)	0.04	(8,9)	1(0.62-1.61)	0.49(0.37-0.63)	0.01	(8,9)
Mitochondrial ribosomal protein S31	1(0.72-1.38)	0.5(0.34-0.75)	0.006	(5,6)					1(0.74-1.36)	0.42(0.23-0.74)	0.009	(5,6)
28S ribosomal protein S34					1(0.17-6.01)	0.55(0.14-2.24)	0.21	(2,3)	1(0.83-1.21)	0.47(0.31-0.72)	0.003	(8,9)
28S ribosomal protein S35	1(0.49-2.02)	0.58(0.37-0.93)	0.06	(3,3)	1(0.7-1.43)	0.42(0.3-0.59)	0.001	(6,6)	1(0.72-1.4)	0.5(0.3-0.82)	0.02	(6,6)
Mitochondrial ribosomal protein S36	1(0.8-1.25)	0.94(0.8-1.11)	0.62	(8,9)	1(0.85-1.17)	1.14(0.93-1.4)	0.26	(8,9)	1(0.91-1.09)	1.04(0.94-1.17)	0.49	(8,9)
39S ribosomal protein L1, mitochondrial	1(0.76-1.32)	1.87(0.86-4.1)	0.06	(3,3)	1(0.46-2.17)	1.2(0.86-1.68)	0.16	(2,3)	1(0.69-1.44)	1.09(0.81-1.46)	0.68	(8,9)
39S ribosomal protein L3, mitochondrial									1(0.89-1.12)	0.79(0.63-1)	0.05	(5,6)
39S ribosomal protein L4, mitochondrial					1(0.76-1.32)	0.86(0.68-1.08)	0.3	(6,6)	1(0.62-1.61)	0.63(0.4-1)	0.04	(3,3)
SRA stem-loop-interacting RNA-binding protein, mitochondrial	1(0.52-1.93)	0.76(0.34-1.73)	0.33	(3,3)	1(0.89-1.12)	0.65(0.46-0.91)	0.02	(5,6)	1(0.84-1.19)	0.6(0.5-0.72)	0.0003	(8,9)
39S ribosomal protein L9, mitochondrial									1(0.85-1.17)	0.88(0.64-1.21)	0.23	(3,3)
39S ribosomal protein L10, mitochondrial	1(0.87-1.15)	1.09(0.61-1.95)	0.58	(3,3)					1(0.78-1.28)	0.85(0.61-1.19)	0.35	(5,6)
39S ribosomal protein L11					1(0.16-6.23)	0.56(0.52-0.6)	0.15	(2,3)	1(0.71-1.41)	0.65(0.53-0.81)	0.02	(5,6)
39S ribosomal protein L12, mitochondrial	1(0.96-1.05)	0.68(0.52-0.89)	0.01	(5,6)	1(0.72-1.4)	0.66(0.62-0.71)	0.03	(5,6)	1(0.91-1.1)	0.71(0.6-0.84)	0.001	(8,9)
39S ribosomal protein L13, mitochondrial	1(0.87-1.15)	1.29(1.15-1.44)	0.004	(3,3)	1(0.56-1.78)	0.62(0.44-0.88)	0.05	(3,3)	1(0.87-1.15)	0.76(0.46-1.25)	0.22	(6,6)
39S ribosomal protein L14, mitochondrial	1(0.88-1.13)	0.66(0.51-0.86)	0.02	(2,3)					1(0.86-1.16)	0.68(0.54-0.85)	0.005	(6,6)
39S ribosomal protein L15	1(0.75-1.34)	1.55(0.67-3.57)	0.25	(5,6)					1(0.65-1.55)	0.72(0.63-0.82)	0.11	(5,6)
39S ribosomal protein L17, mitochondrial	1(0.18-5.43)	0.47(0.19-1.14)	0.05	(2,3)					1(0.85-1.18)	0.77(0.66-0.91)	0.02	(8,9)
39S ribosomal protein L18, mitochondrial									1(0.27-3.65)	0.78(0.55-1.1)	0.18	(2,3)
39S ribosomal protein L19, mitochondria									1(0.73-1.36)	0.76(0.65-0.88)	0.04	(3,3)
39S ribosomal protein L20, mitochondrial									1(0.76-1.32)	0.89(0.43-1.84)	0.58	(3,3)
39S ribosomal protein L22, mitochondrial									1(0.89-1.12)	0.79(0.57-1.1)	0.08	(3,3)
39S ribosomal protein L24, mitochondrial									1(0.16-6.4)	0.51(0.36-0.71)	0.08	(2,3)
39S ribosomal protein L28, mitochondrial									1(0.7-1.43)	0.47(0.17-1.26)	0.11	(5,6)
39S ribosomal protein L38, mitochondrial	1(0.57-1.77)	1.3(0.78-2.15)	0.15	(2,3)	1(0.56-1.78)	1.14(0.67-1.95)	0.51	(3,3)	1(0.89-1.12)	0.77(0.71-0.84)	0.0007	(8,9)

Table continued from previous page												
39S ribosomal protein L39, mitochondrial									1(0.66-1.51)	0.71(0.56-0.91)	0.09	(5,6)
39S ribosomal protein L40, mitochondrial	1(0.72-1.39)	0.7(0.54-0.89)	0.05	(6,6)	1(0.61-1.63)	0.55(0.32-0.92)	0.05	(6,6)	1(0.78-1.28)	0.67(0.32-1.38)	0.22	(5,6)
39S ribosomal protein L41, mitochondrial									1(0.26-3.85)	0.78(0.22-2.78)	0.59	(3,3)
39S ribosomal protein L43, mitochondrial									1(0.6-1.66)	0.56(0.55-0.58)	0.04	(3,3)
39S ribosomal protein L44, mitochondrial	1(0.87-1.16)	0.54(0.43-0.67)	0.0001	(8,9)	1(0.62-1.62)	0.68(0.45-1.03)	0.14	(5,6)	1(0.63-1.58)	0.98(0.8-1.2)	0.94	(8,9)
39S ribosomal protein L45, mitochondrial					1(0.65-1.53)	0.69(0.29-1.68)	0.21	(3,3)	1(0.85-1.18)	0.48(0.27-0.85)	0.02	(5,6)
39S ribosomal protein L46, mitochondrial									1(0.58-1.73)	0.69(0.41-1.18)	0.11	(3,3)
39S ribosomal protein L47, mitochondrial	1(0.76-1.31)	0.72(0.57-0.91)	0.05	(8,9)	1(0.71-1.4)	0.32(0.08-1.25)	0.06	(3,3)	1(0.93-1.08)	0.59(0.51-0.68)	<0.0001	(8,9)
39S ribosomal protein L49, mitochondrial	1(0.83-1.21)	0.66(0.54-0.82)	0.004	(8,9)	1(0.69-1.46)	0.51(0.37-0.71)	0.006	(5,6)	1(0.85-1.18)	0.8(0.64-1.01)	0.09	(8,9)
39S ribosomal protein L50, mitochondrial									1(0.83-1.21)	0.65(0.47-0.9)	0.01	(3,3)
39S ribosomal protein L52, mitochondrial									1(0.39-2.56)	1.15(0.7-1.89)	0.37	(2,3)
39S ribosomal protein L54, mitochondrial	1(0.79-1.26)	0.67(0.37-1.2)	0.08	(3,3)	1(0.81-1.23)	0.74(0.69-0.8)	0.02	(3,3)				
39S ribosomal protein L55, mitochondrial	1(0.73-1.37)	0.84(0.68-1.02)	0.23	(5,6)					1(0.8-1.26)	0.85(0.55-1.3)	0.44	(8,9)
G-rich sequence factor 1					1(0.73-1.37)	0.72(0.61-0.85)	0.05	(8,9)	1(0.81-1.24)	0.9(0.77-1.06)	0.39	(8,9)

Table 4-38: Summary of proteomic findings relating to cytoplasmic ribosomal proteins

	HP		ENT		CB	
Protein groups	Total #	Significant change (p<0.05)	Total #	Significant change (p<0.05)	Total #	Significant change (p<0.05)
40S ribosomal protein	32	0	31	1, increased	32	1, decreased
60S ribosomal protein	40	3, all decreased	41	2, all increased	41	1, decreased
Ribosomal protein S6 kinases	4	0	4	0	5	1, increased

Table 4-39: Proteomic findings relating to translational initiation factors

	HP				ENT				CB			
General name	Abundance (C)	Abundance (AD)	p	N_C,N_{AD}	Abundance (C)	Abundance (AD)	p	N_C,N_{AD}	Abundance (C)	Abundance (AD)	p	N_C,N_{AD}
Translation initiation factor												
Eukaryotic translation initiation factor 1A	1(0.87-1.15)	0.77(0.6-0.99)	0.05	(8,9)	1(0.87-1.14)	0.67(0.56-0.8)	0.0009	(8,9)				
Eukaryotic translation initiation factor 1	1(0.73-1.37)	0.92(0.7-1.22)	0.66	(8,9)	1(0.85-1.18)	0.76(0.61-0.96)	0.04	(8,9)	1(0.6-1.67)	1.07(0.69-1.68)	0.81	(8,9)
Eukaryotic translation initiation factor 2 subunit 2	1(0.94-1.06)	0.92(0.88-0.97)	0.03	(8,9)	1(0.92-1.09)	0.95(0.87-1.05)	0.39	(8,9)	1(0.94-1.06)	1.05(0.98-1.14)	0.24	(8,9)
Translation initiation factor eIF-2B subunit gamma					1(0.84-1.19)	0.87(0.52-1.46)	0.37	(3,3)	1(0.93-1.07)	0.81(0.75-0.88)	0.0005	(8,9)
Eukaryotic translation initiation factor 3A	1(0.91-1.1)	0.86(0.75-0.99)	0.07	(8,9)	1(0.85-1.17)	0.78(0.62-0.98)	0.06	(8,9)	1(0.95-1.05)	0.82(0.75-0.91)	0.001	(8,9)
Eukaryotic translation initiation factor 3B	1(0.89-1.13)	0.86(0.72-1.03)	0.14	(8,9)	1(0.89-1.13)	0.83(0.74-0.93)	0.02	(8,9)	1(0.92-1.08)	0.85(0.78-0.92)	0.004	(8,9)
Eukaryotic translation initiation factor 3C-like	1(0.87-1.15)	0.8(0.69-0.93)	0.02	(8,9)	1(0.84-1.19)	0.74(0.48-1.15)	0.17	(8,9)	1(0.94-1.07)	0.86(0.8-0.94)	0.006	(8,9)
Eukaryotic translation initiation factor 3D	1(0.82-1.22)	0.8(0.7-0.93)	0.05	(5,6)	1(0.49-2.04)	0.74(0.56-0.99)	0.36	(6,6)	1(0.93-1.07)	0.88(0.76-1.01)	0.08	(8,9)
Eukaryotic translation initiation factor 3E	1(0.93-1.07)	0.81(0.7-0.92)	0.008	(8,9)	1(0.77-1.31)	0.87(0.69-1.09)	0.36	(8,9)	1(0.91-1.1)	0.86(0.79-0.93)	0.02	(8,9)
Eukaryotic translation initiation factor 3F	1(0.87-1.15)	0.79(0.68-0.94)	0.03	(8,9)	1(0.87-1.15)	0.73(0.57-0.94)	0.03	(8,9)	1(0.96-1.04)	0.88(0.78-0.99)	0.04	(8,9)
Eukaryotic translation initiation factor 3G	1(0.91-1.1)	0.84(0.71-0.99)	0.05	(8,9)	1(0.78-1.28)	0.9(0.75-1.08)	0.42	(8,9)	1(0.87-1.15)	0.76(0.65-0.88)	0.007	(8,9)
Eukaryotic translation initiation factor 3H	1(0.81-1.23)	0.7(0.6-0.81)	0.006	(8,9)	1(0.3-3.37)	1.11(0.21-5.95)	0.76	(3,2)	1(0.87-1.15)	0.75(0.61-0.91)	0.02	(8,9)
Eukaryotic translation initiation factor 3K									1(0.86-1.16)	0.73(0.63-0.86)	0.004	(8,9)
Eukaryotic translation initiation factor 3L	1(0.91-1.1)	0.83(0.75-0.93)	0.008	(8,9)	1(0.89-1.13)	0.78(0.52-1.17)	0.21	(8,9)	1(0.91-1.1)	0.76(0.66-0.87)	0.002	(8,9)
Eukaryotic translation initiation factor 3M	1(0.9-1.11)	1.11(0.77-1.59)	0.52	(5,6)	1(0.81-1.24)	0.87(0.65-1.17)	0.38	(8,9)	1(0.91-1.1)	0.81(0.69-0.96)	0.03	(8,9)
Eukaryotic translation initiation factor 4 gamma 1	1(0.9-1.12)	0.85(0.78-0.94)	0.02	(8,9)	1(0.86-1.16)	0.66(0.56-0.77)	0.0005	(8,9)	1(0.93-1.07)	0.83(0.77-0.89)	0.0005	(8,9)
Eukaryotic translation initiation factor 4 gamma 2	1(0.89-1.13)	0.8(0.65-0.99)	0.06	(8,9)	1(0.92-1.09)	0.75(0.6-0.94)	0.02	(8,9)	1(0.93-1.08)	0.84(0.76-0.92)	0.004	(8,9)
Eukaryotic translation initiation factor 4 gamma 3	1(0.77-1.3)	1.03(0.78-1.37)	0.84	(8,9)	1(0.78-1.27)	0.61(0.48-0.78)	0.004	(8,9)	1(0.88-1.14)	0.82(0.61-1.1)	0.18	(8,9)
Eukaryotic initiation factor 4A-II	1(0.87-1.15)	0.85(0.72-1)	0.1	(8,9)	1(0.84-1.19)	0.85(0.74-0.99)	0.13	(8,9)	1(0.9-1.11)	0.84(0.75-0.94)	0.02	(8,9)
Eukaryotic initiation factor 4A-III	1(0.9-1.12)	0.81(0.72-0.9)	0.006	(8,9)	1(0.75-1.33)	0.87(0.71-1.06)	0.37	(8,9)	1(0.9-1.11)	0.93(0.86-1.02)	0.25	(8,9)
Eukaryotic translation initiation factor 4B isoform 1	1(0.94-1.07)	1.04(0.92-1.17)	0.53	(8,9)	1(0.88-1.13)	1(0.94-1.07)	0.95	(8,9)	1(0.91-1.1)	1.11(1.04-1.18)	0.05	(8,9)
Eukaryotic translation initiation factor 4E	1(0.93-1.08)	0.88(0.79-0.98)	0.04	(6,6)	1(0.78-1.28)	1(0.9-1.11)	1	(8,9)	1(0.94-1.07)	0.93(0.88-0.98)	0.05	(8,9)
Eukaryotic translation initiation factor 4H	1(0.79-1.27)	0.7(0.54-0.89)	0.03	(8,9)	1(0.89-1.12)	0.7(0.55-0.9)	0.01	(8,9)	1(0.9-1.11)	0.84(0.77-0.91)	0.01	(8,9)
Eukaryotic translation initiation factor 5	1(0.89-1.12)	0.77(0.66-0.9)	0.008	(8,9)	1(0.83-1.21)	0.7(0.54-0.9)	0.02	(8,9)	1(0.89-1.12)	0.81(0.71-0.93)	0.01	(8,9)
Eukaryotic translation initiation factor 5A-1	1(0.91-1.1)	0.73(0.6-0.88)	0.006	(8,9)	1(0.89-1.12)	0.69(0.57-0.83)	0.002	(8,9)	1(0.96-1.04)	0.86(0.79-0.93)	0.003	(8,9)
Eukaryotic translation initiation factor 5B	1(0.61-1.63)	1.45(0.64-3.24)	0.18	(3,3)	1(0.81-1.23)	1.14(0.9-1.45)	0.3	(5,6)	1(0.81-1.24)	1.54(1.04-2.28)	0.05	(8,9)

Table 4-40: Proteomic findings relating to elongation factors and regulators

	HP				ENT				CB			
General name	**Abundance (C)**	**Abundance (AD)**	**p**	**N_C,N_{AD}**	**Abundance (C)**	**Abundance (AD)**	**p**	**N_C,N_{AD}**	**Abundance (C)**	**Abundance (AD)**	**p**	**N_C,N_{AD}**
Elongation factor												
Elongation factor 1-alpha 1	1(0.88-1.14)	1.26(1.03-1.53)	0.04	(8,9)	1(0.91-1.1)	1.02(0.88-1.17)	0.82	(8,9)	1(0.95-1.05)	0.97(0.88-1.07)	0.52	(8,9)
Elongation factor 1-alpha 2	1(0.91-1.1)	0.6(0.49-0.72)	0.0001	(8,9)	1(0.85-1.18)	0.67(0.55-0.81)	0.002	(8,9)	1(0.93-1.08)	0.82(0.74-0.9)	0.002	(8,9)
Eukaryotic translation elongation factor 1 beta 2	1(0.89-1.12)	0.6(0.52-0.69)	<0.0001	(8,9)	1(0.83-1.21)	0.6(0.47-0.77)	0.002	(8,9)	1(0.9-1.11)	0.74(0.57-0.96)	0.03	(8,9)
Eukaryotic translation elongation factor 1 gamma	1(0.93-1.08)	0.66(0.57-0.77)	0.0001	(8,9)	1(0.83-1.2)	0.67(0.56-0.81)	0.003	(8,9)	1(0.95-1.06)	0.85(0.75-0.97)	0.02	(8,9)
Elongation factor 1-delta	1(0.9-1.11)	0.83(0.69-0.99)	0.06	(8,9)	1(0.83-1.2)	0.71(0.58-0.87)	0.01	(8,9)	1(0.95-1.06)	0.89(0.81-0.98)	0.03	(8,9)
Elongation factor 2	1(0.94-1.06)	0.89(0.8-0.99)	0.05	(8,9)	1(0.94-1.07)	0.81(0.73-0.89)	0.0008	(8,9)	1(0.95-1.05)	0.89(0.83-0.95)	0.006	(8,9)
Elongation factor Tu, mitochondrial	1(0.8-1.26)	0.81(0.65-1.02)	0.16	(8,9)	1(0.78-1.28)	0.7(0.5-0.99)	0.08	(8,9)	1(0.8-1.26)	0.51(0.37-0.7)	0.001	(8,9)
Elongation factor G, mitochondrial	1(0.84-1.2)	0.89(0.52-1.52)	0.65	(8,9)	1(0.7-1.43)	0.69(0.49-0.98)	0.03	(3,3)	1(0.9-1.11)	0.47(0.35-0.64)	0.0003	(8,9)
Regulators												
Cold-inducible RNA-binding protein	1(0.82-1.22)	0.77(0.64-0.93)	0.04	(8,9)	1(0.83-1.21)	0.58(0.4-0.83)	0.01	(8,9)	1(0.86-1.16)	0.64(0.48-0.84)	0.006	(8,9)
Protein argonaute-2	1(0.75-1.34)	1.23(1.01-1.49)	0.16	(5,6)	1(0.81-1.23)	1.37(1.08-1.75)	0.04	(8,9)	1(0.93-1.07)	1.11(1-1.23)	0.08	(8,9)
Ribonuclease UK114	1(0.9-1.11)	1.39(1.23-1.56)	0.0003	(8,9)	1(0.88-1.14)	1.25(1.08-1.45)	0.02	(8,9)	1(0.9-1.11)	1.32(1.15-1.53)	0.003	(8,9)

4.3.3.8. Chaperones – protein maturation

Protein regulation is mainly governed by the ubiquitin-proteasome system (UPS) and molecular chaperones such as the heat shock proteins (HSPs) [330]. Molecular chaperones, together with co-chaperones, assist the folding of proteins and prevent toxic protein aggregation [330].

In this study, two mitochondrial chaperones showed altered abundance in AD brain; 10 kDa heat shock protein, mitochondrial (HSP10) was elevated in CB and heat shock protein 75 kDa, mitochondrial HSP75 was strongly decreased in all three brain regions examined. The small heat shock proteins (sHSPs) form a intracellular family of molecular chaperones composed of ten proteins, HSPB1 to HSPB10 [331]. We detected three sHSPs (HSPB1, HSPB6, and HSPB8), all of which increased in abundance where statistical significance was reached.

In this study, heat shock 70 kDa protein 1A/1B was increased in all brain regions, whereas heat shock 70 kDa protein 4L, 12A, and 13 were decreased in abundance where statistical significance was reached. All of the HSP90s and their co-chaperones that were altered in AD were decreased in abundance, most significantly in HP and ENT. Co-chaperones that interact with HSP 70 and HSP 90 were also decreased in general (with the exception of J-domain proteins subfamily A members). ER chaperones calreticulin and calnextin were also decreased in the AD brain (**Table 4-41**).

Bcl-2-associated athanogene (BAG) proteins are molecular chaperone that interact with HSP70. BAG3 and BAG4 were increased while BAG5 was decreased in the AD brain. Subunits of prefoldin and cytosolic chaperonin CCT were generally decreased in the AD brain (**Table 4-42**).

Table 4-41: Proteomic findings relating to chaperones (I)

	HP				ENT				CB			
General name	Abundance (C)	Abundance (AD)	p	N_C,N_{AD}	Abundance (C)	Abundance (AD)	p	N_C,N_{AD}	Abundance (C)	Abundance (AD)	p	N_C,N_{AD}
Mitochondrial and small HSPs												
10 kDa heat shock protein, mitochondrial (HSP10)	1(0.88-1.13)	1.01(0.87-1.17)	0.88	(8,9)	1(0.79-1.26)	1.04(0.86-1.24)	0.78	(8,9)	1(0.93-1.07)	1.11(1.02-1.19)	0.04	(8,9)
Heat shock protein 75 kDa, mitochondrial (HSP75)	1(0.84-1.19)	0.56(0.45-0.71)	0.0004	(8,9)	1(0.92-1.09)	0.66(0.53-0.83)	0.003	(8,9)	1(0.85-1.18)	0.65(0.52-0.82)	0.003	(8,9)
Heat shock protein beta-1 (HSP27)	1(0.84-1.2)	1.77(1.41-2.23)	0.0004	(8,9)	1(0.85-1.18)	1.53(1.28-1.83)	0.001	(8,9)	1(0.89-1.12)	1.01(0.9-1.14)	0.87	(8,9)
Heat shock protein beta-6 (HSP20)	1(0.8-1.25)	1.77(1.42-2.21)	0.0007	(8,9)	1(0.51-1.98)	1.43(0.99-2.05)	0.25	(5,6)	1(0.79-1.27)	1.41(1.15-1.72)	0.02	(6,6)
Heat shock protein beta-8 (HSP22)	1(0.87-1.15)	1.15(1.02-1.29)	0.09	(8,9)	1(0.58-1.71)	1.83(1.51-2.22)	0.03	(8,9)	1(0.93-1.08)	1.08(0.98-1.19)	0.16	(8,9)
Heat shock protein beta-11	1(0.69-1.45)	0.91(0.69-1.2)	0.64	(8,9)	1(0.61-1.63)	0.55(0.36-0.83)	0.03	(5,6)	1(0.86-1.16)	0.86(0.75-0.98)	0.09	(8,9)
HSP 70 and associated												
Heat shock 70 kDa protein 1A/1B	1(0.9-1.11)	1.31(1.13-1.51)	0.003	(8,9)	1(0.91-1.1)	1.28(1.11-1.47)	0.004	(8,9)	1(0.93-1.08)	1.28(1.15-1.42)	0.0008	(8,9)
Heat shock 70 kDa protein 4L	1(0.91-1.09)	0.61(0.53-0.71)	<0.0001	(8,9)	1(0.87-1.16)	0.67(0.61-0.74)	0.0001	(8,9)	1(0.91-1.09)	0.85(0.77-0.93)	0.01	(8,9)
Heat shock 70 kDa protein 12A	1(0.78-1.28)	0.82(0.68-1)	0.16	(8,9)	1(0.81-1.24)	0.76(0.62-0.95)	0.06	(8,9)	1(0.95-1.05)	0.9(0.81-1.01)	0.09	(8,9)
Heat shock 70 kDa protein 13	1(0.38-2.63)	0.96(0.76-1.21)	0.88	(3,3)	1(0.79-1.27)	0.7(0.54-0.91)	0.03	(8,9)	1(0.88-1.13)	0.81(0.73-0.9)	0.01	(8,9)
Small glutamine-rich tetratricopeptide repeat-containing protein alpha	1(0.85-1.18)	0.6(0.52-0.68)	0.0001	(8,9)	1(0.8-1.25)	0.56(0.48-0.66)	0.0002	(8,9)	1(0.89-1.12)	0.91(0.85-0.98)	0.14	(8,9)
Small glutamine-rich tetratricopeptide repeat-containing protein beta	1(0.84-1.19)	0.66(0.61-0.72)	0.0004	(8,9)	1(0.85-1.18)	0.57(0.52-0.62)	<0.0001	(8,9)	1(0.92-1.09)	0.8(0.73-0.86)	0.0003	(8,9)
HSP 70-binding protein 1	1(0.81-1.23)	0.95(0.76-1.18)	0.68	(8,9)	1(0.83-1.2)	1.07(0.95-1.21)	0.46	(8,9)	1(0.93-1.08)	1.19(1.04-1.36)	0.02	(8,9)
DnaJ homolog subfamily A member 1	1(0.91-1.09)	1.15(1.03-1.28)	0.04	(8,9)	1(0.89-1.13)	1.15(1.05-1.27)	0.05	(8,9)	1(0.94-1.06)	1.09(0.99-1.19)	0.09	(8,9)
DnaJ homolog subfamily A member 3, mitochondrial	1(0.86-1.16)	0.95(0.76-1.18)	0.64	(8,9)	1(0.73-1.37)	0.93(0.76-1.14)	0.65	(8,9)	1(0.86-1.16)	0.87(0.79-0.96)	0.08	(8,9)
DnaJ homolog subfamily B member 1	1(0.88-1.14)	0.85(0.76-0.95)	0.04	(8,9)	1(0.86-1.17)	0.83(0.72-0.96)	0.05	(8,9)	1(0.94-1.06)	0.98(0.87-1.1)	0.69	(8,9)
DnaJ homolog subfamily B member 4	1(0.83-1.21)	0.83(0.72-0.96)	0.09	(8,9)	1(0.84-1.19)	0.77(0.66-0.89)	0.02	(8,9)	1(0.87-1.16)	0.79(0.73-0.85)	0.006	(8,9)
DnaJ homolog subfamily C member 10									1(0.81-1.23)	0.75(0.63-0.89)	0.02	(6,6)
DnaJ homolog, subfamily C, member 11	1(0.62-1.62)	0.67(0.24-1.82)	0.31	(5,4)	1(0.18-5.64)	1.06(0.52-2.15)	0.82	(2,3)	1(0.89-1.13)	0.83(0.77-0.9)	0.009	(8,9)
HSP 90												
HSP90-alpha	1(0.94-1.07)	0.73(0.63-0.84)	0.0008	(8,9)	1(0.92-1.09)	0.7(0.59-0.83)	0.001	(8,9)	1(0.92-1.09)	0.89(0.79-1.01)	0.09	(8,9)
HSP90-beta	1(0.84-1.19)	0.74(0.62-0.88)	0.01	(8,9)	1(0.92-1.09)	0.67(0.55-0.81)	0.001	(8,9)	1(0.93-1.08)	0.92(0.84-1.01)	0.13	(8,9)
HSP90 co-chaperone Cdc37	1(0.9-1.11)	0.87(0.81-0.94)	0.03	(8,9)	1(0.91-1.1)	0.89(0.84-0.95)	0.03	(8,9)	1(0.94-1.07)	1.14(0.99-1.3)	0.08	(8,9)
Heat shock protein 90kDa beta	1(0.93-1.08)	0.71(0.58-0.86)	0.004	(8,9)	1(0.92-1.09)	0.67(0.54-0.83)	0.002	(8,9)	1(0.95-1.05)	0.88(0.8-0.97)	0.02	(8,9)
Activator of heat shock 90kDa protein ATPase homolog 1	1(0.86-1.16)	0.79(0.71-0.89)	0.01	(8,9)	1(0.92-1.09)	0.69(0.58-0.82)	0.0008	(8,9)	1(0.85-1.18)	0.91(0.82-1.01)	0.27	(8,9)
Calreticulin/calnexin												
Calreticulin	1(0.94-1.06)	0.69(0.58-0.82)	0.001	(8,9)	1(0.8-1.24)	0.63(0.52-0.76)	0.002	(8,9)	1(0.93-1.08)	0.84(0.75-0.94)	0.008	(8,9)
Calnexin	1(0.82-1.22)	1.12(0.88-1.43)	0.42	(8,9)	1(0.83-1.21)	0.98(0.81-1.18)	0.84	(8,9)	1(0.92-1.09)	0.88(0.81-0.95)	0.02	(8,9)

Table 4-42: Proteomic findings relating to chaperones (II)

	HP				ENT				CB			
General name	Abundance (C)	Abundance (AD)	p	N_C,N_{AD}	Abundance (C)	Abundance (AD)	p	N_C,N_{AD}	Abundance (C)	Abundance (AD)	p	N_C,N_{AD}
BAG												
BAG 3	1(0.87-1.15)	1.7(1.45-1.99)	<0.0001	(8,9)	1(0.84-1.18)	1.42(1.13-1.78)	0.01	(8,9)	1(0.92-1.08)	1.32(1.21-1.44)	0.0001	(8,9)
BAG 4	1(0.82-1.23)	0.96(0.87-1.07)	0.71	(8,9)	1(0.8-1.25)	1.31(1.14-1.5)	0.03	(5,6)	1(0.87-1.15)	1(0.84-1.19)	0.99	(8,9)
BAG 5	1(0.6-1.66)	1(0.85-1.19)	0.98	(5,6)	1(0.9-1.11)	0.77(0.63-0.93)	0.02	(8,9)	1(0.95-1.05)	0.98(0.91-1.06)	0.66	(8,9)
Prefoldin and CCT												
Prefoldin subunit 4	1(0.94-1.07)	0.92(0.83-1.02)	0.14	(8,9)	1(0.85-1.18)	0.93(0.8-1.07)	0.45	(8,9)	1(0.93-1.07)	1.13(1.05-1.21)	0.01	(8,9)
Prefoldin subunit 5	1(0.92-1.08)	0.87(0.79-0.96)	0.02	(8,9)	1(0.92-1.09)	0.97(0.86-1.09)	0.61	(8,9)	1(0.9-1.11)	1.02(0.94-1.11)	0.71	(8,9)
Prefoldin subunit 6	1(0.89-1.13)	0.94(0.86-1.01)	0.3	(8,9)	1(0.89-1.13)	1(0.85-1.18)	0.97	(8,9)	1(0.94-1.07)	1.07(1.01-1.13)	0.09	(8,9)
T-complex protein 1 subunit alpha (CCT1)	1(0.91-1.1)	0.87(0.84-0.91)	0.01	(8,9)	1(0.9-1.12)	0.84(0.82-0.87)	0.008	(8,9)	1(0.96-1.05)	0.99(0.96-1.02)	0.56	(8,9)
T-complex protein 1 subunit beta (CCT2)	1(0.87-1.15)	0.83(0.74-0.92)	0.02	(8,9)	1(0.93-1.08)	0.79(0.73-0.86)	0.0003	(8,9)	1(0.95-1.05)	0.93(0.89-0.97)	0.03	(8,9)
T-complex protein 1 subunit gamma (CCT3)	1(0.88-1.13)	0.88(0.83-0.94)	0.06	(8,9)	1(0.93-1.08)	0.88(0.84-0.91)	0.005	(8,9)	1(0.95-1.05)	0.96(0.93-0.98)	0.08	(8,9)
T-complex protein 1 subunit delta (CCT4)	1(0.91-1.1)	0.84(0.79-0.89)	0.003	(8,9)	1(0.9-1.11)	0.95(0.82-1.1)	0.51	(8,9)	1(0.93-1.08)	0.98(0.93-1.03)	0.57	(8,9)
T-complex protein 1 subunit epsilon (CCT5)	1(0.9-1.11)	0.89(0.83-0.96)	0.04	(8,9)	1(0.84-1.19)	0.85(0.78-0.93)	0.08	(8,9)	1(0.9-1.11)	0.97(0.91-1.03)	0.54	(8,9)
T-complex protein 1 subunit zeta (CCT6)	1(0.93-1.08)	0.91(0.88-0.94)	0.02	(8,9)	1(0.96-1.05)	0.88(0.84-0.93)	0.0006	(8,9)	1(0.9-1.11)	0.92(0.88-0.95)	0.09	(8,9)
T-complex protein 1 subunit eta (CCT7)	1(0.92-1.09)	0.85(0.83-0.88)	0.003	(8,9)	1(0.9-1.12)	0.85(0.8-0.9)	0.01	(8,9)	1(0.96-1.04)	0.98(0.95-1)	0.26	(8,9)
T-complex protein 1 subunit theta (CCT8)	1(0.92-1.08)	0.86(0.81-0.92)	0.005	(8,9)	1(0.89-1.13)	0.85(0.81-0.9)	0.02	(8,9)	1(0.95-1.05)	1.02(0.97-1.07)	0.54	(8,9)
Miscellaneous												
Heat shock protein 105 kDa (HSP105)	1(0.89-1.13)	0.86(0.75-0.98)	0.06	(8,9)	1(0.86-1.16)	0.85(0.76-0.94)	0.05	(8,9)	1(0.94-1.06)	1.11(1.02-1.21)	0.03	(8,9)
Heat shock cognate 71 kDa protein	1(0.95-1.06)	0.9(0.8-1.01)	0.08	(8,9)	1(0.83-1.2)	0.87(0.79-0.95)	0.13	(8,9)	1(0.93-1.08)	1.03(0.95-1.12)	0.52	(8,9)
Heat shock factor-binding protein 1	1(0.8-1.25)	0.92(0.81-1.05)	0.48	(8,9)	1(0.84-1.19)	0.79(0.71-0.88)	0.02	(8,9)	1(0.92-1.09)	0.88(0.81-0.97)	0.03	(8,9)
Protein disulfide isomerase A4	1(0.87-1.15)	0.93(0.84-1.03)	0.37	(8,9)	1(0.89-1.13)	0.83(0.72-0.96)	0.03	(8,9)	1(0.92-1.09)	0.87(0.82-0.92)	0.006	(8,9)
Hypoxia up-regulated protein 1	1(0.84-1.19)	0.77(0.69-0.86)	0.01	(8,9)	1(0.82-1.22)	0.79(0.67-0.94)	0.06	(8,9)	1(0.92-1.09)	0.8(0.75-0.86)	0.0004	(8,9)
p53 and DNA damage-regulated protein 1					1(0.56-1.77)	1.76(1.03-3.01)	0.04	(3,3)				

4.3.3.9. Protein degradation

The 26S proteasome, present in all cells of the CNS, is responsible for the majority of cellular proteolysis. The 26S proteasome is a large complex consisting of two portions: the catalytic 20S proteasome and the 19S regulatory particle. The 20S proteasome is made up of two α-rings and two β-rings, each comprising seven structurally similar α- and seven β-subunits, respectively [332]. In this study, numerous proteasome subunits (both α- and β-subunits) were detected, across all brain regions examined. Of these subunits, all of those that showed significant differences between the AD and control were increased in abundance. Of three brain regions examined, CB showed the most number of proteasome subunits with significant increase (**Table 4-43**).

The 19S regulatory particle consists of two sub-complexes: the base and the lid. The base is composed of six ATPase subunits (RPT1-RPT6) and three non-ATPase subunits (RPN1, RPN2, and RPN13). In this study, all six RPTs plus RPN1 were significantly decreased where statistical significance was reached (most consistently in ENT). RPN10 is assumed to sit at the interface of the lid and base, and its abundance was decreased in ENT. The lid is composed of nine non-ATPase subunits: RPN3, RPN5–RPN9, RPN11, RPN12 and RPN15 [332]. Herein, we observed significant decrease in the abundance of RPN3 and RPN5-RPN9 (**Table 4-44**).

Proteins that are essential for neddylation-deneddylation pathway, cullins and COP9 signalsome complex (CSN) subunits were decreased in the AD brain; all eight subunits of CSN were found to be decreased in AD brain, most consistently so in HP and ENT. Cullin-1, cullin-2 and cullin-3 were decreased wherever statistical significance was reached (**Table 4-45**).

4.3.3.10. 14-3-3 proteins

In this study, all six detected 14-3-3 protein isoforms were significantly and consistently decreased in all three brain regions in AD brain; the levels were decreased to 60%-80% in HP, 60%-70% in ENT, and 80%-90% in CB (**Table 4-46**).

Table 4-43: Proteomic findings relating to the 20S Proteosome

	HP				ENT				CB			
General name	**Abundance (C)**	**Abundance (AD)**	**p**	**N_C,N_{AD}**	**Abundance (C)**	**Abundance (AD)**	**p**	**N_C,N_{AD}**	**Abundance (C)**	**Abundance (AD)**	**p**	**N_C,N_{AD}**
20S proteasome												
Proteasome subunit alpha type-1	1(0.93-1.07)	1.15(1.04-1.27)	0.02	(8,9)	1(0.84-1.19)	1.08(0.94-1.25)	0.42	(8,9)	1(0.95-1.05)	1.14(1.07-1.22)	0.002	(8,9)
Proteasome subunit alpha type-2	1(0.9-1.11)	1.1(0.95-1.26)	0.24	(8,9)	1(0.9-1.11)	1.29(1.11-1.51)	0.007	(8,9)	1(0.95-1.05)	1.11(1.04-1.18)	0.009	(8,9)
Proteasome subunit alpha type-4	1(0.89-1.12)	1.07(0.94-1.22)	0.39	(8,9)	1(0.89-1.13)	1.1(1-1.21)	0.16	(8,9)	1(0.91-1.09)	1.19(1.09-1.29)	0.006	(8,9)
Proteasome subunit alpha type-6	1(0.95-1.06)	1.03(0.92-1.16)	0.58	(8,9)	1(0.9-1.12)	1.15(1.04-1.26)	0.05	(8,9)	1(0.97-1.03)	1.09(1.01-1.17)	0.03	(8,9)
Proteasome subunit alpha type-7	1(0.93-1.08)	1.12(1.04-1.21)	0.03	(8,9)	1(0.87-1.14)	1.13(0.93-1.37)	0.25	(8,9)	1(0.93-1.07)	1.09(1.01-1.18)	0.07	(8,9)
Proteasome subunit beta type-1	1(0.93-1.07)	1.06(0.92-1.22)	0.42	(8,9)	1(0.89-1.13)	1.22(1.06-1.42)	0.03	(8,9)	1(0.94-1.07)	1.08(0.96-1.2)	0.2	(8,9)
Proteasome subunit beta type-2	1(0.86-1.16)	1.08(0.94-1.24)	0.4	(8,9)	1(0.85-1.18)	1.22(1.01-1.48)	0.08	(8,9)	1(0.94-1.07)	1.09(0.99-1.19)	0.11	(8,9)
Proteasome subunit beta type-3	1(0.92-1.09)	1.06(0.96-1.18)	0.28	(8,9)	1(0.82-1.22)	1.21(1.02-1.43)	0.11	(8,9)	1(0.93-1.08)	1.1(1.04-1.16)	0.03	(8,9)
Proteasome subunit beta type-4	1(0.93-1.07)	1.13(1.02-1.25)	0.04	(8,9)	1(0.87-1.15)	1.15(0.98-1.35)	0.15	(8,9)	1(0.93-1.08)	1.07(0.99-1.15)	0.18	(8,9)
Proteasome subunit beta type-7	1(0.9-1.11)	1.02(0.87-1.2)	0.79	(8,9)	1(0.82-1.22)	1.02(0.86-1.21)	0.85	(8,9)	1(0.94-1.07)	1.12(1.04-1.21)	0.01	(8,9)
Assembly and regulation												
Proteasome activator complex subunit 1 (PA28a)	1(0.94-1.07)	1.16(1.01-1.32)	0.04	(8,9)	1(0.85-1.17)	1.1(1.01-1.21)	0.23	(8,9)	1(0.9-1.11)	1.03(0.96-1.09)	0.63	(8,9)
Proteasome activator complex subunit 2 (PA28b)	1(0.87-1.14)	1.14(0.97-1.35)	0.17	(8,9)	1(0.89-1.12)	1.15(1.04-1.28)	0.05	(8,9)	1(0.91-1.1)	1.1(0.97-1.26)	0.18	(8,9)
Proteasome assembly chaperone 1	1(0.65-1.54)	0.85(0.67-1.09)	0.47	(8,9)					1(0.84-1.19)	1.42(1.04-1.93)	0.02	(3,3)
Proteasome-associated protein ECM29 homolog (ECM29)	1(0.86-1.16)	0.95(0.81-1.13)	0.63	(8,9)	1(0.85-1.18)	0.7(0.56-0.87)	0.009	(8,9)	1(0.93-1.07)	0.86(0.79-0.94)	0.006	(8,9)

Table 4-44: Proteomic findings relating to the 19S regulatory particle

	HP				ENT				CB			
General name	Abundance (C)	Abundance (AD)	p	N_C,N_{AD}	Abundance (C)	Abundance (AD)	p	N_C,N_{AD}	Abundance (C)	Abundance (AD)	p	N_C,N_{AD}
19S regulatory particle												
26S protease regulatory subunit 7 (RPT1)	1(0.88-1.14)	0.85(0.77-0.93)	0.03	(8,9)	1(0.9-1.12)	0.76(0.64-0.91)	0.01	(8,9)	1(0.93-1.07)	0.89(0.84-0.94)	0.007	(8,9)
26S protease regulatory subunit 4 (RPT2)	1(0.87-1.15)	0.82(0.69-0.97)	0.05	(8,9)	1(0.88-1.13)	0.83(0.72-0.96)	0.04	(8,9)	1(0.94-1.06)	0.85(0.78-0.93)	0.003	(8,9)
26S protease regulatory subunit 6B (RPT3)	1(0.85-1.18)	0.97(0.88-1.08)	0.75	(8,9)	1(0.93-1.08)	0.8(0.68-0.95)	0.02	(8,9)	1(0.94-1.06)	0.89(0.81-0.97)	0.02	(8,9)
26S protease regulatory subunit 10B (RPT4)	1(0.87-1.15)	0.93(0.82-1.04)	0.34	(8,9)	1(0.83-1.2)	0.83(0.71-0.97)	0.09	(8,9)	1(0.94-1.07)	0.92(0.85-0.99)	0.07	(8,9)
26S protease regulatory subunit 6A (RPT5)	1(0.88-1.13)	0.85(0.77-0.93)	0.03	(8,9)	1(0.93-1.07)	0.82(0.73-0.91)	0.003	(8,9)	1(0.94-1.07)	0.89(0.8-0.99)	0.05	(8,9)
26S protease regulatory subunit 8 (RPT6)	1(0.86-1.16)	0.88(0.76-1.02)	0.17	(8,9)	1(0.9-1.11)	0.83(0.72-0.96)	0.03	(8,9)	1(0.94-1.06)	0.92(0.84-1)	0.08	(8,9)
26S proteasome non-ATPase regulatory subunit 2 (RPN1)	1(0.9-1.11)	0.89(0.79-1.01)	0.12	(8,9)	1(0.89-1.12)	0.81(0.7-0.93)	0.02	(8,9)	1(0.95-1.05)	0.92(0.85-1)	0.06	(8,9)
26S proteasome non-ATPase regulatory subunit 4 (RPN10)	1(0.91-1.1)	0.94(0.84-1.05)	0.35	(8,9)	1(0.82-1.22)	0.68(0.61-0.75)	0.002	(8,9)	1(0.89-1.13)	0.99(0.92-1.07)	0.86	(8,9)
26S proteasome non-ATPase regulatory subunit 3 (RPN3)	1(0.87-1.15)	0.84(0.76-0.94)	0.04	(8,9)	1(0.84-1.19)	0.85(0.76-0.95)	0.09	(8,9)	1(0.93-1.07)	0.89(0.84-0.95)	0.01	(8,9)
26S proteasome non-ATPase regulatory subunit 12 (RPN5)	1(0.85-1.17)	0.92(0.78-1.08)	0.39	(8,9)	1(0.9-1.12)	0.84(0.74-0.95)	0.03	(8,9)	1(0.95-1.06)	0.96(0.91-1.02)	0.32	(8,9)
26S proteasome non-ATPase regulatory subunit 11 (RPN6)	1(0.86-1.17)	0.85(0.79-0.93)	0.05	(8,9)	1(0.85-1.18)	0.74(0.63-0.89)	0.01	(8,9)	1(0.86-1.16)	0.82(0.75-0.89)	0.02	(8,9)
26S proteasome non-ATPase regulatory subunit 6 (RPN7)	1(0.82-1.22)	1.02(0.92-1.13)	0.86	(8,9)	1(0.89-1.13)	0.91(0.8-1.03)	0.22	(8,9)	1(0.92-1.09)	0.9(0.86-0.95)	0.03	(8,9)
26S proteasome non-ATPase regulatory subunit 7 (RPN8)	1(0.83-1.21)	0.88(0.74-1.03)	0.23	(8,9)	1(0.85-1.18)	0.87(0.78-0.97)	0.13	(8,9)	1(0.91-1.1)	0.85(0.73-1)	0.06	(8,9)
26S proteasome non-ATPase regulatory subunit 13 (RPN9)	1(0.86-1.16)	0.81(0.7-0.92)	0.02	(8,9)	1(0.9-1.11)	0.83(0.71-0.96)	0.03	(8,9)	1(0.97-1.03)	0.88(0.82-0.95)	0.004	(8,9)
Assembly												
26S proteasome non-ATPase regulatory subunit 5 (S5B)	1(0.91-1.1)	0.87(0.76-0.99)	0.07	(8,9)	1(0.78-1.28)	0.74(0.55-0.99)	0.09	(8,9)	1(0.93-1.08)	0.91(0.82-1.01)	0.1	(8,9)
26S proteasome non-ATPase regulatory subunit 9 (p27)	1(0.91-1.1)	1.1(0.95-1.28)	0.22	(8,9)	1(0.85-1.18)	1.29(1.16-1.42)	0.009	(8,9)	1(0.84-1.2)	1.07(0.9-1.26)	0.54	(8,9)

Table 4-45: Proteomic findings relating to deneddylation

	HP				ENT				CB			
General name	Abundance (C)	Abundance (AD)	p	N_C,N_{AD}	Abundance (C)	Abundance (AD)	p	N_C,N_{AD}	Abundance (C)	Abundance (AD)	p	N_C,N_{AD}
CSN												
COP9 signalosome complex subunit 1	1(0.88-1.13)	0.85(0.77-0.93)	0.03	(8,9)	1(0.88-1.14)	0.73(0.63-0.85)	0.003	(8,9)	1(0.96-1.05)	0.97(0.92-1.03)	0.41	(8,9)
COP9 signalosome complex subunit 2	1(0.92-1.08)	0.77(0.67-0.89)	0.002	(8,9)	1(0.95-1.05)	0.72(0.6-0.86)	0.003	(8,9)	1(0.97-1.03)	0.94(0.89-0.99)	0.04	(8,9)
COP9 signalosome complex subunit 3	1(0.85-1.18)	0.86(0.75-0.99)	0.12	(8,9)	1(0.85-1.18)	0.87(0.75-1.01)	0.16	(8,9)	1(0.93-1.08)	0.93(0.87-1)	0.13	(8,9)
COP9 signalosome complex subunit 4	1(0.93-1.08)	0.79(0.68-0.91)	0.005	(8,9)	1(0.82-1.22)	0.65(0.56-0.75)	0.001	(8,9)	1(0.95-1.05)	0.94(0.88-1.01)	0.13	(8,9)
COP9 signalosome complex subunit 5	1(0.84-1.19)	0.82(0.71-0.94)	0.05	(8,9)	1(0.87-1.15)	0.84(0.71-1.01)	0.1	(8,9)	1(0.91-1.1)	0.95(0.85-1.05)	0.4	(8,9)
COP9 signalosome complex subunit 6	1(0.91-1.1)	0.72(0.66-0.8)	<0.0001	(8,9)	1(0.86-1.17)	0.62(0.51-0.77)	0.0007	(8,9)	1(0.89-1.12)	0.88(0.82-0.95)	0.05	(8,9)
COP9 signalosome complex subunit 7a	1(0.9-1.12)	0.73(0.67-0.79)	0.0001	(8,9)	1(0.91-1.1)	0.86(0.8-0.92)	0.009	(8,9)	1(0.84-1.19)	0.89(0.79-1.01)	0.24	(8,9)
COP9 signalosome complex subunit 7b	1(0.81-1.23)	1.25(1.13-1.38)	0.05	(8,9)	1(0.8-1.25)	0.91(0.77-1.07)	0.45	(8,9)	1(0.8-1.26)	0.94(0.65-1.35)	0.72	(8,9)
COP9 signalosome complex subunit 8	1(0.88-1.14)	0.8(0.71-0.89)	0.007	(8,9)	1(0.83-1.2)	0.67(0.6-0.76)	0.001	(8,9)	1(0.94-1.07)	0.96(0.86-1.06)	0.41	(8,9)
Cullin												
Cullin-1	1(0.82-1.22)	0.75(0.69-0.83)	0.01	(8,9)	1(0.86-1.17)	0.95(0.85-1.06)	0.54	(8,9)	1(0.92-1.09)	0.88(0.86-0.9)	0.007	(8,9)
Cullin-2	1(0.88-1.14)	0.72(0.63-0.81)	0.0007	(8,9)	1(0.86-1.17)	0.72(0.58-0.88)	0.009	(8,9)	1(0.96-1.04)	0.94(0.85-1.02)	0.14	(8,9)
Cullin-3	1(0.94-1.07)	0.89(0.82-0.95)	0.01	(8,9)	1(0.93-1.07)	0.95(0.86-1.05)	0.31	(8,9)	1(0.95-1.05)	0.99(0.94-1.05)	0.76	(8,9)
Cullin-4A	1(0.8-1.26)	1.21(1.1-1.33)	0.09	(6,6)	1(0.8-1.26)	0.8(0.54-1.18)	0.27	(8,9)	1(0.83-1.2)	0.97(0.87-1.08)	0.72	(8,9)
Cullin-4B	1(0.78-1.28)	1.12(0.95-1.31)	0.4	(8,9)	1(0.88-1.14)	1.12(1-1.25)	0.16	(8,9)	1(0.93-1.07)	1.05(0.97-1.13)	0.3	(8,9)
Cullin-5	1(0.92-1.09)	0.97(0.85-1.1)	0.66	(8,9)	1(0.91-1.1)	0.96(0.9-1.02)	0.38	(8,9)	1(0.91-1.1)	1.01(0.94-1.08)	0.89	(8,9)
Cullin-associated NEDD8-dissociated protein 1	1(0.86-1.16)	0.9(0.76-1.07)	0.29	(8,9)	1(0.91-1.1)	1(0.92-1.09)	0.99	(8,9)	1(0.96-1.04)	1.13(1.06-1.21)	0.003	(8,9)
Ncullin-associated NEDD8-dissociated protein 2	1(0.6-1.66)	1.12(0.93-1.35)	0.58	(5,6)	1(0.73-1.37)	0.56(0.28-1.11)	0.09	(6,6)	1(0.89-1.13)	1.04(0.76-1.44)	0.78	(8,9)

Table 4-46 Proteomic findings relating to 14-3-3 proteins

	HP				ENT				CB			
General name	Abundance (C)	Abundance (AD)	p	N_C,N_{AD}	Abundance (C)	Abundance (AD)	p	N_C,N_{AD}	Abundance (C)	Abundance (AD)	p	N_C,N_{AD}
14-3-3												
14-3-3 protein beta/alpha	1(0.87-1.15)	0.64(0.53-0.78)	0.0009	(8,9)	1(0.88-1.13)	0.62(0.53-0.73)	0.0001	(8,9)	1(0.92-1.09)	0.86(0.81-0.91)	0.005	(8,9)
14-3-3 protein gamma	1(0.82-1.23)	0.62(0.51-0.75)	0.001	(8,9)	1(0.9-1.11)	0.62(0.5-0.77)	0.0006	(8,9)	1(0.94-1.07)	0.83(0.79-0.88)	0.0002	(8,9)
14-3-3 protein zeta/delta	1(0.85-1.17)	0.59(0.51-0.69)	0.0001	(8,9)	1(0.86-1.16)	0.67(0.58-0.78)	0.0005	(8,9)	1(0.93-1.08)	0.83(0.76-0.91)	0.003	(8,9)
14-3-3 protein eta	1(0.83-1.2)	0.62(0.51-0.74)	0.0006	(8,9)	1(0.88-1.13)	0.69(0.56-0.85)	0.004	(8,9)	1(0.91-1.1)	0.76(0.65-0.9)	0.005	(8,9)
14-3-3 protein epsilon	1(0.91-1.09)	0.78(0.69-0.88)	0.002	(8,9)	1(0.87-1.15)	0.71(0.64-0.79)	0.0004	(8,9)	1(0.94-1.06)	0.92(0.88-0.97)	0.02	(8,9)
14-3-3 protein theta	1(0.89-1.13)	0.68(0.56-0.82)	0.002	(8,9)	1(0.93-1.08)	0.65(0.52-0.81)	0.002	(8,9)	1(0.89-1.13)	0.81(0.74-0.89)	0.007	(8,9)

4.3.3.11. Axonal transport and amyloid biology

In this study, both kinesins and dyneins were decreased in abundance in AD, most significantly in ENT (**Table 4-47**). Specifically, both heavy and light chains of kinesins, kinesin-associated protein, and kinesin-like proteins were decreased in the AD brain, as were both heavy and light chains of cytoplasmic dynein-1. Dynactin, an essential cofactor for the cytoplasmic dyenin-1[333], showed significant decrease in many subunits.

Initial data analysis showed significant differences in the abundance of APP (amyloid beta A4 protein), in only ENT among the three brain regions (**Figure 4-5**). Further examination of all the peptides detected for this protein revealed strong accumulation of Aβ (1-40) and/or Aβ (1-42) in the AD brain, but not other peptides (**Figure 4-5**). Proteins involved in APP processing showed decreased abundance in the HP and ENT of AD brain. On the other hand, changes in apolipoproteins were only apparent in the CB (**Table 4-49**).

4.3.3.12. Immune response

In this study, complement-component proteins and pro-inflammatory molecules were increased in abundance (statistical threshold reached) in the AD brain, most consistently in HP and ENT (**Table 4-50**). Immunoglobulin-component proteins were also increased where the statistical threshold was passed (**Table 4-51**). Erythrocyte-component proteins were most significantly increased in the ENT and proteins involved in coagulation were in general, increased in the AD brain (**Table 4-52**).

Table 4-47: Proteomic findings relating to axonal transport

	HP				ENT				CB			
General name	Abundance (C)	Abundance (AD)	p	N_C,N_{AD}	Abundance (C)	Abundance (AD)	p	N_C,N_{AD}	Abundance (C)	Abundance (AD)	p	N_C,N_{AD}
Kinesin												
Kinesin-1 heavy chain	1(0.93-1.08)	0.94(0.8-1.1)	0.41	(8,9)	1(0.8-1.25)	0.72(0.58-0.9)	0.03	(8,9)	1(0.94-1.06)	0.91(0.81-1.01)	0.09	(8,9)
Kinesin heavy chain isoform 5A	1(0.67-1.49)	0.84(0.54-1.3)	0.5	(8,9)	1(0.57-1.76)	0.45(0.28-0.71)	0.02	(5,6)	1(0.86-1.16)	0.62(0.46-0.85)	0.008	(8,9)
Kinesin heavy chain isoform 5C	1(0.83-1.2)	0.68(0.61-0.75)	0.001	(8,9)	1(0.87-1.16)	0.54(0.46-0.64)	<0.0001	(8,9)	1(0.94-1.06)	0.79(0.73-0.86)	0.0001	(8,9)
Kinesin light chain 1	1(0.82-1.22)	0.8(0.7-0.92)	0.05	(8,9)	1(0.87-1.15)	0.66(0.6-0.73)	0.0001	(8,9)	1(0.93-1.08)	0.83(0.77-0.9)	0.002	(8,9)
Kinesin light chain 2	1(0.83-1.2)	0.85(0.73-0.98)	0.1	(5,6)	1(0.81-1.23)	0.66(0.5-0.86)	0.01	(8,9)	1(0.91-1.1)	0.92(0.8-1.04)	0.22	(8,9)
Kinesin-associated protein 3	1(0.56-1.8)	0.88(0.57-1.35)	0.65	(6,6)	1(0.73-1.37)	0.63(0.49-0.81)	0.01	(5,6)	1(0.87-1.15)	0.88(0.75-1.03)	0.18	(8,9)
Kinesin-like protein KIF2A	1(0.8-1.25)	0.76(0.66-0.87)	0.03	(8,9)	1(0.89-1.13)	0.69(0.57-0.83)	0.002	(8,9)	1(0.95-1.06)	0.91(0.85-0.98)	0.04	(8,9)
Kinesin-like protein KIF21A	1(0.83-1.2)	0.85(0.77-0.94)	0.1	(8,9)	1(0.91-1.1)	0.84(0.7-1.01)	0.08	(8,9)	1(0.93-1.07)	0.88(0.8-0.96)	0.02	(8,9)
Kinesin-like protein KIF1A	1(0.85-1.18)	0.79(0.65-0.96)	0.05	(8,9)	1(0.86-1.16)	0.82(0.68-0.98)	0.07	(8,9)	1(0.92-1.09)	1.18(0.98-1.43)	0.09	(8,9)
Kinesin-like protein KIF21B	1(0.17-6.03)	0.91(0.69-1.2)	0.62	(2,3)	1(0.67-1.5)	0.75(0.6-0.95)	0.08	(3,3)				
Dynein												
Cytoplasmic dynein 1 heavy chain 1	1(0.8-1.25)	0.86(0.72-1.03)	0.25	(8,9)	1(0.86-1.17)	0.76(0.65-0.9)	0.01	(8,9)	1(0.95-1.05)	0.86(0.78-0.94)	0.007	(8,9)
Cytoplasmic dynein 1 light intermediate chain 1	1(0.73-1.36)	0.8(0.68-0.95)	0.17	(8,9)	1(0.84-1.18)	0.78(0.69-0.87)	0.01	(8,9)	1(0.94-1.07)	0.89(0.78-1.01)	0.09	(8,9)
Cytoplasmic dynein 1 light intermediate chain 2	1(0.81-1.23)	0.86(0.72-1.03)	0.24	(8,9)	1(0.85-1.18)	0.75(0.68-0.82)	0.004	(8,9)	1(0.9-1.11)	0.88(0.8-0.97)	0.06	(8,9)
Cytoplasmic dynein 1 intermediate chain 1	1(0.9-1.11)	0.79(0.72-0.86)	0.001	(8,9)	1(0.84-1.19)	0.77(0.7-0.84)	0.01	(8,9)	1(0.92-1.09)	0.96(0.9-1.02)	0.37	(8,9)
Dynein cytoplasmic 1 intermediate chain 2	1(0.88-1.14)	0.94(0.79-1.13)	0.55	(8,9)	1(0.83-1.21)	0.66(0.54-0.81)	0.003	(8,9)	1(0.84-1.2)	0.81(0.72-0.92)	0.04	(8,9)
Dynein light chain 1, cytoplasmic	1(0.81-1.23)	0.76(0.65-0.88)	0.02	(8,9)	1(0.81-1.23)	0.71(0.63-0.81)	0.007	(8,9)	1(0.91-1.1)	0.83(0.72-0.94)	0.01	(8,9)
Dynein light chain 2, cytoplasmic	1(0.86-1.16)	0.86(0.73-1.01)	0.13	(8,9)	1(0.81-1.23)	1.12(0.92-1.36)	0.38	(8,9)	1(0.83-1.21)	1.05(0.89-1.25)	0.65	(8,9)
Dynein light chain 1, axonemal	1(0.73-1.36)	0.99(0.64-1.53)	0.96	(8,9)	1(0.43-2.35)	0.89(0.24-3.22)	0.76	(3,3)	1(0.61-1.63)	0.93(0.68-1.26)	0.73	(5,6)
Dynein light chain 4, axonemal	1(0.07-13.65)	1.07(0.65-1.76)	0.81	(2,3)								
Dynein light chain Tctex-type 1	1(0.51-1.97)	0.78(0.31-1.96)	0.41	(3,3)	1(0.69-1.45)	0.73(0.54-0.99)	0.15	(8,9)	1(0.77-1.3)	1.12(0.63-2.01)	0.66	(5,6)
Dynein light chain Tctex-type 3	1(0.92-1.08)	0.78(0.71-0.86)	0.0002	(8,9)	1(0.83-1.2)	0.79(0.69-0.91)	0.03	(5,6)	1(0.89-1.13)	0.9(0.83-0.97)	0.1	(8,9)
Dynein light chain roadblock-type 1	1(0.85-1.18)	0.78(0.69-0.88)	0.01	(8,9)	1(0.78-1.28)	0.7(0.65-0.74)	0.01	(8,9)	1(0.91-1.1)	0.94(0.83-1.05)	0.33	(8,9)
Dynactin subunit 1	1(0.89-1.13)	0.7(0.62-0.79)	0.0002	(8,9)	1(0.93-1.07)	0.69(0.59-0.81)	0.0006	(8,9)	1(0.93-1.08)	0.82(0.72-0.94)	0.01	(8,9)
Dynactin subunit 2	1(0.89-1.13)	0.78(0.7-0.87)	0.003	(8,9)	1(0.84-1.19)	0.73(0.67-0.8)	0.004	(8,9)	1(0.92-1.08)	0.92(0.83-1.02)	0.14	(8,9)
Dynactin subunit 3	1(0.9-1.11)	0.8(0.74-0.88)	0.002	(8,9)	1(0.91-1.1)	0.71(0.66-0.77)	<0.0001	(8,9)	1(0.9-1.11)	0.87(0.82-0.92)	0.02	(8,9)
Dynactin subunit 4	1(0.9-1.11)	0.83(0.73-0.94)	0.02	(8,9)	1(0.88-1.13)	0.8(0.72-0.89)	0.007	(8,9)	1(0.93-1.08)	0.93(0.87-1)	0.11	(8,9)
Dynactin subunit 5	1(0.78-1.28)	0.8(0.56-1.15)	0.11	(3,3)	1(0.7-1.42)	0.64(0.51-0.8)	0.01	(3,3)	1(0.78-1.29)	0.9(0.78-1.05)	0.23	(3,3)
Dynactin subunit 6	1(0.82-1.21)	1.02(0.74-1.41)	0.91	(8,9)	1(0.79-1.27)	0.9(0.79-1.02)	0.36	(8,9)	1(0.75-1.33)	1.35(1.02-1.78)	0.1	(8,9)

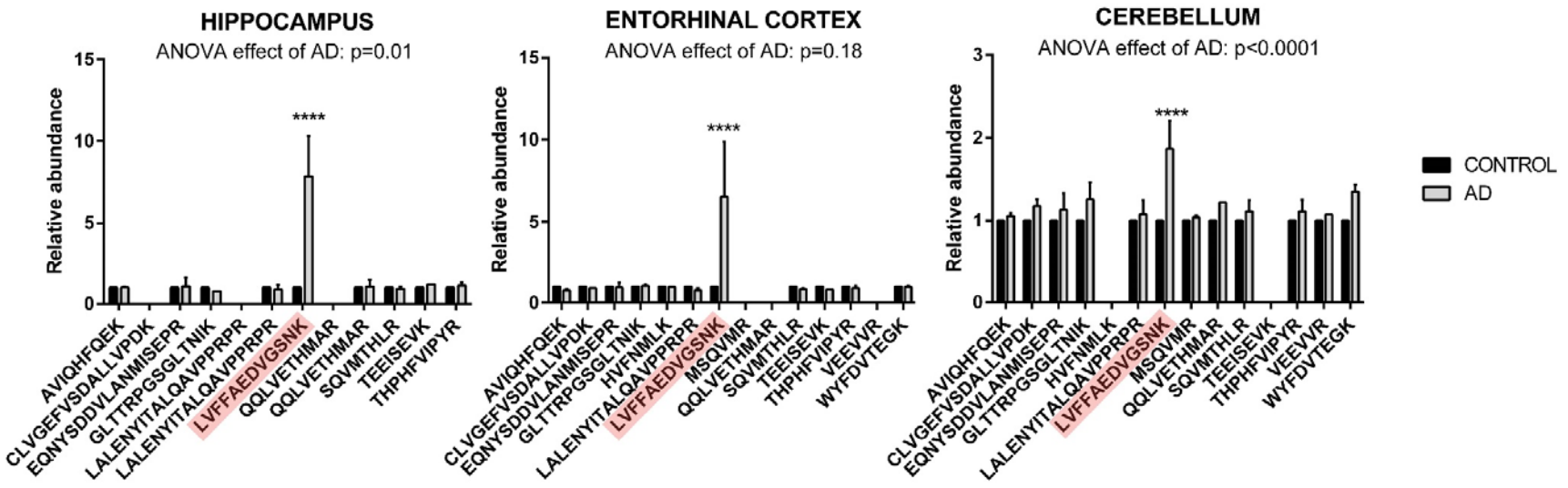

Figure 4-5 Relative abundances for individual APP-derived tryptic peptides

Two-Way ANOVAs (AD x peptides) were used to determine the overall effect of AD on the protein (inserted under each graph heading with p referring to the significance of the effect of AD on all peptides combined). Significant differences between AD and control were analysed for each individual peptide using Sidak's multiple comparisons test. Control values (solid black bars) were scaled to "1" during normalisation with AD values relative to controls. Where significant in the post-test, asterisks were inserted above the bars. Peptides specific to either Aβ (1-40) and/or Aβ (1-42) were highlighted in pink. Abbreviations: ****, p<0.0001.

Table 4-48: Proteomic findings relating to amyloid biology

	HP				ENT				CB			
General name	Abundance (C)	Abundance (AD)	p	N_C,N_{AD}	Abundance (C)	Abundance (AD)	p	N_C,N_{AD}	Abundance (C)	Abundance (AD)	p	N_C,N_{AD}
Amyloid												
Amyloid beta A4 protein	1(0.58-1.73)	1.43(1.2-1.71)	0.18	(8,9)	1(0.79-1.27)	1.54(1.13-2.09)	0.02	(8,9)	1(0.59-1.7)	1.14(0.75-1.72)	0.66	(8,9)
Amyloid beta A4 precursor protein-binding family B member 1	1(0.78-1.28)	0.76(0.62-0.94)	0.07	(8,9)	1(0.63-1.59)	0.76(0.5-1.14)	0.26	(5,6)	1(0.89-1.12)	0.91(0.83-1)	0.15	(8,9)
Amyloid-like protein 2	1(0.74-1.35)	1.41(1.05-1.9)	0.06	(5,6)	1(0-267.47)	1.55(0.93-2.58)	0.5	(2,3)	1(0.93-1.08)	1.06(0.92-1.22)	0.4	(8,9)
APP processing												
Presenilin-2					1(0.6-1.68)	1(0.65-1.52)	0.98	(3,3)	1(0.79-1.26)	1.29(1-1.68)	0.08	(5,6)
Integral membrane protein 2C	1(0.69-1.46)	0.76(0.65-0.88)	0.12	(6,6)	1(0.22-4.6)	0.53(0.37-0.76)	0.05	(2,3)				
Cajalin 2 (amyloid-beta precursor protein intracellular domain associated protein 1)	1(0.64-1.57)	0.58(0.44-0.78)	0.03	(8,9)	1(0.77-1.29)	0.77(0.5-1.16)	0.23	(8,9)	1(0.87-1.15)	0.9(0.74-1.08)	0.28	(8,9)
Reticulon-3	1(0.89-1.13)	0.87(0.78-0.97)	0.06	(8,9)	1(0.88-1.14)	0.89(0.78-1.03)	0.2	(8,9)	1(0.92-1.09)	0.97(0.87-1.08)	0.62	(8,9)
Reticulon-4	1(0.89-1.13)	0.83(0.77-0.89)	0.008	(8,9)	1(0.89-1.12)	0.76(0.7-0.83)	0.0006	(8,9)	1(0.93-1.07)	0.96(0.88-1.05)	0.42	(8,9)
Reticulon-4 receptor					1(0.85-1.17)	0.71(0.54-0.92)	0.02	(8,9)	1(0.89-1.12)	0.91(0.76-1.08)	0.29	(8,9)

Table 4-49: Proteomic findings relating to apolipoproteins

	HP				ENT				CB			
General name	Abundance (C)	Abundance (AD)	p	N_C,N_{AD}	Abundance (C)	Abundance (AD)	p	N_C,N_{AD}	Abundance (C)	Abundance (AD)	p	N_C,N_{AD}
Apolipoprotein												
Apolipoprotein A-I	1(0.75-1.33)	0.95(0.77-1.19)	0.77	(8,9)	1(0.63-1.58)	0.87(0.71-1.06)	0.52	(8,9)	1(0.69-1.45)	0.7(0.54-0.91)	0.09	(8,9)
Apolipoprotein A-II	1(0.76-1.32)	0.9(0.66-1.23)	0.57	(8,9)	1(0.71-1.42)	0.9(0.76-1.08)	0.55	(8,9)	1(0.71-1.41)	0.67(0.52-0.86)	0.04	(8,9)
Apolipoprotein A-I-binding protein / NAD(P)HX epimerase	1(0.92-1.08)	1.1(0.98-1.23)	0.13	(8,9)	1(0.85-1.17)	1.17(1.02-1.33)	0.11	(8,9)	1(0.86-1.16)	1.22(1.14-1.31)	0.02	(8,9)
Apolipoprotein B-100	1(0.82-1.22)	1.31(1.1-1.55)	0.03	(8,9)	1(0.81-1.24)	1.11(0.81-1.51)	0.49	(5,6)	1(0.81-1.23)	1.09(0.8-1.48)	0.59	(8,9)
Apolipoprotein C-I									1(0.75-1.33)	0.59(0.4-0.88)	0.02	(5,6)
Apolipoprotein C-III	1(0.86-1.16)	1.12(0.91-1.36)	0.29	(6,6)	1(0.81-1.23)	1.18(0.99-1.4)	0.14	(5,6)	1(0.68-1.46)	0.91(0.68-1.2)	0.64	(8,9)
Apolipoprotein D	1(0.86-1.17)	1.09(0.98-1.22)	0.3	(8,9)	1(0.85-1.17)	1.05(0.84-1.32)	0.67	(8,9)	1(0.8-1.25)	1.38(1.16-1.65)	0.02	(8,9)
Apolipoprotein E	1(0.73-1.38)	1.07(0.85-1.36)	0.69	(8,9)	1(0.76-1.32)	1.27(1.03-1.57)	0.13	(8,9)	1(0.9-1.11)	1.33(1.19-1.48)	0.0005	(8,9)
Apolipoprotein O	1(0.87-1.15)	1.06(0.93-1.21)	0.49	(8,9)	1(0.79-1.26)	0.92(0.63-1.34)	0.67	(8,9)	1(0.87-1.15)	1.01(0.79-1.28)	0.95	(8,9)
Apolipoprotein L2	1(0.9-1.12)	0.84(0.7-1)	0.06	(6,6)	1(0.89-1.13)	0.93(0.6-1.45)	0.72	(5,6)	1(0.84-1.19)	1.1(0.89-1.37)	0.43	(8,9)

Table 4-50: Proteomic findings relating to immune response

	HP				ENT				CB			
General name	Abundance (C)	Abundance (AD)	p	N_C,N_{AD}	Abundance (C)	Abundance (AD)	p	N_C,N_{AD}	Abundance (C)	Abundance (AD)	p	N_C,N_{AD}
Complement												
Complement C1q subcomponent subunit B	1(0.73-1.37)	1.21(0.93-1.57)	0.3	(8,9)	1(0.61-1.63)	0.98(0.7-1.36)	0.92	(5,6)	1(0.81-1.23)	1.52(1.1-2.11)	0.02	(5,6)
Complement C1q subcomponent subunit C	1(0.76-1.31)	1.46(1.23-1.72)	0.02	(8,9)	1(0.71-1.4)	1.66(1.46-1.89)	0.009	(8,9)	1(0.88-1.14)	1.49(1.32-1.68)	0.0001	(8,9)
Complement C1q-like protein 3	1(0.62-1.61)	1.7(0.99-2.92)	0.04	(2,3)	1(0.07-14.88)	1.41(0.63-3.15)	0.33	(2,3)	1(0.29-3.46)	0.41(0.09-1.81)	0.12	(3,3)
Complement C3	1(0.88-1.14)	1.67(1.48-1.88)	<0.0001	(8,9)	1(0.79-1.26)	1.57(1.3-1.88)	0.003	(8,9)	1(0.81-1.23)	1.38(1.08-1.76)	0.03	(8,9)
C4b-binding protein alpha	1(0.67-1.49)	1.68(1.06-2.67)	0.05	(5,6)	1(0.67-1.5)	1.84(1.6-2.12)	0.01	(6,6)	1(0.7-1.43)	1.53(1.19-1.96)	0.04	(8,8)
Complement C4-B;Complement C4-A	1(0.83-1.21)	1.85(1.54-2.23)	0.0001	(8,9)								
Complement C4-B	1(0.53-1.88)	2(1.43-2.81)	0.02	(3,3)								
Complement C4-B; Complement C4-A	1(0.84-1.19)	1.68(1.38-2.05)	0.0003	(8,9)	1(0.72-1.4)	1.63(1.21-2.2)	0.02	(8,9)	1(0.78-1.28)	1.54(1.16-2.04)	0.02	(8,9)
Complement C5									1(0.4-2.52)	0.95(0.71-1.28)	0.64	(2,3)
Complement component C6 precursor									1(0.93-1.08)	1.07(0.8-1.43)	0.57	(5,6)
Complement component C9	1(0.67-1.49)	1.96(1.33-2.88)	0.01	(6,6)	1(0.23-4.33)	2.04(1.05-3.96)	0.16	(3,3)	1(0.5-1.98)	1.22(0.43-3.46)	0.54	(3,3)
Complement factor B	1(0.66-1.52)	1.51(1.26-1.8)	0.06	(8,9)	1(0.6-1.68)	1.34(0.97-1.86)	0.25	(6,6)	1(0.61-1.63)	1.39(0.83-2.33)	0.3	(8,9)
Complement factor H	1(0.7-1.44)	2.02(1.39-2.94)	0.004	(3,3)	1(0.15-6.64)	1.81(1.01-3.23)	0.31	(3,3)	1(0.77-1.3)	1.44(0.98-2.1)	0.07	(5,6)
Plasma protease C1 inhibitor	1(0.86-1.16)	2.09(1.8-2.44)	<0.0001	(8,9)	1(0.66-1.5)	2.63(2.25-3.08)	0.0005	(8,9)	1(0.77-1.31)	1.9(1.49-2.42)	0.0009	(8,9)
Pro-inflammatory molecules												
Alpha-1-acid glycoprotein 1	1(0.83-1.21)	2.7(2.18-3.34)	<0.0001	(8,9)	1(0.74-1.34)	3.02(2.44-3.75)	<0.0001	(8,9)	1(0.74-1.34)	2.54(1.93-3.35)	0.0001	(8,9)
Alpha-1-acid glycoprotein 2	1(0.75-1.33)	2.4(1.71-3.36)	0.0003	(8,9)	1(0.7-1.42)	2.55(1.98-3.28)	0.0002	(8,9)	1(0.69-1.46)	1.8(1.36-2.4)	0.01	(8,9)
Serum amyloid A-1 protein	1(0.19-5.17)	3.8(1.8-8.05)	0.09	(5,6)	1(0.5-2.01)	1.85(1.24-2.76)	0.08	(6,6)	1(0.16-6.19)	4.4(2.61-7.45)	0.1	(8,9)
Serum amyloid P-component	1(0.79-1.27)	2.06(1.21-3.51)	0.02	(5,6)	1(0.69-1.46)	2.74(1.84-4.08)	0.0009	(5,6)	1(0.16-6.09)	1.75(1.01-3.04)	0.31	(3,3)
Alpha-2-macroglobulin	1(0.81-1.23)	1.52(1.33-1.74)	0.002	(8,9)	1(0.77-1.3)	1.34(1.1-1.62)	0.05	(8,9)	1(0.73-1.37)	1.28(1.04-1.57)	0.15	(8,9)
Macrophage migration inhibitory factor	1(0.76-1.31)	1.04(0.92-1.17)	0.78	(8,9)	1(0.8-1.25)	1.17(1.01-1.37)	0.18	(8,9)	1(0.77-1.29)	1.26(1.1-1.45)	0.09	(8,9)
SAM domain and HD domain-containing protein 1	1(0.76-1.32)	1.4(1.24-1.58)	0.03	(8,9)	1(0.81-1.23)	1.35(1.1-1.66)	0.03	(8,9)	1(0.91-1.1)	0.95(0.85-1.05)	0.38	(8,9)
Chitinase-3-like protein 1	1(0.7-1.43)	1.3(0.76-2.21)	0.17	(3,3)	1(0.8-1.25)	1.39(0.98-1.98)	0.07	(6,6)				

Table 4-51: Proteomic findings relating to immunoglobulin-related molecules

	HP				ENT				CB			
General name	Abundance (C)	Abundance (AD)	p	N_C,N_{AD}	Abundance (C)	Abundance (AD)	p	N_C,N_{AD}	Abundance (C)	Abundance (AD)	p	N_C,N_{AD}
Antibody immunoglobulin												
Ig alpha-1 chain C region	1(0.89-1.13)	2.21(1.75-2.8)	<0.0001	(8,9)	1(0.71-1.41)	2.82(2.07-3.84)	0.0001	(8,9)	1(0.74-1.35)	2.23(1.5-3.33)	0.002	(8,9)
Ig gamma-1 chain C region	1(0.61-1.65)	2.82(2.02-3.94)	0.002	(8,9)	1(0.6-1.67)	2.64(1.94-3.59)	0.003	(8,9)	1(0.61-1.64)	2.07(1.72-2.49)	0.01	(8,9)
Ig gamma-2 chain C region	1(0.08-12.62)	2.71(0.94-7.88)	0.23	(3,3)	1(0.74-1.36)	1.93(1.1-3.38)	0.03	(5,6)	1(0.57-1.75)	1.6(1.09-2.33)	0.13	(8,9)
Ig gamma-3 chain C region	1(0.8-1.24)	2.15(1.5-3.07)	0.001	(8,9)	1(0.72-1.39)	1.83(1.35-2.47)	0.007	(8,9)	1(0.71-1.4)	1.8(1.21-2.68)	0.02	(8,9)
Ig kappa chain V-I region Gal					1(0.23-4.38)	3.01(1.65-5.48)	0.07	(3,3)				
Ig kappa chain V-I region Gal					1(0.75-1.33)	1.41(1.04-1.92)	0.06	(5,6)				
Ig kappa chain V-III region VG	1(0.76-1.32)	1.63(1.38-1.92)	0.004	(8,9)					1(0.08-12.05)	1.15(0.37-3.57)	0.69	(2,3)
Ig kappa chain V-III region VH					1(0.5-2.01)	2.08(1.42-3.03)	0.006	(2,3)	1(0.6-1.68)	0.9(0.56-1.44)	0.56	(3,3)
Ig kappa chain C region	1(0.78-1.29)	2.13(1.79-2.54)	0.0001	(8,9)	1(0.78-1.28)	2.18(1.7-2.79)	0.0001	(8,9)	1(0.67-1.48)	1.83(1.44-2.32)	0.01	(8,9)
Ig kappa chain V-III region HAH	1(0.77-1.3)	1.68(1.35-2.08)	0.003	(8,9)					1(0.72-1.39)	1.45(1.24-1.7)	0.04	(8,9)
Ig kappa chain V-III region HAH; Ig kappa chain V-III region HIC	1(0.59-1.71)	2.14(1.56-2.92)	0.01	(6,6)								
Ig kappa chain V-III region NG9					1(0.72-1.38)	1.65(1.33-2.06)	0.01	(8,9)	1(0.6-1.68)	0.7(0.5-0.97)	0.16	(5,6)
Ig lambda-2 chain C regions	1(0.79-1.27)	1.99(1.64-2.42)	0.0001	(8,9)	1(0.55-1.83)	2.24(1.76-2.83)	0.02	(8,9)				
Ig lambda-3 chain C regions									1(0.71-1.4)	1.88(1.49-2.36)	0.003	(8,9)
Immunoglobulin lambda-like polypeptide 5	1(0.72-1.38)	3.08(2.27-4.17)	<0.0001	(8,9)	1(0.56-1.8)	3.01(2.45-3.7)	0.004	(6,6)	1(0.87-1.15)	1.79(1.28-2.5)	0.009	(3,3)
Ig mu chain C region	1(0.73-1.38)	1.93(1.5-2.47)	0.002	(8,9)	1(0.62-1.62)	1.84(1.35-2.52)	0.03	(8,9)	1(0.61-1.65)	1.46(1.16-1.84)	0.13	(8,9)
Ig heavy chain V-I region HG3	1(0.67-1.49)	2.44(1.65-3.6)	0.002	(8,9)					1(0.62-1.6)	1.88(1.38-2.55)	0.02	(8,9)
Ig heavy chain V-I region Mot					1(0.58-1.72)	1.96(1.3-2.96)	0.04	(8,9)				
Ig heavy chain V-III region TEI	1(0.85-1.18)	1.97(1.55-2.51)	0.0001	(8,9)	1(0.75-1.33)	2.41(1.91-3.05)	0.0002	(5,6)	1(0.4-2.49)	2.01(1.17-3.45)	0.12	(5,6)
Immunoglobulin superfamily member 21	1(0.77-1.3)	0.89(0.75-1.05)	0.38	(8,9)	1(0.86-1.16)	1.05(0.88-1.25)	0.63	(8,9)	1(0.88-1.14)	1.38(1.17-1.62)	0.003	(8,9)

Table 4-52: Proteomic findings relating to blood components

	HP				ENT				CB			
General name	Abundance (C)	Abundance (AD)	p	N_C,N_{AD}	Abundance (C)	Abundance (AD)	p	N_C,N_{AD}	Abundance (C)	Abundance (AD)	p	N_C,N_{AD}
Blood components												
Hemoglobin subunit alpha	1(0.85-1.17)	1.34(0.87-2.05)	0.17	(8,9)	1(0.78-1.29)	1.51(1.08-2.1)	0.04	(8,9)	1(0.77-1.29)	1.1(0.73-1.65)	0.65	(8,9)
Hemoglobin subunit beta	1(0.82-1.22)	1.24(0.79-1.94)	0.34	(8,9)	1(0.83-1.21)	1.39(1.03-1.86)	0.05	(8,9)	1(0.78-1.28)	1.02(0.65-1.61)	0.91	(8,9)
Hemoglobin subunit delta	1(0.78-1.28)	1.32(0.8-2.18)	0.27	(8,9)	1(0.77-1.29)	1.57(1.08-2.29)	0.04	(8,9)	1(0.78-1.29)	1.13(0.81-1.58)	0.49	(8,9)
Solute carrier family 4, member 1	1(0.74-1.34)	1.44(1.06-1.95)	0.06	(8,9)	1(0.86-1.16)	1.46(1.19-1.8)	0.003	(8,9)	1(0.79-1.26)	0.96(0.66-1.38)	0.82	(8,9)
Erythrocyte membrane protein band 4.1	1(0.74-1.34)	0.98(0.79-1.21)	0.9	(8,9)	1(0.33-3.03)	1.4(0.35-5.67)	0.46	(3,3)	1(0.95-1.05)	0.87(0.8-0.95)	0.009	(8,9)
Hemopexin	1(0.83-1.2)	1.78(1.5-2.12)	0.0001	(8,9)	1(0.7-1.43)	1.78(1.43-2.22)	0.007	(8,9)	1(0.81-1.23)	1.26(1.09-1.47)	0.05	(8,9)
Haptoglobin	1(0.77-1.29)	3.39(2.52-4.56)	<0.0001	(8,9)	1(0.69-1.45)	3.12(2.38-4.08)	0.0001	(8,9)	1(0.71-1.41)	2.56(1.78-3.68)	0.0005	(8,9)
Haptoglobin-related protein					1(0.7-1.42)	1.5(1.19-1.88)	0.02	(3,3)				
Serotransferrin	1(0.73-1.37)	0.91(0.78-1.06)	0.54	(8,9)	1(0.78-1.29)	0.73(0.58-0.91)	0.04	(8,9)	1(0.76-1.32)	0.96(0.8-1.16)	0.8	(8,9)
Ceruloplasmin	1(0.8-1.26)	2.17(1.79-2.64)	<0.0001	(8,9)	1(0.82-1.22)	1.59(1.36-1.87)	0.0008	(8,9)	1(0.76-1.31)	1.76(1.41-2.2)	0.002	(8,9)
Coagulation												
Fibrinogen alpha	1(0.77-1.29)	2.88(1.75-4.74)	0.001	(8,9)	1(0.66-1.51)	2.31(1.49-3.57)	0.005	(8,9)	1(0.72-1.39)	2.16(1.32-3.54)	0.01	(8,9)
Fibrinogen beta	1(0.74-1.36)	2.15(1.36-3.4)	0.006	(8,9)	1(0.73-1.36)	2.03(1.38-2.98)	0.005	(8,9)	1(0.73-1.37)	1.76(1.12-2.77)	0.03	(8,9)
Fibrinogen gamma	1(0.75-1.33)	2.2(1.39-3.47)	0.005	(8,9)	1(0.7-1.43)	2.2(1.39-3.48)	0.007	(8,9)	1(0.76-1.32)	1.74(1.12-2.72)	0.03	(8,9)
Prothrombin	1(0.69-1.45)	1.81(0.97-3.37)	0.03	(3,3)					1(0.14-7.07)	1.51(0.92-2.49)	0.46	(3,3)
Antithrombin-III	1(0.84-1.19)	1.29(1-1.66)	0.07	(6,6)	1(0.73-1.37)	1.22(1.01-1.48)	0.23	(8,9)	1(0.82-1.21)	1.08(0.91-1.28)	0.51	(8,9)
Coagulation factor XIII	1(0.58-1.74)	1.65(1.38-1.98)	0.07	(8,9)	1(0.66-1.51)	1.31(0.98-1.74)	0.19	(5,6)	1(0.78-1.28)	1.03(0.76-1.39)	0.86	(8,9)
Kininogen-1	1(0.67-1.49)	1.63(1.18-2.25)	0.04	(6,6)					1(0.91-1.1)	1.21(1.02-1.44)	0.04	(5,6)

4.4. Discussion

4.4.1. Energy production

Global and regional impairment in brain metabolism and energetics is central to the pathogenesis of AD as evidence by epidemiological, neuropathological, and functional neuroimaging studies [334]. In AD, dysfunction in brain energy metabolism has previously been described as a shift from primarily aerobic glycolysis (i.e. glycolysis followed by complete oxidation in mitochondria) to the ketogenic/fatty acid β-oxidation pathway, with impaired mitochondrial bioenergetics [232].

4.4.1.1. Glucose metabolism

The AD brain characteristically exhibits defective cerebral perfusion [192] and glucose uptake [217], which was believed to underlie hypometabolism and cognitive decline [225]. Interestingly, our data showed extreme elevation in the levels of free glucose in all seven regions of brain examined in this study (Chapter Three). Glucose is normally metabolised through the glycolytic pathway to pyruvate and in the presence of oxygen, is oxidised to CO_2 and water in the mitochondria with maximum energy extraction. However, during periods of excessive glucose levels or defective glycolysis, the polyol and pentose-phosphate pathways (minor routes of glucose clearance under usual physiological circumstances) may be activated to metabolise glucose by alternative routes [227,242].

In line with the elevation in glucose levels, this proteomic study has shown significant changes in pathways involved in glucose metabolism. In the glycolysis pathway, enzymes catalysing the first three steps were either unchanged or decreased, and most significantly decreased in the ENT. However, enzymes including and subsequent to aldolase in the pathway, mainly showed increased in abundance where the changes were significant. This pattern was clearest in ENT, as shown in **Figure 4-6**.

An intriguing observation was that the glycolytic enzymes showing decreased abundance were those that do not participate in gluconeogenesis, a metabolic pathway that runs in the opposite direction to glycolysis and generates glucose from non-carbohydrate substrates. Most enzymatic steps in the glycolytic pathway are reversible (catalysed by the same enzyme during gluconeogenesis) except for steps 1 and 3 in which the gluconeogenic reactions are catalysed by glucose-6-phosphatase and fructose-1,6-bisphosphatase, respectively. Fructose-1,6-bisphosphatase catalyses the reverse reaction to phosphofructokinase in glycolysis, and it was significantly increased in the ENT whereas phosphofructokinase was significantly decreased in this brain region. This change may imply that gluconeogenesis was favoured in this brain region, but this pattern was not seen in other brain regions. Supporting this observation, Go-enrichment analysis detected increased abundance of proteins involved in “cellular carbohydrate biosynthetic processes” in ENT only. This may be, in part, associated with altered “D-myo-inositol” related processes as reported by IPA in ENT. As glycolysis and gluconeogenesis share most of the enzymes, and only a few were altered in abundance, it is hard to infer with certainty which pathway is dominant within the brain at this stage.

Elevated glucose levels also appeared to have activated other glucose-clearance pathways within the AD brain, namely the pentose-phosphate pathway and the polyol pathway. As discussed in Chapter Three, the most striking feature of the metabolic disturbance was the strong elevation in the polyol pathway metabolites in all seven brain regions of AD brain. In line with this finding, significant elevation in sorbitol dehydrogenase was observed in all three regions in AD brain. However, the rate-limiting enzyme of the polyol pathway aldose reductase was only significantly elevated in the CB (**Figure 4-7**). Elevated aldose reductase may explain the relatively smaller build-up of glucose in CB compared to the other brain regions. To the best of our knowledge, this is the first time that polyol pathway activation has been reported in the context of AD. As increased flux through the polyol pathway is a well-established molecular mechanism driving tissue damage in diabetes [227], our finding provides strong support for a link between AD and diabetes.

Also consistent with the general increase in pentoses as observed in the GC-MS study (Chapter Three), all pentose-phosphate pathway enzymes that were altered significantly, showed increased abundance. Furthermore, proteins that provide direct links between glycolysis and the pentose-phosphate pathway were also increased (where statistical significance was reached). This finding is consistent with the previously reported activation of the pentose-phosphate pathway in those patients with mild cognitive impairment that progressed to AD [211]. The changes in enzymes involved in the pentose-phosphate and polyol pathways were most significant in CB: this finding is consistent with the pathway analysis which indicated increased “pentose-phosphate shunt” and “pentose metabolic process” in CB.

Decreased levels of the glucose transporters GLUT1 and GLUT3 have previously been associated with defective glucose uptake in AD brain [335]. However in this study, only GLUT1 showed significant decrease and then only in CB. Levels of GLUT3 were not significantly altered in any of the brain regions examined. The decreased GLUT1 levels in CB may be associated with the decrease in low-density-lipoprotein receptor-related protein 1 (LRP1), which plays a role in receptor-mediated endocytosis associated with protein signalling: loss of LRP1 expression has previously been reported in AD brain, and LRP1-deficiency was shown to impair insulin signalling and reduce glucose transporters [336]. This state may also underlie the smaller fold-elevation of glucose in CB compared to other brain regions.

Glycogen synthesis and degradation are further important aspects of glucose metabolism. They both occur in the brain, probably mainly in astrocytes. Here we found decreased levels of glucan branching enzyme (also known as glycogen branching enzyme) and of glycogen synthase kinase. The former plays a critical role in glycogen synthesis, and glycogen synthase kinase regulates glycogen synthesis by phosphorylating glycogen synthase. These findings are consistent with impaired brain glycogen synthesis. On the other hand, glycogen catabolism may be increased in the CB, based on the finding of increased glycogen phosphorylase, the key enzyme in glycogenolysis.

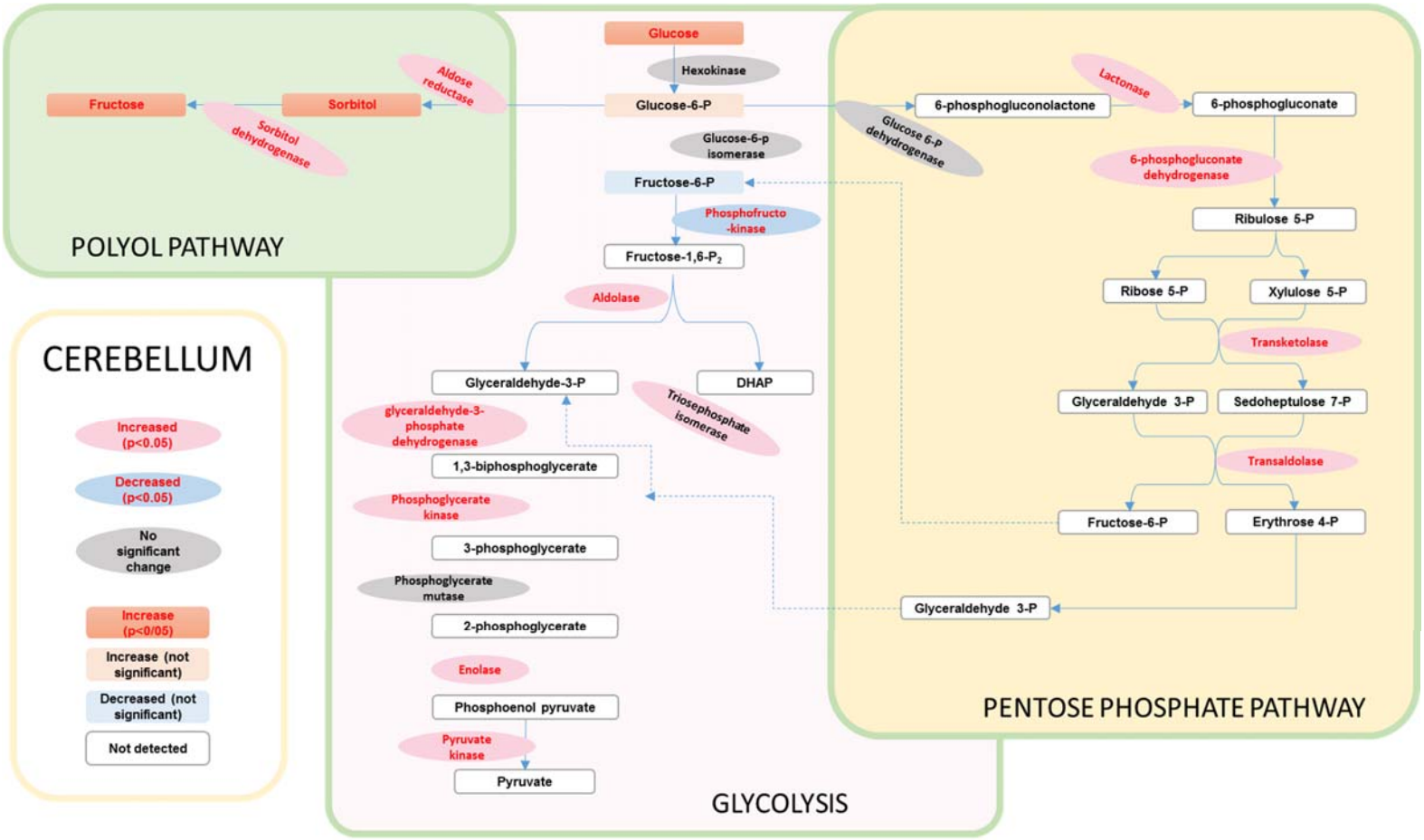

Figure 4-6 Glucose metabolism in CB of AD brain

In line with the accumulation of glucose, major changes in glucose-clearence pathways were present in the AD brain. With the exception of phosphofructokinase, altered glycolytic enzymes were all increased in abundance. Elevated glucose levels also appeared to have activated the pentose-phosphate pathway and the polyol pathway; enzymes involved in pentose-phosphate and polyol pathways were significantly elevated. Consistently, accumulation of polyol pathway metabolites (sorbitol and fructose) and pentoses were detected in the AD brain (as discussed in Chapter Three). Abbreviations: DHAP, dihydroxyacetone phosphate.

Taken together, our results indicate that diminished glucose transporter activity is unlikely to be the main cause of decreased glucose uptake in AD brain. Rather, a lowered trans-cell membrane glucose concentration gradient due to intracellular glucose accumulation is likely to be the key underlying mechanism. Glucose is taken up into cells via facilitated diffusion, driven by the transmembrane concentration gradient. If the intracellular free glucose levels rise, then the transmembrane gradient falls, causing a decline in the motive force driving glucose uptake into the cell. If so, the decline in the facilitated diffusion of glucose is the proximal mechanism of decreased glucose uptake into brain cells in AD.

4.4.1.2. Lipid metabolism

Altered lipid metabolism is important in CNS disorders as the brain not only has high lipid content but also high oxygen consumption, rendering it particularly susceptible to oxidative damage from lipid oxidation/peroxidation [337]. The intriguing fact that hydrogen-rich fatty acids are used poorly as a brain fuel has been suggested to be associated with their detrimental effect on mitochondrial integrity through ROS production [338].

In this study, levels of fatty-acid synthesising enzymes and fatty-acid transporting carnitine were decreased in the AD brain, particularly in HP and ENT. This is indicative of decreased availability of fatty acids as an energy source in the AD brain. However, enzymes catalysing FAO showed a less distinctive pattern of change. Enzymes involved in FAO were in general up-regulated in HP and ENT but down-regulated in CB. Similarly, enzymes involved in FAO or unsaturated fatty acids were elevated in HP and ENT, but not CB. Consistent with this observation, “Fatty Acid β-oxidation III” was suggested by IPA to be altered significantly in HP and ENT. Changes in enzymes catalysing oxidation of odd-numbered saturated fatty acids observed here were insufficient to enable recognition of a trend. In contrast to the global reduction in fatty acid synthesis and transport, FAO is likely to be up-regulated in HP and ENT while being down-regulated (or relatively unaffected) in CB.

The observed decrease in the glycerolipid metabolising enzymes (diacylglycerol lipase alpha and acylglycerol kinase) in CB may be associated with the elevated levels of DGs in the CB (discussed in Chapter Three). Decreased glycerolipid lipase activity can decrease fatty acid production and might hence explain the diminished levels of FAO enzymes in CB specifically. In HP and ENT, release of fatty acids from glycerolipid may supply enough substrate for FAO activity. In support of FAO-associated oxidative stress, the pathway analysis identified an elevation in various processes related to oxidative stress in HP and ENT, especially the response towards hydrogen peroxide. Therefore, CB may have been subjected to less oxidative stress in comparison with the other two regions (**Figure 4-8**).

Phospholipid is the major component of all cell membranes and various classes of phospholipids have been shown to be altered in the AD brain [339]. In our metabolomics study, increased lyso-phospholipids and decreased levels of phospholipid containing long-acyl chains or alky/plasmalogen substituents were consistently observed in heavily affected brain regions (HP and ENT) whereas the changes were

ambiguous with mixed trends in the least affected region (CB) (details in Chapter Three). The proteomic study on the other hand, showed neither a clear global trend nor a region-specific effect for the enzymes involved in phospholipid metabolism. CB was the only brain region exhibiting robust changes in proteins of this category (three proteins up-regulated, four down-regulated and further three trending to be decreased). This is consistent with CB showing both increased and decreased levels of phospholipids as detailed in the previous chapter.

The observed increases in the levels of phospholipid scrambling proteins in HP and ENT is consistent with a disturbed process of phospholipid migration across the membrane and disturbed plasma membrane phospholipid symmetry. Although scrambling proteins were not altered in CB, P4-ATPase flippase complex proteins, involved in the translocation of phospholipid through neuronal membranes [323], were increased in this region. Therefore, phospholipid transport may also be altered in CB, albeit through a different mechanism from that in HP and ENT. Furthermore, phospholipid-scrambling-mediated changes in membrane phospholipid symmetry are critically involved in the blood coagulation in conjunction with fibrin [340]. Therefore, the observed increase in phospholipid-scrambling proteins may be part of the activated coagulation system as suggested by the pathway analysis.

Sphingolipids, also known as glycosylceramides, are lipids containing sphingoid bases as their backbone attached to aliphatic amino alcohols. The best studied sphingolipids in the brain include ceramide and sphingomyelin. Sphingolipids are particularly abundant in the myelin sheath around the axon of the neurons and, not surprisingly, impaired sphingolipid metabolism is associated with neurodegeneration, as reported in AD [280]. Sphingolipid metabolism not only influences the membrane homeostasis, but also generates intermediates such as sphingosine, ceramide, and sphingosine-1P which are bioactive molecules involved in cellular signalling [341,342]. In the HP, the observed increase in proteins involved in sphingosine metabolism and signalling is in line with the change in metabolite levels, such as sphingosine-1P (as discussed in detail in Chapter Three).

4.4.1.3. TCA cycle

Pyruvate dehydrogenase links glycolysis to the TCA cycle by converting pyruvate to acetyl-CoA. The significantly decreased levels of PDHC components observed in this study are consistent with previously reported decreases in PDHC activity found in AD brain by both immunochemical and molecular studies [343,344]. In accord with decreased PDHC components, IPA indicated altered “Acetyl-CoA Biosynthesis I” in all three brain regions.

Interestingly, in CB (but not in HP and ENT), enzymes involved in conversion and/or interconversion of pyruvate to malate and lactate (malic enzyme, malate dehydrogenase, and lactate dehydrogenase) were increased in abundance, possibly as a compensatory mechanism in response to PDHC defects (shown in **Figure 4-7**).

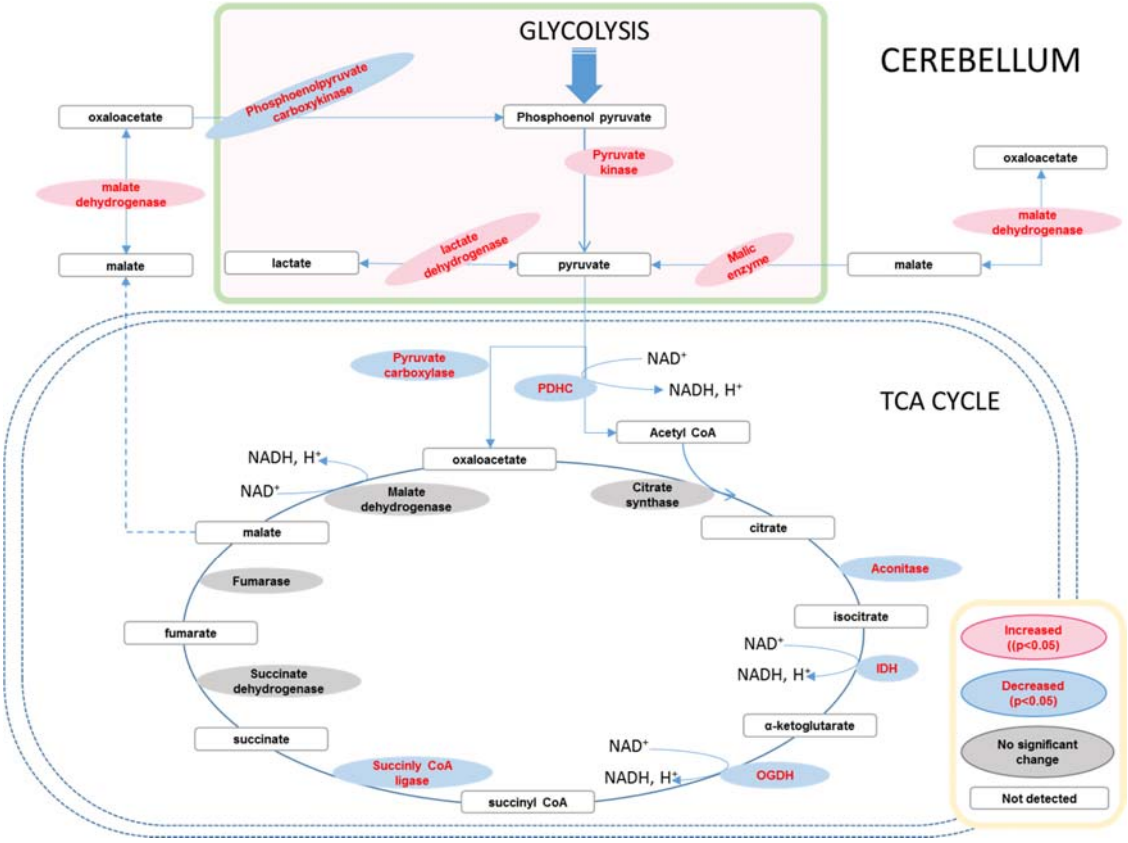

Figure 4-7 TCA cycle in CB of AD brain

Pyruvate dehydrogenase complex (PDHC) converts pyruvate to acetyl-CoA and links glycolysis to the TCA cycle. In the CB of AD brain, PDHC and four enzymes of the TCA cycle (aconitase, isocitrate dehydrogenase (IDH), 2-oxoglutarate dehydrogenase (OGDH), and succinyl-CoA ligase) were decreased. In contrast, enzymes involved in the generation of pyruvate (malic enzyme, malate dehydrogenase, pyruvate kinase and lactate dehydrogenase) were increased in abundance. Abbreviations: PDHC, Pyruvate dehydrogenase complex; IDH, isocitrate dehydrogenase; OGDH, 2-oxoglutarate dehydrogenase.

Acetyl-CoA enters the TCA cycle and, via a series of sequential enzymatic reactions, generates NADH which then feeds into OxPhos to support ATP production. In all three brain regions, we found significantly decreased levels of isocitrate dehydrogenase, 2-oxoglutarate dehydrogenase, and succinyl-CoA ligase (Figure 4-7). The oxoglutarate dehydrogenase complex (OGDC) catalyses the key step (and arguably rate-limiting step) of the TCA cycle. Decreases in subunits making up OGDC, combined with decreased PDHC across all three brain regions, suggest a global impairment of TCA cycle flux in AD brain. In line with this, both pathway analyses indicated compromised “TCA cycle” in HP and CB. A disrupted TCA cycle would consequently lead to decreased electron supply (i.e. reduction in NADH/FADH2 level) to the ETC for ATP production, with consequent lowering of ATP availability that could, for example, lower rates of glycolysis by impairing the necessary, ATP-dependent substrate-levels phosphorylation events.

4.4.1.4. Electron transport chain and mitochondrial oxidative stress

Neurons have especially high energy demands compared to most other cell types and are particularly dependent on efficient ETC function [345]. Mitochondria consume large amounts of oxygen during OxPhos and when electrons leak from the ETC, superoxide anions ($O_2^{-\bullet}$) and consequently other ROS are generated [346]. Therefore, mitochondrial energy production is closely linked to oxidative stress associated with mitochondrial ROS production.

Complex I is the point of entry in the mitochondrial ETC for NADH-reducing equivalents, and it behaves as an adjustable pacemaker of respiratory ATP production in human cells [347]. In this study, the abundance of complex I proteins was strikingly decreased in the CB of AD brain. Although there were alterations in the levels of some complex I proteins also in HP and ENT, this was not comparable to the consistency observed in CB. Decreased levels of these proteins would severely affect the electron transport from NADH to the next ETC complex. Complex III and IV proteins were not altered in HP and ENT. However in CB, decreased abundance of two and three proteins were observed in complex III and IV respectively. Complex II and complex V were relatively unaffected in the AD brain (**Figure 4-8**).

In AD brain, OxPhos defects have been described as a generalised depression in the activity of ETC complexes, most markedly in complex IV activity [348]. Defects in ETC were also reported in Parkinson's disease, where complex I activity was found to be significantly decreased, along with the activity of complex II and IV which were less strikingly impaired [349]. Our study suggests severely compromised ETC system in the CB of AD. However in contrast to described depression of ETC activity centred around complex IV [348], our results showed striking depression of the proteins that make up complex I. The profound defect in complex I, accompanied by less significant changes in complex III, IV, and V in CB of the AD brain is similar to the ETC defect as described in Parkinson's disease [349].

Impaired ETC has been shown to increase generation of ROS in cells that are ETC-inhibited and contain damaged mtDNA [350]. Oxidative stress caused by mitochondrial ROS is often considered an underlying cause of neurodegenerative diseases such as AD and Parkinson's Disease [351]. During mitochondrial respiration, redox enzymes such as NADPH oxidase can generate superoxide and play an important role in cellular stress response-related signalling [352]. Superoxide can also be converted to hydrogen peroxide spontaneously or through the action of superoxide dismutase (SOD) and subsequently, hydrogen peroxide can be converted into water and oxygen gas by catalase [353]. In this study, we observed a general increase in the levels of NADPH oxidase, cytoplasmic SOD1, mitochondrial SOD2, extracellular SOD3, and catalase (most significantly in HP and ENT). Collectively, these results are consistent with increased ROS production in the AD brain, particularly in the HP and ENT. We also found increased redox-active proteins such as SH3 domain-binding glutamic acid-rich-like proteins, and peroxide reductase glutathione peroxidase-1, which play important roles in modulating redox-dependent cellular responses in the mitochondria [354], which finding is further consistent with increased oxidative stress in the AD brain.

Increased outer mitochondrial membrane monoamine oxidase, MAO-B, in HP and ENT is also consistent with the notion of increased ROS production in these two brain regions. MAO-B plays an important role in dopamine degradation [355] and hydrogen peroxide produced during the oxidative deamination of catecholamines was previously suggested to contribute to neurodegeneration in AD [346].

A family of thiol-dependent peroxidases known as peroxiredoxins (PRDXs) is able to reduce hydrogen peroxide, alkyl hydroperoxides, and peroxynitrite [356]. We found all PRDXs, except for PRDX-5, to be increased in the AD brain. PRDXs that are increased in this study mainly act as redox sensors in hydrogen peroxide-dependent intracellular signalling [356], suggesting response towards increased ROS in the AD brain. The decreased PRDX, PRDX-5, is the only member of the family that acts mainly as a cytoprotective antioxidant enzyme. PRDX5 uses cytosolic thioredoxin 1 or mitochondrial thioredoxin 2 as physiologic reductants to reduce alkyl hydroperoxides or peroxynitrite with high rate constants, whereas the reaction with hydrogen peroxide is slower [356]. In this study, thioredoxin 1 was increased whereas the mitochondrial thioredoxin 2 and thioredoxin reductase 2 were decreased. These again imply compromised anti-oxidative capacity in mitochondria. Decreased oxidation resistance protein 1, which functions in protection against oxidative damage [357], and NmrA-like family domain-containing protein 1, which reduces nitric oxide production [358], further suggest impaired oxidative stress defence in the AD brain.

Hydroxyacylglutathione hydrolase (glyoxalase II) and DJ-1 protein (glyoxalase III) catalyse the conversion of methylglyoxal, considered a toxic compound [359], into lactate [359]. In this study, we observed significant elevation of both glyoxalase enzymes in the CB, possibly reflecting an increased need for clearance of glyoxal, which has been suggested to disrupt the energetic metabolism in the brain [360]. Therefore, the increased glyoxalase system may act as a mechanism against disrupted energetic metabolism associated with the glyoxal level, in CB.

In the mitochondria, defects in OxPhos lead to the accumulation of ROS, which in turn, further damages proteins critical for maintaining proper OxPhos and TCA cycle function. Due to the close proximity of mitochondrial matrix components (TCA cycle enzymes) to the ROS-producing complexes of the ETC in the inner membrane of mitochondria, major oxidative damage can occur to matrix- resident proteins. For example, the TCA enzyme aconitase is especially prone to oxidative damage [345]. This is a vicious cycle that damage mitochondrial energy production.

Mitochondrial dysfunction has been suggested to occur before the onset of memory deficit and neurological phenotype, and also before the formation of amyloid deposits in a mouse model of familial AD [361]. Our observations support this idea in the sense that the most dramatic decrease in ETC complex proteins was apparent in the CB (at the time of patient's death), the brain region with the least neuropathology and volumetric loss. Mitochondria also play a key role in apoptosis [362,363].

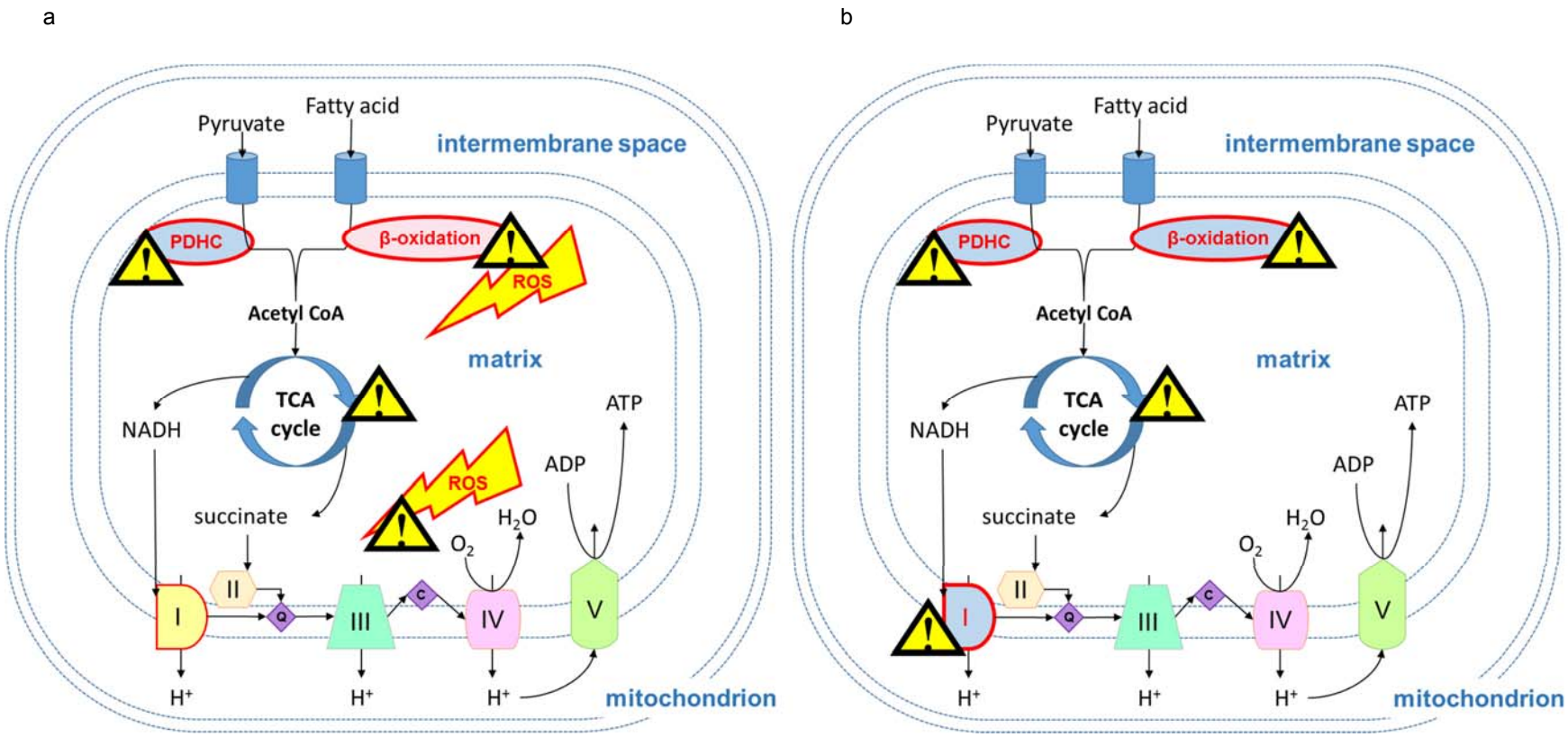

Figure 4-8 Mitochondrial energy production in AD brain.

Acetyl CoA derived from carbohydrate and fat (via pyruvate metabolism and β-oxidation, respectively) is transformed into cellulcar energy (ATP) through the TCA cycle and electron transport chain (ETC) in the mitochondria. Diminished pyruvate metabolism and impaired TCA cycle were common features of all brain regions in the AD group. (a) HP and ENT of AD brain exhibited elevated β-oxidation and normal ETC function, both of which may contribute to mitochondrial production of reactive oxygen species (ROS). (b) CB of AD brain exhibited decreased β-oxidation and impaired ETC function resulting from severe reduction in Complex I componenets. Overall, CB is likely to be subject to limited ROS-related insults when compared to HP and ENT. Abbreviations: PDHC, pyruvate dehydrogenase complex; ROS, reactive oxygen species; exclamation marks, severely affected; thunderbolts means, under ROS-related insult.

Therefore, this study provides further evidence that the mitochondrial deficits may occur prior to the loss of neurons through apoptosis and subsequent progression to brain atrophy in the brain of AD patients.

Another interesting aspect of brain energetics is the "neuronal Warburg effect" where energy-demanding neurons switch from OxPhos to glucose fermentation for the benefit of limiting ROS accumulation, at the expense of ATP yield [364]. Glucose fermentation ends with the conversion of pyruvate to lactate instead of the TCA cycle substrate acetyl-CoA, which relies on OxPhos for energy production. GC-MS results showed significantly increased lactate levels in HP and MCx, but not other brain regions. The proteomic study showed decreased abundance in PDHC proteins in all three brain regions and markedly down-regulated ETC proteins in CB. While this is consistent with the neuronal Warburg effect hypothesis, diminished OxPhos was more profound in CB. CB was also the only brain region to show increased abundance of lactate dehydrogenase. The fact that CB, the "unaffected" region in AD, has the most severely damaged OxPhos apparatus may be explained by a phenomenon called the "inverse-Warburg effect". Demetrious and Simon hypothesised that natural selection favours neurons with more OxPhos activity in an environment of limited energy substrates such as in AD. However, these "superior" neurons eventually die from oxidative stress resulting from OxPhos-associated ROS production [365]. OxPhos was less affected in HP and ENT compared to CB, which may imply more neuronal death in HP and ENT compared to CB, and hence more volumetric loss (**Figure 4-8**). However, this is only one aspect among many that contribute towards oxidative stress in AD, such as accumulation of Aβ. The global increase in enzymes responsive to oxidative stress, such as NOX, SOD, catalase, and glutathione peroxidase 1 proteins indicate the presence of ROS defence mechanism across different brain regions.

4.4.2. Amino acids and neurotransmitters

Amino acid homeostasis is crucial for the maintenance of neurotransmitters such as glutamate, which is believed to be critically involved in the pathogenesis in AD [366]. In the AD brains examined herein, we observed significant changes in proteins involved in the metabolism and regulation of BCAA, the amino group donors for glutamate synthesis in the brain [328].

We found proteins involved in BCAA catabolism (aminotransferase, various dehydrogenases, and carboxylase) to be decreased in the AD brain, most significantly in HP and CB. Proteins of branched-chain alpha-ketoacid dehydrogenase complex, the most important regulatory complex in BCAA catabolism [367], were significantly decreased (lipoamide acyltransferase, dihydrolipoyl dehydrogenase, and 2-oxoisovalerate dehydrogenase α and β). This was consistent with the IPA result showing "Branched-chain α-keto acid dehydrogenase complex" to be significantly altered in HP and CB ($p=0.02$ and $p=0.0009$ respectively).

Increases in the valine metabolising enzyme 3-hydroxyisobutyrate dehydrogenase in ENT and CB were also observed while the level of valine was significantly decreased in CB only, suggesting increased

valine metabolism. The pathway analysis also suggested altered “Valine degradation I” in CB only (p=0.019).

Methylcrotonyl-CoA carboxylase (MCC), consisting of α and β subunits, is critical in leucine metabolism [368]. In the HP, we found MCCC1 (α subunit) to be decreased whereas MCCC2 (β subunit) increased, suggesting disturbance in leucine metabolism in this brain region.

Taken together, AD brain appears to have impaired BCAA catabolism/synthesis, which may affect the glutamate level in the brain.

Proteins involved in the metabolism/synthesis of glycine, serine and threonine were mostly decreased in the CB, including aminomethyltransferase, serine hydroxymethyl transferase 2 (mitochondrial) and threonine synthase-like 1. However, no significant changes in pathways related to these amino acids were detected.

The Saccharopine pathway serves as a minor lysine degradation pathway in adult mammalian brain [369]. Proteins of this pathway were increased in HP and pathway analysis showed change in “Lysine degradation II” (in HP only, p=0.0097). Consistent with this finding, lysine levels were significantly decreased in HP, but not any other brain regions (Chapter Three). Combined observation suggests increased lysine degradation in HP.

The essential amino acid tryptophan is not only a precursor of serotonin but is also degraded to several other neuroactive compounds, including kynurenic acid, 3-hydroxykynurenine, and quinolinic acid. The synthesis of these metabolites is regulated by an enzymatic cascade, known as the kynurenine pathway [370]. Proteins of the kynurenine pathway (kynurenine aminotransferase III and kynurenine-oxoglutarate transaminase 1) and tryptophan metabolising N-acetylserotonin O-methyltransferase-like protein were decreased in the AD brain (ENT particularly), consistent with altered tryptophan metabolism. In line with this, we found strongly elevated tryptophan in all brain regions except for CB (Chapter Three). Although “Tryptophan degradation X” was only detected to be altered in HP in the pathway analysis, it is most likely to be affected in both HP and ENT (less likely in CB) considering both proteomics and metabolomics results takent together.

Nitrogen homeostasis has been discussed in the context of the urea cycle (**Figure 4-9**). Protein breakdown and amino acid catabolism generate nitrogen that enters the urea cycle in the form of ammonium ion or glutamate. Two critical enzymes of the urea cycle were decreased in HP: ornithine aminotransferase and carbamoyl-phosphate synthase. In the brain, arginine and ornithine are converted to glutamate and GABA, the major excitatory and inhibitory neurotransmitters, and the key enzyme for the Arg→Orn→Glu→GABA pathway is ornithine aminotranferase [371]. Decreases in carbamoyl-phosphate synthase and its allosteric effector N-acetylglutamic acid (Chapter Three) also imply compromised urea cycle and transdeamination routes, which may consequently lead to glutamate accumulation (details as described in Chapter Three). Glutaminase (GLS), an enzyme that catalyses the hydrolysis of glutamine to yield glutamate and ammonia, was also decreased in all AD brain regions studied, and may be directly related to the dysregulated glutamate level in the AD brain (**Figure 4-9**).

Increased glutathione transferase zeta 1, which catalyzes the degradation of both phenyalanine and tyrosine, was observed across three brain regions. BH4 is an essential cofactor for the degradation of aromatic amino acids (such as phenylalanine, tyrosine, and tryptophan) and synthesis of monoamine neurotransmitters such as serotonin and dopamine [372]. Proteins that participate in the synthesis of BH4 (including sepiapterin reductase and pterin-4-alpha-carbinolamine dehydratase) were increased in all three brain regions. IPA suggested significantly altered “Tetrahydrobioproterin Biosynthesis I” and “Tetrahydrobioproterin Biosynthesis II” pathways. Combined with the observed elevations in phenylalanine tyrosine, and tryptophan in the AD brain (Chapter Three), increased abundance of proteins involved in aromatic amino-acid degradation strongly suggests increased degradation of these amino acids. This may also represent a compensatory mechanism to restore levels of neurotransmitters; lowered levels of serotonin and dopamine have been reported in AD brain [272,273].

Disturbances in neurotransmitters may arise from altered degradation process in AD. Glutamate decarboxylase is the main type of GABA-producing enzyme and decreased levels of two glutamate decarboxylase isoenzymes were suggested to lead to diminished synthesis of neurotransmitter and GABA function [373]. In line with this, we found a decrease in both glutamate decarboxylase 1 and 2, in the CB of AD brain, which suggests diminished glutamate degradation and concomitant GABA production in this region. Consistently, IPA identified significantly altered “Glutamate degradation III, via 4-aminobutyrate” in CB. Furthermore, 4-aminobutyrate aminotransferase, a key enzyme in GABA degradation [374], and amine oxidase A (MAO A), a major neurotransmitter-degrading enzyme in the CNS [375], were both increased in the CB of AD brain. Increases in these enzymes can lead to increased GABA degradation, which may further exaggerate the decrease in GABA level caused by reduced glutamate decarboxylation in CB.

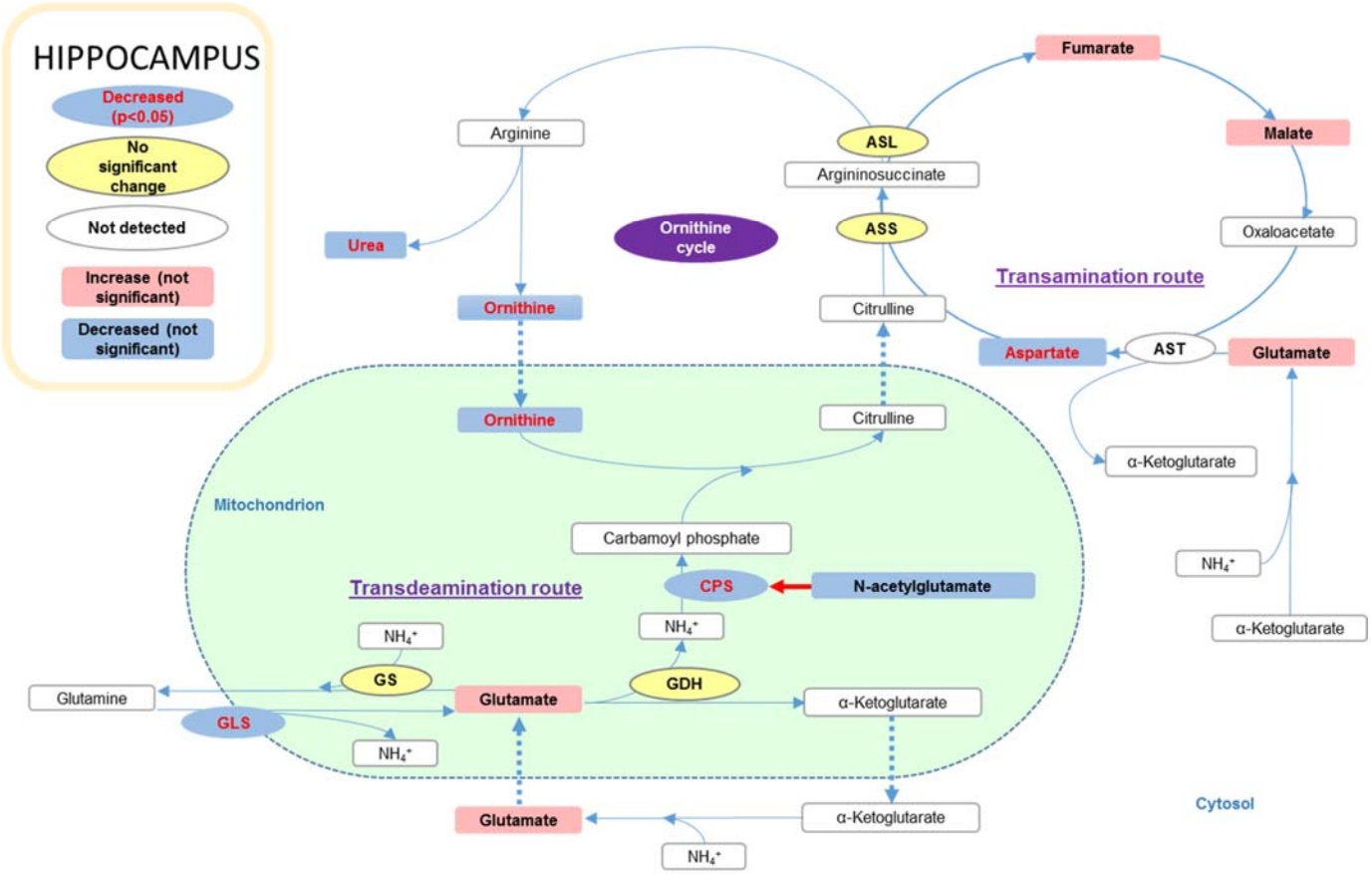

Figure 4-9 Nitrogen homeostasis in HP of AD brain

Protein breakdown and amino acid catabolism generate nitrogen that enters the urea cycle in the form of ammonium ion or glutamate. Nitrogen homeostasis is maintained through transdeamination and transamination routes. In the HP of AD brain, carbamoyl-phosphate synthase (CPS) and its allosteric effector N-acetylglutamate were decreased. At the metabolite level, there was significant decrease in aspartate and ornithine while glutamate appeared to accumulate in HP. Combined, these suggest impairment of key enzymatic steps in both transdeamination and transamination routes. Abbreviations: CPS, carbamoyl-phosphate synthase; GLS, glutaminase; GS, glutamine synthetase; GDH, glutamate dehydrogenase; ASL, argininosuccinate lyase; ASS, argininosuccinate synthase; AST, aspartate transaminase.

Overall, the changes in GABA-receptor-related proteins were not particularly marked and none of the pathway analyses detected significant alterations in processes related to GABA receptors. This may be related to the observed global decrease in GABA abundance in the AD brain (Chapter Three). However, consistent with the detected changes in GABA-producing and -degrading enzymes, significant changes in GABA receptors were more apparent in the CB, where GABA receptor subunit alpha-6 and GABA type B receptor subunit 1 were decreased, while GABA receptor-associated protein-like 2 was increased. Changes in glutamate receptors were again only apparent in the CB. Significant decreases in four glutamate receptors may underlie the altered "Glutamate Receptor Signalling" identified by IPA in CB.

In summary, this result is consistent with a severe imbalance between glutamate and GABA especially in the CB of late stage AD brain. Significant pathological effect may arise from this imbalance, combined with altered glutamate receptor signalling.

4.4.3. Cell cycle: transcription and translation

4.4.3.1. Transcription and pre-mRNA processing

The pathway from gene activation in the nucleus to mRNA translation and decay at specific locations in the cytoplasm is both streamlined and highly interconnected [376]. Replication of the eukaryotic chromosome requires synthesis of not only DNA, but also the histone proteins needed to package the newly replicated DNA into nucleosomes and chromatin. Total cellular levels of histone mRNA parallels the rate of DNA synthesis [377].

In this study, an overall increase in histone protein levels combined with increases in proteins associated with nucleosome and chromatin structure suggests possible increase in cellular DNA content. Such change was echoed in the pathway analysis; in HP and ENT, proteins involved in "chromatin assembly", "chromatin assembly or disassembly", "nucleosome organization", and "protein-DNA complex subunit organisation" were identified as increased. In HP and CB, the category of proteins involved in "nucleosome assembly" was increased. In HP only, proteins participating in "DNA conformation change", "DNA packaging", "chromatin organization" and "protein-DNA complex assembly" were also ientifed as increased in abundance.

Proteins that catalyze the methylation, acetylation and deacetylation of histones are known to epigenetically modify chromatin structure and thus regulate gene expression [378,379]. Histone-lysine N-methyltransferase SETD3 and SETD7, and protein arginine N-methyltransferase 1 can catalyze methylation of histones and act as transcriptional activators [380-382]. These three proteins and histone deacetylase 6 were all decreased in abundance where statistical significance was reached, consistent with impaired transcriptional regulation through histone modification in AD brain. In line with this finding, proteins involved in transcriptional activation and elongation, as well as those that participate in DNA repair, were decreased in abundance. Proteins of the *Drosophila* behaviour/human splicing (DBHS)

family, including PTB-associated splicing factor (PSF), non-POU domain-containing, octamer-Binding (NONO), and paraspeckle component 1 (PSPC1), play roles in transcriptional and posttranscriptional gene regulatory functions, as well as DNA repair. Additionally, mammalian DBHS proteins associate with the architectural long noncoding RNA NEAT1 to form paraspeckles, which are subnuclear bodies that alter gene expression via the nuclear retention of RNA [383]. We found both NONO and PSPC1 to be significantly decreased in AD (significantly in HP and ENT). Other proteins involved in transcription activation, CCR4-NOT transcription complex subunit 1, transcriptional activator protein Pur-alpha, and nucleolar transcription factor, were all decreased in abundance in CB of AD brain. Generally decreased elongation factors are further consistent with decreased transcription. Notably, proteins that act as transcriptional repressors were mainly increased in the AD brain (e.g. TSC22 domain family protein 1 and pre-B-cell leukaemia transcription factor-interacting protein 1), which are also consistent with lowered transcriptional activity in the AD brain.

RNA helicases participate in all biological processes that involve RNA, including transcription, splicing and translation, and they are classified into families such as DEAD-box helicase (DDX) and DEAH- box helicase (DHX) families, based on the sequence of the helicase domain [384]. Four DDX helicases and two DHX helicases were detected in this study, mostly decreased in the AD brain. These changes were again reflected in the pathway analysis, where proteins involved in the pathways of “DNA-templated transcription”, “nucleobase-containing compound biosynthetic process” and “RNA biosynthetic process” were decreased in CB. IPA also detected significantly altered “Assembly of RNA Polymerase I Complex” in CB.

Overall, the observed pattern of increased DNA material with restricted transcription is suggestive of interphase in the mitotic cell-cycle. IPA detected altered “cell cycle: G2/M DNA Damage Checkpoint Regulation” in all three brain regions ($p<0.05$ in all regions). The Go-enrichment analysis showed that proteins involved in “cell cycle G2/M phase transition” and “G2/M transition of mitotic cell cycle”, were decreased in HP and ENT. In ENT, proteins involved in “cell cycle process”, “mitotic cell cycle”, and “mitotic cell cycle process”, were also decreased, which may be associated with impaired mitotic signalling, “RAN signalling”. Although entry to the mitotic phase appeared to be impaired, the reactivation of the cell cycle likely had a detrimental effect on neurons. Cell-cycle reactivation in mature neurons takes part in the activation of apoptotic processes and has been characterised as a neuropathological marker for AD [385].

4.4.3.2. Pre-mRNA processing and alternative splicing

Following transcription, pre-mRNA is further processed to yield mRNA (or pre-tRNAs to yield mature tRNAs). Pre-mRNA processing connects not only to transcriptional regulation but also to translation and mRNA decay [376]. We observed decreased abundance in proteins involved in pre-mRNA processing, including the heterogeneous nuclear ribonucleoproteins (hnRNPs). The hnRNPs are a complex and diverse family of RNA-binding proteins with multiple functions in the processing of heterogeneous nuclear RNAs into mature messenger RNAs [386]. Decreased hnRNP and pre-mRNA processing factors suggests impaired pre-mRNA processing in the AD brain.

Pre-mRNA splicing is a critical step in the posttranscriptional regulation of gene expression and is governed by the spliceosome. The spliceosome consists of four large RNA-protein complexes, called the U1, U2, U4/U6 and U5 small nuclear ribonucleoproteins (snRNPs) [387]. There are also five small nuclear RNA (snRNA) molecules, namely U1, U2, U4, U5, and U6 snRNA [388]. We found a general increase in snRNPs, snRNAs and associated splicing factors (including numerous serine/arginine-rich splicing factors) in all three regions of AD brain.

However, in contrast to the increase in spliceosome components, proteins involved in the assembly spliceosome (serine-threonine kinase receptor-associated protein, pre-mRNA-processing-splicing factor 8, and and U5 small nuclear ribonucleoprotein 200 kDa helicase) were decreased. Serine-threonine kinase receptor-associated functions in the pathway of snRNP biogenesis and is also a marker for the SMN complex, which is active in snRNP assembly [389]. Pre-mRNA-processing-splicing factor 8 occupies a central position in the catalytic core of the spliceosome, and mediates molecular rearrangements of spliceosomal proteins and snRNAs [390]. U5 small nuclear ribonucleoprotein 200 kDa helicase is a component of the U5 snRNP and U4/U6-U5 tri-snRNP complexes and involved in spliceosome assembly/disassemby and activation [391,392].

The observed increase in spliceosome components and decreased spliceosome assembly proteins suggest disrupted spliceosome assembly, and hence, defective splicing activity in the AD brain. Previously, a human brain-insoluble proteome in AD by mass spectrometry has revealed that multiple U1 snRNP subunits form cytoplasmic tangle-like structures in AD, accompanied by dysregulated RNA processing with accumulation of unspliced RNA species [393]. Furthermore, U1-70K knockdown or antisense oligonucleotide inhibition of U1 snRNP increased the protein level of amyloid precursor protein [393]. Our results indicate major defects in pre-mRNA processing and the splicing machinery, which may play an important role in production and aggregation of mis-spliced transcripts in the AD brain.

4.4.3.3. Translation

Processed mRNA is exported out of the nucleus for protein synthesis by ribosomes located in the cytosol, or attached to the ER. Ribosomal dysfunction has previously been associated with decreased protein synthesis, decreased levels of rRNA and tRNA, and increased RNA oxidation [329]. Ding and colleagues reported ribosomal dysfunction in the cortical areas (but not in CB) of subjects with mild cognitive impairment and AD, and they suggested that impairments in protein synthesis occur in the earliest stages of AD, possibly mediated by both altered ribosomal nucleic acids and the polyribosomal complex itself [329]. In this study however, the profiled changes occurred in tissue from patients with later stages of AD, with Braak scores of IV or above.

Synthesis of tRNA is critical for translation processes, as tRNAs contain the anticodon triplets of the genetic code and decreased in tRNA levels have previously been associated with impaired ribosomal function [329]. Here, widespread decreases in both cytoplasmic and mitochondrial tRNA synthesising proteins was observed, most consistently in CB. In line with severely compromised tRNA synthesis in

mitochondria, mitochondrial ribosomal proteins were also decreased in AD brain across all three brain regions. The decreased abundance of mitochondrial ribosomal proteins not only correlated well with that of the tRNA synthesising proteins, but also with that of the ETC complex proteins in a brain region-specific manner (CB being the most severely affected). This is not surprising as mitochondrial ribosomes are responsible for translating the 13 mRNAs for essential proteins of the OxPhos system [394]. The combined effect of decreased mitochondrial ribosomal proteins and tRNA synthesising proteins in the AD brain may be responsible for the overall defects in protein synthesis and the ETC activity.

Furthermore, 3-hydroxyacyl-CoA dehydrogenase type 2, a protein that is critical for tRNA maturation [395], was also strongly decreased in all brain regions. In line with this, the Go-enrichment analysis showed a decrease in “tRNA aminoacylation for protein translation”, “tRNA aminoacylation”, and “tRNA metabolic process” in CB. IPA analysis detected the affected process of “tRNA Charging” in both ENT and CB. Interestingly, in contrast to the severely affected mitochondrial ribosomal proteins, the levels of cytoplasmic ribosomal proteins were not affected to a marked extent in AD brain.

Apart from the compromised tRNA synthesis and ribosomal integrity, additional evidence supported impaired translational processes in the AD brain which included a general decrease in translation initiation factors and elongation factors. Decreased cold-inducible RNA-binding protein, a RNA chaperone that facilitates translation [396] also suggests inefficient translation. Furthermore, enzymes that cease translation processing were increased in the AD brain. Protein argonaute-2 (increased in ENT) is a component of the RNA-induced silencing complex with mRNA cleavage activity, and is the catalytic engine for gene silencing through RNA interference (RNAi) [397]. Ribonuclease UK114 is responsible for the inhibition of translation [398]. Increased levels of argonaute-2 and ribonuclease UK114 further indicate impairment in the translational process.

Taken together, the AD brain appears to have globally decreased translational capability and therefore, defective protein production. However, in contrast to the previous study [329], the most heavily affected region in this study was the CB.

4.4.4. Proteostasis

Defective proteostasis is generally thought to contribute to the neuropathogenesis since the most well described pathological hallmark of AD it the accumulation of misfolded proteins, intracellular neurofibrillary tangles made of misfolded hyperphosphorylated microtubule-associated protein tau, and extracellular depositions of amyloid plaques made up of misfolded and aggregated Aβ [330]. There are two systems that play pivotal roles in the quality control of proteins: chaperones that facilitate their proper folding and the ubiquitin-proteasome system (UPS) that mainly governs proper protein degradation [330].

4.4.4.1. Chaperones

Mitochondrial chaperones are critical for preventing harmful aggregation of redox-modified proteins within the mitochondria [399]. As mitochondria play key roles in energy production, the observed strong decrease in mitochondrial HSP75 across all three brain regions may have implications for several aspects of energy metabolism. Previously, HSP75-deficiency was associated with increased mitochondrial respiration and FAO, leading to accumulation of TCA cycle intermediates while suppressing glucose metabolism [400]. In this study, the decrease in HSP75 may be associated with the suggested increase of FAO in HP and ENT, along with impaired TCA cycle and glucose metabolism in all three regions of AD brain.

The sHSPs bind and prevent aggregation of misfolded proteins by transferring the proteins to larger HSPs with ATPase activity (such as HSP 70) for refolding [401]. We found increased sHSPs in the AD brain (HSPB1, HSPB6, and HSPB8), all of which were previously shown to be present in the brain constitutively [402]. It has been proposed that in response to cellular stress (such as the altered level of phosphorylated tau in AD), sHSPs can be over-expressed [402], presumably performing their function of transferring proteins to larger HSPs (such as HSP70) to prevent misfolded proteins from aggregating [401].

HSP70 and HSP90 proteins are ATP-dependent molecular chaperones that are critical for activation and stabilisation of a wide variety of proteins, many of which are involved in important cellular pathways [403]. Here, different HSP70 proteins showed differential changes in the AD brain: HPS70 1A/1B was elevated while HSP70 4L, 12A and 13 were decreased. The chaperone activity of HSP70 proteins is dependent on their ATPase activity, which is controlled by co-chaperones of the family of J-domain proteins [404]. J-domain proteins (DnaJ homologues) of different subfamilies also showed differential changes in the AD brain; subfamily A was increased while subfamilies B and C were decreased when only significant results were considered. Another HSP70-interacting protein family is the BAG family proteins, known to participate in stress response and apoptosis [405]. BAG3 and BAG4 are known to have anti-apoptotic roles via their interaction with HSP70 [406], BAG5 was shown to be induced by Aβ1-42 and suggested to have a neuroprotective effect [407]. Here we found BAG3 and BAG4 to be increased while BAG5 was decreased in the AD brain. HSP 70 binding protein 1 that binds and inhibits HSP70 [408], was decreased in CB. We suggest that there may be integrated regulation over various HSP70 proteins by J-domain proteins and BAG proteins under pathological conditions such as AD. However, how these HSPs and co-chaperones were coordinated during the changes remain uncertain.

We also found decreased HSP90 proteins and their co-chaperones in the AD brain, most strongly in HP and ENT. Small glutamine-rich tetratricopeptide repeat-containing protein is a co-chaperone that interacts with both Hsp70 and Hsp90 [409]. Both small glutamine-rich tetratricopeptide repeat-containing proteins, -alpha and -beta were decreased significantly in the AD brain. This was consistent with the pathway analysis showing decreased “de novo posttranslational protein folding” and “protein modification by small protein removal” in HP and ENT.

To summarise, although sHSPs were elevated, marked decreases in important HSP70 and HSP90 proteins with their associated co-chaperones would lead to decreased chaperone activity in the AD brain. Increased abundance of chaperones with anti-apoptotic effect (BAG3 and BAG4), along with decreased abundance of proteins mediating heat shock response (heat shock factor binding factor 1) and neuroprotective proteins (BAG5 and hypoxia up-regulated protein 1) possibly reflect increased response mechanisms towards apoptotic signals, loss of heat shock defence, and neuroprotective defence in the AD brain. Furthermore, decreased levels of the ER chaperones calreticulin and calnexin suggest impairment of the calreticulin/calnexin cycle, and possibly dysregulation of the glycoprotein quality control system in the AD brain [410].

Prefoldin is a chaperone that cooperates with cytosolic chaperonin CCT and plays an important role in folding of actin and tubulin [411]. The eukaryotic cytosolic chaperonin CCT is composed of eight different but homologous subunits, CCT1 to CCT8 [412]. Prefoldins and all eight CCT subunits were detected and most markedly decreased in HP, then ENT, and least affected in CB, suggesting there is a gradient in the severity of disruption in actin and tubulin folding. Consistent with the changes in chaperones described above, pathway analysis suggested decreased “de novo protein folding” in HP, decrease in various “cellular protein modification” processes in ENT, but no change in either protein folding/modification in CB.

4.4.4.2. Protein degradation

The UPS as the name suggests is composed of the ubiquitination system and proteasome system. Herein, we report disturbance of both systems in the AD brain. The proteasome plays an important role in maintaining neuronal homeostasis through regulation of cellular proteolysis; proteasomes not only degrade ubiquitinated proteins, but also oxidised, damaged and aggregated proteins [413].

The 26S proteasome, responsible for the majority of cellular proteolysis, is composed of the catalytic 20S proteasome and the 19S regulatory particle. Interestingly, of the proteins that were significantly altered in AD brain, those that belong to the 20S proteasome showed increased abundance whereas the 19S regulatory particle proteins showed decreased abundance. The change in 20S proteins were the most marked in CB while the change in 19S proteins were the most significant in ENT and CB. Proteasome-assembly chaperones and proteasome activator complex, both involved in the assembly of the 20S proteasome [332], were increased in the AD brain. Proteasome-associated protein ECM29 homologue, proposed to facilitate 26S transport to secretory compartments engaged in quality control and to other sites of enhanced proteolysis [414], was significance decreased. Taken together, these results suggest altered proteasome function characterised by: 1) increased 20S components and assembly proteins, and 2) decreased 19S components.

The neddylation-deneddylation pathway controls the selective ubiquitination of important cellular regulators targeted for proteolysis by the ubiquitin proteasome system [415]. During this process, cullin can be neddylated (activated) and transfer ubiquitin, or be deneddylated (deactivated) by COP9 signalosome complex (CSN) [415,416]. CSN is an eight-subunit complex that plays a regulatory role

towards cullin family proteins which target numerous cellular proteins for proteasomal degradation [417]. We found significantly decreased levels of cullin family proteins and CSN proteins in the AD brain. This fits well with an altered "Protein Ubiquitination Pathway" in all three brain regions, as suggested by IPA. Go-enrichment reported decreased "cullin deneddylation" and "protein deneddylation" in both HP and ENT. Interestingly, according to Go-enrichment, "regulation of protein processing" and "regulation of proteolysis" was increased in CB but not the other two regions, which may possibly represent a more regulated proteostasis in this brain region.

Previously, proteasomal inhibition has been proposed to contribute to neurodegeneration in AD, as both addition of Aβ peptide and exposure to oxidative stress were shown to inhibit proteasome activity (Markesbery, 1997; Mattson, 1997). When the production of misfolded proteins exceeds the capacity of chaperone-mediated refolding and UPS, the aggresome macroautophagy pathway plays a major role in sequestration and clearance of toxic protein aggregates [418]. In this study, one of the most markedly and consistently decreased protein families was that of the 14-3-3 proteins, which play an indispensable role in aggresome formation. 14-3-3 proteins recruit chaperone-associated misfolded proteins to dynein motors (significantly decreased in AD brain) for transportation to aggresomes, where they are degraded by lysosome-dependent macroautophagy [418]. In mammals, the 14-3-3 family contains seven isoforms and these proteins reside mainly in the synapses and neuronal cytoplasm [419]. The severe decrease in the entire family of 14-3-3 as seen in this study suggests that the aggresome macroautophagy pathway is highly likely to be compromised in the AD brain, along with other cellular processes involving 14-3-3. The 14-3-3 proteins have previously been suggested to be neuroprotective by preventing cell cycle re-entry and apoptosis though their interaction with substrate proteins [420]. Therefore, decreased 14-3-3 is consistent with the described pattern of change indicating cell cycle re-entry in previous paragraphs.

4.4.5. Aβ aggregation

Communication between neurons is achieved through information transfer along the length of their axons. Therefore, microtubule-based axonal transport governed by molecular motors, namely kinesins and dyneins, is crucial for maintaining neuronal viability and function [421]. Microtubules in the axon allow both retrograde and anterograde movements for transport of membrane-bound organelles; retrograde transport brings cargo back to the cell body and is believed to be mediated by dyneins. On the other hand, anterograde transport is facilitated by kinesins (Morfini, Pigino, Beffert, Busciglio, & Brady, 2002). Here, we detected decreased levels of kinesins, dyneins, and dynactins across all three brain regions of AD brain, with ENT being the most severely affect. This change suggests a severe disturbance in both anterograde and retrograde axonal transport in AD. Consistently, the pathway analysis flagged decreased "microtubule-based movement" in ENT and CB, and decreased "microtubule-based process" and "organelle transport along microtubules" in ENT.

There is accumulating evidence that Aβ accumulation in AD is associated with defective axonal transport of APP via the fast anterograde component [422]. Aβ is generated by the sequential action of two proteases, β-secretase and γ-secretase which cleave amyloid precursor protein (APP) [20]. In this

study, we found no marked change in APP levels overall. However, significantly elevated Aβ peptide levels were present in all brain regions. The degree of Aβ elevation was much higher in HP and ENT, compared to CB, which may be explained by the change in proteins involved in the regulation of APP processing. Integral membrane protein 2C serves as a negative regulator of Aβ peptide production and was suggested to inhibit the processing of APP by blocking its access to α- and β-secretase [423]. Reticulon-3 and -4 are negative regulators of β-secretase that inhibit enhanced processing of APP at the β-secretase site [424]. Decreases in these proteins may underlie the impaired negative regulation over APP processing at the β-secretase site and heavy accumulation of Aβ in HP and ENT particularly. In line with this, altered "Amyloid Processing" was detected in all three brain regions by IPA.

The relatively mild accumulation of Aβ peptide in CB, compared to HP and ENT, may also be related to the significantly increased ApoD and ApoE in CB. ApoE is involved in both clearance and degradation of Aβ in the brain, and it has been suggested that ApoD may play a compensatory role when ApoE function is compromised [425]. Increases in both ApoE and ApoD may be a compensatory mechanism (in CB) to clear increased Aβ levels in the AD brain. Pathway analysis has flagged the "Neuroprotective Role of THOP1 in AD" in only CB. Increased expression of the oligopeptidase thimet oligopeptidase 1 (THOP1) is believed to express a neuroprotective response to Aβ toxicity [426], further suggesting that CB exhibits compensatory mechanisms to respond to Aβ accumulation.

4.4.6. Inflammation

In AD, toxicity associated with aggregated Aβ was suggested to be mediated by pro-inflammatory cytokines derived from activated microglia *in vivo*. Aβ aggregates can trigger receptors that respond to pathogen-associated patterns and initiate immune responses [427]. However, unlike invasive pathogens, elevation of Aβ persists in AD and hence the immune response towards Aβ aggregation fuels a chronic reaction of the innate immune system. Cell-mediated immune mechanisms are also believed to be involved in the pathogenesis of AD, based on the ability of the immune system to generate antibodies against Aβ, that may promote removal of Ab from the brain [306]. Such chronic neuroinflammation was suggested to contribute to the degeneration and functional decline of neurons [427].

The consistent increase in complement factors observed in this study was in line with the Go-enrichment analysis showing increased "complement activation" and "complement activation, classical pathway" in all three brain regions. HP also exhibited increased "regulation of complement activation" and altered "Complement System" according to Go-enrichment and IPA, respectively.

Pro-inflammatory proteins involved in the acute phase response, namely alpha-1-acid glycoprotein 1 and 2, were significantly increased in the AD brain, consistent with both pathway analyses suggesting altered acute phase response (and signalling) in all three brain regions. According to Go-enrichment, "regulation of acute inflammatory response" was up-regulated in HP. Other pro-inflammatory molecules, serum amyloid A-1 protein and serum amyloid P-component were also increased, further suggesting general pro-inflammatory response in the AD brain.

The observed increase in alpha-2-macroglobulin, a humoral defence protein [428], and the consistently elevated immunoglobulin component proteins were again in line with the pathway analysis. Go-enrichment reported increased abundance of proteins involved in "humoral immune response mediated by circulating immunoglobulin" in all three brain regions, and "humoral immune response" in HP and ENT, "regulation of humoral immune response" in HP, and "immunoglobulin mediated immune response" in ENT. Similar pathways were not flagged in CB, probably due to the fact that fewer immunoglobulin component proteins reached significance in CB than in HP and ENT.

We found increased levels of proteins that participate in the innate immune response, including macrophage migration inhibitory factor and SAM domain and HD domain-containing protein 1 [429] [430], particularly in the HP and ENT of AD brain. Furthermore, the erythrocyte component haemopexin, which is known to activate macrophages and neutrophils [431], was also increased in HP and ENT. Our results are thus consistent with an increased innate immune response in the AD brain, particularly in HP and ENT. Pathway analysis identified altered "Dendritic Cell Maturation" and "B Cell development", and "Altered T cell and B cell Signalling in Rheumatoid arthritis" in HP of AD brain. In the ENT, increased "B cell mediated immunity" and altered "B Cell Receptor Signalling" and "4-1BB Signalling in T Lymphocytes" were detected. No adaptive immune response was flagged for CB.

In this study, we found increased erythrocyte components and proteins involved in sequestering haemolysis products (haemoglobin and haeme). Haemolysis results in release of haemoglobin and haeme that are sequestered by haptoglobin and haemopexin respectively [432], and both were increased in the AD brain. Haeme iron recycling following macrophage-mediated erythrocyte degradation is a major source of iron for erythropoiesis [433]. Serotransferrin, an iron-binding transport protein (which sequesters Fe^{3+} ions released by haeme degradation), was decreased in ENT while copper-containing ferroxidase ceruloplasmin was increased in all brain regions. These findings may be consistent with disrupted erythropoiesis, particularly in the ENT of AD brain.

We have also observed strongly elevated coagulation-related proteins in this study. Fibrinogen is cleaved by thrombin and polymerised to form fibrin, which provides structural network essential for clotting [434]. Fibrinogen alpha, beta, and gamma were all strongly increased in all three brain regions. In the HP, we further identified increased prothrombin, antitrhombin-III, coagulation factor XIII, and kininogen-1. In both HP and CB, IPA suggested altered "Coagulation System" and Go-enrichment suggested increased "regulation of response to wounding" and "platelet degranulation". Go-enrichment detected increased levels of proteins involved in "blood coagulation, fibrin clot formation" while IPA suggested altered "Intrinsic Prothrombin Activation pathway" and "Extrinsic Prothorombin Activation Pathway" in the HP. Our findings indicate global activation of coagulation processes in the AD brain and prothorombin activation in the HP.

Overall, inflammatory response and immune system appeared to be activated in all brain regions with decreases in proteins participating in antigen processing and presentation of peptide/antigen via MHC class II. Disrupted erythropoiesis and increased coagulation may also play a critical role in immune response via changes in blood components.

4.5. Conclusion

In this study, we have observed wide-spread metabolic defects in glucose metabolism in AD brain. The marked elevation in free glucose levels appeared not only to be associated with disruption of glycolysis, but also prompted activation of polyol pathway and pentose-phosphate pathway activity, most significantly in CB. Interestingly, our results suggested a possible increase in gluconeogenesis in ENT, but not other regions. Based on our observations, the glucose accumulation in the AD brain is likely the main underlying cause of decreased cerebral glucose uptake observed in AD patients.

Defects in other aspects of brain energetics were also apparent in the AD brain. FAO was elevated in HP and ENT, possibly contributing to more severe oxidative stress in these regions. This change may partially represent a compensatory mechanism to restore inefficient energy supply in these brain regions, although with detrimental effects in the long term. Phospholipid metabolism was also altered in AD; however, loss of membrane integrity and altered signalling may have been the major outcome of this, although contribution to altered energetics should not be overlooked.

We observed a global reduction in mitochondrial enzymes critically involved in energy production across all brain regions in this study. PDHC was decreased in all brain regions, presumably disrupting supply of acetyl-CoA as a consequence. Not surprisingly, the TCA cycle was also globally compromised. Interestingly, ETC function appeared to be most severely affected in CB. Decreased OxPhos in CB would result in relatively less OxPhos-associated oxidative stress when compared to HP and ENT. Together with the increased FAO-associated ROS production in HP and ENT, this provides further evidence that HP and ENT were subject to more extensive oxidative damage in AD.

The disturbance in BCAA catabolism was observed in HP and CB of AD brain. Increased levels of proteins involved tyrosine, phenylalanine, and tryptophan degradation and were consistent with the increase in these amino acids as shown in Chapter Three; this may represent a mechanism to compensate for loss of neurotransmitters such as dopamine and serotonin in AD brain. HP appeared to exhibit the most changes in amino acid metabolism and nitrogen homeostasis among the brain regions studied herein. Unexpectedly, severe imbalance between glutamate and GABA was apparent only in CB.

Increased histones and processes involved in nucleosome organisation and chromatin assembly were indicative of cell cycle reactivation. Although entry to the mitotic phase was apparently disrupted, the reactivation of the cell cycle in mature neurons is known to take part in apoptotic process and likely has a detrimental effect on brain structure and function.

Major defects in tRNA charging/translation processes were observed in AD brain, most significantly in the CB. This observation may be associated with relatively preserved protein folding and degradation systems in the CB. According to this study, chaperone activity was heavily impaired in HP and ENT, but not in CB. Consistently, UPS was compromised in HP and ENT. CB on the other hand, exhibited increased regulation towards regulation of protein processing and proteolysis.

Highly relevant to protein aggregation in the brain, defects in aggresome formation and associated clearance of harmful peptides (e.g. Aβ) were most likely present in all brain regions, based on our observation of remarkably consistent reductions in 14-3-3 proteins, which also implies severe dysfunction in related signalling processes. Defective axonal transport observed in this study further supports the hypothesis of Aβ aggregation and compromised neuronal function in the AD brain. The high degree of Aβ accumulation in HP and ENT may result from more severely impaired regulation of APP processing and axonal transport, along with lower capacity for Aβ clearance, when compared to CB.

Alterations in immune-response proteins and associated inflammatory proteins were observed in all brain regions: these included increased complement activation and acute-phase response proteins. However, alterations in antibody-mediated humoral response and adaptive immune response were more marked in HP and ENT. Presence of an adaptive immune response may represent long-standing immune assault (e.g. by aggregated Aβ) in the brain regions that are known to be affected by the disease first, such as HP and ENT.

In summary, AD brain exhibits global defects in glycolysis, pyruvate metabolism and the TCA cycle, aggresome formation and axonal transport. Furthermore, there were strong indications of cell cycle re-entry and immune response in all three regions of the AD brain. HP and ENT, which are known to be more severely affected by the disease process, showed signs of marked increases in FAO, a heavily impaired ubiquitin-proteasome system, defective regulation of APP processing, and alterations in adaptive immune response proteins. Intriguingly, CB, which is suggested to be relatively spared by the disease process, showed unexpectedly large amount of changes at the molecular level, to a level comparable to the heavily affected regions. In the CB, the observation of more apparent activation of proteins that mediate the alternative minor glucose-clearance pathways (polyol and pentose-phosphate pathways), decreased OxPhos, increased regulation of protein processing and proteolysis, and increased Aβ clearing apolipoproteins, may represent compensatory/protective mechanisms towards various pathological stimuli in the disease. Therefore, while definitely affected by AD at the molecular level, CB may relatively spared becasuse of the activation of these neuroprotective mechanisms.

Chapter 5. **Conclusions and future directions**

5.1. Conclusions

In this thesis document, I have presented my comprehensive molecular analysis of aortic tissue from a rabbit model of atherosclerosis and of *post-mortem* brain tissue from human AD patients, via a series of linked proteomic and metabolomic studies. These were case-control studies in each case.

The analysis of of the atherosclerotic rabbit tissue has been published in Atherosclerosis [435], a leading journal in the field.

In the study profiling protein changes associated with hypercholesterolaemia-induced vasculopathy in the rabbit, we found ten times more proteins to be up-regulated than down-regulated: this may be explained by the dramatic intimal thickening in addition to large numbers of disease-related proteins associated with the aortic wall. Many of the proteins identified were related to inflammatory processes or protein synthesis, and are generally consistent with the current literature.

The main conclusions arising from this study include the following: 1) Alteration in actin cytoskeletal organization underlies not only the phenotypic change in arteries during vascular remodelling, but also the loss of vascular contractile function during this process. 2) The evident shift in metabolic regulation towards increase glycolytic and TCA cycle activity is an integral part of the vascular remodelling process occurring in response to the high cholesterol diet. 3) The most significant and novel finding of this study was the elevation of Gpnmb in the context of atherosclerosis: the mechanism of this effect is yet to be identified.

Metabolic profiling and proteome analysis have revealed that AD brain exhibits global defects in energy production, which is characterised by alterations in glycolytic pathway components with concomitant activation of the pentose-phosphate and polyol pathways. The finding of polyol pathway activation provides a novel link between T2D and AD.

Over the course of this PhD programme, compelling evidence supporting the involvement of glucose in AD, in line with our own findings, has emerged in the literature; for example, impaired glycaemia not only increases the risk of dementia [48] but also correlates positively with cognitive decline in mild cognitive impairment and progression to AD [49]. Furthermore, acute hyperglycaemia has been demonstrated to increase Aβ production through alteration of neuronal activity *in vivo*, in a transgenic mouse model of AD [36], further supporting the significant role of glucose accumulation in the brain during AD pathogenesis.

Based on our original findings, we hypothesize that the accumulation of free glucose in the AD brain is likely to be the main underlying cause of the decreased cerebral glucose uptake observed in AD patients

by *in-vivo* imaging techniques such as 2-[^{18}F]-fluoro-2-deoxy-D-glucose positron emission tomography (FDG-PET).

In line with the substantive evidence for impaired glycolysis generated in this thesis, we also observed a global reduction of pyruvate metabolism and disturbance in TCA cycle enzymes in the AD brain. Intriguingly, OxPhos appeared to be severely diminished only in CB, possibly sparing this brain region from oxidative damage arising from OxPhos at the expense of compromising energy supply.

We also observed severe perturbation in levels of many brain phospholipids: I hypothesize that this alteration in lipid composition is linked to the impaired fuel metabolism and directly contributes to disturbed membrane structure and impaired signalling functions of neurons in AD brain. Notably, FAO was severely elevated only in HP and ENT, possibly exposing these brain regions to a high degree of FAO-associated oxidative stress.

Taken together, a combination of better-regulated FAO and decreased OxPhos in CB may result in relatively limited oxidative stress in this region when compared for example to HP or ENT. Further supporting the notion of CB being less affected in AD, this region also exhibited relatively preserved pathways for protein folding and protein degradation, as well as Aβ-clearance when compared to HP or ENT. Similarly, evidence for activation of the adaptive immune response was only apparent in HP and ENT, whereas CB only showed signs consistent with activation of the acute immune response, further suggesting that activation of this pathogenic cascade may commence at a later stage of AD in CB as compared with HP or ENT.

It is clear from my work that both the extent and the pattern of changes differ among brain regions: This may be accounted for by responses of different nerve cells from different brain regions, having variable susceptibility to pathological insults. This may also represent the different stages in the development of responses to AD; that is, brain regions that are known to be earliest affected by AD showed presence of severe disturbances in many molecular pathways as a result of long-standing assault during the disease process. On the other hand, brain regions that are known to be affected by the disease during a later phase showed better preserved molecular integrity and possibly even signs of activation of protective responses towards the AD-associated assault. Nevertheless, molecular perturbation in AD brain is evidently global, as it was widespread through all brain regions examined in this study.

Overall, these data indicate that impaired glucose metabolism/polyol pathway activation, which is also typically present in T2D-associated tissue damage [228], may provide a critical mechanistic connection between T2D and AD. Impaired glucose metabolism is also a likely contributor to the vasculopathy observed in diabetes (termed diabetic vasculopathy); prolonged exposure to high blood glucose leads to glycosylation of proteins and lipids that subsequently promote atherosclerosis, which accounts for the majority of deaths among diabetic patients [436]. Glycosylated proteins and lipids can interact with receptors, such as those found in endothelial cells of the arterial wall, and induce atherosclerosis-promoting events such as proinflammatory responses and oxidative stress [436], known to be present in

all three diseases. Therefore, our findings point to a common potential mechanism present in all three diseases.

Another possible link between AD and atherosclerosis may be the elevation of Gpnmb, since two brain regions from AD patients (HP and ENT) also showed greater than 2-fold increases in Gpnmb levels (both $p<0.005$), as also demonstrated in the aorta of the atherosclerotic rabbit.. This makes Gpnmb a high priority target for further functional characterisation studies, with relevance to both atherosclerosis and AD.

5.2. Implications and suggestions for further work

We have generated a comprehensive data set describing atherosclerosis-related molecular changes in the aortic tissue of a well-recognized animal model for atherosclerosis. This dataset can serve as a platform for 1) comparisons of molecular changes to address individual research findings in other contexts, and 2) monitoring drug action for new emerging treatments developed for atherosclerosis.

This dataset will also serve as a comparator for another ongoing proteomic analysis of the cerebral arteries from patients with AD and vasculopathy, to generate a detailed comparison between the molecular signatures of vasculopathy in atherosclerosis compared with that in AD.

Given our finding of glucose accumulation in the AD brain, it will be of great interest to examine an equivalent dataset derived from the *post-mortem* brains of diabetic patients. For this purpose, we are currently in the process of acquiring samples of human brain from T2D patients through the National Disease Research Interchange (NDRI, USA) tissue bank. This planned study is once again designed to examine and compare multiple functionally distinctive brain regions.

Clinical studies based on this thesis, which have been designed to determine the levels of polyol metabolites in the blood plasma of AD patients are also underway to test the potential of free glucose and/or fructose levels to act as AD biomarkers.

The data generated from the proteomics study require further validation with a targeted (semi) quantitative method, such as multiple reaction monitoring (MRM), as employed for the rabbit study.

Datasets presented in this thesis document provide detailed descriptions of the molecular changes in both protein and metabolite levels in different anatomical regions of the human brain in AD with dementia. These valuable and rare molecular profiles of AD brain will be made available for the dementia research community through a community resource housing all of these data, once we have completed our ongoing analysis (within 2 years from the time of thesis submission).

Establishment of such a community resource will enable other researchers to: 1) validate AD animal models with more sophisticated examinations of molecular profiles at different stages of disease development; 2) generate arrays of molecular targets for rigorous testing of drug efficacy in future

clinical trials; and 3) explore the possibility of establishing biomarkers derived from some of the identified molecular changes for the purpose of improved diagnosis/prognosis determination.

Functional studies are also needed to improve characterisation of the molecular events that potentially implicate Gpnmb in the mechanism of atherosclerosis and of AD.

References

1. van Oijen, M.*, et al.* Atherosclerosis and risk for dementia. *Ann Neurol* **61**, 403-410 (2007).
2. Hofman, A.*, et al.* Atherosclerosis, apolipoprotein E, and prevalence of dementia and Alzheimer's disease in the Rotterdam Study. *Lancet* **349**, 151-154 (1997).
3. Kang, J. & Rivest, S. Lipid metabolism and neuroinflammation in Alzheimer's disease: a role for liver X receptors. *Endocr Rev* **33**, 715-746 (2012).
4. Ott, A.*, et al.* Diabetes mellitus and the risk of dementia: The Rotterdam Study. *Neurology* **53**, 1937-1942 (1999).
5. Janson, J.*, et al.* Increased Risk of Type 2 Diabetes in Alzheimer Disease. *Diabetes* **53**, 474-481 (2004).
6. Ellis, R.J.*, et al.* Cerebral amyloid angiopathy in the brains of patients with Alzheimer's disease: the CERAD experience, Part XV. *Neurology* **46**, 1592-1596 (1996).
7. Weller, R.O.*, et al.* Cerebral amyloid angiopathy: amyloid beta accumulates in putative interstitial fluid drainage pathways in Alzheimer's disease. *Am J Pathol* **153**, 725-733 (1998).
8. Weller, R.O., Subash, M., Preston, S.D., Mazanti, I. & Carare, R.O. Perivascular drainage of amyloid-beta peptides from the brain and its failure in cerebral amyloid angiopathy and Alzheimer's disease. *Brain Pathol (Zurich, Switzerland)* **18**, 253-266 (2008).
9. Kalback, W.*, et al.* Atherosclerosis, vascular amyloidosis and brain hypoperfusion in the pathogenesis of sporadic Alzheimer's disease. *Neurolo Res* **26**, 525-539 (2004).
10. Yanni, A.E. The laboratory rabbit: an animal model of atherosclerosis research. *Laboratory Animals* **38**, 246-256 (2004).
11. Finking, G. & Hanke, H. Nikolaj Nikolajewitsch Anitschkow (1885-1964) established the cholesterol-fed rabbit as a model for atherosclerosis research. *Atherosclerosis* **135**, 1-7 (1997).
12. Woodruff-Pak, D.S. Animal models of Alzheimer's disease: therapeutic implications. *J Alzheimers Dis* **15**, 507-521 (2008).
13. Sparks, D.L. Cholesterol metabolism and brain amyloidosis: evidence for a role of copper in the clearance of Abeta through the liver. *Curr Alzheimer Res* **4**, 165-169 (2007).
14. Sparks, D.L.*, et al.* Trace copper levels in the drinking water, but not zinc or aluminum influence CNS Alzheimer-like pathology. *J Nutr Health Aging* **10**, 247-254 (2006).
15. Sparks, D.L. & Schreurs, B.G. Trace amounts of copper in water induce β-amyloid plaques and learning deficits in a rabbit model of Alzheimer's disease. *Proc Natl Acad Sci U S A* **100**, 11065-11069 (2003).
16. Drouin-Ouellet, J.*, et al.* Cerebrovascular and blood-brain barrier impairments in Huntington's disease: Potential implications for its pathophysiology. *Ann Neurol* (2015).
17. Lin, C.Y.*, et al.* Neurovascular abnormalities in humans and mice with Huntington's disease. *Exp Neurol* **250**, 20-30 (2013).
18. Rektor, I.*, et al.* Vascular pathology in patients with idiopathic Parkinson's disease. *Parkinsonism Relat Disord* **15**, 24-29 (2009).
19. Prince, M., Guerchet, M. & Prina, M. Policy brief for heads of government: The global impact of dementia 2013-2050. *London: Alzheimers Dis Int* **2013**, 1- 8 (2013).
20. Querfurth, H.W. & LaFerla, F.M. Alzheimer's disease. *N Engl J Med* **362**, 329-344 (2010).
21. Brookmeyer, R., Johnson, E., Ziegler-Graham, K. & Arrighi, H.M. Forecasting the global burden of Alzheimer's disease. *Alzheimers Dement* **3**, 186-191 (2007).
22. Citron, M. Alzheimer's disease: strategies for disease modification. *Nat Rev Drug Discov* **9**, 387-398 (2010).
23. Wimo, A., Jonsson, L., Bond, J., Prince, M. & Winblad, B. The worldwide economic impact of dementia 2010. *Alzheimers Dement* **9**, 1-11 e13 (2013).
24. Sindi, S., Mangialasche, F. & Kivipelto, M. Advances in the prevention of Alzheimer's Disease. *F1000Prime Rep* **7**, 50 (2015).
25. Hardy, J.A. & Higgins, G.A. Alzheimer's disease: the amyloid cascade hypothesis. *Science* **256**, 184-185 (1992).
26. Bettens, K., Sleegers, K. & Van Broeckhoven, C. Genetic insights in Alzheimer's disease. *Lancet. Neurol* **12**, 92-104 (2013).
27. Morris, G.P., Clark, I.A. & Vissel, B. Inconsistencies and controversies surrounding the amyloid hypothesis of Alzheimer's disease. *Acta Neuropathol Commun* **2**, 135 (2014).
28. Braak, H. & Braak, E. Neuropathological stageing of Alzheimer-related changes. *Acta Neuropathol* **82**, 239-259 (1991).
29. Serrano-Pozo, A., Frosch, M.P., Masliah, E. & Hyman, B.T. Neuropathological alterations in Alzheimer disease. *Cold Spring Harb Perspect Med* **1**, a006189 (2011).

30. Ferreira, S.T. & Klein, W.L. The Abeta oligomer hypothesis for synapse failure and memory loss in Alzheimer's disease. *Neurobiol Learn Mem* **96**, 529-543 (2011).
31. Watt, A.D.*, et al.* Oligomers, fact or artefact? SDS-PAGE induces dimerization of beta-amyloid in human brain samples. *Acta Neuropathol* **125**, 549-564 (2013).
32. Herrup, K. The case for rejecting the amyloid cascade hypothesis. *Nat Neurosci* **18**, 794-799 (2015).
33. Vellas, B.*, et al.* Designing drug trials for Alzheimer's disease: what we have learned from the release of the phase III antibody trials: a report from the EU/US/CTAD Task Force. *Alzheimers Dement* **9**, 438-444 (2013).
34. Musiek, E.S. & Holtzman, D.M. Three dimensions of the amyloid hypothesis: time, space and 'wingmen'. *Nat Neurosci* **18**, 800-806 (2015).
35. Snyder, H.M.*, et al.* Vascular contributions to cognitive impairment and dementia including Alzheimer's disease. *Alzheimers Dement* **11**, 710-717 (2015).
36. Macauley, S.L.*, et al.* Hyperglycemia modulates extracellular amyloid-beta concentrations and neuronal activity in vivo. *J Clin Invest* (2015).
37. Zekry, D., Hauw, J.J. & Gold, G. Mixed dementia: epidemiology, diagnosis, and treatment. *J Am Geriatr Soc* **50**, 1431-1438 (2002).
38. de la Torre, J.C. Alzheimer disease as a vascular disorder: nosological evidence. *Stroke* **33**, 1152-1162 (2002).
39. Association, A.P. *Diagnostic and Statistical Manual of Mental Disorders*, (American Psychiatric Association, Washington DC, 1994).
40. Jellinger, K.A. Alzheimer disease and cerebrovascular pathology: an update. *J Neural Transm (Vienna)* **109**, 813-836 (2002).
41. Breteler, M.M. Vascular involvement in cognitive decline and dementia. Epidemiologic evidence from the Rotterdam Study and the Rotterdam Scan Study. *Ann N Y Acad Sci* **903**, 457-465 (2000).
42. Povova, J.*, et al.* Epidemiological of and risk factors for Alzheimer's disease: a review. *Biomed Pap Med Fac Univ Palacky Olomouc Czech Repub* **156**, 108-114 (2012).
43. Breteler, M.M. Vascular risk factors for Alzheimer's disease: an epidemiologic perspective. *Neurobiol Aging* **21**, 153-160 (2000).
44. Skoog, I. Vascular aspects in Alzheimer's disease. *J Neural Transm Suppl* **59**, 37-43 (2000).
45. Schmidt, R., Schmidt, H. & Fazekas, F. Vascular risk factors in dementia. *J Neurol* **247**, 81-87 (2000).
46. Puglielli, L., Tanzi, R.E. & Kovacs, D.M. Alzheimer's disease: the cholesterol connection. *Nat Neurosci* **6**, 345-351 (2003).
47. Huang, C.C.*, et al.* Diabetes mellitus and the risk of Alzheimer's disease: a nationwide population-based study. *PLoS One* **9**, e87095 (2014).
48. Crane, P.K.*, et al.* Glucose Levels and Risk of Dementia. *N Engl J Med* **369**, 540-548 (2013).
49. Morris, J.K., Vidoni, E.D., Honea, R.A. & Burns, J.M. Impaired glycemia increases disease progression in mild cognitive impairment. *Neurobiol Aging* **35**, 585-589 (2014).
50. Sarasa, M. & Pesini, P. Natural non-trasgenic animal models for research in Alzheimer's disease. *Curr Alzheimer Res* **6**, 171-178 (2009).
51. Ross, R. Atherosclerosis--an inflammatory disease. *N Engl J Med* **340**, 115-126 (1999).
52. Glass, C.K. & Witztum, J.L. Atherosclerosis: The road ahead. *Cell* **104**, 503-516 (2001).
53. Lusis, A.J. Atherosclerosis. *Nature* **407**, 233-241 (2000).
54. Marais, A.D. Dietary lipid modification for mild and severe dyslipidaemias. *Proc Nutr Soc* **72**, 337-341 (2013).
55. Kolodgie, F.D.*, et al.* Hypercholesterolemia in the rabbit induced by feeding graded amounts of low-level cholesterol. Methodological considerations regarding individual variability in response to dietary cholesterol and development of lesion type. *Arterioscler Thromb Vasc Biol* **16**, 1454-1464 (1996).
56. Bocan, T.M.*, et al.* The relationship between the degree of dietary-induced hypercholesterolemia in the rabbit and atherosclerotic lesion formation. *Atherosclerosis* **102**, 9-22 (1993).
57. Sung, H.J.*, et al.* Proteomic analysis of differential protein expression in atherosclerosis. *Biomarkers* **11**, 279-290 (2006).
58. Kaga, E., Karademir, B., Baykal, A.T. & Ozer, N.K. Identification of differentially expressed proteins in atherosclerotic aorta and effect of vitamin E. *J Proteomics* **92**, 260-273 (2013).
59. Cizek, S.M.*, et al.* Risk factors for atherosclerosis and the development of preatherosclerotic intimal hyperplasia. *Cardiovas Pathol* **16**, 344-350 (2007).

60. Yu, Q., Zhang, Y. & Xu, C.B. Apolipoprotein B, the villain in the drama? *Eur J Pharmacol* **748**, 166-169 (2015).
61. Knouff, C.*, et al.* Apo E structure determines VLDL clearance and atherosclerosis risk in mice. *J Clin Invest* **103**, 1579-1586 (1999).
62. Carmena, R., Duriez, P. & Fruchart, J.C. Atherogenic lipoprotein particles in atherosclerosis. *Circulation* **109**, III2-7 (2004).
63. Jiang, X.*, et al.* An engineered transthyretin monomer that is nonamyloidogenic, unless it is partially denatured. *Biochem* **40**, 11442-11452 (2001).
64. Hammarstrom, P., Jiang, X., Hurshman, A.R., Powers, E.T. & Kelly, J.W. Sequence-dependent denaturation energetics: A major determinant in amyloid disease diversity. *Proc Natl Acad Sci U S A* **99 Suppl 4**, 16427-16432 (2002).
65. Liz, M.A., Gomes, C.M., Saraiva, M.J. & Sousa, M.M. ApoA-I cleaved by transthyretin has reduced ability to promote cholesterol efflux and increased amyloidogenicity. *J Lipid Res* **48**, 2385-2395 (2007).
66. Westermark, P., Sletten, K., Johansson, B. & Cornwell, G.G., 3rd. Fibril in senile systemic amyloidosis is derived from normal transthyretin. *Proc Natl Acad Sci U S A* **87**, 2843-2845 (1990).
67. Coelho, T. Familial amyloid polyneuropathy: new developments in genetics and treatment. *Curr Opin Neurol* **9**, 355-359 (1996).
68. Jacobson, D.R.*, et al.* Variant-sequence transthyretin (isoleucine 122) in late-onset cardiac amyloidosis in black Americans. *N Engl J Med* **336**, 466-473 (1997).
69. Speidl, W.S., Kastl, S.P., Huber, K. & Wojta, J. Complement in atherosclerosis: friend or foe? *J Thromb Haemost* **9**, 428-440 (2011).
70. Gennaro, R.*, et al.* C5a fragment of bovine complement. Purification, bioassays, amino-acid sequence and other structural studies. *Eur J Biochem* **155**, 77-86 (1986).
71. Podack, E.R., Tschoop, J. & Muller-Eberhard, H.J. Molecular organization of C9 within the membrane attack complex of complement. Induction of circular C9 polymerization by the C5b-8 assembly. *J Exp Med* **156**, 268-282 (1982).
72. Jones, A.L., Hulett, M.D. & Parish, C.R. Histidine-rich glycoprotein: A novel adaptor protein in plasma that modulates the immune, vascular and coagulation systems. *Immunol Cell Biol* **83**, 106-118 (2005).
73. Hajjar, D.P., Boyd, D.B., Harpel, P.C. & Nachman, R.L. Histidine-rich glycoprotein inhibits the antiproliferative effect of heparin on smooth muscle cells. *J Exp Med* **165**, 908-913 (1987).
74. Heiss, A.*, et al.* Hierarchical role of fetuin-A and acidic serum proteins in the formation and stabilization of calcium phosphate particles. *J Biol Chem* **283**, 14815-14825 (2008).
75. Jahnen-Dechent, W., Schafer, C., Ketteler, M. & McKee, M.D. Mineral chaperones: a role for fetuin-A and osteopontin in the inhibition and regression of pathologic calcification. *J Mol Med (Berlin)* **86**, 379-389 (2008).
76. Cuspidi, C. & Sala, C. Is fetuin-A a biomarker of preclinical atherosclerosis in essential hypertension? *Hypertens Res* **36**, 104-106 (2013).
77. Speeckaert, M., Huang, G., Delanghe, J.R. & Taes, Y.E. Biological and clinical aspects of the vitamin D binding protein (Gc-globulin) and its polymorphism. *Clin Chim Acta* **372**, 33-42 (2006).
78. Speeckaert, M.M., Speeckaert, R., van Geel, N. & Delanghe, J.R. Vitamin D binding protein: a multifunctional protein of clinical importance. *Adv Clin Chem* **63**, 1-57 (2014).
79. Raymond, M.A.*, et al.* Endothelial stress induces the release of vitamin D-binding protein, a novel growth factor. *Biochem Biophys Res Commun* **338**, 1374-1382 (2005).
80. Gasparri, C.*, et al.* Proteomics reveals high levels of vitamin D binding protein in myocardial infarction. *Front Biosci (Elite Ed)* **2**, 796-804 (2010).
81. Darde, V.M.*, et al.* Analysis of the plasma proteome associated with acute coronary syndrome: does a permanent protein signature exist in the plasma of ACS patients? *J Proteome Res* **9**, 4420-4432 (2010).
82. Djousse, L., Rothman, K.J., Cupples, L.A., Levy, D. & Ellison, R.C. Serum albumin and risk of myocardial infarction and all-cause mortality in the Framingham Offspring Study. *Circulation* **106**, 2919-2924 (2002).
83. Lowrie, E.G. & Lew, N.L. Death risk in hemodialysis patients: the predictive value of commonly measured variables and an evaluation of death rate differences between facilities. *Am J Kidney Dis* **15**, 458-482 (1990).
84. Ishizaka, N.*, et al.* Association between serum albumin, carotid atherosclerosis, and metabolic syndrome in Japanese individuals. *Atherosclerosis* **193**, 373-379 (2007).

85. Abdelhalim, M.A. & Moussa, S.A. Biochemical changes of hemoglobin and osmotic fragility of red blood cells in high fat diet rabbits. *Pak J Biol Sci* **13**, 73-77 (2010).
86. Kozlov, A.V., Sergienko, V.I., Vladimirov Iu, A. & Azizova, O.A. The antioxidant system of transferrin-ceruloplasmin in experimental hypercholesterolemia. *Biull Eksp Biol Med* **98**, 668-671 (1984).
87. Asetskaia, I.L., *et al.* Ceruloplasmin-transferrin antioxidant system in in experimental and clinical atherosclerosis. *Vestn Akad Med Nauk SSSR*, 41-45 (1990).
88. Kibel, A., Belovari, T. & Drenjancevic-Peric, I. The role of transferrin in atherosclerosis. *Med Hypotheses* **70**, 793-797 (2008).
89. Miller, F.J., Jr., Gutterman, D.D., Rios, C.D., Heistad, D.D. & Davidson, B.L. Superoxide production in vascular smooth muscle contributes to oxidative stress and impaired relaxation in atherosclerosis. *Circ Res* **82**, 1298-1305 (1998).
90. Cai, H. Hydrogen peroxide regulation of endothelial function: origins, mechanisms, and consequences. *Cardiovasc Res* **68**, 26-36 (2005).
91. Jeyabal, P.V., Rubio, V., Chen, H., Zhang, J. & Shi, Z.Z. Regulation of cell-matrix adhesion by OLA1, the Obg-like ATPase 1. *Biochem Biophys Res Commun* **444**, 568-574 (2014).
92. Mao, R.F., *et al.* OLA1 protects cells in heat shock by stabilizing HSP70. *Cell Death Dis* **4**, e491 (2013).
93. Ozols, J. Structure of cytochrome b5 and its topology in the microsomal membrane. *Biochim Biophys Acta* **997**, 121-130 (1989).
94. Ahuja, S.*, et al*. A model of the membrane-bound cytochrome b5-cytochrome P450 complex from NMR and mutagenesis data. *J Biol Chem* **288**, 22080-22095 (2013).
95. Okuwaki, M., Kato, K. & Nagata, K. Functional characterization of human nucleosome assembly protein 1-like proteins as histone chaperones. *Genes Cells* **15**, 13-27 (2010).
96. Civelek, M., Manduchi, E., Riley, R.J., Stoeckert, C.J., Jr. & Davies, P.F. Chronic endoplasmic reticulum stress activates unfolded protein response in arterial endothelium in regions of susceptibility to atherosclerosis. *Circ Res* **105**, 453-461 (2009).
97. Ho, J.J.*, et al.* Active stabilization of human endothelial nitric oxide synthase mRNA by hnRNP E1 protects against antisense RNA and microRNAs. *Mol Cell Biol* **33**, 2029-2046 (2013).
98. Laury-Kleintop, L.D., Gleason, M. & Tulenko, T.N. Expression of the heterogenous nuclear ribonucleoprotein complex K protein and the prolyl-4-hydroxylase alpha-subunit in atherosclerotic arterial smooth muscle cells. *Biochem Biophys Res Commun* **260**, 382-389 (1999).
99. Thiele, B.J. *et al.* RNA-binding proteins heterogeneous nuclear ribonucleoprotein A1, E1, and K are involved in post-transcriptional control of collagen I and III synthesis. *Circ Res* **95**, 1058-1066 (2004).
100. Tchorzewski, M. The acidic ribosomal P proteins. *Int J Biochem Cell Biol* **34**, 911-915 (2002).
101. Malla, R.R., *et al.* Cathepsin B and uPAR knockdown inhibits tumor-induced angiogenesis by modulating VEGF expression in glioma. *Cancer Gene Ther* **18**, 419-434 (2011).
102. Benes, P., Vetvicka, V. & Fusek, M. Cathepsin D--many functions of one aspartic protease. *Crit Rev Oncol Hematol* **68**, 12-28 (2008).
103. Hakala, J.K.*, et al.* Lysosomal enzymes are released from cultured human macrophages, hydrolyze LDL in vitro, and are present extracellularly in human atherosclerotic lesions. *Arterioscler Thromb Vasc Biol* **23**, 1430-1436 (2003).
104. Tang, W.*, et al.* Association of SERPINA9 gene variants with carotid artery atherosclerosis: the Atherosclerosis Risk in Communities (ARIC) Carotid MRI Study. *Int J Mol Epidemiol Genet*. **4**, 258-267 (2013).
105. Sueishi, K., Ichikawa, K., Kato, K., Nakagawa, K. & Chen, Y.X. Atherosclerosis: coagulation and fibrinolysis. *Semin Thromb Hemost* **24**, 255-260 (1998).
106. Wagsater, D., *et al.* Serine protease inhibitor A3 in atherosclerosis and aneurysm disease. *Int J Mol Med* **30**, 288-294 (2012).
107. Kiang, J.G. & Tsokos, G.C. Heat shock protein 70 kDa: molecular biology, biochemistry, and physiology. *Pharmacol Ther* **80**, 183-201 (1998).
108. Dai, E., *et al.* Calreticulin, a potential vascular regulatory protein, reduces intimal hyperplasia after arterial injury. *Arterioscler Thromb Vasc Biol* **17**, 2359-2368 (1997).
109. Moremen, K.W. & Molinari, M. N-linked glycan recognition and processing: the molecular basis of endoplasmic reticulum quality control. *Curr Opin Struct Biol* **16**, 592-599 (2006).
110. Hendershot, L.M., Valentine, V.A., Lee, A.S., Morris, S.W. & Shapiro, D.N. Localization of the gene encoding human BiP/GRP78, the endoplasmic reticulum cognate of the HSP70 family, to chromosome 9q34. *Genomics* **20**, 281-284 (1994).

111. Nagata, K. Expression and function of heat shock protein 47: a collagen-specific molecular chaperone in the endoplasmic reticulum. *Matrix Biol* **16**, 379-386 (1998).
112. Randow, F. & Seed, B. Endoplasmic reticulum chaperone gp96 is required for innate immunity but not cell viability. *Nat Cell Biol* **3**, 891-896 (2001).
113. Schild, H. & Rammensee, H.G. gp96--the immune system's Swiss army knife. *Nat Immunol* **1**, 100-101 (2000).
114. Muller, C.*, et al.* Protein disulfide isomerase modification and inhibition contribute to ER stress and apoptosis induced by oxidized low density lipoproteins. *Antioxid Redox Signal* **18**, 731-742 (2013).
115. Madrigal-Matute, J., *et al.* Heat shock protein 90 inhibitors attenuate inflammatory responses in atherosclerosis. *Cardiovasc Res* **86**, 330-337 (2010).
116. Businaro, R., *et al.* Heat-shock protein 90: a novel autoantigen in human carotid atherosclerosis. *Atherosclerosis* **207**, 74-83 (2009).
117. Kim, J., *et al.* The role of heat shock protein 90 in migration and proliferation of vascular smooth muscle cells in the development of atherosclerosis. *J Mol Cell Cardiol* **72**, 157-167 (2014).
118. Liu, T., Daniels, C.K. & Cao, S. Comprehensive review on the HSC70 functions, interactions with related molecules and involvement in clinical diseases and therapeutic potential. *Pharmacol Ther* **136**, 354-374 (2012).
119. Arispe, N., Doh, M. & De Maio, A. Lipid interaction differentiates the constitutive and stress-induced heat shock proteins Hsc70 and Hsp70. *Cell Stress Chaperones* **7**, 330-338 (2002).
120. Grundtman, C., Kreutmayer, S.B., Almanzar, G., Wick, M.C. & Wick, G. Heat shock protein 60 and immune inflammatory responses in atherosclerosis. *Arterioscler Thromb Vasc Biol* **31**, 960-968 (2011).
121. Melki, R., Batelier, G., Soulie, S. & Williams, R.C., Jr. Cytoplasmic chaperonin containing TCP-1: structural and functional characterization. *Biochemistry* **36**, 5817-5826 (1997).
122. Dunn, A.Y., Melville, M.W. & Frydman, J. Review: cellular substrates of the eukaryotic chaperonin TRiC/CCT. *J Struct Biol* **135**, 176-184 (2001).
123. Nigro, P., Pompilio, G. & Capogrossi, M.C. Cyclophilin A: a key player for human disease. *Cell Death Dis* **4**, e888 (2013).
124. Zerial, M. & McBride, H. Rab proteins as membrane organizers. *Nat Rev Mol Cell Biol* **2**, 107-117 (2001).
125. Mukhopadhyay, A., Quiroz, J.A. & Wolkoff, A.W. Rab1a regulates sorting of early endocytic vesicles. *Am J Physiol Gastrointest Liver Physiol* **306**, G412-424 (2014).
126. Gromov, P.S., *et al.* Human rab11a: transcription, chromosome mapping and effect on the expression levels of host GTP-binding proteins. *FEBS Lett* **429**, 359-364 (1998).
127. Takahashi, S., *et al.* Rab11 regulates exocytosis of recycling vesicles at the plasma membrane. *J Cell Sci* **125**, 4049-4057 (2012).
128. Hu, J., *et al.* A class of dynamin-like GTPases involved in the generation of the tubular ER network. *Cell* **138**, 549-561 (2009).
129. Rismanchi, N., Soderblom, C., Stadler, J., Zhu, P.P. & Blackstone, C. Atlastin GTPases are required for Golgi apparatus and ER morphogenesis. *Hum Mol Genet*. **17**, 1591-1604 (2008).
130. Song, C.*, et al.* Novel immunohistochemical monoclonal antibody against rat B cell receptor Associated Protein 31 (BAP31). *Hybridoma (Larchmt)* **28**, 363-367 (2009).
131. Wakana, Y.*, et al.* Bap31 is an itinerant protein that moves between the peripheral endoplasmic reticulum (ER) and a juxtanuclear compartment related to ER-associated Degradation. *Mol Biol Cell* **19**, 1825-1836 (2008).
132. Kelly, B.T. & Owen, D.J. Endocytic sorting of transmembrane protein cargo. *Curr Opin Cell Biol* **23**, 404-412 (2011).
133. Chavrier, P. & Goud, B. The role of ARF and Rab GTPases in membrane transport. *Curr Opin Cell Biol* **11**, 466-475 (1999).
134. Zhong, X., *et al.* AAA ATPase p97/valosin-containing protein interacts with gp78, a ubiquitin ligase for endoplasmic reticulum-associated degradation. *J Biol Chem* **279**, 45676-45684 (2004).
135. Moriyama, K., *et al.* Destrin, a mammalian actin-depolymerizing protein, is closely related to cofilin. Cloning and expression of porcine brain destrin cDNA. *J Biol Chem* **265**, 5768-5773 (1990).
136. Shapland, C., Hsuan, J.J., Totty, N.F. & Lawson, D. Purification and properties of transgelin: a transformation and shape change sensitive actin-gelling protein. *J Cell Biol* **121**, 1065-1073 (1993).

137. Shifrin, Y., *et al.* The role of FilGAP-filamin A interactions in mechanoprotection. *Mol Biol Cell* **20**, 1269-1279 (2009).
138. Shen, J., *et al.* Arterial injury promotes medial chondrogenesis in Sm22 knockout mice. *Cardiovasc Res* **90**, 28-37 (2011).
139. Yu, N., Erb, L., Shivaji, R., Weisman, G.A. & Seye, C.I. Binding of the P2Y2 nucleotide receptor to filamin A regulates migration of vascular smooth muscle cells. *Circ Res* **102**, 581-588 (2008).
140. Brown, N.H., *et al.* Talin is essential for integrin function in Drosophila. *Dev Cell* **3**, 569-579 (2002).
141. Malinin, N.L., Pluskota, E. & Byzova, T.V. Integrin signaling in vascular function. *Curr Opin Hematol* **19**, 206-211 (2012).
142. Moser, M., Legate, K.R., Zent, R. & Fassler, R. The tail of integrins, talin, and kindlins. *Science* **324**, 895-899 (2009).
143. Kordowska, J., Huang, R. & Wang, C.L. Phosphorylation of caldesmon during smooth muscle contraction and cell migration or proliferation. *J Biomed Sci* **13**, 159-172 (2006).
144. Vukovic, I., Arsenijevic, N., Lackovic, V. & Todorovic, V. The origin and differentiation potential of smooth muscle cells in coronary atherosclerosis. *Exp Clin Cardiol* **11**, 123-128 (2006).
145. Li, Z., *et al.* Desmin is essential for the tensile strength and integrity of myofibrils but not for myogenic commitment, differentiation, and fusion of skeletal muscle. *J Cell Biol* **139**, 129-144 (1997).
146. Persoons, M.C., Daemen, M.J., van Kleef, E.M., Grauls, G.E., Wijers, E. & Bruggeman, C.A. Neointimal smooth muscle cell phenotype is important in its susceptibility to cytomegalovirus (CMV) infection: a study in rat. *Cardiovasc Res* **36**, 282-288 (1997).
147. van der Loop, F.T., Schaart, G., Timmer, E.D., Ramaekers, F.C. & van Eys, G.J. Smoothelin, a novel cytoskeletal protein specific for smooth muscle cells. *J Cell Biol* **134**, 401-411 (1996).
148. Bar, H., *et al.* Smoothelin is an indicator of reversible phenotype modulation of smooth muscle cells in balloon-injured rat carotid arteries. *Basic Res Cardiol* **97**, 9-16 (2002).
149. van der Loop, F.T., Gabbiani, G., Kohnen, G., Ramaekers, F.C. & van Eys, G.J. Differentiation of smooth muscle cells in human blood vessels as defined by smoothelin, a novel marker for the contractile phenotype. *Arterioscler Thromb Vasc Biol* **17**, 665-671 (1997).
150. Yokobori, T.*, et al.* Plastin3 is a novel marker for circulating tumor cells undergoing the epithelial-mesenchymal transition and is associated with colorectal cancer prognosis. *Cancer Res* **73**, 2059-2069 (2013).
151. Szkandera, J.*, et al.* A common gene variant in PLS3 predicts colon cancer recurrence in women. *Tumour Biol* **34**, 2183-2188 (2013).
152. Katanasaka, Y., Asai, T., Naitou, H., Ohashi, N. & Oku, N. Proteomic characterization of angiogenic endothelial cells stimulated with cancer cell-conditioned medium. *Biol Pharm Bull* **30**, 2300-2307 (2007).
153. Mullins, R.D., Heuser, J.A. & Pollard, T.D. The interaction of Arp2/3 complex with actin: nucleation, high affinity pointed end capping, and formation of branching networks of filaments. *Proc Natl Acad Sci U S A* **95**, 6181-6186 (1998).
154. Blindt, R.*, et al.* Upregulation of the cytoskeletal-associated protein Moesin in the neointima of coronary arteries after balloon angioplasty: a new marker of smooth muscle cell migration? *Cardiovasc Res* **54**, 630-639 (2002).
155. Jia, W., Gao, X.J., Zhang, Z.D., Yang, Z.X. & Zhang, G. S100A4 silencing suppresses proliferation, angiogenesis and invasion of thyroid cancer cells through downregulation of MMP-9 and VEGF. *Eur Rev Med Pharmacol Sci* **17**, 1495-1508 (2013).
156. Schneider, M., Hansen, J.L. & Sheikh, S.P. S100A4: a common mediator of epithelial-mesenchymal transition, fibrosis and regeneration in diseases? *J Mol Med (Berlin)* **86**, 507-522 (2008).
157. Nowotny, M.*, et al.* Characterization of the interaction of calcyclin (S100A6) and calcyclin-binding protein. *J Biol Chem* **275**, 31178-31182 (2000).
158. Bao, L.*, et al.* The S100A6 calcium-binding protein regulates endothelial cell-cycle progression and senescence. *FEBS J* **279**, 4576-4588 (2012).
159. Ostergaard, M., Hansen, G.A., Vorum, H. & Honore, B. Proteomic profiling of fibroblasts reveals a modulating effect of extracellular calumenin on the organization of the actin cytoskeleton. *Proteomics* **6**, 3509-3519 (2006).
160. Coppinger, J.A.*, et al.* Characterization of the proteins released from activated platelets leads to localization of novel platelet proteins in human atherosclerotic lesions. *Blood* **103**, 2096-2104 (2004).

161. Calabia-Linares, C.*, et al.* Endosomal clathrin drives actin accumulation at the immunological synapse. *J Cell Sci* **124**, 820-830 (2011).
162. Tabas, I., Williams, K.J. & Boren, J. Subendothelial lipoprotein retention as the initiating process in atherosclerosis: update and therapeutic implications. *Circulation* **116**, 1832-1844 (2007).
163. Rohwedder, I.*, et al.* Plasma fibronectin deficiency impedes atherosclerosis progression and fibrous cap formation. *EMBO Mol Med* **4**, 564-576 (2012).
164. Moore, C.J. & Winder, S.J. Dystroglycan versatility in cell adhesion: a tale of multiple motifs. *Cell Commun Signal* **8**, 3 (2010).
165. Rauch, U.*, et al.* Increased neointimal thickening in dystrophin-deficient mdx mice. *PLoS ONE* **7**, e29904 (2012).
166. Shanahan, C.M., Cary, N.R., Osbourn, J.K. & Weissberg, P.L. Identification of osteoglycin as a component of the vascular matrix. Differential expression by vascular smooth muscle cells during neointima formation and in atherosclerotic plaques. *Arterioscler Thromb Vasc Biol* **17**, 2437-2447 (1997).
167. Indolfi, C.*, et al.* Inhibition of cellular ras prevents smooth muscle cell proliferation after vascular injury in vivo. *Nat Med* **1**, 541-545 (1995).
168. Mayr, M.*, et al.* Proteomic and metabolomic analyses of atherosclerotic vessels from apolipoprotein E-deficient mice reveal alterations in inflammation, oxidative stress, and energy metabolism. *Arterioscler Thromb Vasc Biol* **25**, 2135-2142 (2005).
169. Rose, A.A.N.*, et al.* ADAM10 releases a soluble form of the GPNMB/Osteoactivin extracellular domain with angiogenic properties. *PLoS ONE* **5**(2010).
170. Furochi, H.*, et al.* Osteoactivin fragments produced by ectodomain shedding induce MMP-3 expression via ERK pathway in mouse NIH-3T3 fibroblasts. *FEBS Lett* **581**, 5743-5750 (2007).
171. Henney, A.M.*, et al.* Localization of stromelysin gene expression in atherosclerotic plaques by in situ hybridization. *Proc Natl Acad Sci U S A*. **88**, 8154-8158 (1991).
172. Galis, Z.S., Sukhova, G.K., Lark, M.W. & Libby, P. Increased expression of matrix metalloproteinases and matrix degrading activity in vulnerable regions of human atherosclerotic plaques. *J Clin Invest* **94**, 2493-2503 (1994).
173. Nachtigal, M., Al-Assaad, Z., Mayer, E.P., Kim, K. & Monsigny, M. Galectin-3 expression in human atherosclerotic lesions. *Am J Pathol* **152**, 1199-1208 (1998).
174. Margadant, C., van den Bout, I., van Boxtel, A.L., Thijssen, V.L. & Sonnenberg, A. Epigenetic regulation of galectin-3 expression by beta1 integrins promotes cell adhesion and migration. *J Biol Chem* **287**, 44684-44693 (2012).
175. Markowska, A.I., Liu, F.T. & Panjwani, N. Galectin-3 is an important mediator of VEGF- and bFGF-mediated angiogenic response. *J Exp Med* **207**, 1981-1993 (2010).
176. Pankov, R.*, et al.* Integrin dynamics and matrix assembly: tensin-dependent translocation of alpha(5)beta(1) integrins promotes early fibronectin fibrillogenesis. *J Cell Biol* **148**, 1075-1090 (2000).
177. Pickering, J.G.*, et al.* alpha5beta1 integrin expression and luminal edge fibronectin matrix assembly by smooth muscle cells after arterial injury. *Am J Pathol* **156**, 453-465 (2000).
178. Park, J.E.*, et al.* Annexin A3 is a potential angiogenic mediator. *Biochem Biophys Res Commun* **337**, 1283-1287 (2005).
179. Cederholm, A. & Frostegard, J. Annexin A5 as a novel player in prevention of atherothrombosis in SLE and in the general population. *Ann N Y Acad Sci* **1108**, 96-103 (2007).
180. Han, J.*, et al.* Reconstructing and deconstructing agonist-induced activation of integrin alphaIIbbeta3. *Curr Biol* **16**, 1796-1806 (2006).
181. Liu, T.A.*, et al.* 14-3-3epsilon overexpression contributes to epithelial-mesenchymal transition of hepatocellular carcinoma. *PLoS ONE* **8**, e57968 (2013).
182. Schiavo, G., Greensmith, L., Hafezparast, M. & Fisher, E.M. Cytoplasmic dynein heavy chain: the servant of many masters. *Trends Neurosci* **36**, 641-651 (2013).
183. Gu, Y. & Ihara, Y. Evidence that collapsin response mediator protein-2 is involved in the dynamics of microtubules. *J Biol Chem* **275**, 17917-17920 (2000).
184. Tominaga, M. & Tomooka, Y. Novel genes cloned from a neuronal cell line newly established from a cerebellum of an adult p53(-/-) mouse. *Biochem Biophys Res Commun* **297**, 473-479 (2002).
185. Doran, A.C., Meller, N. & McNamara, C.A. Role of smooth muscle cells in the initiation and early progression of atherosclerosis. *Arterioscler Thromb Vasc Biol* **28**, 812-819 (2008).
186. Gerthoffer, W.T. Mechanisms of vascular smooth muscle cell migration. *Circ Res* **100**, 607-621 (2007).
187. 2014 Alzheimer's disease facts and figures. *Alzheimers Dement* **10**, e47-e92 (2014).

188. Becker, R.E., Greig, N.H., Giacobini, E., Schneider, L.S. & Ferrucci, L. A new roadmap for drug development for Alzheimer's disease. *Nat Rev Drug Discov* **13**, 156 (2014).
189. Kaddurah-Daouk, R.*, et al.* Alterations in metabolic pathways and networks in Alzheimer/'s disease. *Transl Psychiatry* **3**, e244 (2013).
190. Wu, W. & Small, S.A. Imaging the earliest stages of Alzheimer's disease. *Curr Alzheimer Res* **3**, 529-539 (2006).
191. Jobst, K.A.*, et al.* Rapidly progressing atrophy of medial temporal lobe in Alzheimer's disease. *Lancet* **343**, 829-830 (1994).
192. Bradley, K.M.*, et al.* Cerebral perfusion SPET correlated with Braak pathological stage in Alzheimer's disease. *Brain* **125**, 1772-1781 (2002).
193. Mirra, S.S.*, et al.* The Consortium to Establish a Registry for Alzheimer's Disease (CERAD). Part II. Standardization of the neuropathologic assessment of Alzheimer's disease. *Neurology* **41**, 479-486 (1991).
194. Begley, P.*, et al.* Development and performance of a gas chromatography-time-of-flight mass spectrometry analysis for large-scale nontargeted metabolomic studies of human serum. *Anal Chem* **81**, 7038-7046 (2009).
195. Dunn, W.B.*, et al.* Procedures for large-scale metabolic profiling of serum and plasma using gas chromatography and liquid chromatography coupled to mass spectrometry. *Nat. Protoc* **6**, 1060-1083 (2011).
196. Brown, M.*, et al.* Mass spectrometry tools and metabolite-specific databases for molecular identification in metabolomics. *Analyst* **134**, 1322-1332 (2009).
197. Brown, M.*, et al.* Automated workflows for accurate mass-based putative metabolite identification in LC/MS-derived metabolomic datasets. *Bioinformatics* **27**, 1108-1112 (2011).
198. Gabbay, K.H. Hyperglycemia, polyol metabolism, and complications of diabetes mellitus. *Annu Rev Med* **26**, 521-536 (1975).
199. Engelke, U.F.*, et al.* Mitochondrial involvement and erythronic acid as a novel biomarker in transaldolase deficiency. *Biochim Biophys Acta* **1802**, 1028-1035 (2010).
200. Landaas, S. & Jakobs, C. The occurrence of 2-hydroxyisovaleric acid in patients with lactic acidosis and ketoacidosis. *Clin Chim Acta* **78**, 489-493 (1977).
201. Chang, C.Y., Ke, D.S. & Chen, J.Y. Essential fatty acids and human brain. *Acta Neurol Taiwan* **18**, 231-241 (2009).
202. Lajtha, A. *Metabolism in the Nervous System*, Springer US 1983., Boston, MA, (1983).
203. Weckwerth, W. *Metabolomics: Methods and Protocols*, Humana Press, (2007).
204. Maitre, M. The gamma-hydroxybutyrate signalling system in brain: organization and functional implications. *Prog Neurobiol* **51**, 337-361 (1997).
205. Trushina, E. & Mielke, M.M. Recent advances in the application of metabolomics to Alzheimer's Disease. *Biochim Biophys Acta* **1842**, 1232-1239 (2014).
206. Han, X. Multi-dimensional mass spectrometry-based shotgun lipidomics and the altered lipids at the mild cognitive impairment stage of Alzheimer's disease. *Biochim Biophys Acta* **1801**, 774-783 (2010).
207. Han, X.*, et al.* Metabolomics in early Alzheimer's disease: identification of altered plasma sphingolipidome using shotgun lipidomics. *PLoS One* **6**, e21643 (2011).
208. Kaddurah-Daouk, R.*, et al.* Metabolomic changes in autopsy-confirmed Alzheimer's disease. *Alzheimers Dement* **7**, 309-317 (2011).
209. Ibanez, C.*, et al.* Toward a predictive model of Alzheimer's disease progression using capillary electrophoresis-mass spectrometry metabolomics. *Anal Chem* **84**, 8532-8540 (2012).
210. Czech, C.*, et al.* Metabolite profiling of Alzheimer's disease cerebrospinal fluid. *PLoS One* **7**, e31501 (2012).
211. Oresic, M.*, et al.* Metabolome in progression to Alzheimer's disease. *Transl Psychiatry* **1**, e57 (2011).
212. Trushina, E., Dutta, T., Persson, X.-M.T., Mielke, M.M. & Petersen, R.C. Identification of altered metabolic pathways in plasma and CSF in mild cognitive impairment and Alzheimer's disease using metabolomics. *PLoS ONE* **8**, e63644 (2013).
213. Inoue, K.*, et al.* Metabolic profiling of Alzheimer's disease brains. *Sci. Rep.* **3**(2013).
214. Chan, R.B.*, et al.* Comparative lipidomic analysis of mouse and human brain with Alzheimer disease. *J Biol Chem* **287**, 2678-2688 (2012).
215. Blass, J.P. & Gibson, G.E. Cerebrometabolic aspects of delirium in relationship to dementia. *Dement Geriatr Cogn Disord* **10**, 335-338 (1999).
216. Mosconi, L.*, et al.* FDG-PET changes in brain glucose metabolism from normal cognition to pathologically verified Alzheimer's disease. *Eur J Nucl Med Mol Imaging* **36**, 811-822 (2009).

217. Arnaiz, E.*, et al.* Impaired cerebral glucose metabolism and cognitive functioning predict deterioration in mild cognitive impairment. *Neuroreport* **12**, 851-855 (2001).
218. Blennow, K., de Leon, M.J. & Zetterberg, H. Alzheimer's disease. *Lancet* **368**, 387-403 (2006).
219. Mattson, M.P. & Magnus, T. Ageing and neuronal vulnerability. *Nat Neurosci* **7**, 278-294 (2006).
220. Mosconi, L.*, et al.* FDG-PET changes in brain glucose metabolism from normal cognition to pathologically verified Alzheimer's disease. *Eur J Nucl Med Mol Imaging* **36**, 811-822 (2009).
221. Schönberger, S.J., Edgar, P.F., Kydd, R., Faull, R.L. & Cooper, G.J.S. Proteomic analysis of the brain in Alzheimer's disease: molecular phenotype of a complex disease process. *Proteomics* **1**, 1519-1528 (2001).
222. Arnáiz, E.*, et al.* Impaired cerebral glucose metabolism and cognitive functioning predict deterioration in mild cognitive impairment. *Neuroreport* **12**, 851-855 (2001).
223. Drzezga, A.*, et al.* Cerebral metabolic changes accompanying conversion of mild cognitive impairment into Alzheimer's disease: a PET follow-up study. *Eur J Nucl Med Mol Imaging* **30**, 1104-1113 (2003).
224. Simpson, I.A., Chundu, K., Davies-Hill, T., Honer, W.G. & Davies, P. Decreased concentrations of GLUT1 and GLUT3 glucose transporters in the brains of patients with Alzheimer's disease. *Ann Neurol* **35**, 546-551 (1994).
225. Costantini, L.C., Barr, L.J., Vogel, J.L. & Henderson, S.T. Hypometabolism as a therapeutic target in Alzheimer's disease. *BMC Neuroscience* **9 Suppl 2**, S16 (2008).
226. Talbot, K.*, et al.* Demonstrated brain insulin resistance in Alzheimer's disease patients is associated with IGF-1 resistance, IRS-1 dysregulation, and cognitive decline. *J Clin Invest* **122**, 1-23 (2012).
227. Brownlee, M. The pathobiology of diabetic complications: a unifying mechanism. *Diabetes* **54**, 1615-1625 (2005).
228. Brownlee, M. Biochemistry and molecular cell biology of diabetic complications. *Nature* **414**, 813-820 (2001).
229. Williamson, J.R.*, et al.* Hyperglycemic pseudohypoxia and diabetic complications. *Diabetes* **42**, 801-813 (1993).
230. Dringen, R., Hoepken, H., Minich, T. & Ruedig, C. Pentose phosphate pathway and NADPH metabolism. In*: Handbook of neurochemistry and molecular neurobiology. Brain energetics, integration of molecular and cellular processes*, Springer c2007., New York, (2007).
231. Kasischke, K. Lactate fuels the neonatal brain. *Front Neuroenergetics* **3**, 4 (2011).
232. Yao, J., Rettberg, J.R., Klosinski, L.P., Cadenas, E. & Brinton, R.D. Shift in brain metabolism in late onset Alzheimer's disease: implications for biomarkers and therapeutic interventions. *Mol Aspects Med* **32**, 247-257 (2011).
233. Guzman, M. & Blazquez, C. Ketone body synthesis in the brain: possible neuroprotective effects. *Prostaglandins, Leukot Essent Fatty Acids* **70**, 287-292 (2004).
234. Owen, O.E.*, et al.* Brain metabolism during fasting. *J Clin Invest* **46**, 1589-1595 (1967).
235. Pan, J.W., Rothman, D.L., Behar, K.L., Stein, D.T. & Hetherington, H.P. Human brain [bgr]-hydroxybutyrate and lactate increase in fasting-induced ketosis. *J Cereb Blood Flow Metab* **20**, 1502-1507 (2000).
236. Liebich, H.M. & Forst, C. Hydroxycarboxylic and oxocarboxylic acids in urine: products from branched-chain amino acid degradation and from ketogenesis. *J Chromatogr* **309**, 225-242 (1984).
237. Cunnane, S.*, et al.* Brain fuel metabolism, aging, and Alzheimer's disease. *Nutrition (***27**, 3-20 (2011).
238. Reger, M.A.*, et al.* Effects of β-hydroxybutyrate on cognition in memory-impaired adults. *Neurobiol Aging* **25**, 311-314 (2004).
239. Kashiwaya, Y.*, et al.* A ketone ester diet exhibits anxiolytic and cognition-sparing properties, and lessens amyloid and tau pathologies in a mouse model of Alzheimer's disease. *Neurobiol Aging* **34**, 1530-1539 (2013).
240. Maalouf, M., Sullivan, P.G., Davis, L., Kim, D.Y. & Rho, J.M. Ketones inhibit mitochondrial production of reactive oxygen species production following glutamate excitotoxicity by increasing NADH oxidation. *Neuroscience* **145**, 256-264 (2007).
241. Izumi, Y., Ishii, K., Katsuki, H., Benz, A.M. & Zorumski, C.F. beta-Hydroxybutyrate fuels synaptic function during development. Histological and physiological evidence in rat hippocampal slices. *J Clin Invest* **101**, 1121-1132 (1998).
242. Sochor, M., Baquer, N.Z. & McLean, P. Glucose overutilization in diabetes: evidence from studies on the changes in hexokinase, the pentose phosphate pathway and glucuronate-

xylulose pathway in rat kidney cortex in diabetes. *Biochem Biophys Res Commun* **86**, 32-39 (1979).
243. Asakura, T., Adachi, K., Minagami, S. & Yoshikawa, H. Non-glycolytic sugar metabolism in human erythrocytes. I. Xylitol metabolism. *J Biochem* **62**, 184-193 (1967).
244. Pitkanen, E. The conversion of D-xylose into D-threitol in patients without liver disease and in patients with portal liver cirrhosis. *Clin Chim Acta* **80**, 49-54 (1977).
245. Hanover, J.A. Glycan-dependent signaling: O-linked N-acetylglucosamine. *FASEB J* **15**, 1865-1876 (2001).
246. Fulop, N.*, et al.* Aging leads to increased levels of protein O-linked N-acetylglucosamine in heart, aorta, brain and skeletal muscle in Brown-Norway rats. *Biogerontology* **9**, 139-151 (2008).
247. Shimohama, S., Tanino, H., Sumida, Y., Tsuda, J. & Fujimoto, S. Alteration of myo-inositol monophosphatase in Alzheimer's disease brains. *Neurosci Lett* **245**, 159-162 (1998).
248. Shughrue, P.*, et al.* Chronic treatment with scyllo-inositol reduces brain myo-inositol levels and enhances performance in a rat model of social withdrawal. *Alzheimers Dement* **9**, P157 (2013).
249. Finegold, D., Lattimer, S.A., Nolle, S., Bernstein, M. & Greene, D.A. Polyol pathway activity and myo-inositol metabolism. A suggested relationship in the pathogenesis of diabetic neuropathy. *Diabetes* **32**, 988-992 (1983).
250. Kruman, II*, et al.* Suppression of uracil-DNA glycosylase induces neuronal apoptosis. *J Biol Chem* **279**, 43952-43960 (2004).
251. Kovacs, Z.*, et al.* Post mortem degradation of nucleosides in the brain: comparison of human and rat brains for estimation of in vivo concentration of nucleosides. *J Neurosci Methods* **148**, 88-93 (2005).
252. Becker, B.F. Towards the physiological function of uric acid. *Free Radic Biol Med* **14**, 615-631 (1993).
253. Yu, Z.F., Bruce-Keller, A.J., Goodman, Y. & Mattson, M.P. Uric acid protects neurons against excitotoxic and metabolic insults in cell culture, and against focal ischemic brain injury in vivo. *J Neurosci Res* **53**, 613-625 (1998).
254. Kim, T.S.*, et al.* Decreased plasma antioxidants in patients with Alzheimer's disease. *Int J Geriatr Psychiatry* **21**, 344-348 (2006).
255. Rinaldi, P.*, et al.* Plasma antioxidants are similarly depleted in mild cognitive impairment and in Alzheimer's disease. *Neurobiol Aging* **24**, 915-919 (2003).
256. Irizarry, M.C.*, et al.* Plasma urate and progression of mild cognitive impairment. *Neuro-degener Dis* **6**, 23-28 (2009).
257. Euser, S.M., Hofman, A., Westendorp, R.G. & Breteler, M.M. Serum uric acid and cognitive function and dementia. *Brain* **132**, 377-382 (2009).
258. Degrell, I. & Niklasson, F. Purine metabolites in the CSF in presenile and senile dementia of Alzheimer type, and in multi infarct dementia. *Arch Gerontol Geriatr* **7**, 173-178 (1988).
259. Kronenberg, G.*, et al.* Folate deficiency induces neurodegeneration and brain dysfunction in mice lacking uracil DNA glycosylase. *J Neurosci* **28**, 7219-7230 (2008).
260. Dietschy, J.M. & Turley, S.D. Cholesterol metabolism in the brain. *Curr Opin Lipidol* **12**, 105-112 (2001).
261. Vance, J.E. Dysregulation of cholesterol balance in the brain: contribution to neurodegenerative diseases. *Dis Model Mech* **5**, 746-755 (2012).
262. Mailman, T., Hariharan, M. & Karten, B. Inhibition of neuronal cholesterol biosynthesis with lovastatin leads to impaired synaptic vesicle release even in the presence of lipoproteins or geranylgeraniol. *J Neurochem* **119**, 1002-1015 (2011).
263. Takeoka, M., Soman, T.B., Shih, V.E., Caviness, V.S., Jr. & Krishnamoorthy, K.S. Carbamyl phosphate synthetase 1 deficiency: a destructive encephalopathy. *Pediatr Neurol* **24**, 193-199 (2001).
264. Sporn, M.B., Dingman, W., Defalco, A. & Davies, R.K. Formation of urea from arginine in the brain of the living rat. *Nature* **183**, 1520-1521 (1959).
265. Howell, B.W., Lagace, M. & Shore, G.C. Activity of the carbamyl phosphate synthetase I promoter in liver nuclear extracts is dependent on a cis-acting C/EBP recognition element. *Mol Cell Biol* **9**, 2928-2933 (1989).
266. Kanamori, K., Ross, B.D. & Kondrat, R.W. Rate of glutamate synthesis from leucine in rat brain measured in vivo by 15N NMR. *J Neurochem* **70**, 1304-1315 (1998).
267. Lowe, S.L., Bowen, D.M., Francis, P.T. & Neary, D. Ante mortem cerebral amino acid concentrations indicate selective degeneration of glutamate-enriched neurons in Alzheimer's disease. *Neuroscience* **38**, 571-577 (1990).

268. Francis, P.T. Glutamatergic systems in Alzheimer's disease. *Int J Geriatr Psychiatry* **18**, S15-21 (2003).
269. Perry, E.K., Gibson, P.H., Blessed, G., Perry, R.H. & Tomlinson, B.E. Neurotransmitter enzyme abnormalities in senile dementia: Choline acetyltransferase and glutamic acid decarboxylase activities in necropsy brain tissue. *J Neurol Sci* **34**, 247-265 (1977).
270. Rigotti, D.J., Inglese, M. & Gonen, O. Whole-brain N-acetylaspartate as a surrogate marker of neuronal damage in diffuse neurologic disorders. *Am J Neuroradiol* **28**, 1843-1849 (2007).
271. Fernstrom, J.D. & Fernstrom, M.H. Tyrosine, phenylalanine, and catecholamine synthesis and function in the brain. *J Nutr* **137**, 1539S-1547S (2007).
272. Garcia-Alloza, M.*, et al.* Cholinergic–serotonergic imbalance contributes to cognitive and behavioral symptoms in Alzheimer's disease. *Neuropsychologia* **43**, 442-449 (2005).
273. Storga, D., Vrecko, K., Birkmayer, J.G. & Reibnegger, G. Monoaminergic neurotransmitters, their precursors and metabolites in brains of Alzheimer patients. *Neurosci Lett* **203**, 29-32 (1996).
274. Matthews, K.L.*, et al.* Noradrenergic changes, aggressive behavior, and cognition in patients with dementia. *Biol Psychiatry* **51**, 407-416 (2002).
275. Degrell, I., Hellsing, K., Nagy, E. & Niklasson, F. Amino acid concentrations in cerebrospinal fluid in presenile and senile dementia of Alzheimer type and multi-infarct dementia. *Arch Gerontol Geriatr* **9**, 123-135 (1989).
276. Harrison, F.E. & May, J.M. Vitamin C function in the brain: vital role of the ascorbate transporter SVCT2. *Free Radic Biol Med* **46**, 719-730 (2009).
277. Seijo-Martinez, M.*, et al.* L-2-hydroxyglutaric aciduria: clinical, neuroimaging, and neuropathological findings. *Arch Neurol* **62**, 666-670 (2005).
278. Latini, A.*, et al.* Induction of oxidative stress by L-2-hydroxyglutaric acid in rat brain. *J Neurosci Res* **74**, 103-110 (2003).
279. Rzem, R.*, et al.* A gene encoding a putative FAD-dependent L-2-hydroxyglutarate dehydrogenase is mutated in L-2-hydroxyglutaric aciduria. *Proc Natl Acad Sci U S A* **101**, 16849-16854 (2004).
280. He, X., Huang, Y., Li, B., Gong, C.X. & Schuchman, E.H. Deregulation of sphingolipid metabolism in Alzheimer's disease. *Neurobiol Aging* **31**, 398-408 (2010).
281. Goni, F.M. & Alonso, A. Sphingomyelinases: enzymology and membrane activity. *FEBS Lett* **531**, 38-46 (2002).
282. Huang, Y.*, et al.* Elevation of the level and activity of acid ceramidase in Alzheimer's disease brain. *Eur J Neurosci* **20**, 3489-3497 (2004).
283. Satoi, H.*, et al.* Astroglial expression of ceramide in Alzheimer's disease brains: a role during neuronal apoptosis. *Neuroscience* **130**, 657-666 (2005).
284. Gomez-Munoz, A., Kong, J., Salh, B. & Steinbrecher, U.P. Sphingosine-1-phosphate inhibits acid sphingomyelinase and blocks apoptosis in macrophages. *FEBS Lett* **539**, 56-60 (2003).
285. Hla, T. Signaling and biological actions of sphingosine 1-phosphate. *Pharmacol Res* **47**, 401-407 (2003).
286. Malaplate-Armand, C.*, et al.* Soluble oligomers of amyloid-beta peptide induce neuronal apoptosis by activating a cPLA2-dependent sphingomyelinase-ceramide pathway. *Neurobiol Dis* **23**, 178-189 (2006).
287. Fonteh, A.N.*, et al.* Alterations in cerebrospinal fluid glycerophospholipids and phospholipase A2 activity in Alzheimer's disease. *J Lipid Res* **54**, 2884-2897 (2013).
288. Farooqui, A.A. & Horrocks, L.A. Brain phospholipases A2: a perspective on the history. *Prostaglandins Leukot Essent Fatty Acids* **71**, 161-169 (2004).
289. Nitsch, R.M.*, et al.* Evidence for a membrane defect in Alzheimer disease brain. *Proc Natl Acad Sci U S A* **89**, 1671-1675 (1992).
290. Guan, Z.*, et al.* Decrease and structural modifications of phosphatidylethanolamine plasmalogen in the brain with Alzheimer disease. *J Neuropathol Exp Neurol* **58**, 740-747 (1999).
291. Tajima, Y.*, et al.* Lipidomic analysis of brain tissues and plasma in a mouse model expressing mutated human amyloid precursor protein/tau for Alzheimer's disease. *Lipids Health Dis* **12**, 68 (2013).
292. Bennett, S.A.*, et al.* Using neurolipidomics to identify phospholipid mediators of synaptic (dys)function in Alzheimer's Disease. *Front Physiol* **4**, 168 (2013).
293. Han, X., Holtzman, D.M. & McKeel, D.W., Jr. Plasmalogen deficiency in early Alzheimer's disease subjects and in animal models: molecular characterization using electrospray ionization mass spectrometry. *J Neurochem* **77**, 1168-1180 (2001).

294. Stokes, C.E. & Hawthorne, J.N. Reduced phosphoinositide concentrations in anterior temporal cortex of Alzheimer-diseased brains. *J Neurochem* **48**, 1018-1021 (1987).
295. Rigoni, M.*, et al.* Equivalent effects of snake PLA2 neurotoxins and lysophospholipid-fatty acid mixtures. *Science* **310**, 1678-1680 (2005).
296. Coleman, R.A. & Mashek, D.G. Mammalian triacylglycerol metabolism: synthesis, lipolysis, and signaling. *Chem Rev* **111**, 6359-6386 (2011).
297. Wendel, A.A., Lewin, T.M. & Coleman, R.A. Glycerol-3-phosphate acyltransferases: rate limiting enzymes of triacylglycerol biosynthesis. *Bioch Biophys Acta* **1791**, 501-506 (2009).
298. Tu-Sekine, B. & Raben, D.M. Regulation and roles of neuronal diacylglycerol kinases: a lipid perspective. *Crit Rev Biochem Mol Biol* **46**, 353-364 (2011).
299. Reisenberg, M., Singh, P.K., Williams, G. & Doherty, P. The diacylglycerol lipases: structure, regulation and roles in and beyond endocannabinoid signalling. *Philos Trans R Soc Lond B Biol Sci* **367**, 3264-3275 (2012).
300. Wang, S.P.*, et al.* Metabolism as a tool for understanding human brain evolution: Lipid energy metabolism as an example. *J Hum Evol* **77**, 41-49 (2014).
301. Compton, J., van Amelsvoort, T. & Murphy, D. HRT and its effect on normal ageing of the brain and dementia. *Br J Clin Pharmacol* **52**, 647-653 (2001).
302. Compton, J., van Amelsvoort, T. & Murphy, D. Mood, cognition and Alzheimer's disease. *Best Pract Res Clin Obstet Gynaecol* **16**, 357-370 (2002).
303. Puglielli, L., Tanzi, R.E. & Kovacs, D.M. Alzheimer's disease: the cholesterol connection. *Nat Neurosci* **6**, 345-351 (2003).
304. Braak, H. & Braak, E. Evolution of neuronal changes in the course of Alzheimer's disease. *J Neural Transm Suppl* **53**, 127-140 (1998).
305. Dickson, D.W. Neuropathological diagnosis of Alzheimer's disease: a perspective from longitudinal clinicopathological studies. *Neurobiol Aging* **18**, S21-26 (1997).
306. Mattson, M.P. Pathways towards and away from Alzheimer's disease. *Nature* **430**, 631-639 (2004).
307. Buxbaum, J.D.*, et al.* Alzheimer amyloid protein precursor in the rat hippocampus: transport and processing through the perforant path. *J Neurosci* **18**, 9629-9637 (1998).
308. Mandelkow, E.M., Stamer, K., Vogel, R., Thies, E. & Mandelkow, E. Clogging of axons by tau, inhibition of axonal traffic and starvation of synapses. *Neurobiol Aging* **24**, 1079-1085 (2003).
309. Ferreira, I.L., Resende, R., Ferreiro, E., Rego, A.C. & Pereira, C.F. Multiple defects in energy metabolism in Alzheimer's disease. *Curr Drug Targets* **11**, 1193-1206 (2010).
310. Rudy, C.C., Hunsberger, H.C., Weitzner, D.S. & Reed, M.N. The role of the tripartite glutamatergic synapse in the pathophysiology of Alzheimer's disease. *Aging Dis* **6**, 131-148 (2015).
311. Chen, K.H., Reese, E.A., Kim, H.W., Rapoport, S.I. & Rao, J.S. Disturbed neurotransmitter transporter expression in Alzheimer's disease brain. *J Alzheimers Dis* **26**, 755-766 (2011).
312. Shevchenko, G., Konzer, A., Musunuri, S. & Bergquist, J. Neuroproteomics tools in clinical practice. *Biochim Biophys Acta* (2015).
313. Hawkridge, A.M. & Muddiman, D.C. Mass spectrometry-based biomarker discovery: toward a global proteome index of individuality. *Annu Rev Anal Chem (Palo Alto Calif).* **2**, 265-277 (2009).
314. Musunuri, S.*, et al.* Micellar extraction possesses a new advantage for the analysis of Alzheimer's disease brain proteome. *Anal Bioanal Chem* **407**, 1041-1057 (2015).
315. Musunuri, S.*, et al.* Quantification of the brain proteome in Alzheimer's disease using multiplexed mass spectrometry. *J Proteome Res* **13**, 2056-2068 (2014).
316. Manavalan, A.*, et al.* Brain site-specific proteome changes in aging-related dementia. *Exp Mol Med* **45**, e39 (2013).
317. Andreev, V.P.*, et al.* Label-free quantitative LC-MS proteomics of Alzheimer's disease and normally aged human brains. *J Proteome Res* **11**, 3053-3067 (2012).
318. Chen, S., Lu, F.F., Seeman, P. & Liu, F. Quantitative proteomic analysis of human substantia nigra in Alzheimer's disease, Huntington's disease and Multiple sclerosis. *Neurochem Res* **37**, 2805-2813 (2012).
319. Erol, A. Are paradoxical cell cycle activities in neurons and glia related to the metabolic theory of Alzheimer's disease? *J Alzheimers Dis* **19**, 129-135 (2010).
320. McShea, A., Wahl, A.F. & Smith, M.A. Re-entry into the cell cycle: a mechanism for neurodegeneration in Alzheimer disease. *Med Hypotheses* **52**, 525-527 (1999).
321. Buhaescu, I. & Izzedine, H. Mevalonate pathway: a review of clinical and therapeutical implications. *Clin Bioch* **40**, 575-584 (2007).

322. Foxton, R.H., Land, J.M. & Heales, S.J. Tetrahydrobiopterin availability in Parkinson's and Alzheimer's disease; potential pathogenic mechanisms. *Neurochem Res* **32**, 751-756 (2007).
323. Kato, U.*, et al.* Role for phospholipid flippase complex of ATP8A1 and CDC50A proteins in cell migration. *J Biol Chem* **288**, 4922-4934 (2013).
324. Patel, M.S., Nemeria, N.S., Furey, W. & Jordan, F. The pyruvate dehydrogenase complexes: structure-based function and regulation. *J Biol Chem* **289**, 16615-16623 (2014).
325. Hirai, K.*, et al.* Mitochondrial abnormalities in Alzheimer's disease. *J Neurosci* **21**, 3017-3023 (2001).
326. Papa, S.*, et al.* The oxidative phosphorylation system in mammalian mitochondria. *Adv Exp Med Biol* **942**, 3-37 (2012).
327. Yudkoff, M.*, et al.* Brain glutamate metabolism: neuronal-astroglial relationships. *Dev Neurosci* **15**, 343-350 (1993).
328. Yudkoff, M. Brain metabolism of branched-chain amino acids. *Glia* **21**, 92-98 (1997).
329. Ding, Q., Markesbery, W.R., Chen, Q., Li, F. & Keller, J.N. Ribosome dysfunction is an early event in Alzheimer's disease. *J Neurosci* **25**, 9171-9175 (2005).
330. Sulistio, Y.A. & Heese, K. The Ubiquitin-Proteasome System and Molecular Chaperone Deregulation in Alzheimer's Disease. *Mol Neurobiol* (2015).
331. Kappe, G.*, et al.* The human genome encodes 10 alpha-crystallin-related small heat shock proteins: HspB1-10. *Cell Stress Chaperones* **8**, 53-61 (2003).
332. Murata, S., Yashiroda, H. & Tanaka, K. Molecular mechanisms of proteasome assembly. *Nat Rev Mol Cell Biol* **10**, 104-115 (2009).
333. Urnavicius, L.*, et al.* The structure of the dynactin complex and its interaction with dynein. *Science* **347**, 1441-1446 (2015).
334. Kapogiannis, D. & Mattson, M.P. Disrupted energy metabolism and neuronal circuit dysfunction in cognitive impairment and Alzheimer's disease. *Lancet. Neurol* **10**, 187-198 (2011).
335. Simpson, I.A., Chundu, K.R., Davies-Hill, T., Honer, W.G. & Davies, P. Decreased concentrations of GLUT1 and GLUT3 glucose transporters in the brains of patients with Alzheimer's disease. *Ann Neurol* **35**, 546-551 (1994).
336. Liu, C.C.*, et al.* Neuronal LRP1 Regulates glucose metabolism and insulin signaling in the brain. *J Neurosci* **35**, 5851-5859 (2015).
337. Adibhatla, R.M. & Hatcher, J.F. Lipid oxidation and peroxidation in CNS health and disease: from molecular mechanisms to therapeutic opportunities. *Antioxid Redox Signal* **12**, 125-169 (2010).
338. Schonfeld, P. & Reiser, G. Why does brain metabolism not favor burning of fatty acids to provide energy? Reflections on disadvantages of the use of free fatty acids as fuel for brain. *J Cereb Blood Flow Metab* **33**, 1493-1499 (2013).
339. Fabelo, N.*, et al.* Altered lipid composition in cortical lipid rafts occurs at early stages of sporadic Alzheimer's disease and facilitates APP/BACE1 interactions. *Neurobiol Aging* **35**, 1801-1812 (2014).
340. Lhermusier, T., Chap, H. & Payrastre, B. Platelet membrane phospholipid asymmetry: from the characterization of a scramblase activity to the identification of an essential protein mutated in Scott syndrome. *J Thromb Haemost* **9**, 1883–1891).
342. van Echten-Deckert, G., Hagen-Euteneuer, N., Karaca, I. & Walter, J. Sphingosine-1-phosphate: boon and bane for the brain. *Cell Physiol Biochem* **34**, 148-157 (2014).
343. Sheu, K.F., Kim, Y.T., Blass, J.P. & Weksler, M.E. An immunochemical study of the pyruvate dehydrogenase deficit in Alzheimer's disease brain. *Ann Neurol* **17**, 444-449 (1985).
344. Sorbi, S., Bird, E.D. & Blass, J.P. Decreased pyruvate dehydrogenase complex activity in Huntington and Alzheimer brain. *Ann Neurol* **13**, 72-78 (1983).
345. Karbowski, M. & Neutzner, A. Neurodegeneration as a consequence of failed mitochondrial maintenance. *Acta Neuropathol* **123**, 157-171 (2012).
346. Cadenas, E. & Davies, K.J. Mitochondrial free radical generation, oxidative stress, and aging. *Free Radic Biol Med* **29**, 222-230 (2000).
347. Papa, S. & De Rasmo, D. Complex I deficiencies in neurological disorders. *Trends Mol Med* **19**, 61-69 (2013).
348. Parker, W.D., Jr., Parks, J., Filley, C.M. & Kleinschmidt-DeMasters, B.K. Electron transport chain defects in Alzheimer's disease brain. *Neurology* **44**, 1090-1096 (1994).
349. Parker, W.D., Jr., Boyson, S.J. & Parks, J.K. Abnormalities of the electron transport chain in idiopathic Parkinson's disease. *Ann Neurol* **26**, 719-723 (1989).
350. Indo, H.P.*, et al.* Evidence of ROS generation by mitochondria in cells with impaired electron transport chain and mitochondrial DNA damage. *Mitochondrion* **7**, 106-118 (2007).

351. Guo, C., Sun, L., Chen, X. & Zhang, D. Oxidative stress, mitochondrial damage and neurodegenerative diseases. *Neural Regen Res* **8**, 2003-2014 (2013).
352. Jiang, F., Zhang, Y. & Dusting, G.J. NADPH oxidase-mediated redox signaling: roles in cellular stress response, stress tolerance, and tissue repair. *Pharmacol Rev* **63**, 218-242 (2011).
353. Schrader, M. & Fahimi, H.D. Peroxisomes and oxidative stress. *Biochim Biophys Acta* **1763**, 1755-1766 (2006).
354. Handy, D.E.*, et al.* Glutathione peroxidase-1 regulates mitochondrial function to modulate redox-dependent cellular responses. *J Biol Chem* **284**, 11913-11921 (2009).
355. Matsumoto, C., Shinkai, T., Hori, H., Ohmori, O. & Nakamura, J. Polymorphisms of dopamine degradation enzyme (COMT and MAO) genes and tardive dyskinesia in patients with schizophrenia. *Psychiatry Res* **127**, 1-7 (2004).
356. Knoops, B., Goemaere, J., Van der Eecken, V. & Declercq, J.P. Peroxiredoxin 5: structure, mechanism, and function of the mammalian atypical 2-Cys peroxiredoxin. *Antioxid Redox Signal* **15**, 817-829 (2011).
357. Volkert, M.R., Elliott, N.A. & Housman, D.E. Functional genomics reveals a family of eukaryotic oxidation protection genes. *Proc Natl Acad Sci U S A* **97**, 14530-14535 (2000).
358. Mazzocco, M.*, et al.* The identification of a novel human homologue of the SH3 binding glutamic acid-rich (SH3BGR) gene establishes a new family of highly conserved small proteins related to Thioredoxin Superfamily. *Gene* **291**, 233-239 (2002).
359. Sousa Silva, M., Gomes, R.A., Ferreira, A.E., Ponces Freire, A. & Cordeiro, C. The glyoxalase pathway: the first hundred years... and beyond. *Biochem J* **453**, 1-15 (2013).
360. Schmidt, B.*, et al.* Effects of glyoxal or methylglyoxal on the metabolism of amino acids, lactate, glucose and acetate in the cerebral cortex of young and adult rats. *Brain Res* **1315**, 19-24 (2010).
361. Trushina, E.*, et al.* Defects in mitochondrial dynamics and metabolomic signatures of evolving energetic stress in mouse models of familial Alzheimer's disease. *PLoS One* **7**, e32737 (2012).
362. Thornton, C. & Hagberg, H. Role of mitochondria in apoptotic and necroptotic cell death in the developing brain. *Clin Chim Acta* **451**, (Pt A) 35-8 (2015).
363. Wang, C. & Youle, R.J. The role of mitochondria in apoptosis*. *Annu Rev Genet* **43**, 95-118 (2009).
364. Bading, H. Nuclear calcium signalling in the regulation of brain function. *Nat Rev Neurosci* **14**, 593-608 (2013).
365. Demetrius, L.A. & Simon, D.K. An inverse-Warburg effect and the origin of Alzheimer's disease. *Biogerontology* **13**, 583-594 (2012).
366. Gazulla, J. & Cavero-Nagore, M. [Glutamate and Alzheimer's disease]. *Rev Neurol* **42**, 427-432 (2006).
367. Harris, R.A., Joshi, M., Jeoung, N.H. & Obayashi, M. Overview of the molecular and biochemical basis of branched-chain amino acid catabolism. *J Nutr* **135**, 1527S-1530S (2005).
368. Baumgartner, M.R.*, et al.* The molecular basis of human 3-methylcrotonyl-CoA carboxylase deficiency. *J Clin Invest* **107**, 495-504 (2001).
369. Hallen, A., Jamie, J.F. & Cooper, A.J. Lysine metabolism in mammalian brain: an update on the importance of recent discoveries. *Amino Acids* **45**, 1249-1272 (2013).
370. Schwarcz, R., Bruno, J.P., Muchowski, P.J. & Wu, H.Q. Kynurenines in the mammalian brain: when physiology meets pathology. *Nat Rev Neurosci* **13**, 465-477 (2012).
371. Seiler, N. & Daune-Anglard, G. Endogenous ornithine in search for CNS functions and therapeutic applications. *Metab Brain Dis* **8**, 151-179 (1993).
372. Ichinose, H., Nomura, T. & Sumi-Ichinose, C. Metabolism of tetrahydrobiopterin: its relevance in monoaminergic neurons and neurological disorders. *Chem Rec (New York, N.Y.)* **8**, 378-385 (2008).
373. Burbaeva, G.*, et al.* A role of glutamate decarboxylase in Alzheimer's disease. *Zh Nevrol Psikhiatr Im S S Korsakova* **114**, 68-72 (2014).
374. Kwon, O.S., Park, J. & Churchich, J.E. Brain 4-aminobutyrate aminotransferase. Isolation and sequence of a cDNA encoding the enzyme. *J Biol Chem* **267**, 7215-7216 (1992).
375. Abell, C.W. & Kwan, S.W. Molecular characterization of monoamine oxidases A and B. *Prog Nucleic Acid Res Mol Biol* **65**, 129-156 (2001).
376. Moore, M.J. & Proudfoot, N.J. Pre-mRNA processing reaches back to transcription and ahead to translation. *Cell* **136**, 688-700 (2009).
377. Baumbach, L.L., Stein, G.S. & Stein, J.L. Regulation of human histone gene expression: transcriptional and posttranscriptional control in the coupling of histone messenger RNA stability with DNA replication. *Biochemistry* **26**, 6178-6187 (1987).

378. Olzscha, H., Sheikh, S. & La Thangue, N.B. Deacetylation of chromatin and gene expression regulation: a new target for epigenetic therapy. *Crit Rev Oncog* **20**, 1-17 (2015).
379. Horsburgh, S., Robson-Ansley, P., Adams, R. & Smith, C. Exercise and inflammation-related epigenetic modifications: focus on DNA methylation. *Exerc Immunol Rev* **21**, 26-41 (2015).
380. Eom, G.H.*, et al.* Histone methyltransferase SETD3 regulates muscle differentiation. *J Biol Chem* **286**, 34733-34742 (2011).
381. Liang, X.Q., Du, Y.P., Wang, D.L. & Yang, Y. The biological functions of lysine methyltransferase PR-SET7]. *Yi Chuan* **35**, 241-254 (2013).
382. Wysocka, J., Allis, C.D. & Coonrod, S. Histone arginine methylation and its dynamic regulation. *Front Biosci* **11**, 344-355 (2006).
383. Passon, D.M.*, et al.* Structure of the heterodimer of human NONO and paraspeckle protein component 1 and analysis of its role in subnuclear body formation. *Proc Natl Acad Sci U S A* **109**, 4846-4850 (2012).
384. Abdelhaleem, M. RNA helicases: regulators of differentiation. *Clin Biochem* **38**, 499-503 (2005).
385. Lopes, J.P., Oliveira, C.R. & Agostinho, P. Cell cycle re-entry in Alzheimer's disease: a major neuropathological characteristic? *Curr Alzheimer Res* **6**, 205-212 (2009).
386. Jean-Philippe, J., Paz, S. & Caputi, M. hnRNP A1: the Swiss army knife of gene expression. *Int J Mol Sci* **14**, 18999-19024 (2013).
387. Lee, Y. & Rio, D.C. Mechanisms and regulation of alternative pre-mRNA splicing. *Annu Rev Biochem* **84**, 291-323 (2015).
388. Valadkhan, S. snRNAs as the catalysts of pre-mRNA splicing. *Curr Opin Chem Biol* **9**, 603-608 (2005).
389. Carissimi, C.*, et al.* Unrip is a component of SMN complexes active in snRNP assembly. *FEBS Lett* **579**, 2348-2354 (2005).
390. Grainger, R.J. & Beggs, J.D. Prp8 protein: at the heart of the spliceosome. *RNA (New York)* **11**, 533-557 (2005).
391. Liu, S., Rauhut, R., Vornlocher, H.P. & Luhrmann, R. The network of protein-protein interactions within the human U4/U6.U5 tri-snRNP. *RNA (New York)* **12**, 1418-1430 (2006).
392. Nguyen, T.H.*, et al.* Structural basis of Brr2-Prp8 interactions and implications for U5 snRNP biogenesis and the spliceosome active site. *Structure (London)* **21**, 910-919 (2013).
393. Bai, B.*, et al.* U1 small nuclear ribonucleoprotein complex and RNA splicing alterations in Alzheimer's disease. *Proc Natl Acad Sci U S A* **110**, 16562-16567 (2013).
394. O'Brien, T.W. Properties of human mitochondrial ribosomes. *IUBMB Life* **55**, 505-513 (2003).
395. Holzmann, J.*, et al.* RNase P without RNA: identification and functional reconstitution of the human mitochondrial tRNA processing enzyme. *Cell* **135**, 462-474 (2008).
396. Zhou, M., Yang, W.L., Ji, Y., Qiang, X. & Wang, P. Cold-inducible RNA-binding protein mediates neuroinflammation in cerebral ischemia. *Biochim Biophys Acta* **1840**, 2253-2261 (2014).
397. Liu, J.*, et al.* Argonaute2 is the catalytic engine of mammalian RNAi. *Science* **305**, 1437-1441 (2004).
398. Oka, T.*, et al.* Isolation and characterization of a novel perchloric acid-soluble protein inhibiting cell-free protein synthesis. *J Biol Chem* **270**, 30060-30067 (1995).
399. Deocaris, C.C., Kaul, S.C. & Wadhwa, R. On the brotherhood of the mitochondrial chaperones mortalin and heat shock protein 60. *Cell Stress Chaperones* **11**, 116-128 (2006).
400. Yoshida, S.*, et al.* Molecular chaperone TRAP1 regulates a metabolic switch between mitochondrial respiration and aerobic glycolysis. *Proc Natl Acad Sci U S A* **110**, E1604-1612 (2013).
401. Jakob, U., Gaestel, M., Engel, K. & Buchner, J. Small heat shock proteins are molecular chaperones. *J Biol Chem* **268**, 1517-1520 (1993).
402. Brownell, S.E., Becker, R.A. & Steinman, L. The protective and therapeutic function of small heat shock proteins in neurological diseases. *Front Immunol* **3**, 74 (2012).
403. Li, J. & Buchner, J. Structure, function and regulation of the hsp90 machinery. *Biomed J* **36**, 106-117 (2013).
404. Mayer, M.P. & Bukau, B. Hsp70 chaperones: cellular functions and molecular mechanism. *Cell Mol Life Sci* **62**, 670-684 (2005).
405. Doong, H., Vrailas, A. & Kohn, E.C. What's in the 'BAG'?--A functional domain analysis of the BAG-family proteins. *Cancer Lett* **188**, 25-32 (2002).
406. Annunziata, C.M.*, et al.* BAG-4/SODD and associated antiapoptotic proteins are linked to aggressiveness of epithelial ovarian cancer. *Clin Cancer Res* **13**, 6585-6592 (2007).

407. Guo, K., Li, L., Yin, G., Zi, X. & Liu, L. Bag5 Protects Neuronal Cells from Amyloid beta-induced Cell Death protects neuronal cells from amyloid β-induced cell death. *J Mol Neurosci* **55**, 815-820 (2015).
408. Raynes, D.A. & Guerriero, V., Jr. Inhibition of Hsp70 ATPase activity and protein renaturation by a novel Hsp70-binding protein. *J Biol Chem* **273**, 32883-32888 (1998).
409. Dutta, S. & Tan, Y.J. Structural and functional characterization of human SGT and its interaction with Vpu of the human immunodeficiency virus type 1. *Biochemistry* **47**, 10123-10131 (2008).
410. Bedard, K., Szabo, E., Michalak, M. & Opas, M. Cellular functions of endoplasmic reticulum chaperones calreticulin, calnexin, and ERp57. *Int J Cytol* **245**, 91-121 (2005).
411. Millan-Zambrano, G. & Chavez, S. Nuclear functions of prefoldin. *Open Biology* **4**(2014).
412. Chagoyen, M., Carrascosa, J.L., Pazos, F. & Valpuesta, J.M. Molecular determinants of the ATP hydrolysis asymmetry of the CCT chaperonin complex. *Proteins* **82**, 703-707 (2014).
413. Keller, J.N., Hanni, K.B. & Markesbery, W.R. Impaired proteasome function in Alzheimer's disease. *J Neurochem* **75**, 436-439 (2000).
414. Gorbea, C., Goellner, G.M., Teter, K., Holmes, R.K. & Rechsteiner, M. Characterization of mammalian Ecm29, a 26 S proteasome-associated protein that localizes to the nucleus and membrane vesicles. *J Biol Chem* **279**, 54849-54861 (2004).
415. Schmaler, T. & Dubiel, W. Control of deneddylation by the Cop9 signalosome. *Subcell Biochem* **54**, 57-68 (2010).
416. Wu, J.T., Lin, H.C., Hu, Y.C. & Chien, C.T. Neddylation and deneddylation regulate Cul1 and Cul3 protein accumulation. *Nat Cell Biol* **7**, 1014-1020 (2005).
417. Birol, M.*, et al.* Structural and biochemical characterization of the Cop9 signalosome CSN5/CSN6 heterodimer. *PLoS One* **9**, e105688 (2014).
418. Jia, B., Wu, Y. & Zhou, Y. 14-3-3 and aggresome formation: implications in neurodegenerative diseases. *Prion* **8**(2014).
419. Umahara, T., Uchihara, T. & Iwamoto, T. Structure-oriented review of 14-3-3 protein isoforms in geriatric neuroscience. *Geriatr Gerontol Int* **12**, 586-599 (2012).
420. Shimada, T., Fournier, A.E. & Yamagata, K. Neuroprotective function of 14-3-3 proteins in neurodegeneration. *BioMed Res Int* **2013**, 564534 (2013).
421. Vicario-Orri, E., Opazo, C.M. & Munoz, F.J. The pathophysiology of axonal transport in Alzheimer's disease. *J Alzheimers Dis* **43**, 1097-1113 (2015).
422. Stokin, G.B. & Goldstein, L.S. Axonal transport and Alzheimer's disease. *Annu Rev Biochem* **75**, 607-627 (2006).
423. Matsuda, S., Matsuda, Y. & D'Adamio, L. BRI3 inhibits amyloid precursor protein processing in a mechanistically distinct manner from its homologue dementia gene BRI2. *J Biol Chem* **284**, 15815-15825 (2009).
424. Murayama, K.S.*, et al.* Reticulons RTN3 and RTN4-B/C interact with BACE1 and inhibit its ability to produce amyloid beta-protein. *Eur J Neurosci* **24**, 1237-1244 (2006).
425. Elliott, D.A., Weickert, C.S. & Garner, B. Apolipoproteins in the brain: implications for neurological and psychiatric disorders. *Clin Lipidol* **51**, 555-573 (2010).
426. Pollio, G.*, et al.* Increased expression of the oligopeptidase THOP1 is a neuroprotective response to Abeta toxicity. *Neurobiol Dis* **31**, 145-158 (2008).
427. Heneka, M.T., Golenbock, D.T. & Latz, E. Innate immunity in Alzheimer's disease. *Nat Immunol* **16**, 229-236 (2015).
428. Borth, W. Alpha 2-macroglobulin, a multifunctional binding protein with targeting characteristics. *FASEB J* **6**, 3345-3353 (1992).
429. Calandra, T. Macrophage migration inhibitory factor and host innate immune responses to microbes. *Scand J Infect Dis* **35**, 573-576 (2003).
430. Kretschmer, S.*, et al.* SAMHD1 prevents autoimmunity by maintaining genome stability. *Ann Rheum Dis* **74**, e17 (2015).
431. Dutra, F.F. & Bozza, M.T. Heme on innate immunity and inflammation. *Front Pharmacol* **5**, 115 (2014).
432. Schaer, D.J., Vinchi, F., Ingoglia, G., Tolosano, E. & Buehler, P.W. Haptoglobin, hemopexin, and related defense pathways-basic science, clinical perspectives, and drug development. *Front Physiol* **5**, 415 (2014).
433. Korolnek, T. & Hamza, I. Macrophages and iron trafficking at the birth and death of red cells. *Blood* (2015).
434. Levy, J.H., Szlam, F., Tanaka, K.A. & Sniecienski, R.M. Fibrinogen and hemostasis: a primary hemostatic target for the management of acquired bleeding. *Anesth Analg* **114**, 261-274 (2012).

435. Xu, J., Jüllig, M., Middleditch, M.J. & Cooper, G.J.S. Modelling atherosclerosis by proteomics: Molecular changes in the ascending aortas of cholesterol-fed rabbits. *Atherosclerosis* **242**, 268-276 (2015).
436. Aronson, D. & Rayfield, E.J. How hyperglycemia promotes atherosclerosis: molecular mechanisms. *Cardiovasc Diabetol* **1**, 1 (2002).